ISBN 1-56347-242-2

58495>

9 781563 472428

AIAA EDUCATION SERIES

Introductory Aerodynamics and Hydrodynamics of Wings and Bodies: A Software-Based Approach
FREDERICK O. SMETANA

AIAA

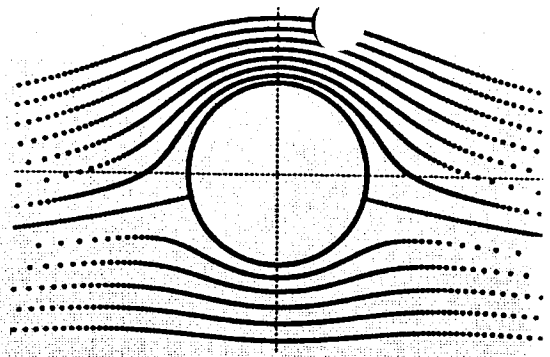

FREDERICK O. SMETANA

Introductory Aerodynamics and Hydrodynamics of Wings and Bodies: A Software-Based Approach

AIAA Education Series

J. S. PRZEMIENIECKI / SERIES EDITOR-IN-CHIEF

Introductory Aerodynamics and Hydrodynamics of Wings and Bodies: A Software-Based Approach

Introductory Aerodynamics and Hydrodynamics of Wings and Bodies: A Software-Based Approach

Frederick O. Smetana
Raleigh, North Carolina

AIAA

EDUCATION SERIES
J. S. Przemieniecki
Series Editor-in-Chief
Air Force Institute of Technology
Wright-Patterson Air Force Base, Ohio

Published by
American Insitute of Aeronautics and Astronautics, Inc.
1801 Alexander Bell Drive, Reston, VA 20191

American Institute of Aeronautics and Astronautics, Inc., Reston, Virginia

Library of Congress Cataloging-in-Publication Data

Smetana, Frederick O., 1928–
Introductory aerodynamics and hydrodynamics of wings and bodies : a software-based approach / Frederick O. Smetana.
p. cm. – (AIAA education series)
Includes bibliographical references and index.
ISBN 1-56347-242-2 (alk. paper)
1. Aerodynamics–Data processing. 2. Hydrodynamics–Data processing. I. Title. II. Series.
TL573.S5723 1997
629.132'3—dc21 97-11859
CIP

Leb wohl, du kühnes, herrliches kind!

—Wotan's farewell to his daughter
Brünnhilde from Act III of
Die Walküre by Richard Wagner

Table of Contents

Preface

THIS book is built around six computer programs that treat various aspects of the determination of the aerodynamic or hydrodynamic characteristics of wings and bodies at low Mach numbers. It is intended to support a first course on the subject. The pedagogical theory on which the book is based is that the material is better understood when the student can devote more effort to formulating the problem and interpreting the answer and less effort to generating the solution. Generating the solutions to many end-of-chapter problems is therefore left to the programs.

There is substantial danger in such an approach: The student will use the program and fail to study the accompanying material to determine the limits of the theory that is programmed. To minimize this risk the book treats the problems to be solved at two levels: 1) one simple enough to be solved readily by hand and 2) the other realistic enough to make computer solution attractive.

The treatment is limited to cases where the freestream flow velocity is much smaller than the local speed of sound. As a result of this limitation, the theory presented applies both to bodies in the atmosphere and to bodies fully submerged in the ocean.

The title should suggest that only the basics of the subject are treated. Many subtitles are left for advanced courses. This includes the idea of wing–body combinations.

The book begins with a determination of the characteristic of the operating environment. Beginning with a derivation of the governing differential equation, it is shown that mathematical models of the ocean and the atmosphere represent three special cases of this equation: 1) a constant density case, 2) a case where the temperature decreases linearly with increasing altitude, and 3) a case where the temperature remains constant with increasing altitude. The pressure–density–temperature relations for these situations are derived. The meaning of the coefficient of dynamic viscosity is also discussed.

The second chapter treats elementary inviscid flow functions and shows how by combining a uniform stream, a source, and a sink, a flow resembling that over a cylinder normal to the stream can be generated. The cylinder may be rotating, in which case it generates a lift. Depictions of the flow-field for a number of cases are provided, and source code for the software that was used to generate the figures is supplied on an accompanying 3.5-in. disk. These codes are in addition to the six principal programs supplied with the book.

The third chapter describes how, through a conformal transformation, the lifting circular cylinder can be mapped into an airfoil shape. The details of performing this transformation are handled by the program **JOUKOW** following the exposition of

the technique in the text. The program contains two enhancements to yield better agreement with experimental data. How these enhancements accomplish this feat is discussed. Typical airfoil shapes generated by this program are shown, as are the pressure distributions they generate at various angles of attack and a portion of a typical text listing.

The extension of the fluid model to accommodate fluid viscosity is treated in Chapter 4. The concept of a boundary layer is introducted, and a method is developed (momentum integral technique) for determining the effective displacement of the freestream due to the presence of a body in the flow. The method also yields the skin friction due to the flow over the surface. In addition, the method provides the basis for determining the size of the body wake or wing wake and, thus, the form drag of the configuration. When added to the skin-friction drag this yields the net fluid resistance on the body. The details of how this is accomplished for fuselagelike or nacellelike bodies are provided in Chapter 7.

Chapter 5 describes the theory behind a major program, **AIRFOIL**, which can determine the lift, drag, and pitching moment characteristics of a specified airfoillike shape. Instructions for entering data into the program are provided, as are typical results. The chapter text discusses limitations imposed by the theory coded on the types of airfoils that can be analyzed and the maximum lift coefficient value for which the code gives results that closely match those determined experimentally. Example results for a variety of airfoils are given.

Chapter 6 discusses how airfoil characteristics at various spanwise stations can be integrated to determine the characteristics of a complete wing through the program **F2D3D**. Included is a discussion of the origins of induced drag and the theoretical foundations of **F2D3D**. Typical program input and output are shown. Because **F2D3D** requires the two-dimensional characteristics to be in functional form, a least-squares fit of experimental data or the tabular data produced by **AIRFOIL** is generated by **POLYFIT**. Two auxillary programs, **2DHELP** and **3DHELP**, help the user set up input files for the two principal programs.

Chapter 7 deals with the determination of the lift, drag, and moment characteristics of a body with a plane of symmetry at small inclination to the flow. The theory, which is programmed in **BODY**, is discussed, and instructions for entering the body geometry and other required data are provided in addition to a program (**BODYGEN**), which generates input data for general ellipsoids. Results for sample cases, including graphics, are given.

Chapter 8 deals with the flowfield generated by a lifting wing. **WASH** determines the streamlines in the downwash field including the rollup of the tip vortices. **WAKE** calculates the momentum deficiency in the downwash field. The combined result of the two programs can be used to determine the magnitude and persistance of the vortical flow components in the field up to three or four chord lengths aft of the wing trailing edge and the streamwise momentum defect faced by a tailplane at various vertical locations. This is important to the designer when selecting a suitable tailplane area and incidence angle. Chapter 8 also provides some auxillary programs to assist in data entry and graphics preparation.

Chapter 9 is a brief survey of some aspects of what is termed computational fluid dynamics. This is included to indicate to the reader the direction in which the effort is proceeding to make the prediction of the aerodynamic characteristics of complete configurations entirely analytic.

The programs themselves are supplied on high-density diskettes both as personal computer executables and as Fortran source code in ASCII format, which can be user compiled for other platforms. Only the **JOUKOW** program and the auxillary programs have not been previously published. **AIRFOIL, F2D3D, POLYFIT**, and **BODY** appeared in NASA CR-2523 and **WAKE** and **WASH** appeared in NASA CR-2774. For the present work, however, the user interface on the previously published programs has been updated to take advantage of currently available personal graphics systems (for example, the **AIRFOIL** program now generates PostScript files of the airfoil shape, the pressure distributions, and the complete lift, drag, and moment characteristics), and a slightly more accurate version of the program **BODY** is provided. The Input/Output operations were altered (disk files in place of tape files, for example) to better fit current standards and to segregate data into separate files. To facilitate program usage a number of auxillary programs were prepared especially for this book.

The programs taken from the NASA contractor's reports have received favorable comments from the general aviation industry and from home builders for the last 20 years. With the widespread availability of computers capable of running the larger programs quickly, it was felt that now the methods the programs implement could also be incorporated into the undergraduate teaching program to good effect.

Some familiarity with mathematics and physics, at least to the extent of their basic vocabulary, is assumed in the developments of theory in the text. For example, the reader should understand the meaning of superposition as related to the summing of solutions of differential equations or the concept of linear vs nonlinear or ordinary vs partial differential equations.

This book differs from most currently available texts in that it does not seek broad coverage of the subject area; rather, only sufficient theory is provided for understanding the applicability and limitations of the computer programs. The author believes that encyclopedias are not the best textbooks for introductory students. For one thing, an instructor cannot possibly cover all of such a book during the usual course framework. In the student's opinion that portion of the book that is not covered is simply excess weight and cost. At this point in the development of technology, it should also be abundantly clear that the student will someday have to acquire additional books in the course of a career for self-study—books that treat advanced aspects of the topics studied as an undergraduate or that open the door to entirely new fields.

A single method that will quickly lead to the student's being able to perform some useful design or analysis holds student interest much better than a succession of theoretical treatments, the applications of that are never explained. The programs supplied with this book most certainly are not the only ones that could be applied to such instructional purposes; the fundamental pedagogical point to be made,

however, is that students need to be given tools, such as these programs, to assist them in learning the subject matter. In particular, it is important that students be given the opportunity to carry out "what if" studies on their own. Several of the end-of-chapter problems prompt the student in this direction. The author has discovered from personal experience that such studies are an excellant vehicle to facilitate individual learning, as well as being a device that could not have been used before the availability of low-cost personal computers of adequate capability because of the time that would have been required for the various computations.

The author urges the reader not to attempt to use these computer programs blindly. Although this is possible, it is fraught with pitfalls. Computer results, these or any others, should never be accepted without a reasonably good understanding of the underlying theory. Only with such understanding are the programs not used in inappropriate situations, and only with such understanding can the results be properly evaluated. With the increasing reliance now being placed on computer usage it is important that this point be stressed to students early in their educations.

The end-of-chapter problems often seek to teach some new ideas, that is, some ideas not mentioned in the body of the chapter or mentioned only in passing, by having students perform some operation and then asking them to discuss the significance of the result. There are also some problems that permit students to check their understanding of the material. Some problems suggest archival literature from which interesting and informative data can be obtained. In contrast to many books, some of the end-of-chapter problems are really discussion questions in which students are urged to express in words their understanding of the physics of the situation. Although such problems must be graded subjectively, they provide the instructor with an indication of whether students can verbalize significant concepts, important practice for when students seek to convince others of the rightness of their ideas.

To the Student

The author appreciates that students at this level are not called upon to solve differential equations in their engineering courses. This book will make no great demands in that direction either, unless the student is provided with a computer program that enables the task to be accomplished rapidly with a minimum of errors. However, to use the programs effectively the student must understand the procedure that is coded. Unless there is this understanding, there will be little feeling for whether the results given by the computer are valid. In the workplace computer results are often used to design important pieces of hardware. Errors in the result can have serious economic consequences and may even create health and safety hazards.

Only rarely are errors in computed results the fault of the computer. Most of the time they are the result of errors in the input data or the use of the program in inappropriate circumstances. The latter situation can easily happen if the user does

not understand the procedures that have been coded; thus there exists the need to study and understand those procedures and not to use the programs blindly.

Most of the methods, which have been coded in these programs, are what might be called integral methods in that they really involve integrals of differential equations. The integrals are often approximated by a system of algebraic equations. The solution algorithms for these equations are tedious but not especially sophisticated. A general appreciation of how they work should not be that difficult to acquire and should be adequate for successful use of the programs.

The author has found that the study of new subjects is greatly enhanced if the software supplied with the course is used to obtain solutions to what if problems of his own devising and if those solutions are examined to see what lessons they have to teach. For example, one might wish to compute the aerodynamic characteristics of an airfoil over a wide range of angles of attack or a wide range of Reynolds numbers or over a series of airfoils where one geometric parameter is varied over a wide range. At some point in each of these computations the results will become ridiculous. Such an investigation serves to define the region of applicability of the program. There are many tools that can assist in evaluating program results: experimental data, analytical solutions for simple cases, results obtained by other methods, and numbers produced by the program that are obviously impossible on physical grounds. It may be noted that trying to match experimental results for airfoils under conditions where the programs can be expected to work lead to the development of tweaks that improve program performance. Students tend to resist doing such "what if" studies in the interests of saving time, but as the old saying goes: no pain, no gain. The programs execute rapidly. The output is provided as both listings and graphics. Time is not spent on tedious hand calculations, and the errors that usually come with such calculations do not occur. Thus, the student can spend a majority of the time doing what a human still does better than a machine: evaluating the results and learning therefrom.

In this text the author has made the use of software the raison d'etre in the hope that students will find that it facilitates learning and ability to undertake more realistic problems earlier in their careers.

Software Issues

The software is supplied on the attached diskettes. The user will probably find it most convenient to load all of the executable files in one directory on a hard disk. If the user desires to modify the source files, they should be placed in the same directory. If the user desires to run the codes under a non-MSDOS operating system, then, of course, the .EXE files are of no use and may be discarded. The DOSXNT and DOSXMFS files must be in the same directory from which the executable MSDOS files are run. These files create the protected mode environment that is needed to permit large programs to run. One of these files is used when the user is in the MSDOS environment and the other in the Windows 3.1 environment. A recompilation with a newer version of the PowerStation or other FORTRAN

compiler will probably be necessary to run under Windows 95 or Windows NT and, almost certainly, to run under operating system 2 (OS/2).

The FORTRAN source files are written in ASCII and should be readable by most computers. The FORTRAN is quite standard although some compilers will complain (give warnings) about the order of arrays in COMMON blocks or DIMENSION statements. Some Unix compilers the author has seen use only unit 0 to write to the screen although most will accept either unit 0 or unit * commands for screen writes. Unit * has been utilized in these codes.

Users will find it convenient to have available a software PostScript interpreter such as GHOSTSCRIPT, which contains screen drivers and drivers for most popular printers. [GHOSTSCRIPT is a shareware program distributed by the Open Software Foundation, usually as a set of compressed files. It is distributed with a set of public domain font files. It can accept additional proprietary fonts in Type 1 (PostScript) format and can be made to use the True Type fonts distributed with Windows. It supports color Postscript. The GHOSTSCRIPT distribution contains a number of document files, which are very useful in helping first time users get started. As with most shareware programs, however, technical support is not available. The user may also find some commercial software PostScript interpreters that perform the same functions as GHOSTSCRIPT. Many commercial graphics packages contain a skeletal PostScript interpreter (they read files in Adobe Illustrator format) and can perform file conversions.] Use of such a software interpreter is usually preferable to the use of the built-in interpreter in many PostScript-equipped printers because the computer CPU is usually much faster than the CPU in the printer. To print or view the vector PostScript files that the programs write under Windows, a file conversion to a Windows compatible format may be necessary. The author chose to write the graphics in PostScript format because of its portability and because the files are written in ASCII characters, not in a binary format, making it possible for the user to alter it, add titles and legends, change the figure size and shape, and send it by email.

Sample input files are given for most of the programs in the text. Users should try the respective programs with these files to see if the output data given in the text are reproduced. When the same results are achieved it generally means that the program is being used correctly and that the executable file is operating correctly.

Users with access to compilers are encouraged to try modifications to the programs. Modifications may be in the form of the visual appearance of the output, in the tasks the program performs, or in the language in which the programs are written. Users who develop useful modifications or who rewrite the source code(s) in another programming language, and this includes MATLAB m-files, are asked to share their codes with the author and with the scientific community at large.

Even users who do not have a FORTRAN compiler can still find the source code useful in checking the order of input data in a .DAT file, for example, for reviewing the algorithm actually used to solve a problem or to generate a plot, or when checking for suspected coding errors. The author is entirely responsibile for any such errors that remain and would appreciate being notified if and when such

errors are found so that they may be corrected in future releases of the software. The author would also like to hear from users who have suggestions to make regarding ease of use issues or program utility.

Acknowledgment

THE author would like to acknowledge the contributions made by his coauthors in preparing the NASA contractor reports cited. The original code preparation and much of the text was theirs although decisions as to the adequacy of results and suggestions for some of the modifications to codes obtained from elsewhere were the author's. Modifications over the ensuing years to enable the codes to be compiled with more modern compilers and to run on newer hardware were also made by the author, as were the PostScript graphics routines and the provisions for interactive data entry. Mistakes such as remain in the book are the sole responsibility of the author. Portions of Sec. 6.3 and much of Sec. 6.4 are based on the treatment given by Smetana et al. (Ref. 26). The discussion herein provides the theoretical basis for the F2D3D program, which is a modified version of the program presented in Ref. 26.

Finally, the author is especially grateful to James C. Williams, III, for his careful and helpful review of an early version of the manuscript. His suggestions contributed to a complete, and hopefully superior, version of Chapter 2.

Frederick O. Smetana
Raleigh, North Carolina
October 31, 1996

1
The Atmosphere and the Ocean

1.1 Introduction

AERODYNAMICS and hydrodynamics are fields of study concerned with predicting the forces and moments experienced by bodies moving in a fluid medium. The two fluids of greatest interest are air and water. Both are viscous and compressible. As a result of the compressibility, these fluids have sound speeds dependent on the characteristics of the particular medium. We note that the speed of sound in a medium is the speed at which remote regions of the fluid receive information regarding the existence of a weak disturbance elsewhere in the fluid. The speed of sound in water is many times faster than it is in air, while the density of water is about 800 times that of air at sea level. As a result of the denser medium and higher sound speed, vehicles traveling in water move at speeds that are very much smaller that the local speed of sound; that is, they have Mach numbers approaching zero. (The Mach number is the ratio of the vehicle's speed to the speed of sound of the medium in which the vehicle is traveling.) Although transonic and supersonic flight in the atmosphere is now common, we will restrict our consideration, in so far as this book is concerned, to Mach numbers of 0.3 or less. At these Mach numbers the air at any altitude can be considered to be incompressible.

The ocean differs from the atmosphere most notably in that vehicular travel is possible on the surface as well as beneath the surface. We will restrict our consideration to vehicular motion sufficiently far beneath the surface that the effects of surface waves and of wave reflections from the surface on the fluid through which the vehicle must travel are vanishingly small. Under these conditions the same basic theory is valid for flight in the atmosphere or in the ocean. To be sure, the greater density of the water means that vehicle bouancy is always a significant force in undersea travel although it is usually insignificant when applied to heavier-than-air machines.

1.2 Relation of Pressure and Altitude

For us to determine the forces and moments experienced by a vehicle moving in a particular fluid, it is necessary that we first deduce some of the properties of the fluid and their variation with altitude (or depth). Let us consider a small fluid element having dimensions dx, dy, and dz. This element is shown in Fig. 1.1. The mass of the element is $\rho\,dx\,dy\,dz$ where ρ is the density. The weight of the element is simply the mass times the acceleration due to gravity g. If the pressure on the bottom face of the element is p, then the force on this surface is $P\,dx\,dy$ directed upward.

The pressure on the upper surface is $P + \Delta P$, and the force on this surface directed downward is $(P + \Delta P)(dx\,dy)$. If the element is to remain stationary, the forces on it must be in equilibrium. Hence,

$$P\,dx\,dy = g\rho\,dx\,dy\,dz + (P + \Delta P)(dx\,dy)$$

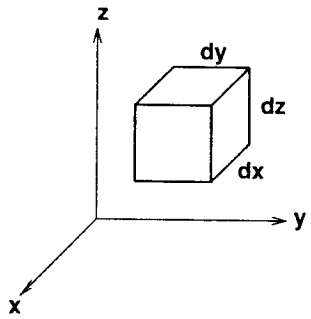

Fig. 1.1 Element of volume.

If we now divide this equation by $dx\,dy$ we have

$$P = g\rho\,dz + P + dP$$

or

$$dP = -g\rho\,dz \tag{1.1}$$

1.2.1 In the Ocean

The solution to differential equation (1.1) tells us how the fluid pressure varies with variations in z (height or depth). To solve Eq. (1.1) we need an additional relationship. For the ocean we will assume that ρ is constant, which is the same as assuming that the fluid is incompressible. Eq. (1.1) then has the solution

$$P_2 - P_1 = -g\rho(z_2 - z_1) \tag{1.2}$$

For convenience we call z_1, the depth at the surface of the ocean, zero. Because our positive direction is up, increasing depth means increasingly negative values of z_2. The pressure at any depth is then

$$P = P_0 + g\rho d \tag{1.3}$$

where P_0 is the atmospheric pressure at the surface and d is the depth of the point of interest measured positively with respect to the surface. From Eq. (1.3) we see that the pressure at a point 100 ft below the surface is $2116.2 + (64)(100) = 8516.2$ psf or about 59 psi. Here, 64 is the weight in pounds of a cubic foot of sea water.

1.2.2 In the Atmosphere

To solve Eq. (1.1) for the atmosphere, we first employ the equation of state for a perfect gas

$$P = \rho\mathcal{R}T \tag{1.4}$$

where $\mathcal{R}$ is the gas constant and T is the temperature measured from absolute zero. $\mathcal{R}$ has the value of 1718 in U.S. customary units (USCU). However, this

equation introduces an additional variable and we must specify a relationship among the variables in order to obtain a solution.

In the troposphere. Measurements in the atmosphere indicate that from the ground up to an altutide of 36,150 ft, the region of the atmosphere called the troposphere, the temperature decreases about 3.56°F for each 1,000-ft increase in altitude. This behavior can be expressed as

$$T = T_0 - \alpha h \tag{1.5}$$

where $\alpha = 0.00356$/ft or 0.0065° K/m.

Pressure–altitude variation in the stratosphere. From 36,150 to 82,300 ft the temperature is constant. In this region, called the stratosphere, Eq. (1.1) can be written

$$dP = -\frac{gP}{\mathcal{R}T}dh$$

or

$$\frac{dP}{P} = -\frac{g\,dh}{\mathcal{R}T} \tag{1.6}$$

Equation (1.6) has the solution

$$\ln P = -(g/\mathcal{R}T)h + C \tag{1.7}$$

If the pressure at h_0 is p_0, then

$$C = \ln P_0 + (gh_0/\mathcal{R}T)$$

and

$$\ln(P/P_0) = -(g/\mathcal{R}T)\,(h - h_0)$$

or

$$P = P_0 \exp\left[-\frac{g(h - h_0)}{\mathcal{R}T}\right] \tag{1.8}$$

In Eq. (1.8) $h > h_0$ so that P is always less than P_0. Here, $h_0 = 36{,}150$ ft, $P_0 = 471.54$ psf, and $T = 389.99$°R.

Pressure–altitude variation in the troposphere. For the case where the temperature decreases linearly with altitude

$$dP = -\frac{gP\,dh}{\mathcal{R}T_0[1 - (\alpha h/T_0)]} \tag{1.9}$$

Equation (1.9) has the solution

$$\ln P = -\frac{g}{\alpha \mathcal{R}} \ln\left(1 - \frac{\alpha h}{T_0}\right) + C \tag{1.10}$$

When $h = 0$, $P = P_0$. Thus,

$$\ln P_0 = C$$

and

$$P = P_0 \left(1 - \frac{\alpha h}{T_0}\right)^{-\frac{g}{\alpha \mathcal{R}}} \tag{1.11}$$

Typical values for P_0, $g/\alpha\mathcal{R}$, T_0, and α/T_0 are 2116.2, 5.26481, 518.69, and 6.86×10^{-6} in USCU.

1.3 Density–Altitude Relationship

After the expressions for the variation of pressure with altitude are known, the expressions for the variation of density with altitude can be found with the aid of the equation of state. Because

$$\frac{\rho}{\rho_0} = \frac{P}{P_0}\frac{T_0}{T} \tag{1.12}$$

the density–altitude relationship in the troposphere is

$$\rho = \rho_0 (1 - 6.86 \times 10^{-6} h)^{4.26} \tag{1.13}$$

and the density–altitude relationship in the stratosphere is

$$\rho = \rho_0 \exp\left[-\frac{g(h - h_0)}{\mathcal{R}T}\right] \tag{1.14}$$

1.4 Density–Temperature Relationship in Water

Sea water, of course, is not a gas and so Eq. (1.4) does not apply. Nevertheless, water has a density–temperature relationship that is quite interesting. Water has its maximum density at 4°C or 39°F. It is less dense at lower temperatures (to 0°C) and decreasingly dense as the temperature increases above 4°C. As a result, the temperature in the ocean below a depth of a few hundred feet in the artic, temperate, or equatorial regions (in fact, everywhere on Earth) is always 4°C. The density difference between sea water at 4°C and sea water at colder or warmer temperatures is not large. For this reason the assumption of constant density is quite reasonable for purposes of force calculations.

1.5 Definition of Altitude

Equations (1.8), (1.11), (1.13), and (1.14) are definitions of the altitudes at which certain pressures or densities are assumed to exist. On any given day, however, the pressure or density at any geometric altitude may be quite different from the values obtained from these equations. The relations are still useful, however, because the forces on the vehicle are dependent on the actual density, not the altitude. Similary, pneumatic altimeters, airspeed indicators, and Mach meters are calibrated according to the standard pressure altitude relationship. Thus, these instruments are said to read pressure altitude, which may or may not be the same as geometric altitude. The altitude pressure indication plus a measurement of the static temperature at that altitude are used to determine the density altitude. Again, it may or may not be the same as the geometric altitude.

In addition to these differences, we must be aware that these formulas are based on a constant value for the acceleration due to gravity. The value of g actually diminishes according to the formula

$$g = g_0 \left(\frac{2.0856 \times 10^7}{2.0856 \times 10^7 + h}\right)^2 \tag{1.15}$$

where h is the geometric distance from the surface of the Earth in feet and g_0 is the sea level value of g. From this relation it is obvious that the vehicle must be a great deal higher than 82,300 ft before the decrease in gravitational attraction becomes noticeable.

1.6 Viscosity

There is one additional property of fluids that is important in calculating the forces experienced by bodies moving through the fluid: viscosity. Viscosity is the property that describes the resistance of the fluid to being sheared. A fluid that shears easily has a low viscosity; one that is difficult to shear has a high viscosity.

The concept of fluid shear is illustrated in Fig. 1.2.

A fluid element consists of two regions, A and B. If region B moves relative to region A the element is said to shear. The coefficient of dynamic viscosity μ is the ratio of force per unit shear area required to separate region B from region A to the difference in velocity between regions A and B divided by the distance

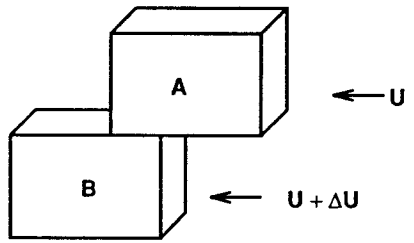

Fig. 1.2 Illustration of concept of viscosity.

between them. Mathematically this is expressed as

$$\mu = \frac{F}{dA} \Big/ \frac{du}{dy} \tag{1.16}$$

where F is the force, dA the shear area, du the change in velocity, and dy the distance between regions A and B. Another measure of viscosity used with liquids is the rate at which the fluid will pass through a given size hole at the bottom of an open top container under the influence of gravity.

For gases the coefficient of viscosity increases roughly with the square root of the absolute temperature. There is also a modest pressure effect, primarily at superatmospheric pressures. Liquids usually exhibit a decrease in viscosity with increasing temperature. (The effect is celebrated in folklore with the phrase: as slow as molasses in January.)

The complex molecular interactions that manifest themselves as viscosity also give rise to heat conduction. In contrast to pressure and temperature, viscosity and heat conduction require that the molecules of the fluid be in relatively close proximity to each other. Thus, the magnitude of the effects we call viscosity and heat conduction decline as the distance between molecules increases. Gases exhibit less viscosity and heat conduction than liquids, and rarefied gases are less viscous than the same gas under denser conditions.

Heat conduction is significant in aerodynamics only for Mach numbers greater than 2.0; thus, it will not be discussed further. Viscosity, on the other hand, is the dominant physical phenomenon leading to the production of most body drag and a significant portion of wing drag. We will discuss methods for quantitative determination of the various drag components in a subsequent chapter.

1.6.1 Example 1

Use Eq. (1.11) to determine the pressure at 36,150 ft.

The result is easily obtained to a greater accuracy than can be obtained with pocket calculators using the following short program:

```
      IMPLICIT REAL*8(A-H,O-Z)
      H=36150.0D0
      A=0.00356D0
      T0=518.69D0
      P0=2116.2D0
      EX=32.2/(1718.0D0*A)
      P=P0*(1.0D0-(A/T0)*H)**EX
      T=518.69D0-A*H
      WRITE(*,1) P,T,EX
1     FORMAT(10X,'P = ',D23.16,
     1/,10X,'T = ',D23.16,
     2/,10X,'EX = ',D23.16)
      STOP
      END
```


The results are printed on the screen. The pressure value is 471.54 . . . . The pressure at any other altitude less than 36,150 ft can be computed with the program merely by changing the value of H. A table of pressure vs altitude can be generated by putting the computation below line 6 in a loop and incrementing the value of H. In this case, it is more satisfactory to write the results to a two-column file.

1.6.2 Example 2

A hemicylindrical shell forms part of the gate trapping a quantity of water (see Fig. 1.3). Determine the vertical force generated by the hemicylinder.

The solution is as follows. The pressure at any point on a hemicylindrical shell can be shown to be

$$P_0 + \rho g h_0 + \rho g r(1 - \cos\theta)$$

where P_0 is the atmosphereic pressure, h_0 is the depth of the top of the hemicylindrical shell, r is the radius of the shell, and θ is measured from the vertical. Here, θ is zero at the top and π at the bottom. The area element on the surface of the shell is $r\,d\theta\,dw$. If we let $dw = 1$, we can say that $r\,d\theta$ is the area element on the surface of the shell per unit length of the shell. The force due to the pressure of the water has a vertical component and a horizontal component. The vertical component is obtained by integrating the product of the pressure and $\cos\theta$ over the shell surface,

$$\int_0^{\pi} [P_0 + \rho g h_0 + \rho g r(1 - \cos\theta)] r \cos\theta\, d\theta = \rho g r^2 \frac{\pi}{2}$$

This force acts up.

For simplicity we have ignored the force due to the air pressure on the downstream side of the shell. In any case, it is less than 1/800 times the force of the water.

We can also obtain the vertical force as a consequence of Archimedes principle, that is, the bouyant force is the difference in the weight of the water excluded from the shell and that of the air contained therein. The weight of the excluded water is the same result we obtained previously, simply

$$\rho g(\pi r^2/2)$$

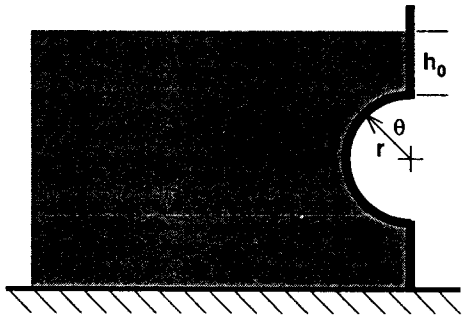

Fig. 1.3 Gate with hemicylindrical shell.

Problems

1.1. Assume the pressure–altitude relation is given by Eq. (1.11). Determine the density of the air in a) Leadville, Colorado (elevation 10,000 ft) when the temperature is −40°F and when it is 100°F; b) Edwards, California (elevation 2500 ft) when the temperature is 20°F and when it is 120°F; c) Death Valley, California (elevation −260 ft) when the temperature is 130°F; and d) Washington, D.C. (elevation about sea level) when the temperature is 59°F.

1.2. If a submarine is designed to withstand a pressure of 1000 psi on its hull, what is the greatest depth to which it can safely descend?

1.3. What is the weight of a sphere of sea water with a radius of 20 ft?

1.4. What is the weight of the same sphere when filled with air at standard temperature and pressure?

1.5. If the sphere in problem 4 were immersed in sea water, what bouyant force would it experience? Assume the container is rigid and weightless.

1.6. The density of gases is roughly proportional to their molecular weight. Air, which is a mixture of gases, can be assumed to have a molecular weight of 29. Octofluorocyclobutane has a molecular formula given by C_4F_8. What would you expect its density to be relative to air at standard temperature and pressure (STP)?

1.7. The surface area of a sphere is given by $4\pi r^2$. A balloon is made of material that weighs 0.025 psf. The balloon has a radius of 100 ft when fully inflated. The balloon is filled with helium at the same temperature and pressure as the surrounding air when fully inflated. What is the maximum altitude to which the balloon will ascend? What is the maximum altitude if the balloon is filled with hydrogen?

1.8. Supply the correct numbers for the constants in Eqs. (1.3), (1.8), and (1.11) in System International (SI) units.

1.9. If the temperature–altitude relation given by Eq. (1.5) holds on a particular day, what should you expect the temperature to be at the 6000-ft level on Mt. Mitchell, North Carolina, if the temperature at sea level on that day is 52°F?

1.10. The force per unit width created by the water on the dam shown in Fig. P1.1 is given by

$$F = \int_0^h P(z)\,dz$$

where z is measured from the surface down. The point where all of the force can be assumed to act is $2h/3$ from the surface. There are two possible failure modes

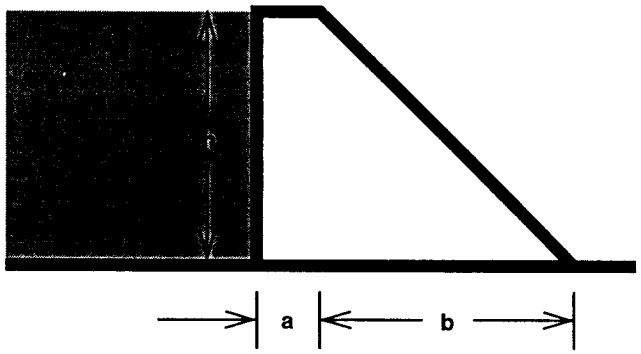

Fig. P1.1 Dam.

for the dam: 1) it can slide down the river bed if its weight is insufficient or 2) it can tip over if b is made too small. If concrete weighs 2.6 times as much as fresh water for equal volumes, what should the relation of b be to h if a is $h/20$?

1.11. Write a computer program to generate a table of pressure, density, and temperature vs geometric altitude to an altitude of 82,300 ft in 100-ft increments. Take $P_0 = 2116.2$ psf, $\rho_0 = 0.002377$ slugs/ft^3, and $T_0 = 518.69$°R. Format the output so that data from 0 to 4900 ft appear on the first page, 5000 to 9900 on the second page, and so forth.

1.12. Generate a table for the same conditions in SI units.

2
Elementary Flow Functions

2.1 Introduction

IT has long been the goal of researchers to describe fluid flow over bodies in mathematical terms. If this can be done, then it is a simple matter, at least conceptually, to determine the change in the forces acting on the body that result from a change in body shape. Unfortunately, successful descriptions thus far have been limited to fairly simple shapes. Nevertheless, the understanding gained from studies of flows over these simple shapes has enabled researchers to generalize the treatment to surprisingly realistic configurations.

All analyses of fluid flow begin with a mathematical statement of some fundamental conservation laws. Our present interest is a statement of the conservation of mass. This law says that the fluid mass entering a unit volume either leaves or accumulates. We may derive a mathematical expression of this statement as follows.

Given an element of volume having dimensions of dx, dy, and dz (see Fig. 2.1) the mass entering the left face has a density ρ and a velocity u. The area of the flow is $dy\,dz$. Assume now that the mass leaving the right face has a slightly different velocity and density. The mass leaving the right face is, therefore, $[\rho u + (\partial \rho u/\partial x)dx]dy\,dz$. We may write similar terms for the mass entering and leaving the volume in the y direction: $\rho v\,dx\,dz$ and $[\rho v + (\partial \rho v/\partial y)dy]dx\,dz$. In the z direction the same procedure leads to $\rho w\,dx\,dy$ and $[\rho w + (\partial \rho w/\partial z)dz]dx\,dy$.

The change in the mass inside the volume is given by

$$\frac{\partial \rho}{\partial t}dx\,dy\,dz$$

Equating the change in the mass inside the volume to the sum of the inflows less the sum of the outflows results in the following equation:

$$\begin{aligned}\frac{\partial \rho}{\partial t}dx\,dy\,dz &= \rho u\,dy\,dz + \rho v\,dx\,dz + \rho w\,dx\,dy - \left(\rho u + \frac{\partial \rho u}{\partial x}dx\right)dy\,dz \\ &\quad - \left(\rho v + \frac{\partial \rho v}{\partial y}dy\right)dx\,dz - \left(\rho w + \frac{\partial \rho w}{\partial z}dz\right)dx\,dy \\ &= -\left(\frac{\partial \rho u}{\partial x} + \frac{\partial \rho v}{\partial y} + \frac{\partial \rho w}{\partial z}\right)dx\,dy\,dz \qquad (2.1)\end{aligned}$$

However, $dx\,dy\,dz$ is simply the differential volume. Dividing both sides by the differential volume we have the law of mass conservation or the continuity equation as applied to a fluid medium

$$\frac{\partial \rho}{\partial t} + \left(\frac{\partial \rho u}{\partial x} + \frac{\partial \rho v}{\partial y} + \frac{\partial \rho w}{\partial z}\right) = 0 \qquad (2.2a)$$

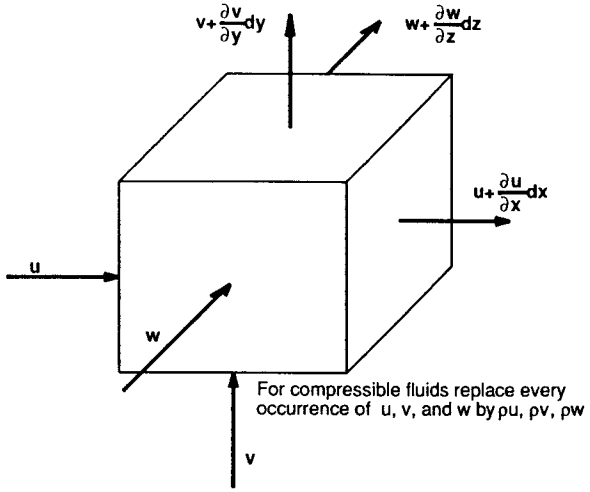

Fig. 2.1 Element of volume.

For steady, incompressible flow in two dimensions, that is with ρ constant, the continuity equation reduces to

$$\frac{\partial u}{\partial x} + \frac{\partial v}{\partial y} = 0 \tag{2.2b}$$

2.2 Potential Functions

It can be shown[1] that the statement that the line integral between two points in a plane is independent of the path of integration between the two points is equivalent to the statement that the line integral around any closed path is zero. This equivalence leads to the following theorem:

In a simply connected region in which $u(x, y)$, $v(x, y)$, and their first partial derivatives are continuous, the necessary and sufficient condition that the integral

$$\int u\,dx + v\,dy$$

around a closed path should be zero and that the integral along a path connecting two points should be independent of the path is

$$\frac{\partial u}{\partial y} = \frac{\partial v}{\partial x} \tag{2.3}$$

Further, if Eq. (2.3) is satisfied for any two functions u and v, there exists a function ϕ for which

$$\frac{\partial \phi}{\partial x} = u; \qquad \frac{\partial \phi}{\partial y} = v \tag{2.4}$$

Therefore,

$$u\,dx + v\,dy = d\phi \tag{2.5}$$

is an exact differential.

Readers interested in the proof may consult Ref. 1 or other advanced calculus texts. We shall not pursue it here; rather we are interested in what conclusions we can draw from the theorem as it relates to steady, inviscid fluid flows.

Suppose we have a flow with a component of velocity in the x direction designated as u and a component of velocity in the y direction designated as v. Further, let u and v be continuous differentiable functions of position. Then if Eq. (2.3) is satisfied we conclude that a velocity potential ϕ exists. We have demonstrated previously that when two-dimensional, inviscid, incompressible flows satisfy the requirement for conservation of mass, the velocity components are related through the equation

$$\frac{\partial u}{\partial x} + \frac{\partial v}{\partial y} = 0 \tag{2.6}$$

Using the relationship between ϕ and u and v we may write Eq. (2.6) as

$$\frac{\partial^2 \phi}{\partial x^2} + \frac{\partial^2 \phi}{\partial y^2} = 0 \tag{2.7}$$

This is Laplace's equation, probably the most studied partial differential equation in the mathematical literature. If a potential function satisfies this equation it is irrotational, as we shall now demonstrate.

2.3 Conditions for Irrotationality

Consider the plane element of area shown in Fig. 2.2. We will treat this element as if it were solid rather than fluid in the interests of keeping the analysis simple. Doing so does not affect the conclusions drawn from the analysis but it does affect the values of the numerical constants in the result. In the more usual treatment, the angular velocity of the fluid element in Fig. 2.2 is mass averaged with the result that the coefficient in Eq. (2.8) is one-half rather than 2. Our purpose in conducting this analysis is to inquire whether, as a result of the difference in velocities shown in Fig. 2.2, the element will rotate and translate or simply translate. We designate a clockwise angular velocity about the center of the element as ω. There are four components to ω

$$\omega = -\frac{u}{dy/2} + \frac{v}{dx/2} - \left(v + \frac{\partial v}{\partial x}dx\right) \Big/ \frac{dx}{2} + \left(u + \frac{\partial u}{\partial y}dy\right) \Big/ \frac{dy}{2}$$

$$\omega = 2\left(\frac{\partial u}{\partial y} - \frac{\partial v}{\partial x}\right) \tag{2.8}$$

We see, therefore, that if

$$\frac{\partial u}{\partial y} - \frac{\partial v}{\partial x} = 0 \tag{2.9}$$

the element will simply translate; that is, it is irrotational.

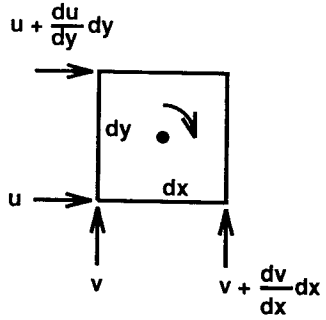

Fig. 2.2 Plane element.

If a potential function ϕ exists such that

$$u = \frac{\partial \phi}{\partial x} \tag{2.10a}$$

$$v = \frac{\partial \phi}{\partial y} \tag{2.10b}$$

ϕ satisfies the continuity equation if and only if the flow is irrotational. The velocity may be said to be the gradient of the ϕ. As a simple example to demonstrate this, we choose the potential function

$$\phi = xy^3 - yx^3$$

Then

$$\frac{\partial \phi}{\partial x} = y^3 - 3yx^2$$

$$\frac{\partial \phi}{\partial y} = 3xy^2 - x^3$$

and

$$\frac{\partial^2 \phi}{\partial x^2} = -6yx$$

$$\frac{\partial^2 \phi}{\partial y^2} = 6xy$$

$$\frac{\partial^2 \phi}{\partial x \partial y} = 3y^2 - 3x^2$$

$$\frac{\partial^2 \phi}{\partial y \partial x} = 3y^2 - 3x^2$$

It is obvious that ϕ is irrotational because

$$\frac{\partial^2 \phi}{\partial x \partial y} - \frac{\partial^2 \phi}{\partial y \partial x} = 0$$

Because ϕ is irrotational it should also satisfy the continuity equation

$$\frac{\partial^2 \phi}{\partial x^2} + \frac{\partial^2 \phi}{\partial y^2} = 0$$

If we substitute the recently computed values for these derviatives we obtain

$$-6xy + 6xy = 0$$

and see that, indeed, the continuity equation is satisfied.

Potential functions are called state functions in thermodynamics because the value of the function depends only on the values of the coordinates. Flows in which there is significant energy dissipation, such as flows where viscosity is important, or flows that contain shock waves are rotational. If they are real flows they must, of course, still satisfy mass conservation (continuity). But to analyze them we must forego the simplicity that follows from representing them by potential functions.

2.4 Laplace's Partial Differential Equation and the Stream Function

Hydrodynamics is the branch of mathematical physics concerned with the properties of functions that satisfy Laplace's partial differential equation. We will restrict our consideration at this level to the two-dimensional form. In rectangular coordinates we can restate Laplace's equation, written here in terms of the stream function, as

$$\frac{\partial^2 \psi}{\partial x^2} + \frac{\partial^2 \psi}{\partial y^2} = 0 \tag{2.11}$$

In polar coordinates Laplace's equation is

$$\frac{\partial^2 \psi}{\partial r^2} + \frac{1}{r^2}\frac{\partial^2 \psi}{\partial \theta^2} + \frac{1}{r}\frac{\partial \psi}{\partial r} = 0 \tag{2.12}$$

Because this equation is a linear partial differential equation, a sum of solutions is also a solution. For example, if

$$\psi = Ur\sin\theta \tag{2.13}$$

and

$$\psi = \frac{K}{2\pi}\ell_n r \tag{2.14}$$

are solutions, then

$$\psi = \frac{K}{2\pi}\ell_n r + Ur\sin\theta \tag{2.15}$$

is also a solution.

We should note that certain stream functions, like certain potential functions, satisfy the Laplace equation. They differ mathematically from potential functions by how their boundary conditions must be specified. The physical basis of stream functions is discussed in the following discussion.

Assume we seek to find functions that model some physical fluid flow. (By model we mean that the graph of the function looks like a picture of the physical flow.) It is readily seen that if the product $r \sin\theta$ is a constant regardless of the value of r or θ, then $\psi = Ur \sin\theta$ represents a straight line. By choosing $(r \sin\theta)_j = (r \sin\theta)_{j-1} + C$

$$\psi = Ur \sin\theta$$

represents a series of straight lines each separated by a distance C from the line below it and by a distance C from the line above it. If these lines are parallel to the direction of the flowing stream and the fluid anywhere between any pair of lines is of the same constant density and it flows at the same constant velocity, then the fluid flow is termed a uniform stream. Now, a curve that is always parallel to the local direction of a flowing stream is called a streamline. A function of x and y or r and θ that describes a series of streamlines is called a stream function. Because there is no flow across streamlines (else the streamline would not be parallel to the local flow direction) the fluid volume per unit depth per unit time flowing between a pair of streamlines remains constant. Obviously, then, there is a relationship between fluid flow as modeled by stream functions and the continuity equation. We shall seek to determine this relationship and some aspects of its characteristics.

Suppose we consider the function

$$\psi = Ur \sin\theta \tag{2.16}$$

We can readily see that this function satisfies the definition for a stream function we have given. In this case, the stream function represents a uniform stream.

We are going to restrict our attention to fluid flows for which the density remains essentially constant. Water and air at low Mach numbers can be treated as constant density fluids for purposes of our analysis. The mass flowing past a given streamwise station can be expressed by

$$\rho v h = \dot{m}/d \tag{2.17}$$

where ρ is the density, v is the average velocity, h is the distance between the boundaries of the flow, d is the depth of the fluid and is assumed to remain constant, and $\dot{m}$ is the time rate of change of the fluid mass. Since $\dot{m}$ must be constant for a steady flow with no additions or removals, the mass flowing between two streamlines remains constant, as we have already noted. When the streamlines converge, the average velocity must increase; when the streamlines diverge, the average velocity must decrease; when the streamlines are parallel, the velocity remains constant. The value of the stream function is then a measure of the mass flow (or the volumetric flow) between a particular streamline and the reference streamline. It has the units of length $\times$ length per unit time.

When one goes from one streamline to an adjacent one the change in the volumetric flow rate is a measure of the velocity of the flow parallel to the stream.

If we take as our coordinates y as being normal to the freestream flow direction and x as being parallel to the freestream flow direction, then

$$\frac{\partial \psi}{\partial y} = u \qquad v_r = \frac{1}{r}\frac{\partial \psi}{\partial \theta} \tag{2.18a}$$

and

$$\frac{\partial \psi}{\partial x} = -v \qquad v_\theta = -\frac{\partial \psi}{\partial r} \tag{2.18b}$$

The negative sign on v indicates that if the value of ψ increases as one moves in the streamwise direction, the streamlines are converging and the velocity component along the y axis points in the negative direction.

In a two-dimensional flow the change in the volumetric flow at a point has two components that must sum to zero to satisfy mass conservation. We expressed this condition by means of the continuity equation (2.26). If we substitute definitions for u and v in terms of the stream function into Eq. (2.26) we obtain

$$\frac{\partial^2 \psi}{\partial x \partial y} - \frac{\partial^2 \psi}{\partial y \partial x} = 0 \tag{2.19}$$

which is true regardless of ψ because the order of differentiation does not matter. If the flow is irrotational and we substitute the expressions for u and v into Eq. (2.9) we find that

$$\frac{\partial^2 \psi}{\partial y^2} + \frac{\partial^2 \psi}{\partial x^2} = 0 \tag{2.20}$$

which is Laplace's equation. Thus, we are led to the very important conclusion that when applied to steady, incompressible, inviscid flows this equation provides a complete description of the flow.

2.5 Euler's Equations

Moving fluids also obey Newton's laws of motion but in a form that is a little different from the form applied to solid bodies. Newton's second law of motion says that the sum of all of the external forces applied to a fluid element must equal the change in the momentum of the fluid mass in the element. The fluid element depicted in Fig. 2.1 has a volume given by $dx\,dy\,dz$. Multiplying the volume by the density gives the mass of the fluid element or $\rho\,dx\,dy\,dz$. Because we will consider only cases in which the fluid mass is conserved, the change in momentum across the fluid element in the ith direction is

$$\left(\rho \frac{\partial u_i}{\partial t} + \rho u_j \frac{\partial u_i}{\partial x_j}\right) dx\,dy\,dz$$

where the repeated subscript j indicates that the expression actually represents

a sum of three terms, a term with $j = 1$, one with $j = 2$, and one with $j = 3$, corresponding to the x, y, and z directions. Because the net force can be applied in an arbitrary direction, it must be considered to have components in all three directions. Generally, the net force has contributions from the pressure differences across the element, from viscous stresses acting on the element, and, in the case of water, from the gravitational attraction acting on the fluid mass in the element. The latter, however, acts only normal to the Earth's surface. The mass in an element of air is considered to be so small that one can safely neglect the effects of gravity in that case. To be consistent with the other analyses in this chapter we will also neglect the effects of fluid viscosity as they affect the motion of the fluid element. The net force in the ith direction acting on the $dydz$ face of the element because of hydrostatic pressure is simply

$$-\frac{\partial p}{\partial x}dx\,dy\,dz$$

Equating the net force to the change in momentum in the x direction yields

$$-\frac{\partial p}{\partial x} = \rho\frac{\partial u}{\partial t} + \rho u\frac{\partial u}{\partial x} + \rho v\frac{\partial u}{\partial y} + \rho w\frac{\partial u}{\partial z} \tag{2.21a}$$

after dividing out the volume element $dx\,dy\,dz$ on both sides of the equation. The equations for the y and z directions are similar,

$$-\frac{\partial p}{\partial y} = \rho\frac{\partial v}{\partial t} + \rho u\frac{\partial v}{\partial x} + \rho v\frac{\partial v}{\partial y} + \rho w\frac{\partial v}{\partial w} \tag{2.21b}$$

$$-\frac{\partial p}{\partial z} = \rho g + \rho\frac{\partial w}{\partial t} + \rho u\frac{\partial w}{\partial x} + \rho v\frac{\partial w}{\partial y} + \rho w\frac{\partial w}{\partial z} \tag{2.21c}$$

Writing the equations in this fashion assumes that the z direction is normal to the Earth's surface.

This inviscid form of the equations of motion are generally termed the Euler equations because Euler was one of the first to study the equations of motion extensively in connection with hydrodynamics problems. Euler's studies began during the later years of the 18th century. In the early 19th century, Navier[2] and Stokes[3] undertook studies of the motion of fluids when the forces applied to the fluid element contained viscous stresses, as well as the hydrostatic pressure.

The inclusion of viscous stress in the equations of motion greatly complicates their solution because they are then nonlinear in general. Analytical solutions have been found for only a few cases with very simple boundaries. We shall consider a few of the possible analytical solutions in Chapter 4. In general, solving the Navier–Stokes equations, as they are called, has become a specialized industry populated by mathematical physicists running powerful computational hardware. We will consider the task faced by these scientists in somewhat more detail in Chapter 9.

2.6 Bernoulli's Equation

If we restrict application of the Euler equations to situations where the flow is steady and two dimensional, we can write the equations as

$$-\frac{\partial p}{\partial x} = \rho u\frac{\partial u}{\partial x} + \rho w\frac{\partial u}{\partial z} \tag{2.22a}$$

$$-\frac{\partial p}{\partial z} = \rho g + \rho u\frac{\partial w}{\partial x} + \rho w\frac{\partial w}{\partial z} \tag{2.22b}$$

It is convenient for what we wish to do next to write these equations in terms of the streamline coordinates, that is, coordinates that are parallel and normal to a streamline at any point rather than in terms of fixed Cartesian coordinates. In such coordinates,[4] the equations become

$$V\frac{\partial V}{\partial s} + \frac{1}{\rho}\frac{\partial p}{\partial s} + g\frac{\partial z}{\partial s} = 0 \tag{2.23a}$$

$$\frac{V^2}{R} + \frac{1}{\rho}\frac{\partial \rho}{\partial n} + g\frac{\partial z}{\partial n} = 0 \tag{2.23b}$$

where V is the magnitude of the velocity vector, R is the radius of streamline curvature, n is the distance normal to the streamline, and s is the distance along the streamline.

For most problems of interest the radius of streamline curvature is fairly large, and the other terms in the equation of motion normal to the streamline are much smaller than those in the equation of motion along the streamline. Therefore, we will discard the equation of motion normal to a streamline. As a consequence, the remaining equation has only one independent variable and, therefore, can be written as an ordinary differential equation

$$V\,dV + \frac{1}{\rho}dp + g\,dz = 0$$

Upon integration we can write this as

$$\frac{V^2}{2}\Big|_1^2 + \frac{p}{\rho}\Big|_1^2 + gz\Big|_1^2 = 0$$

or

$$\left(\frac{V^2}{2}\right)_2 + \left(\frac{p}{\rho}\right)_2 + (gz)_2 = \left(\frac{V^2}{2}\right)_1 + \left(\frac{p}{\rho}\right)_1 + (gz)_1 \tag{2.24}$$

This is known as Bernoulli's equation. It is valid everywhere along a streamline in incompressible flow, and if the flow is initially uniform, inviscid, and irrotational it is valid anywhere in the flowfield. It is, as we have seen, an integral of the momentum equation along a streamline. When multiplied by ρ it has the units of force per unit area. When applied to situations in the atmosphere, the third term

on each side of the equation can be discarded because it is then much smaller than the other two. This equation has been used to relate pressure measurements to flow velocity for the past 150 years.

2.7 Elementary Solutions of Laplace's Equation

Four elementary solutions of Laplace's equation have been found to be extremely useful in building models of flow over solid bodies of interest. We will discuss these four solutions and show that when they are combined, they can represent remarkably realistic flows. The illustrations of the streamlines of the combined flows were created with computer programs the source code of which is supplied on the accompanying disk. The reader may use the codes, if desired, to create illustrations of flows with different values of the constants. The reader is warned, however, that large departures from the example values may move the streamlines outside the boundaries of the figure or cause the function to enter regions of the trignometric or log functions that yield infinite values. Because source code is provided, such problems are correctable.

2.7.1 Uniform Stream

This is the first of the four elementary functions we will discuss. We used this function for the examples cited earlier [see Eq. (2.16)]. It is illustrated in Fig. 2.3a. To show that it is, indeed, a solution of the Laplace equation, we calculate

$$\frac{\partial \psi}{\partial r} = U\sin\theta \qquad \frac{\partial^2 \psi}{\partial r^2} = 0$$

$$\frac{\partial \psi}{\partial \theta} = Ur\cos\theta \qquad \frac{\partial^2 \psi}{\partial \theta^2} = -Ur\sin\theta$$

We substitute these values into Eq. (2.12) to obtain

$$-\frac{1}{r^2}Ur\sin\theta + \frac{1}{r}U\sin\theta = 0 \tag{2.25}$$

which demonstrates that this ψ is a solution to Laplace's equation.

2.7.2 Source

The source is the second elementary stream function shown in Fig. 2.3. The figure represents the case of fluid issuing from a point with equal volumetric flow in all directions. The stream function in this case may be written as

$$\psi = (Q/2\pi)\theta \tag{2.26}$$

where Q is called the strength of the source and has dimensions of volume per unit time per unit depth.

2.7.3 Sink

Figure 2.3c shows a sink. This can be thought of as a negative source in that the fluid coming equally from all directions disappears into a point. For the sink,

$$\psi = -(Q/2\pi)\theta \tag{2.27}$$

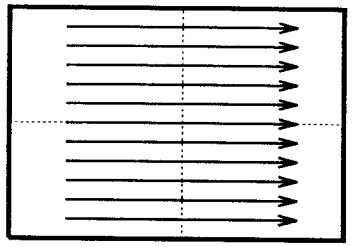

a) Streamlines for a uniform stream.

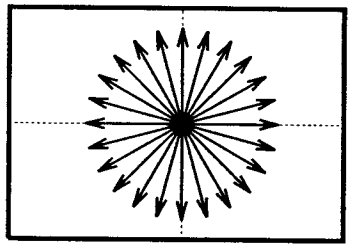

b) Streamlines for a source.

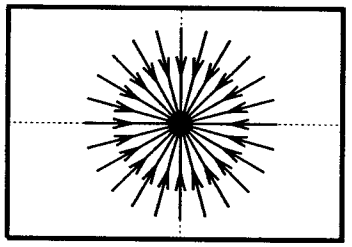

c) Streamlines for a sink.

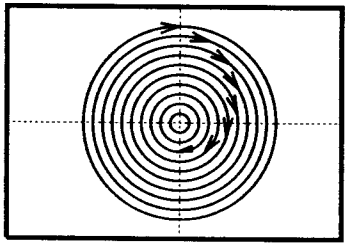

d) Streamlines for a vortex.

Fig. 2.3 Four elementary stream functions.

2.7.4 Vortex

The vortex (shown in Fig. 2.3d) is a flow wherein the fluid circulates about a point. The angular velocity decreases in a logrithmetic fashion as the distance from the point increases. As such the origin of the vortex is a singular point, that is, one where the fluid velocity is infinite. The origins of sources and sinks are also singular points. For a vortex

$$\psi = (K/2\pi)\ell_n r \tag{2.28}$$

K is the vortex strength and has the dimensions of volume per unit time per unit depth.

2.8 Superposition of Elementary Flow Functions

We indicated earlier that because Laplace's equation is linear, a sum of solutions (for example, an addition of certain stream functions) is also a solution. In this section we will generate and examine the streamlines associated with some stream functions produced by various combinations of elementary flow functions. Although for reasons of clarity we have chosen not to indicate the values of the stream function for the various streamlines on the figures, the values can be deduced, if desired, from the provided computer codes, which were used to generate the illustrations. Note, too, that because the relationship between adjacent points on a particular streamline is not always clear the streamlines have been created simply by calculating the coordinates for a very large number of points and plotting each result as a small circle. In some cases streamlines for only one quadrant of the picture were actually calculated; the portion of the picture in the second quadrant is a mirror image of the image in the first quadrant about the y axis. The portion in the fourth quadrant is a mirror image of that in the first quadrant about the x axis. The image in the third quadrant is generated from either that in the second or that in the fourth quadrant.

2.8.1 Source in a Uniform Stream

Shown in Fig. 2.7a is the streamline created by a source in a uniform stream. Note that a sort of boundary is visible (where the streamline is normal to the x axis). This represents the line where the rightward flow of the uniform stream is just balanced by the leftward flow from the source. Because the value of the stream function is zero at this point the flow velocity is also zero. Note that if such points are located in an otherwise flowing stream, they are called stagnation points. As we will see later such points have particular significance. The combined stream function for this case is

$$\psi = \frac{Q}{2\pi}\theta + Ur\sin\theta \tag{2.29}$$

2.8.2 Separated Source and Sink

Shown in Fig. 2.7b are the streamlines created by a source and sink of equal strength separated by a distance $2a$ on the x axis. The stream function for this flow

is

$$\psi = \frac{Q}{2\pi}\left[\tan^{-1}\left(\frac{y}{x-a}\right) - \tan^{-1}\left(\frac{y}{x+a}\right)\right] \tag{2.30}$$

2.8.3 Separated Source and Sink in a Uniform Stream: Rankine Oval

The geometric figure created by the streamline pattern shown in Fig. 2.7c for a separated source and sink in a uniform stream is called a Rankine oval. The boundary of the geometric figure is the $\psi = 0$ line. It is important to note that for negative values of the combined stream function, the streamlines would lie inside the figure. They are not shown here.

Note that the locations of the source and the sink relative to the origin of the closed figure $\psi = 0$ must be included in the combined representation

$$\psi = \frac{Q}{2\pi}\left[\tan^{-1}\left(\frac{y}{x-a}\right) - \tan^{-1}\left(\frac{y}{x+a}\right)\right] + Uy \tag{2.31}$$

2.8.4 Coincident Source and Sink: Doublet

The streamlines resulting from a coincident source and sink are shown in Fig. 2.4a. The stream function itself is

$$\psi = -\frac{\Lambda\sin\theta}{r} \tag{2.32}$$

where Λ is the strength of the doublet.

2.8.5 Doublet in a Uniform Stream

The streamlines created by placing a doublet in a uniform stream are shown in Fig. 2.5a. The stream function for this case is

$$\psi = Ur\left(1 - \frac{a^2}{r^2}\right)\sin\theta \tag{2.33}$$

where $a = \sqrt{\Lambda/U}$.

2.8.6 Sink and Vortex

The combined stream function for a sink and vortex, shown in Fig. 2.6a, can be represented mathematically by the expression

$$\psi = \frac{K}{2\pi}\ell_n r - \frac{Q}{2\pi}\theta \tag{2.34}$$

This stream function closely models the flow patterns one sees in water leaving a large surface through a centrally located drain or on the Earth's surface in the neighborhood of a tornado or hurricane everywhere except at the very center of the flow. Because mass must be conserved, it is natural to ask what happens in the real world to the air mass that "disappears" through the sink. There is a problem

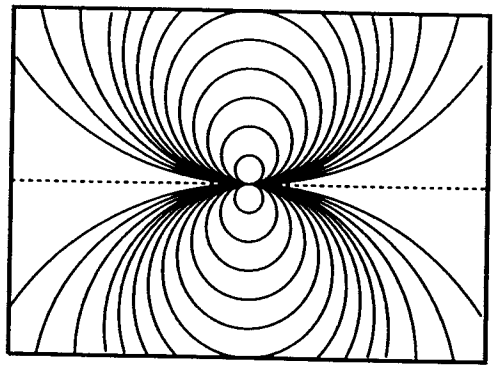

a) Streamlines for a doublet; superposition of a source and sink.

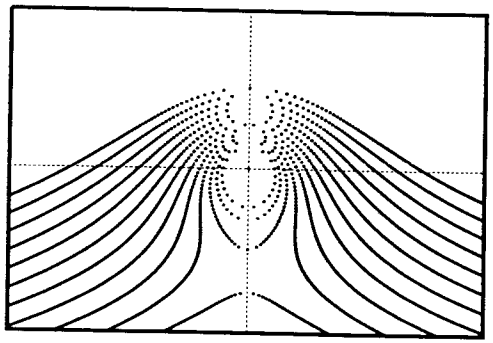

b) Computed streamlines for vortex and uniform stream; $U = 10$, vortex strength = 78.5, stream function increment = 2, $\theta = 1$ deg.

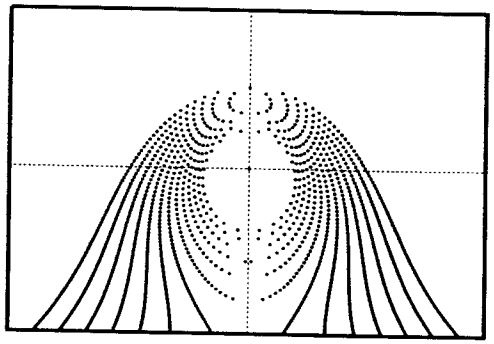

c) Computed streamlines for vortex and uniform stream; $U = 10$, vortex strength = 157, stream function increment = 2, $\theta = 1$ deg.

Fig. 2.4 Superposition of elementary functions.

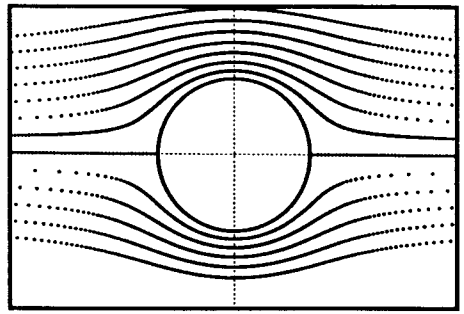

a) Computed streamlines for doublet and uniform stream; $U = 10$, stream function increment = 2, $\theta = 1$ deg.

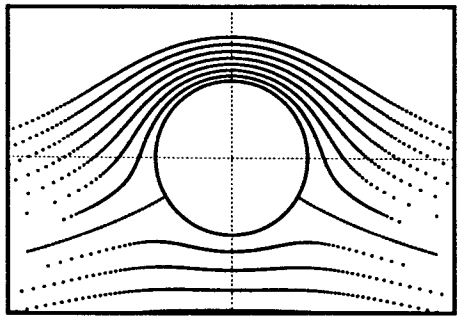

b) Computed streamlines for vortex, doublet and uniform stream; $U = 10$, vortex strength = 31.4, stream function increment = 2, $\theta = 1$ deg.

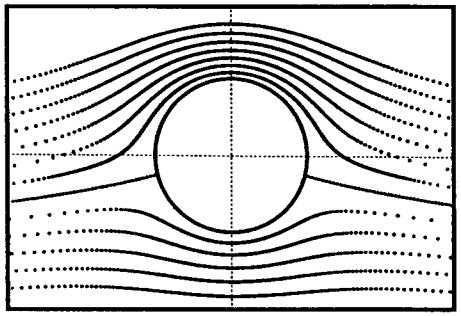

c) Computed streamlines for vortex, doublet, and uniform stream; $U = 10$, vortex strength = 15.7, stream function increment = 2, $\theta = 1$ deg.

Fig. 2.5 Superposition of elementary functions.

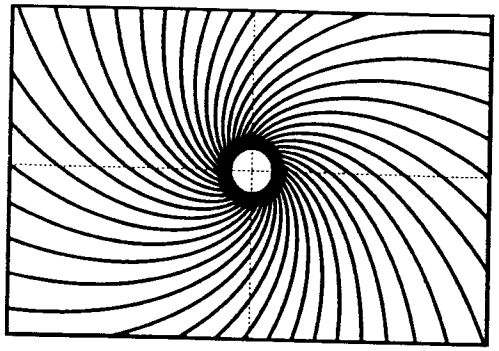

a) Computed streamlines for a sink and a vortex; Q = 109.9, sink strength = −78.5, stream function increment = 2.75, R = 0.01.

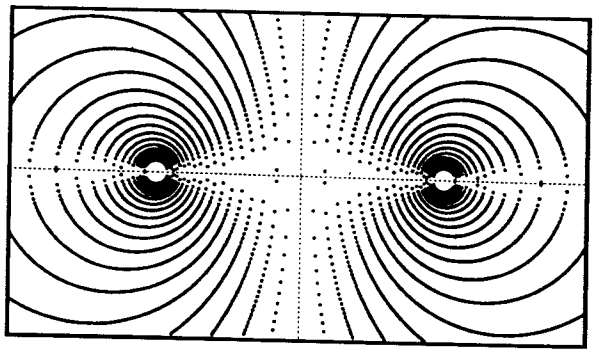

b) Computed streamlines for two counter-rotating vortices; vortex strength = 109.9, stream function increment = 3.0, DX = 0.01.

Fig. 2.6 Superposition of elementary flows.

with the theoretical vortex as a model for real flows. As one approaches the origin, the model breaks down, as is seen by the appearance of an eye in a tornado or hurricane. It is well known that in the eye of such storms the air becomes relatively calm in contrast to the very high horizontal velocities just outside the eye. In fact, the mass entering the eye from the rest of the storm moves vertically upward in sort of a tube formed by the eye and is disgourged horizontally from the top of the storm. The vertical air motion in the eye is not readily apparent to an observer on the surface, however. To simulate the eye the streamlines in the picture terminate at a finite distance from the origin.

2.8.7 *Vortex and Uniform Flow*

This stream function,

$$\psi = Ur\sin\theta + \frac{K}{2\pi}\ell_n r \tag{2.35}$$

is shown with two different vortex strengths in Figs. 2.4b and 2.4c.

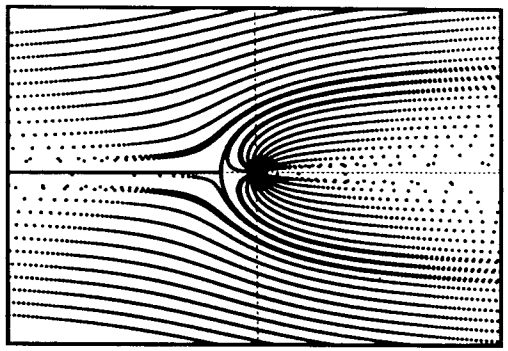

a) Computed streamlines for a source in a uniform stream; U = 10, source strength = 78.5, stream function increment = 4, θ = 0.01 rad.

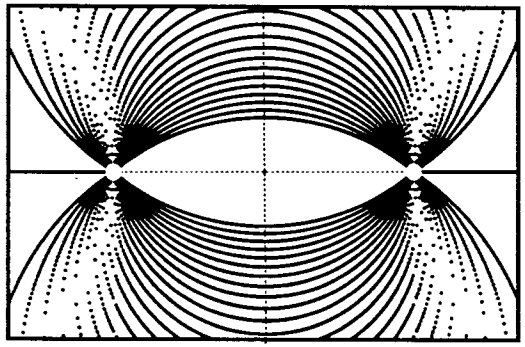

b) Computed streamlines for a source and a sink; source sink strength = 109.9, stream function increment = 1.5, DX = 0.01.

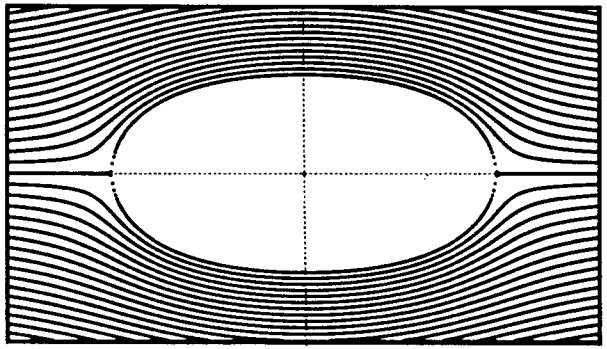

c) Computed streamlines for source, sink and uniform flow; U = 12, source sink strength = 109.9, stream function increment = 3.0, DX = 0.01.

Fig. 2.7 Superposition of elementary flows.

2.8.8 Counter-Rotating Vortices

When two vortices of equal strength but rotating in opposite directions are separated by a distance $2a$ they create the streamline patterns shown in Fig. 2.6. The stream function for the pair can be written as

$$\psi = \frac{K}{2\pi}\ell_n\left(\frac{\sqrt{(x+a)^2+y^2}}{\sqrt{(x-a)^2+y^2}}\right) \tag{2.36}$$

We have chosen to use Cartesian coordinates rather polar coordinates in this case because the coordinates of points on lines of constant ψ are more easily determined in these coordinates when the function origins are separated.

2.8.9 Circular Cylinder with Circulation in a Uniform Stream

This stream function is created by the combination of a doublet, a uniform stream moving from left to right, and a clockwise vortex coincident with the doublet. Historically, it is the most important of those discussed because it can be used to explain the Magnus effect (though it does not give the correct magnitude of the normal force) and because it forms the basis of the first successful attempt to explain the lift of an airfoil. Figure 2.5 shows that this combination of elementary stream functions models the flow over a circular cylinder with varying amounts of circulation provided by the coincident vortex. In Fig. 2.5a, the vortex strength is zero. Figures 2.5b and c are for two different vortex strengths.

The stream function for this case can be written

$$\psi = Ur\left(1-\frac{a^2}{r^2}\right)\sin\theta + \frac{K}{2\pi}\ell_n r \tag{2.37}$$

The circumferential velocity at any radius is

$$v_\theta = -\frac{\partial\psi}{\partial r} = -\left(U\sin\theta + U\frac{a^2}{r^2}\sin\theta + \frac{K}{2\pi r}\right) \tag{2.38}$$

We define the points on the circle $r = a$ where $v_\theta = 0$ as stagnation points. Because

$$v_r = \frac{1}{r}\frac{\partial\psi}{\partial\theta} = Ur\left(1-\frac{a^2}{r^2}\right)\cos\theta \tag{2.39}$$

is zero when $r = a$, we see that both velocity components are zero at stagnation points. When the vortex strength is zero the stagnation points occur at 0 and π. As the vortex strength increases, the stagnation points both move toward $\theta = 3\pi/2$. Setting $v_\theta = 0$ and letting $a = 1$, we see that

$$2U\sin\theta + \frac{K}{2\pi} = 0 \tag{2.40}$$

from which we deduce that the value of K is $4\pi U$ when both stagnation points are at $3\pi/2$. For larger values of K, the stagnation points move away from the cylinder along the line $\theta = 3\pi/2$. Physically, such large values of K are not realizable.

The maximum value of v_θ always occurs at $\theta = \pi/2$, that is, the top of the cylinder. Its value at this point is

$$v_\theta = 2U + \frac{K}{2\pi} \tag{2.41}$$

The point on the circle where the velocity is the same as freestream can be found by setting $v_\theta = U$ and solving for θ. This value of θ is

$$\sin^{-1}\left[\left(U - \frac{K}{2\pi}\right)\Big/2U\right] \tag{2.42}$$

An important application of this information is the angle relative to the bottom centerline at which the static pressure taps should be located on a pitot static tube so that the static pressure indication is independent of tube angle of attack. Such a device is shown in Fig. 2.8.

Let P_s be the total pressure indication and P be the static pressure indication. Then the airspeed is determined from

$$U = \sqrt{2(P_s - P)/\rho} \tag{2.43}$$

and the Mach number from

$$M = \sqrt{\frac{2}{\gamma-1}\left(\left[\frac{P_s}{P}\right]^{\frac{\gamma-1}{\gamma}} - 1\right)} \tag{2.44}$$

In Eq. (2.44) γ is the ratio of specific heats, 1.4 for air at temperatures less than 400°F. The pressure altitude is a function of static pressure alone. If the static pressure is sensitive to changes in angle of attack, then the indications of all these instruments will be in error. By locating the static pressure taps at ±38 deg (as determined experimentally rather than by the theoretical value of ±30 deg) from the bottom centerline, the point on the tube diameter at which the pressure due to

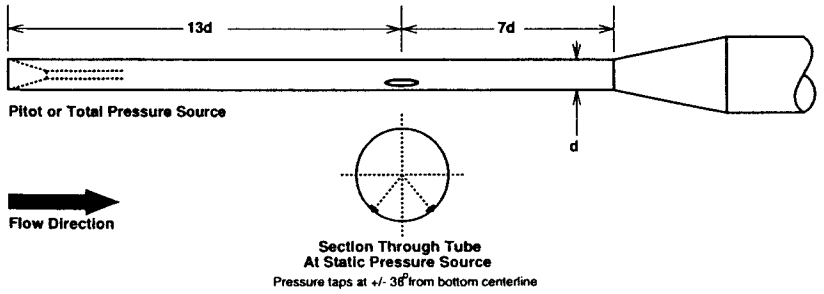

Fig. 2.8 Pitot-static tube.

the crossflow component of the velocity is the same as the freestream value for positive angles of attack to 90 deg and for sideslip angles in the range ±5 deg, the static pressure indication can be made to be independent of changes in angle of attack. The total or stagnation pressure source is countersunk with a 10-deg half-angle cone to the point that the tube lip is sharp. This configuration yields constant total pressure values over the angle-of-attack range of ±27 deg. The static taps each cover about 10 deg circumferentially and can be elongated to about 3.5 times their circumferential dimension in order to improve the airflow rate into and out of the instruments, which are connected to the source. By so doing the lag of the indications of pneumatic instruments to rapid changes in altitude is reduced. To keep the pressure indications from being distorted by ice buildup on the tube, pitot-static tubes are usually heated electrically by helical calrod heaters brazed to the inside wall of the tube. In some designs the interior portion of the tube is a static pressure plenum, with the line from the total pressure source running through it.

2.9 Circulation

We noted earlier that ψ and ϕ are state functions when the flow is irrotational. This means that the change in value of one of these functions around any closed path is zero or

$$\oint_C d\psi = 0 \tag{2.45}$$

There is one exception to this rule, however, and that is when the path encloses a singular point. We note that

$$d\psi = \frac{\partial \psi}{\partial r} dr + \frac{\partial \psi}{\partial \theta} d\theta \tag{2.46}$$

In the case of a vortex

$$d\psi = \frac{\partial \psi}{\partial r} dr = \frac{K}{2\pi r} dr \tag{2.47}$$

We choose as our path a circle of radius r. In that case we may write $dr = r\,d\theta$ and choose as our limits of integration 0 and 2π. Then,

$$\int_0^{2\pi} \frac{K}{2\pi r} r\, d\theta = K \tag{2.48}$$

The circumferential velocity for the source and for the sink is zero; thus, even though the closed path may include the singular point at the origin

$$\oint_C d\psi = 0 \tag{2.49}$$

2.9.1 Magnus Effect

The Magnus effect is a well-known phenomenon associated with rotating cylinders or spheres. When a cylinder at right angles to an oncoming stream rotates at high speed it drags the fluid that is on and next to the surface with it. (This is a result of the viscosity of the fluid.) Because this layer of entrained air (or water) moves faster at $\theta = \pi/2$ (and slower at $\theta = 3\pi/2$) than it normally would, the pressure at $\theta = \pi/2$ is lower than it normally would be (and the pressure at $\theta = 3\pi/2$ is higher than it normally would be). This results in a force on the cylinder normal to the direction of fluid motion. Golf balls are dimpled to enhance this effect. The lacings on baseballs serve the same purpose. One might imagine that the rotational velocity of the cylinder could be set to $\Gamma/2\pi a \cdot \ell = K/2\pi a$ as indicated in Eq. (2.38) to obtain the lift predicted by Eq. (2.50). However, the measured lift forces are usually much smaller.

A vortex imposed on a doublet creates the same flow pattern as is observed experimentally about a rotating cylinder. An integration of the pressure components normal to the oncoming stream at $r = a$ shows that the resultant lift force is

$$L = \rho U \Gamma \tag{2.50}$$

where Γ is the circulation due to the vortex. Γ is K times the length of the cylinder, ℓ. This well-known result was obtained independently by Kutta in 1902 and Joukowski in 1906. One of the most profound insights in all of aerodynamic theory follows from Eq. (2.50): lift is independent of profile shape. This also turns out to be the case in practice as well, despite what the popular media would have one believe regarding the accretion of ice on a wing. Becuase lift is independent of profile shape, the Kutta–Joukowski theory says we can take the results for the flow about a right circular cylinder with circulation and apply them to a specific airfoil. The details of how this may be done are related in Chapter 3.

The Kutta–Joukowski results model the lifting behavior of airfoils very well for angles of attack, up to the point where there is significant flow separation on the upper surface. Flow separation is a consequence of fluid viscosity, the effects of which are discussed in Chapter 4. Separation is present when airfoils move in real fluids. It becomes significant for most airfoils when the lift coefficient, defined by

$$C_L = \frac{L}{\frac{1}{2}\rho U^2 S}$$

is above a value of about 0.8. In this expression, s is the planform area of the lifting surface.

The Kutta–Joukowski model, being inviscid, predicts that the circulation and, hence the lift, will increase with angle of attack all the way to 90 degrees. The effects of ice on the wing surface will generally be to 1) change the pitching moment, 2) reduce the maximum lift because it promotes flow separation at lower angles of attack, and 3) increase the drag. However, for low angles of attack such as those used for cruise flight or even takeoff, normal lift can still be generated although perhaps at a different trim condition and almost certainly with an additional power requirement. The additional weight of ice will increase the

takeoff speed slightly. Ice can be a serious problem if it prevents control surfaces from moving or clogs engine air intakes. If ice accretion is not symmetrical on the two wings, rolling moments and/or yawing moments can be generated.

2.10 Relationship of Stream Function and Potential Function

We now ask the question: If I know the stream function for a flow, how can I develop the potential function from it? Let us take as an example the stream function

$$\psi = 2x(1 + y)$$

Then the velocity components are

$$\frac{\partial \psi}{\partial x} = 2 + 2y = -v \tag{2.51a}$$

$$\frac{\partial \psi}{\partial y} = 2x = u \tag{2.51b}$$

But

$$u = \frac{\partial \phi}{\partial x} = 2x \tag{2.52a}$$

$$v = \frac{\partial \phi}{\partial y} = -2 - 2y \tag{2.52b}$$

Integration of these equations yields

$$\phi = x^2 + f(y) \tag{2.53a}$$

$$\phi = -2y - y^2 + f(x) \tag{2.53b}$$

Evidently, then,

$$\phi = x^2 - 2y - y^2 \tag{2.54}$$

One of the interesting facets of the relationship between ϕ and ψ is that they are orthogonal; that is, lines of constant ϕ and lines of constant ψ are everywhere at right angles. How may we demonstrate this? To simplify matters, let ϕ and ψ be -8 and 0, although almost any constant value will suffice. Then solve both expressions for y

$$y_1 = -1$$

$$y_2 = -1 \pm \tfrac{1}{2}\sqrt{4x^2 - 4}$$

The first expression is a straight line parallel to the x axis. The slope of the second expression is

$$\frac{dy}{dx} = \frac{\pm\frac{1}{2}(8x)}{\sqrt{4x^2 - 4}}$$

which is infinite at $x = 1$ and $y = -1$, proving that at $(1, -1)$, $\phi = -8$ and $\psi = 0$ are orthogonal.

2.11 Stream Function Generation Software

To obtain accurate plots of the stream functions, the coordinates of points along particular streamlines were evaluated using Fortran programs, which also generated the PostScript plotting files. Source code for these programs is provided on the accompanying disk. It may be noted that the PostScript rasterizer locates points on the paper to within 0.003 in. As noted earlier, rather than attempt to incorporate sufficient logic to connect points on the same streamline, the programs generally compute the coordinates for several hundred to a thousand points per quadrant spread over a number of streamlines and plot the results as filled circles. By spacing the points close together the effect of a continuous streamline is created in most cases. Cases where this is not true are those in which one coordinates varies widely with small changes in the other. No attempt was made to supply more points in such regions.

The programs are on the order of 125 lines long, each including comments. The size of the executable files depends largely on the compiler used, but with the Microsoft PowerStation compiler they each require about 103,000 bytes. Some of the PostScript output files can be very large, about a megabyte in length. The files are

STREAM0.FOR—doublet and coincident vortex in a uniform stream,
STREAM1.FOR—vortex in a uniform stream,
STREAM2.FOR—separated source and sink in a uniform stream,
STREAM3.FOR—source in a uniform stream,
STREAM4.FOR—separated source and sink,
STREAM5.FOR—sink in a uniform stream, and
STREAM6.FOR—separated, counter-rotating vortices.

Streamlines for the doublet are circular and, thus, can be drawn without computation. The streamlines for the doublet in a uniform stream can be drawn using STREAM0.FOR by setting the vortex strength to zero.

Where one coordinate of the stream functions can be written simply in terms of the the other, that form is used in the computation. For example, the source in a uniform stream was rewritten as

$$r = \frac{\left(\psi - \dfrac{Q}{2\pi}\theta\right)}{U \sin\theta} \tag{2.55}$$

and θ was then varied in small increments to obtain the ouput points. In some cases a Newton–Raphson scheme is used to find one coordinate in terms of the other and, finally, for those cases involving inverse trignometric functions, a function in the form

$$Z = \tan^{-1}\left(\frac{y}{x - a}\right) - \tan^{-1}\left(\frac{y}{x + a}\right) + \frac{2\pi}{Q}(Uy - \psi) \tag{2.56}$$

is evaluated as both variables are increased over their expected ranges in very small increments. The first occurence of a change in the sign of Z is then an

indication that the current values satisfy the equation approximately. Such a crude procedure is too time consuming if not carried out on a computer. That such a simple-minded procedure is effective and readily programmed is further indication that the computer can have a significant impact on the way we do tasks, as well as performing established procedures more rapidly.

The programs can be used to produce plot files for other values of the strengths of the elementary functions and/or the uniform stream velocity. The user should recognize, however, that large changes from the values used in the programs may produce plots that lie outside the outlined region. If many plots are desired, it is probably wise to replace the assignment statements used to specify parameter values with file reads, either from the console or from a previously written data file.

2.12 Concluding Remarks

In this chapter we sought to present those elements of fluid dynamics theory on which current mathematical models of airfoil lift are based. We showed how the law of conservation of mass is developed as a partial differential equation and how two-dimensional inviscid, incompressible flows obeying this law can be represented by a stream function, the partial derivatives of which with respect to the spatial coordinates represent the velocity components of the flow. When such flows are irrotational we showed that there exists another function, the velocity potential, the partial derivatives of which with respect to the spatial coordinates also represent the velocity components.

We then considered the development of a version of Newton's second law of motion applicable to fluids and showed how an integral of the law along one coordinate direction yielded a very useful relationship, Eq. (2.24). In fact, the three terms in Eq. (2.24) represent three components of the energy in the flow. As written, Eq. (2.24) applies only to conservative systems, that is, systems in which no energy is added or removed from the flow.

We continued by showing that by using the velocity components in terms of the stream function in the condition for irrotationality one obtains Laplace's partial differential equation. Since the Laplace equation is a linear partial differential equation, a sum of solutions, stream functions or potential functions that satisfy it can be added to obtain a new solution. We then displayed four elementary stream functions, which can be used to represent simple flows: a uniform flow, a source, a sink, and a vortex. We showed that by combining various aspects of these elementary stream functions we could adequately represent more complex flows. We gave a series of examples and an application of the result. We considered the concept of circulation as the generating mechanism in airfoil lift and its relationship to the strength of one or more vortices, which may be components of the overall stream function. Finally, we showed that stream functions and potential function are orthogonal. Knowing one enables the other to be found, at least for simple cases.

The chapter concludes with a description of the accompanying computer programs, which were used to generate the flowfield diagrams shown in the text. This section indicates how the provided source codes can be modified to generate diagrams for flows not discussed in the text.

With the exception of a theoretical treatment of viscous effects, which has been delayed until Chapter 4, this chapter presents at least briefly all of the analytical concepts on which the mathematical models of lifting wings and bodies embodied in the attached computer codes are built and from which certain aerodynamic characteristics of these wings and bodies can be deduced. It is important that the code user gain at least a reasonable understanding of these methods as well as the flow and boundary conditions under which they can be safely applied. How this is done by users is left to their own devices, but answering the end-of-chapter problems, devising alternate combinations of elementary flow functions to model specific flow situations, and checking the degree to which these models produce results that agree with experimental data are recommended procedures that the author has found to be effective in his own case.

Problems

2.1. Following the procedure used to obtain Eq. (2.1), derive a set of equations expressing Newton's second law of motion. Assume that the only force present is pressure. Show all steps.

2.2. Integrate the equation

$$\rho u \frac{\partial u}{\partial x} = -\frac{\partial P}{\partial x}$$

in the x direction. Use the fact that $P = P_s$ when $u = 0$ to evaluate the constant of integration. The result is called Bernoulli's equation.

2.3. Make a copy of Fig. 2.3 and sketch lines of constant potential on the figures.

2.4. Explain, using Eq. (2.37), why the choice of $r = a$ is a convenient way to use the stream function to represent a solid right-circular cylinder.

2.5. Define the pressure coefficient as follows:

$$C_P = \frac{P_L - P_\infty}{\frac{1}{2}\rho U_\infty^2}$$

where the subscript L refers to local conditions. Using the Bernoulli equation we could also write

$$C_P = \frac{P_s - \frac{1}{2}\rho U_L^2 - P_s + \frac{1}{2}\rho U_\infty^2}{\frac{1}{2}\rho U_\infty^2} = 1 - \left(\frac{U_L}{U_\infty}\right)^2$$

Determine the maximum and minimum values of the pressure coefficient on a circular cylinder in a uniform stream with no circulation.

2.6. When $K = 4\pi U$, what are the maximum and minimum values of the pressure coefficient on a circular cylinder in a uniform stream?

2.7. For the stream function

$$\psi = 4r^2\theta$$

a) sketch the streamlines, and b) determine whether the function satisfies the continuity equation.

2.8. Sketch the streamlines for the following stream functions and determine whether the function satisfies the continuity equation:
a) $\psi = 2x(1 + y)$,
b) $\psi = x^3 - 3y$,
c) $\psi = 3x^2 + 2y^2$,
d) $\psi = 2xy$, and
e) $\psi = x^2 y$.

2.9. Calculate and plot the pressure coefficients on a circular cylinder in a uniform stream with $K = 2\pi U$. Plot points every 6 deg. around the cylinder.

2.10. Integrate the pressures determined in problem 2.9 to find the force normal to the stream. Compare with $L = \rho U \Gamma$.

2.11. Integrate the pressures found in problem 2.9 to find the force in the streamwise direction. Why is this result called D'Alembert's paradox? If you do the problem correctly you will get the same result that D'Alembert did. He knew his result was incorrect but could not explain why.

2.12. Determine and plot the $\psi = 0$ streamline for the following cases:
a) source at $x = -a$, sink at $x = a$, $U = 12$, $Q_{\text{source}} = 109.9$, $Q_{\text{sink}} = 55.0$;
b) source at $x = -a$, sink at $x = a$, sink at $x = 2a$, $U = 12$, $Q_{\text{source}} = 109.9$, $Q_{\text{sink}} = 54.95$; and
c) source at $x = -a$, sink at $x = a$, $U = 18$, $Q_{\text{source}} = 109.9$, $Q_{\text{sink}} = 109.9$.
Note that problems 2.12a and 2.12b are symmetric about the x axis but not about the y axis.

2.13. The stream function is not defined for general three-dimensional flows. However, an axisymmetric flow is a special type of three-dimensional flow requiring only two spatial coordinates, r and z, with z being the axial dimension and r being the radial dimension. The continuity equation for this case reads

$$\frac{\partial v_r}{\partial r} + \frac{\partial v_z}{\partial z} + \frac{v_r}{r} = 0$$

Show that the velocity components

$$\frac{1}{r}\frac{\partial \psi}{\partial z} = v_r \qquad -\frac{1}{r}\frac{\partial \psi}{\partial r} = v_z$$

satisfy the continuity equation.

2.14. When the flow is steady and compressible, the two-dimensional continuity equation in rectangular coordinates reads

$$u\frac{\partial \rho}{\partial x} + v\frac{\partial \rho}{\partial y} + \rho\left(\frac{\partial u}{\partial x} + \frac{\partial v}{\partial y}\right) = 0$$

Show that velocity components in the form

$$u = \frac{1}{\rho}\frac{\partial \psi}{\partial y} \qquad v = -\frac{1}{\rho}\frac{\partial \psi}{\partial x}$$

satisfy continuity.

2.15. The velocity components for steady, compressible axisymmetrical flow read

$$v_r = \frac{1}{\rho r}\frac{\partial \psi}{\partial z} \qquad v_z = -\frac{1}{\rho r}\frac{\partial \psi}{\partial r}$$

Construct the continuity equation for this case.

2.16. Given the potential function

$$\phi = \frac{1}{2}\ell_n\left[\frac{(x+a)^2 + y^2}{(x-a)^2 + y^2}\right]$$

find the stream function.

2.17. A stream function is given by

$$\psi = U(a + b)\sinh(\xi - \xi_0)\sin(\eta - \alpha)$$

In this expression

$$x = c\cosh\xi\cos\eta \qquad y = c\sinh\xi\sin\eta$$

$$a = c\cosh\xi_0 \qquad b = c\sinh\xi_0$$

$$a^2 - b^2 = c^2 \qquad \xi_0 = \ell_n\left(\frac{a+b}{a-b}\right)$$

$$\frac{x^2}{c^2\cosh^2\xi} + \frac{y^2}{c^2\sinh^2\xi} = 1$$

$$\frac{x^2}{c^2\cos^2\eta} - \frac{y^2}{c^2\sin^2\eta} = 1$$

Let $b = 0$. Therefore, $c = a$. Also choose $\alpha = \pi/2$ and $c = 4$. Let $U = 12$ and $0 \le \eta \le 2\pi$. In this case, $\xi > 0$. For $\psi = 1, 2, 3, 4, \ldots, 20$ select closely spaced values of ξ and solve for the corresponding values of η. Then determine the matching set of x and y for each value of ψ and plot. Plot also the mirror image about the x axis. Describe the resulting image.

2.18. Now let $b = \sqrt{15}$, $c = 1$, and $U = 12$. Repeat problem 2.17 using these values.

2.19. With $b = 0$, $c = 4$, $U = 12$, and $\alpha = 0$, repeat problem 2.17 using these values.

2.20. With $a = 5$, $b = 3$, $U = 12$, and $\alpha = 0$, repeat problem 2.17. Note: Problems 2.17–2.29 are the problems solved most easily by writing a program similar to one of the STREAMX.FOR programs. If a Fortran compiler is not available, the problem can be set up to be done using a spreadsheet program. If your spreadsheet does not use hyperbolic functions, these can be generated using the exponential function.

2.21. Compare the units of the circulation Γ with those of K and with those of ω as defined by Eq. (2.8).

2.22. The circulation per unit span is defined as the integral of the velocity around any closed path. What will the units of this circulation be?

2.23. What are the units of the stream function?

2.24. The Laplace equation is homogeneous. If one saw, instead, an equation written as

$$\Omega = \frac{\partial^2 \psi}{\partial x^2} + \frac{\partial^2 \psi}{\partial y^2}$$

what would be the significance of Ω?

2.25. The pitot-static tube shown in Fig. 2.8 is a design developed for the U.S. Air Force in the 1960s for use on transonic aircraft. The great length is made necessary by the streamwise extent of flow disturbances when the flight Mach number is near 1.0. For Mach numbers near zero (this includes operation submerged beneath the surface of the ocean) the older designs such as that shown in Fig. P2.1 are satisfactory provided their alignment does not depart by more than ± 5 deg from the direction of the flow. Considering the static pressure ports in Fig. P2.1, how might you estimate the static pressure error at the port location? Does the picture in Fig. 2.5a give you a suggestion? You may wish to consider a means of estimating the error from the relations

$$P_s = P_\infty + \tfrac{1}{2}\rho U_\infty^2$$

$$P_s = P_L + \tfrac{1}{2}\rho \left(v_r^2 + v_\theta^2\right)$$

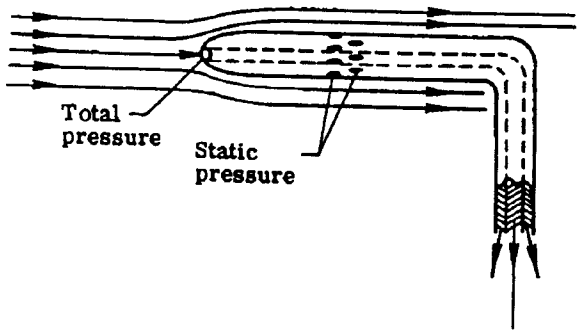

Fig. P2.1 Pitot static tube.

Therefore,

$$\frac{P_L - P_\infty}{\frac{1}{2}\rho U_\infty^2} = 1 - \frac{v_r^2 + v_\theta^2}{U_\infty^2}$$

2.26. Although the nose of the pitot-static tube in Fig. P2.1 is a three-dimensional body what sort of estimate might you make based on the use of a two-dimensional stream function that would indicate the range of angle-of-attack values to which the tube could be inclined and still indicate a reasonably accurate value of total pressure?

2.27. Identify the three flow patterns shown in Figs. P2.2 (examples might be: circulatory flow with no uniform stream, uniform stream) and indicate an appropriate caption to place beside the callout in Fig. P2.2, part c.

2.28. Does the potential function

$$\phi = xy^3 - yx^3$$

a) satisfy continuity and b) satisfy the condition for irrotationality?

2.29. What assumption is implicit regarding ρ in Eq. (2.24)?

2.30. Suggest one means by which the circulation about an airfoil section might be increased beyond that naturally generated. Hint: a method for doing this could also increase the Magnus effect on cylinders and spheres.

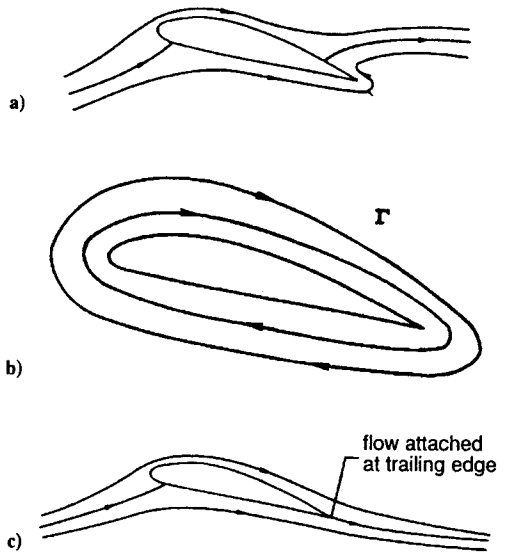

Fig. P2.2 Flow patterns.

2.31. If a cylinder in a uniform stream of velocity V is spinning at an angular velocity of

$$\omega = 3V/D$$

where D is the cylinder diameter, what lift coefficient would be expected assuming the circulatory flow velocity is that given by the formula?

2.32. If the actual lift coefficient for the preceding problem were found to be 0.4, what is the value of the actual circulation?

2.33. Derive an expression for C_L per unit wing chord in terms of Γ, U, and the wing span b.

2.34. A particular airfoil has a maximum lift coefficient of 1.52 and a corresponding drag coefficient of 0.055. With double slotted flaps fully deployed the lift coefficient is 3.48 and the drag coefficient is 0.28. By what factor does the circulation change in going from the clean configuration to full flaps deployed?

2.35. Discuss the mechanism by which the flap deployment is able to increase circulation.

2.36. Consider Eq. (2.24). Assume there is a horizontal pipe through which water is flowing. Pressures and velocities at two stations along the pipe are measured. If

$$\frac{V_1^2}{2} + \frac{p_1}{\rho} \neq \frac{V_2^2}{2} + \frac{p_2}{\rho}$$

to what do you attribute the inequality?

2.37. If the inequality of problem 2.36 exists, can the flow be described by a potential function?

2.38. If the fluid in the pipe were air instead of water, would your answers to problems 2.36 and 2.37 need to change and why?

2.39. Can Eq. (2.24) be used to determine the pressure at various depths in the ocean? Explain.

2.40. Given that

$$\psi = Ar^n \sin(n\theta)$$

$$\phi = Ar^n \cos(n\theta)$$

plot the streamlines and velocity potential when a) $n = 3$, b) $n = 2$, c) $n = 3/2$, and d) $n = 2/3$.

2.41. Consider the flow functions given in problem 2.40. a) In order for the sign of ψ to remain positive what is the permissible range of θ in 2.40a, 2.40b, 2.40c, and 2.40d? b) Can you think of any physical situation which these functions might represent?

2.42. A building is constructed from a hemicylindrical shell. A strong wind with velocity U blows at 90 degrees to the shell axis but parallel to the ground. a) How might you model this situation with a combination of flow functions which we have used in this Chapter? b) Under what conditions does the force of the wind seek to move the building horizontally? c) Assuming the pressure inside the shell is atmospheric, is there a compression or a tension in the shell? d) Outline the procedure by which you would calculate the force in the vertical direction.

2.43. Given the function

$$\psi = \sin\frac{x}{X}\sinh\frac{y}{Y}$$

where X and Y are constants. Then, restricting $0 \leq x \leq \pi X$ and $y \geq 0$ determine whether ϕ can exist. If it does, locate any stagnation points and generate some streamlines.

2.44. Given a flow which can be represented by the stream function

$$\psi = Cxy$$

where C is a constant, determine if the flow is irrotational. Generate some streamlines. What practical situation does it represent? Choose a streamline and calculate the pressures at several points along the streamline.

2.45. A non-rotating circular cylinder is inserted normal to a uniform stream. Assume that the cylinder generates a wake in which the pressure is atmospheric and which begins on the lea side of cylinder at a point on the cylinder where the pressure first equals atmospheric pressure. (Invicid theory says that there should be a region on the lea side where the pressure is above atmospheric. In our example this is the region in the wake.) Compute the drag coefficient of the cylinder per unit span.

2.46. At a point in the flow over the cylinder in problem 2.45 where $\theta = \pi/2$ and $r = 3a$, how does the pressure coefficient compare with the pressure coefficient at the point $\theta = \pi/w$ and $r = a$?

2.47. For the flow situation in problem 2.45, how does the velocity of the fluid immediately next to the surface differ in the viscous and inviscid cases? It is useful in the viscous case to think of the fluid as being composed of point mass molecules which have random velocities as well as mass mean velocities. From what you know of such solid-solid interactions, what is the likely effect on particle momentum of impact with the surface?

3
Airfoils and the Joukowski Transform

3.1 Introduction

HAVING arrived at an understanding of the means by which certain physical flows can be modeled mathematically, we seek to determine how this knowledge was used to construct a satisfactory explanation of the phenomenon of lift. In order to provide the proper framework for our discussion, we need to distinguish between a wing and an airfoil. A wing is a three-dimensional structure while an airfoil is a two-dimensional structure. An airfoil can be thought of as a slice of the wing whose sides are parallel to the direction of the freestream flow. To really appreciate the remarkable achievement of a satisfactory explanation of wing lift derived from mathematical descriptions of elementary fluid flows, it is helpful to review the understanding of the lifting mechanism extant in the general scientific community as it existed around the dawn of the 20th century. We will then go on to examine in detail the mathematical device by which Kutta and Joukowski were able to transform the mathematical description of uniform flow over a rotating cylinder to that for uniform flow over an airfoil. To ease the task of performing such transformations we provide a computer program that does all of the necessary calculations and creates PostScript files of the resulting airfoil shape and the associated pressure distributions at various angles of attack. Instructions for the use of the program are provided in this chapter. FORTRAN source code for the program is given on the accompanying 3.5-in. disks so that users may compile it on platforms other than the IBM personal computer and can modify it if they so desire to suit their own interests.

To ensure that we have a common understanding of airfoil nomenclature, we will define the various terms that may arise during our discussion with the aid of Fig. 3.1. In this figure the airfoil is moving through the fluid medium from left to right. A straight line drawn from the rightmost part of the airfoil to the leftmost point is called the chord. A curved line connecting the two ends of the chord in a manner such that there is an equal distance from the line to the upper surface of the airfoil as from the line to the lower surface at every point along the line is called the mean camber line. The angle the oncoming air flow makes with the airfoil chord is called the angle of attack. The angle between the two airfoil surfaces at the downstream end of the airfoil is termed the trailing-edge angle. The upstream end of the airfoil, termed the leading edge, must always be rounded to some degree. The amount of roundness is specified as the leading-edge radius. Airfoil thickness is usually specified as a percentage of chord. The camber is the maximum distance the mean camber line is displaced from the chord. It may also be stated as a percentage of chord. The chordwise location of the maximum thickness, the amount of camber, the thickness, the leading-edge radius, and the trailing-edge angle taken together as a group are usually sufficient to classify the airfoil shape or profile. The pressure distribution, usually stated as a value of specific points on the upper and lower surface of the airfoil, can be integrated to determine the lift and pitching moment developed by the airfoil at a particular angle of attack.

Airfoils in inviscid flow always have two stagnation points, that is, points on the surface where the flow velocity is zero. The rear stagnation point is always located at the trailing edge. The location of the forward stagnation point depends on the angle of attack. In real fluids, no physical rear stagnation point exists per se because part of the fluid's energy is converted by friction into heat. In the flow region near the airfoil surface, the stagnation pressure actually falls as the fluid moves aft so that at the trailing edge it cannot be as high as it was at the leading edge.

3.2 Historical Perspective

Building on ideas set down by Sir Isaac Newton a hundred years earlier, scientists in the last years of the 18th century concluded that the lift of an airfoil could be calculated in the following manner. Assume the airfoil is flying at an angle of attack α relative to the oncoming wind. The stream of fluid striking this airfoil contains a quantity of mass per unit span given by

$$\rho U c \sin\alpha$$

where c is the length of the airfoil chord (the distance from the nose to the tail). Upon impact with the airfoil, the fluid is turned so that its velocity normal to the airfoil changes from 0 to $U\sin\alpha$ and its velocity parallel to the airfoil changes from U to $U\cos\alpha$. Multiplying this change in velocity normal to the airfoil by the mass involved gives the normal force applied to the airfoil

$$F = \rho c \ell U^2 \sin^2\alpha \tag{3.1}$$

The component of this force normal to the original stream direction is

$$L = \rho c \ell U^2 \sin^2\alpha\cos\alpha \tag{3.2}$$

and the component parallel to the original stream direction is

$$D = \rho c \ell U^2 \sin^3\alpha \tag{3.3}$$

In these equations ℓ is the span, that is, the extent of the wing normal to the flow in the plane of the wing.

According to Eqs. (3.2) and (3.3) the lift-to-drag ratio is infinite at $\alpha = 0$ and decreases as α is increased. To build a flying machine one would like to operate at small values of α. However, the lift at small α is also quite small according to this calculation. Thus, scientists reasoned, one would have to build a very large craft that was nearly weightless in and of itself to lift the weight of a man. With known construction techniques of the time, this was not possible. For a more modest size vehicle, the drag and, thus, the power required would become enormous because the vehicle now had to operate at higher α. Large amounts of power were also impossible to provide with the then-known means of propulsion. It is not surprising that they concluded that man could never fly.

People begin to build crude flying machines in the early part of the 19th century, and it soon became obvious that the lift values predicted on the basis of the foregoing analysis were incorrect when applied to inclined wings in the atmosphere or in the ocean. Some of those people experimenting with flying machines were

scientists, but most were not. The scientists had no theory that could explain the experimental results, and the others said surely if the birds can do it, we can figure out a way and they continued to experiment.

In the latter quarter of the 19th century, John William Strutt, Baron Rayleigh, attempted to model the problem of the motion of the cut tennis ball. He was, of course, familiar with the Magnus effect, a phenomenon artillery men had encountered since the early years of the century. Rayleigh's solution did a better job than the Newtonian theory in explaining the ball's behavior and, in addition, showed the basis of fluid dynamic drag. But it was still a factor of 30 off under some conditions.

The correct explanation, or so we believe today, was developed more or less independently during the period from 1894 to 1909 by Lanchester in England, Kutta in Germany, and Joukowski first in Russia and then in France. Kutta was a mathematician, Joukowski a physicist, and Lanchester an engineer. Lanchaster's work was published first but was more heuristic in nature and as a result was not well understood. In fact, it was Prandtl, who is often given credit for putting forward the successful model explaining induced drag, who stated in a lecture to the Royal Aeronautical Society in 1927 that because he and his group were interested in the same phenomena they were able to understand Lancaster's arguments when people in Britain were not. A fascinating account of this early work is contained in a memoir by Theodore von Kármán,[5] a Hungarian, who at the time was a young contemporary of the first three and a student of Prandtl, having received his doctorate degree at Göttingen in 1908. As Director of the Guggenheim School of Aeronautics at the California Institute of Technology during the 1930s and 1940s, von Kármán played a key role in the development of American aeronautical technology. He was also one of the founders of the Aerojet Corporation, which provided the U.S. military with small rockets for assisting aircraft takeoff and other tasks during World War II. Later the Aerojet Corporation would be one of the pioneers in the development of large solid fuel rockets. His stock in the company made him wealthy. The U.S. Air Force recognized his many contributions to the nation by naming the gas dynamics facility at the Arnold Engineering Center at Tullahoma, Tennessee, in his honor.

The basic idea that everyone came to recognize as important in explaining what had been found experimentally was that a circulation formed around the airfoil similar to that used to model a vortex. Prandtl, some years later, was even able to photograph the manner in which the circulation was created by sprinkling aluminum powder on water into which an airfoil was inserted. When the airfoil was put into motion he took a series of high-speed pictures from the airfoil using reflected light from the aluminum to show the creation of a vortex at the trailing edge and its shedding into the wake. For the vortex to be shed into the wake, an equal strength vortex in the opposite direction must be created over the airfoil because it had been proved that a fluid that is initially irrotational will remain that way. This followed from an 1858 paper, von Helmholtz showed that if there is no initial vorticity in a fluid, vorticity can only be created by friction or by the presence of sharp edges on a body. He went on to demonstrate that when two nearly parallel streams of different velocity meet at an edge they create a continuous sequence of vortices or a vortex sheet. Theoretically, the vortex sheds in a horseshoe from the tips of a three-dimensional airfoil—a wing with the initial starting vortex connecting the two long trailing vortices. The vorticity is completed by what in lifting line theory is called a bound vortex, one which runs along the span of the wing.

Accepting the idea that a circulation is created, the investigators still found it necessary to fix its strength at a particular value for a given angle of attack. They reasoned that as long as vorticity leaves the wing, the circulation increases. When the starting vortex is swept far away, the circulation has reached its maximum value because there is no longer a velocity difference between the flows leaving the upper and lower surfaces. This assumption was put forward independently by both Kutta and Joukowski. It is the salient point in the theory of lift because it fixes the magnitude of the circulation. Stated in this way the rule applies only to airfoils with a zero trailing-edge angle, that is, one that forms a cusp. If the airfoil has a finite trailing-edge angle it is necessary to place the rear stagnation point on the trailing edge, else flows of two different velocities would then exist simultaneously at one point. Because all real airfoils of necessity have finite trailing-edge angles, this is the condition now employed.

With this assumption the problem of computing the pressures, the lift, and the moment on an airfoil obtained by transforming a circle became a purely mathematical one. As noted previously, the theory was essentially complete by 1909—six years after the Wright brothers flew. Their contribution was not in the understanding (at least in an empirical manner) of the lift of wings, which had been done as far back as 1832 by Sir George Cayley. The Wrights' contribution—the one for which they were issued a patent which they successfully defended in court—was for a method of lateral control, specifically wing warping. To place this in its proper context, recall that the three principal problems of powered flight are 1) developing sufficient lift in a lightweight structure, 2) developing sufficient power with a lightweight engine, and 3) controlling the machine once it is built. As noted, the problem of designing a lifting wing was solved at least empirically long before the Wrights began their work. A gasoline engine of suitable power and weight was demonstrated around 1896 by Langley's assistant Manly. The Wrights used their glider tests and wind-tunnel tests to develop a suitable control system, which they then patented. Glenn Curtiss built and flew an airplane (the June Bug) in 1908, which used ailerons for lateral-directional control. The aircraft and the flight received considerable publicity. To defend their patent the Wrights were forced to sue Curtiss for patent infringement. They won their case when the court decided that ailerons were a form of wing warping. (See Refs. 6–18 for related literature on the historical development of the theory of lifts.)

The Kutta–Joukowski theory is in reasonably good agreement with experiment up to an angle of attack for which viscous effects begin to become dominant. It can yield even better agreement with two empirical modifications: 1) reduce the circulation about 10% to account for the viscous boundary layer, and 2) move the stagnation points slightly inside the circle to cause the transformation to produce an airfoil with a finite trailing-edge angle. We will consider the transformation process in detail in Sec. 3.3.

3.3 Conformal Transformations

A transformation can be said to map a region from one plane to a region in another plane. It is conformal if for every point in the first plane there is a unique point in the second plane and the angles between lines in one plane are preserved in the second. If we know for, example, the pressure at some point in the first plane the transformation tells us where this pressure exists in the second plane. Thus, if

the transformation maps a circle in one plane to an airfoil shape in the second, we may take the solution for pressures in the first plane on the $\psi = 0$ line for a doublet and coincident vortex in a uniform stream and from this determine the pressures on the airfoil. We can determine the lift and pitching moment either analytically or by integration of the pressures over the surface. Hence, if we construct an airfoil that has the same shape as that given by the transformation of a circular cylinder we immediately know a majority of its aerodynamic characteristics. To the extent to which this inviscid theory correctly models the flow of real fluids, we have a successful prediction of the lift and pitching moment of a wing of very high aspect ratio where aspect ratio is defined as the span to the second power divided by the planform area. We will couple this idea to that now well known by aerodynamicists as the Kutta condition, which says that we must choose a value for the vortex strength such that at every angle of attack the rear stagnation point of the flow is located at the trailing edge of the airfoil.

3.4 Mapping the Doublet with Circulation in a Uniform Stream to an Airfoil

The transformation devised by Joukowski can be written in the form

$$z = \zeta + \frac{c^2}{\zeta} \tag{3.4}$$

where z, in the target plane, and ζ, in the source plane, are both complex numbers. We will set

$$z = \xi + j\eta \tag{3.5a}$$

and

$$\zeta = x + jy \tag{3.5b}$$

Then,

$$\xi + j\eta = x + jy + \frac{c^2}{x + jy}$$

$$= x + jy + \frac{c^2(x - jy)}{x^2 + y^2} \tag{3.6}$$

from which it is seen that

$$\zeta = x + \frac{xc^2}{x^2 + y^2} \tag{3.7a}$$

$$\eta = y - \frac{yc^2}{x^2 + y^2} \tag{3.7b}$$

These equations give us the coordinates of a point in the z plane in terms of the coordinates of the point in the ζ plane, the plane in which the circle is located.

We now demonstrate that if the center of the circle is at the origin, the circle transforms into a straight line of length $4c$. First, let

$$x = r\cos\theta \tag{3.8a}$$

$$y = r\sin\theta \tag{3.8b}$$

Then, we have

$$\xi = r\cos\theta + \frac{rc^2\cos\theta}{r^2} \tag{3.9a}$$

$$\eta = r\sin\theta - \frac{rc^2\sin\theta}{r^2} \tag{3.9b}$$

We take the radius of the circle to be c with the result that

$$\zeta = \pm 2c \tag{3.10a}$$

$$\eta = 0 \tag{3.10b}$$

By moving the center of the circle away from the origin, we can affect the thickness and camber of the resulting airfoil. Camber is the curvature of mean line between upper and lower surface of the airfoil. We will define F as the displacement of the center along the y axis and ec as the displacement of the center along the x axis. Here, e is a number less than or equal to one. We will also define

$$\beta = \sin^{-1}\left(\frac{F}{c+ec}\right) \tag{3.11}$$

whereas α is the angle of attack and β is related to the camber of the airfoil, which results from the transformation.

Note that coordinates in the ζ plane still must be measured with respect to the origin despite the fact that the center of the circle may be displaced. If θ is measured with respect to the center of the circle, then the coordinates of points on the circle in the ζ plane are

$$y = F + a\sin\theta \tag{3.12a}$$

$$x = ce + a\cos\theta \tag{3.12b}$$

In the z plane the coordinates of the transformed point are

$$\xi = ce + a\cos\theta + \frac{c^2(ce + a\cos\theta)}{(ce + a\cos\theta)^2 + (F + a\sin\theta)^2} \tag{3.13a}$$

$$\eta = F + a\sin\theta - \frac{c^2(F + a\sin\theta)}{(ce + a\cos\theta)^2 + (F + a\sin\theta)^2} \tag{3.13b}$$

Pressures at a particular value of θ on the circle have that same value at the transformed point in the z plane.

In the form just used the transform yields a cusp at the trailing edge. If a, the circle radius, in Eqs. (3.13) is replaced by

$$a = c(1 + fe) \tag{3.14}$$

where the trailing-edge factor f is greater than or equal to 1.0 but usually not more that 2.0, the stagnation points will exist inside the circle leading to a finite angle trailing edge, and the point of maximum thickness on the airfoil exists a little farther aft than when $f = 1.0$.

To guarantee that the trailing edge is a stagnation point we make the circulation

$$K = 4\pi U a \sin(\alpha + \beta) \tag{3.15}$$

Notice that the amount of circulation does not affect the shape of the airfoil, which is determined entirely by the values of c, e, F, and f.

Figure 3.1 illustrates the characteristics of the Joukowski airfoils. The airfoil in Fig. 3.1a is termed a circular arc airfoil because it is made up of sections of circles. In this case the center of the circle is just moved upward on the y axis. The airfoil in Fig. 3.1b is one made by shifting the center of the circle to the right only. E in the program is $1/e$ in the preceding equations. The airfoil in Fig. 3.1c has both thickness and camber but still a cusp trailing edge. The airfoil in Fig. 3.1d has been generated with a greater thickness so that the finite trailing-edge angle is visible. The nominal circle radius for these airfoils is 1.0.

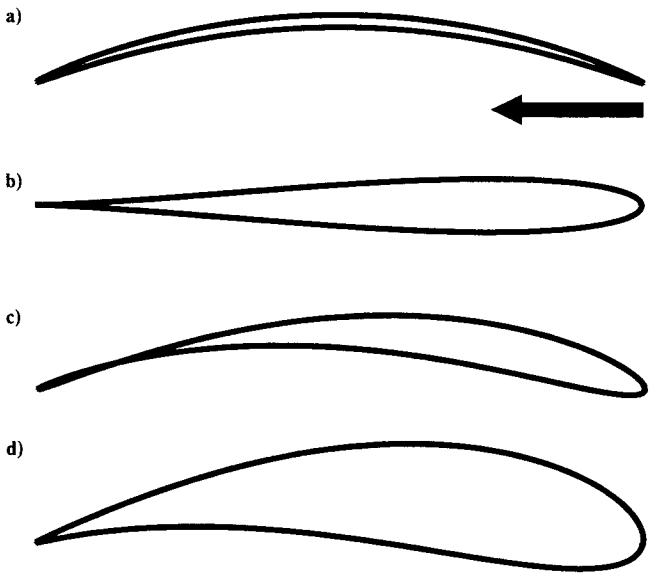

Fig. 3.1 Joukowski airfoils: a) E = 1.0D + 10, F = 0.2, full circulation, and cusp trailing edge; b) E = 14.0, F = 0.0, full circulation, and cusp trailing edge; c) E = 14.0, F = 0.2, full circulation, and cusp trailing edge; and d) E = 7.0, F = 0.2, full circulation, and trailing-edge factor = 1.25.

With the use of this vortex strength, the stream function is

$$\psi = Ur\left(1 - \frac{a^2}{r^2}\right)\sin\theta + \frac{4\pi U a}{2\pi}\sin(\alpha + \beta)\ell_n r \tag{3.16}$$

Then,

$$v_\theta = U\left(1 + \frac{a^2}{r^2}\right)\sin\theta + \frac{2Ua}{r}\sin(\alpha + \beta) \tag{3.17}$$

On the surface of the cylinder $r = a$ and so here

$$v_\theta = 2U\sin\theta + 2U\sin(\alpha + \beta) \tag{3.18}$$

from which we see that $v_\theta = 0$ when $\theta = -(\alpha + \beta)$ and $\theta = \alpha + \beta - \pi$. These are the locations of the stagnation points.

The lift per unit span is

$$\rho U^2 4\pi a \sin(\alpha + \beta) \tag{3.19}$$

To normalize to the lift coefficient we divide by $\frac{1}{2}\rho U^2 \cdot$ chord. The actual chord length is a little more than $4c$, i.e.,

$$4c\left[1 + \frac{e^2}{1 + 2e}\right] \tag{3.20}$$

for a symmetrical Joukowski airfoil. Hence, for such an airfoil

$$C_\ell = 2\pi\left[\frac{1 + 3e + 2e^2}{1 + 2e + e^2}\right]\sin\alpha \tag{3.21}$$

For cambered Joukowski airfoils or airfoils with finite trailing-edge angles, it is preferable to write

$$C_\ell = 8\pi\frac{c(1 + fe)}{\text{chord}}\sin(\alpha + \beta) \tag{3.22}$$

where chord $= |\xi_{max}| + |\xi_{min}|$. The computer program uses this value. Notice the very important result that the lift curve slope is

$$\left.\frac{\partial C_\ell}{\partial\alpha} = 8\pi\frac{c(1 + fe)}{\text{chord}}\right|_{\alpha=0} \tag{3.23}$$

for all airfoils. This is another way of saying that the lift is approximately independent of the airfoil shape, as we noted previously. The lift curve slope does increase slightly as the airfoil thickness increases. This trend is seen for all airfoils, not just those of the Joukowski type.

An analytical expression can be derived for the pitching moment coefficient about specific chordwise locations on symmetrical airfoil (for example, the nose, the quarter-chord, or the aerodynamic center) but for cambered airfoils it is too complex for easy use. In that case it is recommended that the value be obtained

from a process that can be described by an expression such as

$$C_{m_{c/4}} = \frac{\sum[(x - x_{c/4}) \cdot C_{p_s}\Delta x]}{\text{chord}} \tag{3.24}$$

when the summation is carried out over the entire airfoil. Because of the airfoil curvature the segments Δx are not the same length everywhere but rather $\xi_{j+1} - \xi_j$. The program has available pressure coefficients at 180 such values. In the example, the term $x - x_{c/4}$ represents the distance from the quarter-chord to the current segment.

Joukowski airfoils, even those produced by the modifications implemented in the program, have not proven to be as satisfactory as one could wish, primarily because the minimum pressure point on the upper surface occurs too far forward. As a result, the viscous boundary layer faces an unfavorable pressure gradient over most of the upper surface. Consequently, the boundary layer thickens and then separates at lower angles of attack than on more modern airfoils. Joukowski airfoils, therefore, have somewhat higher drag coefficients and lower maximum lift coefficients than newer designs. Of course, this is a result of viscous forces, which are not treated in the theory.

The other less-than-desirable feature of Joukowski airfoils is that one does not know the airfoil shape a priori. Attempts to transform a given shape back into a circle do not always yield a circle. Frequently, one cannot use the theory to predict the pressure distribution on a given shape that for structural or other reasons one may wish to use.

Theoretical developments after Joukowski took one of two paths: 1) construction of a thin airfoil theory in which the airfoil is replaced by a distribution of vortices on the mean camber line and 2) generalization of the Joukowski theory, of which Theodorsen's work is typical. Although it can handle a wider variety of shapes, Theodorsen's method is relatively abstract (entailing two transformations) and the computations are tedious. For that reason it was little used outside of NACA. Even at NACA a strong program was developed during the 1930s to conduct a systematic series of tests to determine the characteristics of whole classes of airfoil sections whose shapes were more the result of careful experimentation into what characteristics were desirable than of guidance from some theory. The published test results[16] on these airfoils (also see Ref. 17) formed the basis for airfoil selection for new aircraft for 30 years.

With the advent of the digital computer, methods such as that described in Chapter 5 have become sufficiently accurate and reliable to enable the designer to optimize the airfoil(s) for the vehicle on which it is to be installed.

3.5 Program JOUKOW

Source code for this program occupies 36,224 bytes. A separate program to generate pressure coefficients plots from tabular data, CP.FOR, occupies 3,200 bytes. CP.FOR is effectively incorporated in JOUKOW.FOR and so it need not be run if all pressure data are generated by JOUKOW. The output files are JOUKOW.TXT, which contain printer plots of the airfoil shape and pressure coefficients; JOUKOW.AIR, a PostScript plot of the profile; and CP.PS, PostScript plots of the pressure distribution. Executable code for JOUKOW is 116,224 as made with the Microsoft PowerStation compiler. At this size execution is very

rapid. JOUKOW.TXT is a large file (247,655 bytes) and CP.PS is much smaller at 133,096 bytes. JOUKOW.AIR requires only 16,096 bytes.

The program generally implements the method for generating the airfoil shape described in Ref. 18, which uses Eqs. (3.4–3.15).

3.5.1 Program Graphics

The program generates two types of graphical output. First are graphs of the airfoil shape and pressure distributions at 12 angles of attack via the printer character set; then, PostScript files of the same data are created. The latter requires a PostScript printer or a software PostScript interpreter to view or print the files.

3.5.2 Program Data Entry

All data entry is by keyboard response to questions displayed on the screen. These ask for the original diameter of the circle to be transformed; the displacement of its center, F, along the y axis and c/E along the x axis; the factor by which to reduce the circulation; and the factor by which the stagnation points are to be embedded, f. One final query gives the user the option to write or not write 12 pressure distribution plots using the printer character set into the text file JOUKOW.TXT.

3.5.3 Typical Results

Prints of typical PostScript output files are shown in Fig. 3.2. A portion of one of the listings is shown in Fig. 3.3. The listings provide the airfoil ordinates at closely

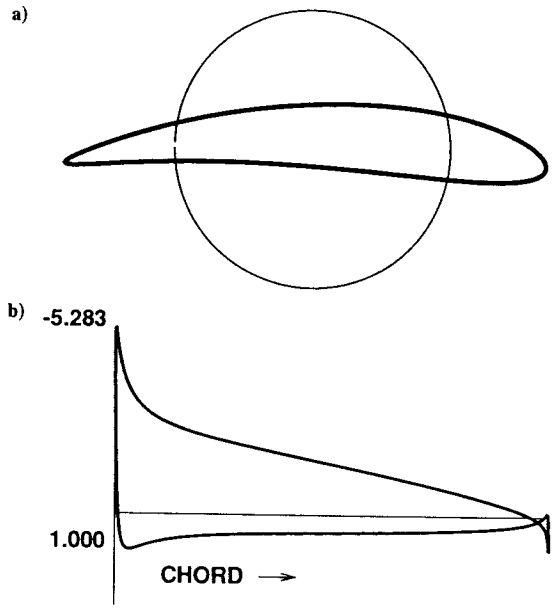

Fig. 3.2 Joukowski airfoil: a) transformed from a circle (airfoil chord is about four times circle radius) and b) pressure distribution, angle of attack = 11.0 deg, leading edge on left and trailing edge on right.

CIRCLE RADIUS = 1.000
HORIZONTAL OFFSET OF CENTER = .1428571
VERTICAL OFFSET OF CENTER = .2000000
FACTOR TO CHANGE HORIZONTAL LOCATION OF REAR STAGNATION POINT = 1.25000
FACTOR TO CHANGE CIRCULATION = .90000

ALPHA = .00000000 LIFT COEFFICIENT = 1.257

J	XI	ETA	CP	VELOCITY
1	-1.969	.019	.3005	.83634143
2	-1.981	.013	.3595	.80031076
3	-1.990	.008	.4423	.74679140
4	-1.996	.004	.5844	.64465457
5	-2.000	.001	.8984	.31873757
6	-2.000	.000	-.1830	-1.08764916
7	-1.997	-.001	-.1731	-1.08311252
8	-1.991	-.001	.0189	-.99052693
9	-1.982	.000	.1163	-.94003118
10	-1.970	.002	.1769	-.90722206
11	-1.954	.005	.2200	-.88319448
12	-1.935	.009	.2531	-.86423561
13	-1.912	.014	.2800	-.84855526
14	-1.886	.019	.3025	-.83519223
15	-1.856	.025	.3217	-.82358767
16	-1.823	.031	.3384	-.81339638
17	-1.787	.037	.3529	-.80439483
18	-1.747	.044	.3657	-.79643272
19	-1.704	.051	.3768	-.78940587
20	-1.657	.058	.3865	-.78324012
21	-1.607	.065	.3949	-.77788156
22	-1.554	.071	.4020	-.77329013
23	-1.497	.078	.4080	-.76943554
24	-1.438	.084	.4128	-.76629439
25	-1.376	.089	.4165	-.76384825
26	-1.311	.094	.4192	-.76208228
27	-1.243	.098	.4209	-.76098417
28	-1.173	.102	.4216	-.76054347
29	-1.101	.104	.4213	-.76075100
30	-1.027	.106	.4200	-.76159843
31	-.950	.107	.4177	-.76307798
32	-.872	.107	.4145	-.76518214
33	-.793	.105	.4103	-.76790350
34	-.712	.103	.4052	-.77123456
35	-.630	.100	.3991	-.77516763
36	-.548	.095	.3921	-.77969470
37	-.464	.090	.3841	-.78480736
38	-.380	.084	.3751	-.79049673
39	-.296	.077	.3652	-.79675336
40	-.212	.069	.3543	-.80356719
41	-.127	.060	.3424	-.81092749
42	-.043	.050	.3295	-.81882277
43	.040	.040	.3157	-.82724075
44	.123	.029	.3008	-.83616827
45	.205	.018	.2850	-.84559123
46	.287	.006	.2681	-.85549449

Fig. 3.3 Example of listing produced by JOUKOW.

spaced chordwise coordinates with sufficient accuracy to permit the construction of a template for fabrication if desired.

The lift coefficents shown are those computed by Eq. (3.22).

3.6 Closure

This chapter has dealt with the use of elementary flow functions and a mathematical transformation both to create a means for representing an airfoil-like shape mathematically and for determining from the transformation the pressures that will exist on the shape and its lift at various angles of attack. Two slight mod-

ifications to the original 1909 theory have been included in a computer program, which performs the operations indicated by the transformation, illustrates the resulting airfoil, determines the lift coefficient at 12 angles of attack, and depicts the pressure distributions at these angles of attack.

The problems at the end of this chapter include some illustrations depicting the nomenclature associated with the aerodynamic characteristics of airfoils and indicate some of the flow characteristics about real airfoils at various angles of attack. What are not shown are wind-tunnel test results of the aerodynamic characteristics of real airfoils, in particular the variation of lift with angle of attack at those angles of attack where the lift is influenced significantly by the fluid viscosity. This will be treated in Chapter 5 where the theory includes a method for determining some viscous effects, as well as some compressible effects. Whereas with the Joukowski transform technique the shape of the airfoil is not known *a priori*, the method in Chapter 5 permits calculation of the characteristics of existing airfoils valid for lift coefficients of 0.8 or less. Other end-of-chapter problems ask the user to generate airfoils with specific characteristics.

The origins of airfoil drag, a characteristic that the Joukowski theory cannot predict, are discussed in the next chapter.

For the angles of attack at which the Joukowski theory provides reliable results, the moment characteristics can be determined from the pressure data. One of the problems describes a semigraphical method.

Although most of the discussion in this chapter has used the word airfoils, it should be understood that the theory applies equally to hydrofoils operating at sufficient depth to eliminate the effect of surface reflections. The forces on a hydrofoil, however, are some 800 times as great as those on an airfoil of the same geometry at the same speed; therefore, the structure must be designed with this in mind. Another difference between airfoils and hydrofoils is the latter is to operate at "high" speeds. The faster the hydrofoil goes the lower is the pressure at some point on the surface. When this pressure is below the vapor pressure of water, the water in this region will vaporize. However, the gas bubble thereby created will collapse when the local pressure returns to an above-vapor-pressure value. The intense scouring action of this collapse quickly erodes the surface beneath it. The process is called cavitation. Supercavitating hydrofoils are designed to ensure that the steam bubble collapses in the wake downstream of the aft end of the hydrofoil.

Problems

3.1. See if you can find information on the first man-powered flight over the English Channel. The desired information is a) Bryan Allen's weight, b) weight of Gossamer Albatross, c) wing span, d) wing area, e) power developed, f) average speed, and g) average altitude. Also, a) discuss why it took so long before man-powered flight became a reality. b) Can you determine from these data the drag of the craft? c) What was the wing loading in pounds per square foot and the power loading in horsepower per square foot? For birds W/S is approximately $W^{0.25}$.

3.2. Glue an 8.5 × 11 in. print of the pressure distribution for some angle of attack on stiff paper. Then cut the picture along the line depicting the pressure

coefficients. When you are finished you should have an irregularly shaped object with most of its area to one end. Then take a draftsman's triangular scale, place the cutout on it so that the chord line is perpendicular to the long axis of the scale, and move the cutout until it balances on the scale. Mark the location on the chord line. This is the x location of the center of pressure. a) Where is this location relative to the nose of the airfoil as a function of the chord length? b) Use this result to obtain the pitching moment coefficient of the airfoil about the quarter chord for the angle of attack at which the data were generated.

3.3. Trace the pressure distribution on millimeter graph paper, count the squares under the curve above the chord line, and record. Count the squares below the chord line that fall between the curve and the chord line. Add the two results. Relate this total to the lift coefficient reported by the program for the angle of attack. What is the result?

3.4. Integrate the components of the pressures on the airfoil at $\alpha = 0$ in the direction of the chord line. What result do you obtain?

3.5. Designate a pressure force coefficient normal to the chord line as C_N. Designate a pressure force coefficient parallel to the chord line as C_A. Then construct the relations

$$C_L = C_N \cos\alpha - C_A \sin\alpha$$

$$C_D = C_N \sin\alpha + C_A \cos\alpha$$

a) What results do you obtain? b) Is it what you expected? c) Why?

3.6. The thickest airfoils found to be practical in use are about 22% thick. a) What value of E is necessary to generate a Joukowski airfoil of that thickness that also has a lift coefficient of 0.4 at $\alpha = 0$ and a finite trailing-edge angle? Use a factor of 1.25 in Eq. (3.14) to multiply $1/E$ to obtain a finite trailing-edge angle. b) What value of F is used? c) Does the factor f in Eq. (3.14) affect the lift coefficient?

3.7. Repeat problem 3.6 but generate an airfoil that is 6% thick. Change the factor multiplying $1/E$ in Eq. (3.14) to 2.0. b) Repeat, but change the lift coefficient at $\alpha = 0$ to 0.2. c) Repeat, but make a symmetrical airfoil. Indicate how you verified the airfoil thickness.

3.8. Figure P3.1 illustrates the nomenclature associated with airfoil aerodynamic characteristics. a) Where is the center of pressure when the pitching moment coefficient about the quarter-chord is negative? b) If the airfoil is cambered as indicated in the figure, at what approximate angle relative to the oncoming flow should it be operated if the lift is to be zero? The angle of attack is zero when the chord line is aligned with the oncoming stream. c) Is the drag likely to change from the value it had when the angle of attack was zero if the angle of attack is changed to the angle of attack for zero lift?

3.9. Consult the $\alpha = 0$ pressure distributions for the airfoils generated in problems 3.6 and 3.7. Do any of them have regions of constant or very slowly increasing

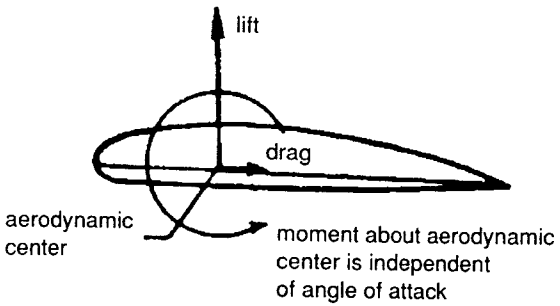

moment coefficient is zero at center of pressure
center of pressure moves forward with increasing angle of attack

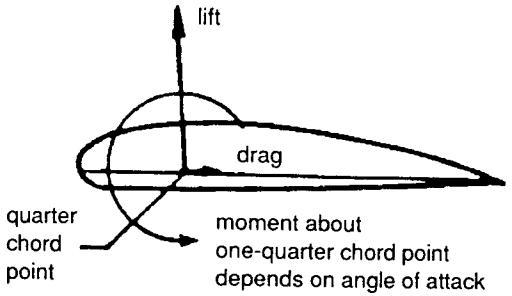

Fig. P3.1 Airfoil aerodynamic characteristics.

values of $-C_P$? Such regions are necessary to keep the viscous boundary layer from thickening and perhaps separating.

3.10. Figure P3.2 shows the condition of the actual flow over an airfoil at various angles of attack. Notice that the viscous boundary layer is relatively thin and its effects are confined primarily to the aft end of the airfoil when the angle of attack is small. This is the reason inviscid airfoil theory can do a good job describing flow behavior for these conditions. Figure P3.2 shows why inviscid airfoil theory fails at higher angles of attack. For angles of attack beyond stall the separated flow region becomes much larger and unsteady, causing a decrease in lift and a significant increase in drag. a) How, from an experimental plot of C_L vs α, might one determine at what angle of attack (or value of lift coefficient) the effects of viscosity are sufficent to modify the behavior of the airfoil? b) Determine what you would expect the characteristics of the airfoil to be at negative angles of attack and explain. c) Determine if you can make a qualitative correlation between the vertical extent of the wake and the drag on the airfoil and explain.

3.11. On what portion of the airfoil should you expect the pressures to differ most from the theoretical expectation?

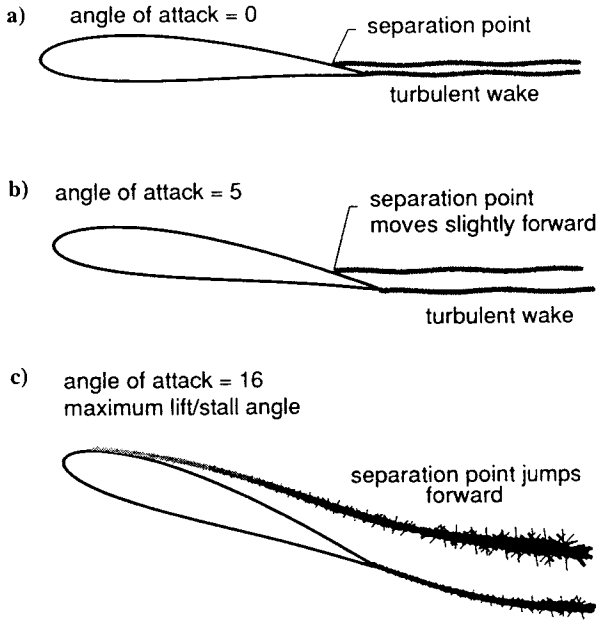

Fig. P3.2 Stall formation.

3.12. Generate a 22% thick Joukowski airfoil that has a lift coefficient at $\alpha = 0$ of 0.4. At what value of x/c is the pressure coefficient on the upper surface most negative at $\alpha = 0$? Let $f = 1.25$ and the circulation factor be 1.0.

3.13. Assume that $P_\infty = 2116$ psf, $\rho_\infty = 0.002378$ slugs/ft^3, and $U_\infty = 316$ ft/s. a) What is the stagnation pressure? b) At what lift coefficient would the minimum pressure point on the airfoil in problem 3.12 first experience a local pressure of $0.528P_s$? c) What is the angle of attack at which this would occur? d) Would you expect this angle of attack to be within the normal operating range of this airfoil and why?

3.14. What would be the value of the circulation/per unit span for problem 3.13?

3.15. At what value of the lift coefficient would the two stagnation points on a circle in a uniform stream come together at $\theta = 270$ deg?

3.16. The following conditions are observed: $q = 64.316$ psf, max $t/c = 0.22$, $\rho = 0.002378$ slugs/ft^3, Joukowski airfoil, $P_\infty = 2116$ psf, $C_{L_{\alpha=0}} = 0.4$, $C_{P_{\min}} = -15$, $q = \frac{1}{2}\rho U^2$, $f = 1.0$, and circulation factor = 1.0. Determine:

a) stagnation pressure,
b) freestream velocity,
c) minimum pressure on airfoil,
d) velocity at minimum pressure point,

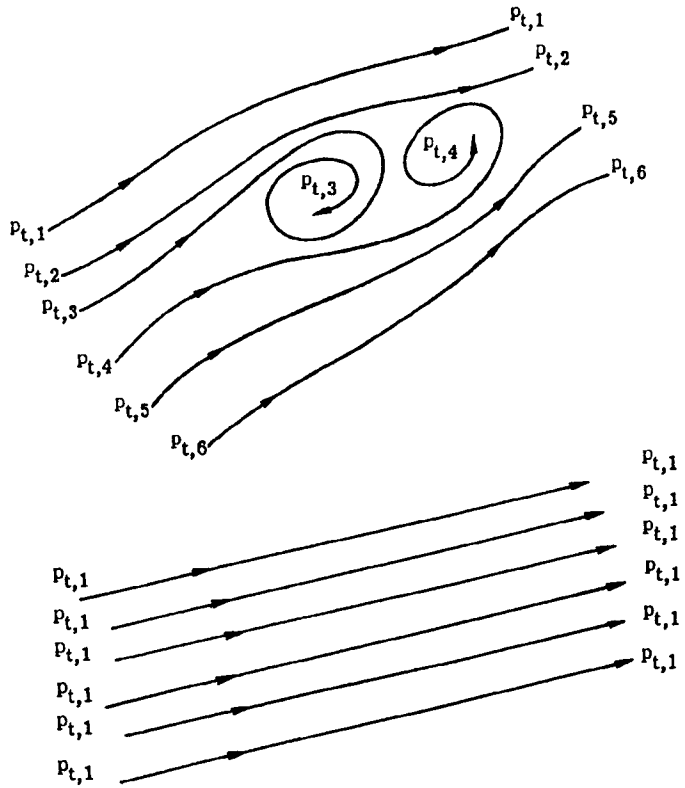

Fig. P3.3 Stagnation pressures on streamlines.

e) lift coefficient of Joukowski airfoil when these conditions exist, and
f) angle of attack of airfoil. How would the answers to problems 3.16c–3.16f change when the circulation factor is 0.9?

3.17. Figure P3.3 shows two examples of the stagnation pressures along streamlines. a) Is either of these flows irrotational? b) If so, which is irrotational? c) Which flow is representative of that approaching the airfoil? d) Which flow is representative of that in an airfoil wake? In these figures p_t is stagnation pressure.

3.18. What is the largest possible positive value of the pressure coefficient?

3.19. Where (as a percent of chord) are the stagnation points in Fig. 3.2?

3.20. Determine the lift curve slope for the airfoils in Fig. 3.1.

3.21. Let $z = \xi + i\eta$ and $\zeta = x + iy$. Draw an airfoil section on millimeter graph paper as smoothly as you can. The chord of this airfoil should be exactly 10 cm long and will serve as the vertical reference. At every millimeter from the

nose to the trailing edge, record values of the other airfoil coordinate for the lower surface in millimeters. Then, going from tail to nose record, again in millimeters, the coordinates of the upper surface at every millimeter along the chord. You should have exactly 200 sets of (ξ, η) values. Let the horizontal reference be the midchord point. Set up a program or a spread sheet that will make ξ and η the real and imaginary parts of the complex number z. Let us say a portion of the FORTRAN code might look like the following:

```
      IMPLICIT REAL*(A-H,O-Z)
      COMPLEX*16 Z,ZETA,CC,HALF,FOUR
      DIMENSION A(200),B(200),X(200),Y(200),Z(200),ZETA(200)
      OPEN(1,FILE='INVERS.DAT',STATUS='OLD')
      DO 1 J=1,200
      READ(1,2) A(J),B(J)
    1 Z(J)=DCMPLX(A(J),B(J))
    2 FORMAT(F5.1,1X,F5.1)
      C=25.0D0
      CC=DCMPLX(C,0.0)
      FOUR=DCMPLX(4.0D0,0.0D0)
      HALF=DCMPLX(0.5D0,0.0D0)
      DO 3 J=1,200
      SIGN=1.0D0
      IF(B(J).LT.0.0D0) SIGN=-1.0D0
    3 ZETA(J)=HALF*(Z(J)+SIGN*CDSQRT(Z(J)*Z(J)-FOUR*CC*CC))
```

a) Plot the real vs imaginary part of ZETA. Connect points by straight line segments. b) Describe the resulting figure in as much detail as you can. c) How would you characterize the process that was carried out? If necessary you can find the square root of a complex number as follows:

```
A=DREAL(Z)
B=DIMAG(Z)
ZM=(A*A+B*B)**0.25
TH=0.5D0*DATAN2(A,B)
ZSQRT=DCMPLX(ZM*DCOS(TH),ZM*DSIN(TH))
```

Z and ZSQRT are complex numbers.

4
Drag, Viscosity, and the Boundary Layer

4.1 Introduction

FROM at least the 18th century onward it has been recognized that all real fluids are viscous to some extent (except for superfluids, which do not exist at room temperature). It has also been generally accepted that the best mathematical description of the motion of such fluids is provided by the Navier–Stokes nonlinear partial differential equations. There are probably fewer than a dozen cases for which exact solutions of these equations are known. Given the difficulty of solving such equations for any but the simplest of boundary conditions, it is not surprising that the study of fluid flow early divided into two camps: 1) theoretical study of the far simpler equations for inviscid flow, which was called hydrodynamics, and 2) a largely empirical investigation of fluild flow, called hydraulics. The second camp was peopled primarily by engineers, who had to get answers to practical problems. Because they could not solve the problems analytically they devised experiments, often at a smaller scale, to determine the flow rates and forces that would exist with the full-scale hardware. For this approach to be productive, they needed to know the proper scaling laws for the forces and flow rates and the correct form of the force coefficients.

The first camp was composed of physicists and mathematicians, who developed analytical solutions to an increasing array of problems, which could be modeled with reasonable accuracy by inviscid flows. Instead of cross fertilizing each other, the two camps tended to drift further apart during the 19th century. We note that the work of Helmholtz, Kichhoff, Lamb, Kutta, and Joukowski was entirely inviscid.

Ludwig Prandtl began his career as a careful experimenter but he also had received solid training in mathematics. His observations revealed that the effects of viscosity were generally confined to a small layer of fluid immediately adjacent to the surface of the body over which the fluid was flowing. This he called the "Grenzschicht" or boundary layer. Prandtl then looked at the Navier–Stokes equations and, by considering the relative importance of the terms in the equations when applied to boundary-layer flow, was able to simplify the equations considerably. Prandtl[19] published the results of these investigations in a seminal paper in 1904. Prandtl's boundary-layer equations form the basis of all modern treatments of the determination of skin friction and the creation of form drag.

We shall emulate Prandtl and show how the boundary-layer equations are obtained from the Navier–Stokes equations. We do this in an attempt to help the reader appreciate the conditions under which a boundary-layer analysis is valid. We will employ a technique for determining boundary-layer growth and for calculating associated skin friction, called the momentum integral method. This is the method used for these purposes by the programs discussed in Chapters 5 and 7. In this chapter we will go through a derivation of the procedure in some detail in the hope that the reader will gain an indication of its strengths and weaknesses, as well as an indication of how the algorithm fits into the drag calculations carried

out by the programs. Then if there is a question about the validity of the results produced by the programs, the reader will know that the procedures by which they are obtained have been set out for inspection.

To provide the reader with some additional association with viscous flows and their characteristics, we will obtain exact solutions to the Navier–Stokes equations for five simple cases and approximate boundary-layer type solutions in three additional cases. The exact solutions and one of the approximate solutions involve internal flows. The remaining two involve external flows. The problems at the end of the chapter deal primarily with these eight cases and some extensions thereof.

4.2 Drag

Because of viscosity, bodies that move through a fluid experience a resistance to motion that we call drag. As a result, energy must be added constantly to the body to maintain its motion. It is convenient to think of the drag on a body as being composed of two components: a skin-friction drag and a profile or form drag. Skin friction results from the rubbing of the fluid on the body surface as the fluid moves over it. The energy dissipation usually results in heat being transferred to the body surface, but this depends on the value of the Prandtl number. As a result of the momentum loss in the boundary layer, the flow leaving the body contains a region with a lower velocity than that in the remainder of the flow. Figure P3.2 illustrates this situation. Figure P3.2 shows a relatively small wake. By the time a large angle of attack is reached the wake is quite thick. In a streamline near the forward stagnation point the static pressure is near the stagnation value and the velocity is low. As the flow makes its way over the airfoil, the pressure drops and the velocity increases. Normally, the presssures then begin to rise toward the stagnation value as the trailing edge of the airfoil is reached. However, when there is extensive separation, as shown in Fig. P3.2, this pressure rise does not occur. The flow leaves the surface and roughly maintains the pressure it had when it separated. By Prandtl's hypothesis the pressures in these separating streamlines are transmitted unabated through the boundary layer to the surface below such that when the pressures on the entire body are integrated there is a net force in the streamwise direction, called the pressure or form drag.

The form drag depends on the extent to which the boundary layer adheres to the body surface. If the boundary layer encounters rising pressures (called an adverse pressure gradient) of sufficient intensity that it cannot overcome them, it separates from the body surface. When this happens the pressures on the aft end of the body are very low relative to the stagnation pressure, and the corresponding form drag is very high.

To relate the drag of one body to that of another, it is common to nondimensionalize it as a coefficient. Thus, we write

$$C_D = \frac{\text{drag force}}{\frac{1}{2}\rho S V^2} \tag{4.1}$$

For most geometrically similar bodies, the drag coefficient is a function only of the Reynolds number when the Mach numbers are less than about 0.5. This means that two bodies of different size but of similar shape have the same drag coefficient if the Reynolds number for the two cases is the same. In Eq. (4.1) ρ is the fluid density, S is the reference area, and V is the fluid velocity. Reynolds number Re_N is expressed by

$$\frac{\rho V L}{\mu} \tag{4.2}$$

where L is a reference length (usually the chord length for airfoils) and μ is the coefficient of dynamic viscosity. The latter is a physical property of the fluid determined by measurement. Its magnitude varies with temperature. For gases it increases with increasing temperature; for liquids its magnitude decreases with increasing temperatures.

4.3 The Boundary-Layer Equations

We begin with a development of the equations expressing the conservation of momentum (also known as Newton's second law of motion as applied to viscous fluids). Much as we did in Chapter 2, we will consider the difference in the momentum of the fluid mass entering an element of fluid and momentum in the fluid mass leaving it and equate these differences to the changes in the forces acting on the fluid mass. Because force is a vector quantity (that is, it has both a magnitude and a direction), we must write an expression of this law in each of the principal directions of our Cartesian coordinate system.

Now we can write the mass of fluid crossing a plane area per unit time as

$$\rho u_1 \, dx_2 \, dx_3 \tag{4.3}$$

If we multiply this mass by its velocity in the x_1 direction, we obtain its momentum in the x_1 direction. Because mass must be conserved, the change in momentum in the x_1 direction is given by

$$\rho u_1 \frac{\partial u_1}{\partial x_1} dx_1 \, dx_2 \, dx_3 \tag{4.4}$$

Now the mass entering a fluid element may also have components in the x_2 and x_3 directions. Each of these components can contribute to the momentum and, thus, to the change in the momentum in the x_1 direction. We can generalize Eq. (4.4) to account for all changes in momentum per unit volume by writing

$$\rho u_j \frac{\partial u_i}{\partial u_j} \tag{4.5}$$

where we interpret the repeated index j to mean summation:

$$\rho u_1 \frac{\partial u_i}{\partial x_1} + \rho u_2 \frac{\partial u_i}{\partial x_2} + \rho u_3 \frac{\partial u_i}{\partial x_3} \tag{4.6}$$

The result given by Eq. (4.5) indicates a change in momentum due to a change in position. In addition, there may also be a temporal change in momentum. Thus, we need to add the term

$$\rho \frac{\partial u_i}{\partial t} \tag{4.6a}$$

to Eq. (4.5) to obtain a complete expression for the change in momentum.

The viscous forces acting on the element per unit area can be of two types: normal stresses and shearing stresses. Such stresses are tensor quantities because they require that we employ two indices to identify them properly. We need to know both the surface (identified by the direction of its normal) on which the stress acts as well as the direction on or along this surface in which it acts. Note that there are, in general, nine such stress components.

A fluid medium cannot resist shearing per se but it does develop a force proportional to the rate at which it is sheared. We express such a force per unit area as

$$\tau_{ij} = \mu \frac{\partial u_i}{\partial x_j} \tag{4.7}$$

Because i and j can each have values 1, 2, and 3, τ_{ij} in general has nine components. The proportionality between the rate of shearing and the stress it creates is expressed by μ. Essentially, it serves the same purpose in fluids as Young's modulus, (the modulus of elasticity) does for solids. Just as Young's modulus is constant for most materials up to an elastic limit, the coefficient of dynamic viscosity, as it is called, is constant or primarily a function of temperature for fluids, which are termed Newtonian. Non-Newtonian fluids are fluids where the proportionality between the rate of shearing and the shearing force is a function of the rate of shearing. Non-Newtonian liquids are more common than non-Newtonian gases.

Conceptually, one may have a bit of difficulty visualizing a normal viscous stress, particularly because its effect, if present, is usually hidden by the hydrostatic pressure. Suffice it to say at this point that normal viscous stresses (exclusive of pressure) are usually not of significant magnitude, except perhaps through shock waves. For completeness, however, we give the generally accepted expression for the viscous stress in common fluids, which reads

$$\tau_{ij} = -\frac{2}{3}\mu\delta_{ij}\frac{\partial u_k}{\partial x_k} + \mu\left(\frac{\partial u_i}{\partial x_j} + \frac{\partial u_j}{\partial x_i}\right) \tag{4.8}$$

Here, δ_{ij} (called the Kronecker delta) has the value of 1 when $i = j$ and 0 when $i \neq j$. The repeated subscript k indicates that the term $\partial u_k/\partial x_k$ represents a sum of three normal gradients.

The units of Eq. (4.6a) are force per unit volume. The units of pressure and viscous stress are force per unit area. Thus, a pressure gradient has the units of force per unit volume and, therefore, according to Newton's second law of motion, is equal to the change in momentum as defined by Eqs. (4.5) and (4.6a),

$$\frac{\partial \tau_{ij}}{\partial x_j} - \frac{\partial P}{\partial x_i} = \rho\left(\frac{\partial u_i}{\partial t} + u_j\frac{\partial u_i}{\partial x_j}\right) \tag{4.9}$$

Because i may take any of three values in a Cartesian coordinate system, Eq. (4.9) is a compact way of writing three equations. Notice that i is the free index in the equation whereas j is a repeated index indicating summation. Because we are dealing with a three-dimensional space, the terms involving j actually represent a sum of three terms.

If we wish to apply Eq. (4.9) to water or other liquids we need to add the term ρg to the left side of the equation when the index i refers to the direction normal to

the Earth's surface. This term is called a body force or a potential to indicate that it is due to a gravitational attraction between the liquid and the Earth. For gases the mass of a small volume is insufficient to produce a significant gravitational attraction; in that case the term is ignored.

Equations (4.9) are a system of second-order nonlinear partial differential equations, second order because τ_{ij} already represents partial derivatives of the velocity components with respect to the position variables. If the density is constant (the case with which we will be concerned) there are four dependent variables: the pressure and the three velocity components. Because Eq. (4.9) represents only three equations, we need another equation to make the system solvable. We find this in the equation for mass conservation

$$\rho\frac{\partial u_j}{\partial x_j} = 0 \tag{4.10}$$

If we limit our discussion to steady flow, the first term on the right-hand side of Eq. (4.9) can be set equal to zero.

If we multiply Eq. (4.10) by u_i and then add it to the steady form of Eq. (4.9) we obtain

$$\frac{\partial \tau_{ij}}{\partial x_j} - \frac{\partial P}{\partial x_i} = \rho u_i\frac{\partial u_j}{\partial x_j} + \rho u_j\frac{\partial u_i}{\partial x_j}$$

or

$$\frac{\partial \tau_{ij}}{\partial x_j} - \frac{\partial P}{\partial x_i} = \rho\frac{\partial u_i u_j}{\partial x_j} \tag{4.11}$$

Prandtl's boundary-layer concept asserts that, except for shock wave effects, the influence of viscous stresses in flow over solid bodies is confined to a layer next to the surface (termed the boundary layer in English), which is thin compared with some characteristic dimension of the body. For our present purpose we will limit consideration to plane flows, that is, to flows in two dimensions. We will also restrict consideration to those cases where the boundary has no more than a small slope with respect to the freestream. If, in addition, it is curved we assume that the radius of curvature is very large. As a consequence of these assumptions, the pressure is essentially constant through the boundary layer. Outside the boundary layer we can determine the variation of the pressure in the streamwise direction from a solution of the inviscid equations of motion. Thus, we have essentially removed the pressure as a dependent variable in the problem.

Let us now consider the order of magnitude of terms in the equation of mass conservation for two-dimensional flow

$$\frac{\partial u_1}{\partial x_1} + \frac{\partial u_2}{\partial x_2} = 0$$

We may write this as

$$\mathcal{O}\left(\frac{U}{L}\right) + \mathcal{O}\left(\frac{u_2}{\delta}\right) = 0 \tag{4.12}$$

where

δ = boundary-layer thickness
L = characteristic dimension
u_2 = velocity component normal to the surface in the boundary layer
U = freestream velocity, parallel to x_1
$\mathcal{O}(\,)$ = order of

We see from this that

$$u_2 = \mathcal{O}\left(\frac{\delta}{L}U\right) \tag{4.13}$$

Because of our assumptions

$$\frac{\delta}{L} \ll 1 \tag{4.14a}$$

$$\frac{u_2}{U} \ll 1 \tag{4.14b}$$

We wish now to apply these considerations to the stress terms

$$\tau_{11} = \frac{4}{3}\mu\frac{\partial u_1}{\partial x_1} - \frac{2}{3}\mu\frac{\partial u_2}{\partial x_2} \tag{4.15a}$$

$$\tau_{12} = \tau_{21} = \mu\left(\frac{\partial u_1}{\partial x_2} + \frac{\partial u_2}{\partial x_1}\right) \tag{4.15b}$$

$$\tau_{22} = \frac{4}{3}\mu\frac{\partial u_2}{\partial x_2} - \frac{2}{3}\mu\frac{\partial u_1}{\partial x_1} \tag{4.15c}$$

The order of magnitude of these terms are as follows:

$$\tau_{11} = \mathcal{O}\left(\mu\frac{U}{L}\right) + \mathcal{O}\left(\mu\frac{u_2}{\delta}\right) = \mathcal{O}\left(\mu\frac{U}{L}\right) \tag{4.16a}$$

$$\tau_{12} = \mathcal{O}\left(\mu\frac{U}{\delta}\right) + \mathcal{O}\left(\mu\frac{u_2}{L}\right) = \mathcal{O}\left(\mu\frac{U}{\delta}\right) \tag{4.16b}$$

$$\tau_{22} = \mathcal{O}\left(\mu\frac{u_2}{\delta}\right) + \mathcal{O}\left(\mu\frac{U}{L}\right) = \mathcal{O}\left(\mu\frac{U}{L}\right) \tag{4.16c}$$

Applying the same rationale to the x_1 momentum equation, Eq. (4.11) with $i = 1$, yields

$$\mathcal{O}\left(\rho\frac{U^2}{L}\right) + \mathcal{O}\left(\rho U\frac{u_2}{\delta}\right) = \mathcal{O}\left(\mu\frac{U}{\delta^2}\right) - \frac{\partial P}{\partial x_1} + \mathcal{O}\left(\mu\frac{U}{\delta^2}\right) \tag{4.17}$$

This can be written as

$$\mathcal{O}\left(\rho\frac{U^2}{L}\right)[\mathcal{O}(1) + \mathcal{O}(1)] = -\frac{\partial P}{\partial x_1} + \mathcal{O}\left(\mu\frac{U}{\delta^2}\right)\left[\mathcal{O}\left(\frac{\delta^2}{L}\right) + \mathcal{O}(1)\right] \tag{4.18}$$

By removing the terms that the foregoing analysis shows are small relative to the other terms, we obtain the Prandtl boundary-layer equations,

$$\rho\frac{\partial u_1^2}{\partial x_1} + \rho\frac{\partial u_1 u_2}{\partial x_2} = -\frac{\partial P}{\partial x_1} + \frac{\partial \tau_{12}}{\partial x_2} \tag{4.19a}$$

$$\rho\frac{\partial u_1}{\partial x_1} + \rho\frac{\partial u_2}{\partial x_2} = 0 \tag{4.19b}$$

From the foregoing it can be seen that

$$\mathcal{O}\left(\rho\frac{U^2}{L}\right) = \mathcal{O}\left(\mu\frac{U}{\delta^2}\right)$$

or

$$\delta^2 = \mathcal{O}\left(\frac{\mu U L}{\rho U^2}\right) = \mathcal{O}\left(L^2\frac{\mu}{\rho U L}\right) = \mathcal{O}\left(\frac{L^2}{Re_N}\right) \tag{4.20}$$

Therefore,

$$\delta \propto \frac{L}{\sqrt{Re_N}} \tag{4.21a}$$

where

$$Re_N = \rho U L/\mu \tag{4.21b}$$

Notice that the momentum equation in the x_2 direction has been discarded because all of its terms are of lower order than the terms retained in the x_1 momentum equation. The reader is urged to follow the procedure indicated and verify the boundary-layer equations.

4.4 Boundary Layer and Displacement Thickness

To develop some of the concepts associated with boundary layers, consider the viscous flow over a flat plate aligned with the stream. In contrast with the inviscid case where the flow slips along the surface unimpeded, viscous flow has zero relative velocity at a solid boundary. The relative velocity increases as a function of distance away from the boundary until it is equal to the freestream velocity. Because the flow is steady over the flat plate, the velocity in the x_1 direction does not change; the freestream pressure is also constant for this configuration. As a result of these assumptions, the boundary-layer equations reduce to

$$\frac{\partial u_1 u_2}{\partial x_2} = \frac{\mu}{\rho}\left[\frac{\partial}{\partial x_2}\left(\frac{\partial u_2}{\partial x_1}\right) + \frac{\partial}{\partial x_2}\left(\frac{\partial u_1}{\partial x_2}\right)\right] \tag{4.22a}$$

$$\frac{\partial u_1}{\partial x_1} + \frac{\partial u_2}{\partial x_2} = 0 \tag{4.22b}$$

Expanding the term on the left side of Eq. (4.22a) yields

$$u_1\frac{\partial u_2}{\partial x_2} + u_2\frac{\partial u_1}{\partial x_2} = \frac{\mu}{\rho}\left[\frac{\partial^2 u_1}{\partial x_2^2} + \frac{\partial}{\partial x_1}\left(\frac{\partial u_2}{\partial x_2}\right)\right] \tag{4.23}$$

From Eqs. (4.4–4.16b) the second term on the right-hand side of Eq. (4.23) is at

least an order of magnitude smaller than the other term and so is neglected. Thus, we have for this case

$$u_1\frac{\partial u_2}{\partial x_2}+u_2\frac{\partial u_1}{\partial x_2}=\frac{\mu}{\rho}\frac{\partial^2 u_1}{\partial x_2^2} \tag{4.24}$$

Now make the following substitutions:

$$\nu=\frac{\mu}{\rho} \tag{4.25a}$$

$$\eta=x_2\sqrt{\frac{U}{\nu x_1}} \tag{4.25b}$$

$$\psi=\sqrt{\nu x_1 U}\,f(\eta) \tag{4.25c}$$

$$u_1=\frac{\partial\psi}{\partial x_2}=\frac{\partial\psi}{\partial\eta}\frac{\partial\eta}{\partial x_2}=Uf'(\eta) \tag{4.25d}$$

$$u_2=-\frac{\partial\psi}{\partial x_1}=\frac{1}{2}\sqrt{\frac{\nu U}{x_1}}(\eta f'-f) \tag{4.25e}$$

With these substitutions, Eq. (4.24) becomes

$$-\frac{U^2}{2x_1}\eta f'f''+\frac{U^2}{2x_1}(\eta f'-f)f''=\nu\frac{U^2}{x_1\nu}f'''$$

or simply,

$$ff''+2f'''=0 \tag{4.26}$$

The effect of these substitutions has been to transform the set of two nonlinear partial differential equations into a single nonlinear ordinary differential equation. This was accomplished by choosing the new independent variable η to be a function of both of the original spatial coordinates. The boundary conditions on this third-order equation are

$$\eta=0\text{: } f=0,\ f'=0; \qquad \eta=\infty\text{: } f'=1 \tag{4.27}$$

A number of ways have been devised to solve this equation, beginning with Blasius.[20] Almost all have been numerical. We choose to use a familiar numerical technique, the Runge–Kutta method. This involves breaking the equation down into three first-order equations,

$$f'=g \tag{4.28a}$$

$$g'=h \tag{4.28b}$$

$$h'=-\tfrac{1}{2}fh \tag{4.28c}$$

Unfortunately, the Runge–Kutta technique requires initial conditions and one of the boundary conditions available is not an initial condition. Therefore, we will have to choose an initial value of h from another solution of the boundary-layer equations (along with $f=0$, $g=0$). We will pick the value found by Howarth,[21] 0.33206. A short computer program, which performs a fourth-order Runge–Kutta

integration on the equation, follows.

```
      IMPLICIT REAL*8(A-H,O-Z)
      REAL*8 K1,K2,K3,K4
      DIMENSION DU(3),U(3),WU(3),XU(3),YU(3),ZU(3),K1(3),K2(3),
     1K3(3),K4(3)
C
      OPEN(61,FILE='BL.DAT',STATUS='UNKNOWN')
C
      DO 1 J=1,3
      U(J)=0.0D0
1     DU(J)=0.0D0
C
C     ESTIMATE OF INITIAL VALUE OF f''
C
      U(3)=0.33206D0
      TDEL=0.001D0
      ICNT=0
      T=0.0D0
      N=3
      WRITE(61,22) T,(U(I),I=1,3)
      T=TDEL
C
C     BEGIN RUNGE-KUTTA FORWARD INTEGRATION
C
      DO 10 J=1,10001
      ICNT=ICNT+1
      DO 5 I=1,N
5     WU(I)=U(I)
      CALL FUN(DU,WU)
      DO 6 I=1,N
      K1(I)=DU(I)*TDEL
6     XU(I)=U(I)+DU(I)*TDEL/2.0
      CALL FUN(DU,XU)
      DO 7 I=1,N
      K2(I)=DU(I)*TDEL
7     YU(I)=U(I)+DU(I)*TDEL/2.0
      CALL FUN(DU,YU)
      DO 8 I=1,N
      K3(I)=DU(I)*TDEL
8     ZU(I)=U(I)+DU(I)*TDEL
      CALL FUN(DU,ZU)
      DO 9 I=1,N
      K4(I)=DU(I)*TDEL
```

```
 9  U(I)=U(I)+1.0D0/6.0D0*(K1(I)+2.0*K2(I)+2.0D0*K3(I)+K4(I))
    IF(ICNT.EQ.20) WRITE(61,22) T,(U(I),I=1,3)
    IF(ICNT.EQ.20) ICNT=0
10  T=T+TDEL
22  FORMAT(1X,F5.2,1X,3(F11.8,1X))
    RETURN
    END
C
    SUBROUTINE FUN(DU,U)
    IMPLICIT REAL*8(A-H,O-Z)
    DIMENSION DU(3),U(3)
C
C     THIS SUBROUTINE PROVIDES THE EQUATIONS TO BE INTEGRATED
C
    DU(1)=U(2)
    DU(2)=U(3)
    DU(3)=-0.5D0*U(1)*U(3)
    RETURN
    END
```

Here the increment in η is 0.001 and $U(2)$ is f' in Eq. (4.26). $U(3)$ is f'', T is η, and

$$U(1) = f(\eta) = \frac{\psi}{\sqrt{\nu U x_1}} \tag{4.29}$$

Because f' approaches the value of 1.0 in an asymptotic fashion, it is customary to select a value of 0.99 as indicating that the freestream value has been reached. This corresponds to a value of η of approximately 5.0. We will designate as δ the value of x_2 corresponding to $\eta = 5.0$. Thus,

$$\delta = \frac{5.0}{\sqrt{\dfrac{U}{\nu x_1}}}$$

or

$$\frac{\delta}{x_1} = \frac{5.0}{\sqrt{\dfrac{U x_1}{\nu}}} \tag{4.30}$$

Notice that the boundary-layer thickness grows as the square root of the Reynolds number based on length in the streamwise direction.

Figure 4.1 shows the velocity distribution f' in a laminar boundary layer as a function of the new space variable η, as well as the gradient of the velocity f''.

A physically meaningful measure for the boundary-layer thickness is the displacement thickness δ^*. The displacement thickness is that distance by which

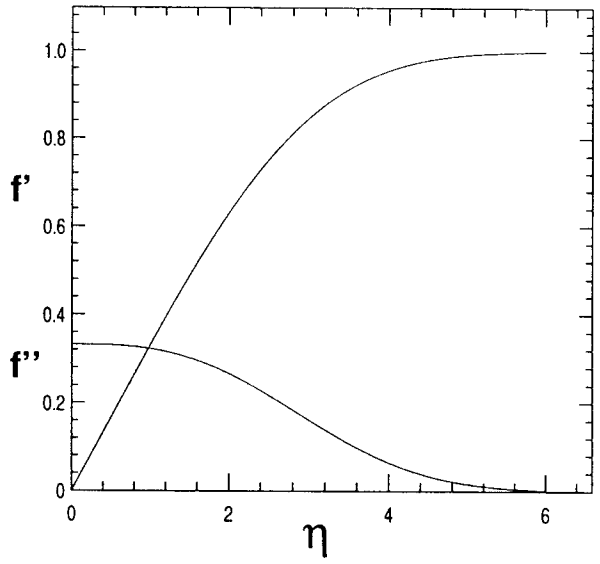

Fig. 4.1 Velocity distribution and its gradient in a laminar boundary layer.

the external potential field of flow is displaced outward as a consequence of the decrease in velocity in the boundary layer. We define the displacement thickness by

$$\delta^* = \int_{x_2=0}^{\infty} \left(1 - \frac{u_1}{U}\right) dx_2 \tag{4.31a}$$

We may also write δ^* as

$$\delta^* = \sqrt{\frac{\nu x_1}{U}} [\eta_1 - f(\eta_1)] \tag{4.31b}$$

where η_1 is a point outside the boundary layer. We can evaluate $\eta_1 - f(\eta_1)$ using the computer program given earlier and obtain a value of 1.7208 for a flat plate. Hence,

$$\delta^* = \frac{1.7208 x_1}{\sqrt{\dfrac{U x_1}{\nu}}} \tag{4.32}$$

Another important quantity is the momentum thickness defined as

$$\theta = \int_{x_2=0}^{\infty} \frac{u_1}{U} \left(1 - \frac{u_1}{U}\right) dx_2 \tag{4.33}$$

For the flat plate at zero incidence

$$\theta = \sqrt{\frac{\nu x_1}{U}} \int_{\eta=0}^{\infty} f'(1 - f')\mathrm{d}\eta$$

or

$$\theta = \frac{0.664 x_1}{\sqrt{\dfrac{U x_1}{\nu}}} \tag{4.34}$$

We can also work out the value of the transverse component of velocity at the outer edge of the boundary layer (when $\eta \to \infty$) as

$$u_2 = \frac{0.8604 U}{\sqrt{\dfrac{U x_1}{\nu}}} \tag{4.35}$$

This means that there is an outward flow because the increasing boundary-layer thickness causes the fluid to be displaced from the wall as it flows along it. This is not a separation because the pressure gradient on the flat plate is zero.

Finally, we can determine the value of the skin friction on the plate. Remember that

$$\tau(x_1) = \mu \left(\frac{\partial u_1}{\partial x_2}\right) = \mu U \sqrt{\frac{U}{\nu x_1}} f''(0)$$

With $f''(0) = 0.33206$, we may write

$$c_f = \frac{2\tau(x_1)}{\rho U^2} = \frac{0.664}{\sqrt{Re_N}} \tag{4.36}$$

When integrated over one surface of the plate we have

$$D = 0.664 b \sqrt{\mu \rho \ell U^3} \tag{4.37}$$

where b is the width of the plate in the direction normal to the flow and ℓ is the length of the plate in the streamwise direction.

A word of caution should be injected at this point. The boundary-layer equations are correctly applied to the flat plate everywhere except in the region near the beginning of the plate, that is, the upstream end of the plate. Here the assumption that $|\partial^2 u_1/\partial x_1^2| \ll |\partial^2 u_1/\partial x_2^2|$ is not satisfied. Note, too, that the numerical values of the various coefficients were derived for a flat plate, that is, for the case where the pressure gradient is always zero. For other pressure distributions, these coefficients will have different values.

4.5 The Momentum Integral Method

In the preceding section we defined some terms commonly used in boundary-layer analysis and showed how one may apply the associated concepts to the simplest of cases: that for flow over a flat plate. The problem of analyzing the flow over more complex bodies quickly grows in difficulty with the complexity of

the body so that for engineering purposes one is driven to consider approximate methods. One of the first methods to find widespread acceptance was developed by von Kármán[22] and is termed the momentum integral method. We will now consider the development of the relevent differential equation. First, we note that in an inviscid stream outside the boundary layer the x_1 momentum equation reduces to

$$\rho U \frac{\mathrm{d}U}{\mathrm{d}x} + \frac{\mathrm{d}P}{\mathrm{d}x} = 0 \tag{4.38}$$

Substitution of Eq. (4.38) into Eq. (4.19a) and integration of the result in the x_2 direction yields the expression

$$\int_{x_2=0}^{h} \left(u_1 \frac{\partial u_1}{\partial x_1} + u_2 \frac{\partial u_1}{\partial x_2} - U \frac{\mathrm{d}U}{\mathrm{d}x_1}\right) \mathrm{d}x_2 = -\frac{\tau_w}{\rho} \tag{4.39}$$

Here h is a point in the x_2 direction outside the boundary layer and τ_w is the shear stress at the wall or boundary.

From the continuity equation,

$$u_2 = -\int_0^{x_2} \frac{\partial u_1}{\partial x_1} \mathrm{d}x_2 \tag{4.40}$$

Substitution of Eq. (4.40) into Eq. (4.39) yields

$$\int_{x_2=0}^{h} \left(u_1 \frac{\partial u_1}{\partial x_1} - \frac{\partial u_1}{\partial x_2} \int_0^{x_2} \frac{\partial u_1}{\partial x_1} \mathrm{d}x_2 - U \frac{\mathrm{d}U}{\mathrm{d}x_1}\right) \mathrm{d}x_2 = -\frac{\tau_w}{\rho} \tag{4.41}$$

Integrating the second term by parts leads to the result

$$\int_{x_2=0}^{h} \left(\frac{\partial u_1}{\partial x_2} \int_0^{x_2} \frac{\partial u_1}{\partial x_1} \mathrm{d}x_2\right) \mathrm{d}x_2 = U \int_0^h \frac{\partial u_1}{\partial x_1} \mathrm{d}x_2 - \int_0^h u_1 \frac{\partial u_1}{\partial x_1} \mathrm{d}x_2$$

so that

$$\int_0^h \left(2u_1 \frac{\partial u_1}{\partial x_1} - U \frac{\partial u_1}{\partial x_1} - U \frac{\mathrm{d}U}{\mathrm{d}x_1}\right) \mathrm{d}x_2 = -\frac{\tau_w}{\rho}$$

which can be contracted to

$$\int_0^h \frac{\partial}{\partial x_1} [u_1 (U - u_1)] \mathrm{d}x_2 + \frac{\mathrm{d}U}{\mathrm{d}x_1} \int_0^h (U - u_1) \mathrm{d}x_2 = -\frac{\tau_w}{\rho} \tag{4.42}$$

Because the integrand in both integrals vanishes outside the boundary layer we can set $h \to \infty$. Now making use of our definitions for displacement thickness and momentum thickness we write

$$\delta^* U = \int_{x_2=0}^{\infty} (U - u_1) \mathrm{d}x_2$$

$$\theta U^2 = \int_{x_2=0}^{\infty} u_1 (U - u_1) \mathrm{d}x_2$$

When these relations are substituted in Eq. (4.42) we have the momentum integral equation as

$$\frac{\tau_w}{\rho} = \frac{\mathrm{d}}{\mathrm{d}x_1}(\theta U^2) + \delta^* U \frac{\mathrm{d}U}{\mathrm{d}x_1} \tag{4.43}$$

Another form of Eq. (4.43)

$$\frac{\mathrm{d}\theta}{\mathrm{d}x_1} + \frac{2\theta + \delta^*}{U}\frac{\mathrm{d}U}{\mathrm{d}x_1} = \frac{\nu}{U^2}\left.\frac{\partial u_1}{\partial x_2}\right|_{x_2=0} \tag{4.44}$$

is perhaps more useful for our present purpose. We note that Eq. (4.43) or Eq. (4.44) is only an approximate description of boundary-layer flow because the process of integration smooths out local departures from mean values.

To solve Eq. (4.44), that is, to find θ, δ^*, and τ_w as functions of x_1, we require an expression for $u_1(x_2)$. We shall assume, following Polhausen,[23] that we can represent this function by the polynomial

$$\frac{u_1}{U} = A\eta + B\eta^2 + C\eta^3 + D\eta^4 \tag{4.45}$$

where η is x_2/δ. We choose this polynomial because it is the lowest-order polynomial that can represent the essential characteristics of what we know of boundary-layer flow and is the highest-order polynomial for which we can evaluate the constants. These are found from the boundary conditions; at $x_2 = 0$

$$u_1 = 0; \qquad \frac{\mathrm{d}P}{\mathrm{d}x} = -\rho U \frac{\mathrm{d}U}{\mathrm{d}x_1} \tag{4.46a}$$

and at $x_2 = \delta$

$$u_1 = U; \qquad \frac{\partial u_1}{\partial x_2} = 0; \qquad \frac{\partial^2 u_1}{\partial x_2^2} = 0 \tag{4.46b}$$

The result is

$$A = 2 + \frac{1}{6}\frac{\delta^2}{\nu}\frac{\mathrm{d}U}{\mathrm{d}x_1} \tag{4.47a}$$

$$B = -\frac{1}{2}\frac{\delta^2}{\nu}\frac{\mathrm{d}U}{\mathrm{d}x_1} \tag{4.47b}$$

$$C = -2 + \frac{1}{2}\frac{\delta^2}{\nu}\frac{\mathrm{d}U}{\mathrm{d}x_1} \tag{4.47c}$$

$$D = 1 - \frac{1}{6}\frac{\delta^2}{\nu}\frac{\mathrm{d}U}{\mathrm{d}x_1} \tag{4.47d}$$

Substitution of these results into Eq. (4.45) gives

$$\frac{u_1}{U} = 2\eta - 2\eta^3 + \eta^4 + \frac{1}{6}\frac{\delta^2}{\nu}\frac{\mathrm{d}U}{\mathrm{d}x_1}(\eta - 3\eta^2 + 3\eta^3 - \eta^4) \tag{4.48}$$

With this definition for u_1/U we have

$$\delta^* = \delta\left[\frac{3}{10} - \frac{1}{120}\frac{\delta^2}{\nu}\frac{\mathrm{d}U}{\mathrm{d}x_1}\right] \tag{4.49a}$$

$$\theta = \delta\left[\frac{37}{315} - \frac{1}{945}\frac{\delta^2}{\nu}\frac{\mathrm{d}U}{\mathrm{d}x_1} - \frac{1}{9072}\left(\frac{\delta^2}{\nu}\frac{\mathrm{d}U}{\mathrm{d}x_1}\right)^2\right] \tag{4.49b}$$

$$\tau_w = \frac{\mu U}{\delta}\left[2 + \frac{1}{6}\frac{\delta^2}{\nu}\frac{\mathrm{d}U}{\mathrm{d}x_1}\right] \tag{4.49c}$$

Substituting these expressions into Eq. (4.44) yields

$$\left[\frac{37}{315} - \frac{3\delta^2}{945\nu}\frac{\mathrm{d}U}{\mathrm{d}x_1} - \frac{5\delta^4}{9072\nu^2}\left(\frac{\mathrm{d}U}{\mathrm{d}x_1}\right)^2\right]\frac{\mathrm{d}\delta}{\mathrm{d}x_1} - \frac{1}{945}\frac{\delta^3}{\nu}\frac{\mathrm{d}^2U}{\mathrm{d}x_1^2}$$
$$- \frac{2\delta^5}{9072\nu^2}\frac{\mathrm{d}U}{\mathrm{d}x_1}\frac{\mathrm{d}^2U}{\mathrm{d}x_1^2} + \frac{2\delta}{U}\left[\frac{37}{315} - \frac{1}{945}\frac{\delta^2}{\nu}\frac{\mathrm{d}U}{\mathrm{d}x_1} - \frac{1}{9072}\left(\frac{\delta^2}{\nu}\frac{\mathrm{d}U}{\mathrm{d}x_1}\right)^2\right]\frac{\mathrm{d}U}{\mathrm{d}x_1}$$
$$+ \frac{\delta}{U}\left[\frac{3}{10} - \frac{1}{120}\frac{\delta^2}{\nu}\frac{\mathrm{d}U}{\mathrm{d}x_1}\right]\frac{\mathrm{d}U}{\mathrm{d}x_1} = \frac{\mu}{\rho U\delta}\left[2 + \frac{1}{6}\frac{\delta^2}{\nu}\frac{\mathrm{d}U}{\mathrm{d}x_1}\right] \tag{4.50}$$

Equation (4.50) is a very nonlinear first-order ordinary differential equation with δ as the dependent variable and x_1 as the independent variable. Notice that U, $\mathrm{d}U/\mathrm{d}x_1$, and $\mathrm{d}^2U/\mathrm{d}x_1^2$ must all be supplied as data obtained from the potential solution (the solution for the flow outside the boundary layer) and that they are all functions of position along the body, x_1. Near $x_1 = 0$ we must select a small finite value for the dependent variable because the equation is singular at $x_1 = 0$. Generally, something on the order of $\sqrt{x_1}$ will be satisfactory. This can be seen for the case of flow over a flat plate where Eq. (4.50) reduces to

$$\frac{37}{315}\frac{\mathrm{d}\delta}{\mathrm{d}x_1} = \frac{2\mu}{\rho U\delta} \tag{4.51}$$

whose solution is

$$\frac{37}{315}\delta^2 = \frac{4\mu x_1}{\rho U}$$

or

$$\delta = \frac{5.84x_1}{\sqrt{\dfrac{Ux_1}{\nu}}} \tag{4.52}$$

The coefficient 5.84 is somewhat greater than the value of approximately 5.0 found by solution of the third-order differential equation. However, u_1/U is less than 0.8% greater than its value at 5.0. We noted that the upper edge of the

boundary layer is defined somewhat nebulously. Thus, the approximations made in developing Eq. (4.50) seem to have been reasonable. We will employ the fact that the momentum integral method overpredicts the displacement thickness to justify an empirical correction to the computed displacement thickness given by the computer program discussed in Chapter 5. In the program the Reynolds number is simply multiplied by a factor of 2 because this results in a slightly thinner boundary layer. Of course, the factor of 2 was chosen because of several values tried it produced the best agreement between predicted values and measured values.

Schlichting[24] describes the more commonly used methods for solving the momentum integral equation for a variety of flow situations. Interested readers will also find therein a discussion of a finite difference approach for solving the equation.

It is evident from Eq. (4.47) that the velocity distribution through the boundary layer is very dependent on the pressure distribution outside the boundary layer. This effect is expressed in Eq. (4.47) by the sign and magnitude of the term dU/dx_1. When dU/dx_1 is positive δ grows more slowly than given by Eq. (4.52). When dU/dx_1 is negative, that is, when the pressure gradient is adverse, δ grows more rapidly than as given by Eq. (4.52). In the face of a sufficiently strong adverse pressure gradient, $\partial u_1/\partial x_2$ will become zero at the wall at some point; the boundary layer then is beginning to separate, that is, to leave the surface of the body. It leaves behind a region of zero mean velocity relative to the body surface in which the pressure is approximately the same throughout. This region is usually at a lower pressure than that on the windward side of the body is and, therefore, is the origin of the body's form or profile drag.

4.5.1 Application to Turbulent Boundary Layers

The preceding development, either explicitly or implicitly, has referred to laminar boundary layers, those flows in which the fluid remains layerlike as it moves over a body surface. Another very important and probably even more common type of viscous flow is turbulent flow, so called because groups of fluid particles in such flows do not appear to follow well-defined paths in the manner of streamlines but rather move in seemingly disorganized fashion. Since the turn of the century researchers have attempted to describe such flows in a satisfactory analytical manner without a great deal of success. As a result, workers who had to devise a means of computing the resistance to motion of a body on which the boundary layer was turbulent have had to resort to semiempirical schemes. That none of the many theoretical models proposed over the years to describe turbulent flows is uniformly satisfactory is probably an indication that an entirely new approach, one divorced from the continuum model basis from which the laminar flow description evolved, must be used.

We may note that the coefficient of dynamic viscosity for air is

$$\mu = 373 \times 10^{-9} \left(\frac{T}{519}\right)^{1.5} \frac{717}{T + 198} \tag{4.53}$$

where μ has dimensions of slugs per foot-seconds and T is in degrees Rankine. One of the devices by which the momentum integral equation has been used to describe turbulent flows has been to replace the expression for the shearing stress

at the wall

$$\tau_w = \mu \left.\frac{\partial u_1}{\partial x_2}\right|_{x_2=0}$$

with an empirical relationship developed by Ludwieg and Tillmann (as quoted by Schlichting[24])

$$\tau_w = \frac{\rho U^2 \left(0.123 \times 10^{-0.678 \frac{\delta^*}{\theta}}\right)}{\left(\frac{U\theta}{\nu}\right)^{0.268}} \tag{4.54}$$

while using an expression for u_1/U given by

$$\frac{u_1}{U} = \left(\frac{x_2}{\delta}\right)^{\frac{1}{n}} \tag{4.55}$$

where n is between 4 and 6 but is usually taken as the latter value.

The use of Eq. (4.54) in Eq. (4.44) still leaves the resulting equation nonintegrable because an explicit relation between δ^* and θ has not been given. One way around this problem is to multiply the reduced x_1 momentum equation (4.43) by u_1 and then integrate the equation with respect to x_2. We obtain what might be termed an energy integral equation

$$\frac{1}{U^3}\frac{d}{dx_1}[U^3\delta^{**}] = \int_0^\delta \frac{\tau_w}{\rho U^2}\left(\frac{u_1}{U}\right) dx_2 \tag{4.56}$$

analogous to the momentum equation, Eq. (4.43). The name, of course, refers to the fact that momentum times velocity has the units of energy. Here,

$$\delta^{**} = \int_0^\delta \frac{u_1}{U}\left(1 - \frac{u_1}{U}\right) dx_2 \tag{4.57}$$

It has been found experimentally that there exists a unique relationship between δ^*/θ and δ^{**}/θ, which can be expressed as

$$\frac{\delta^{**}}{\theta} = \frac{1.269\left(\frac{\delta^*}{\theta}\right)}{\left(\frac{\delta^*}{\theta}\right) - 0.379} \tag{4.58}$$

Further, experiments have led to the conclusion that

$$\int_0^\delta \frac{\tau_w}{\rho U^2}\frac{d}{dx_2}\left(\frac{u_1}{U}\right) dx_2 = \frac{0.56 \times 10^{-2}}{\left(\frac{U\theta}{\nu}\right)^{1/6}} \tag{4.59}$$

Substitution of these experimental results into Eq. (4.56) yields

$$\frac{1}{U^3}\frac{\mathrm{d}}{\mathrm{d}x_1}\left[\frac{1.269U^3\left(\frac{\delta^*}{\theta}\right)\theta}{\left(\frac{\delta^*}{\theta}\right)-0.379}\right]=\frac{0.56\times10^{-2}}{\left(\frac{U\theta}{\nu}\right)^{1/6}} \tag{4.60}$$

whereas Eq. (4.54) substituted into Eq. (4.44) gives

$$\frac{\mathrm{d}\theta}{\mathrm{d}x_1}+\frac{2\theta+\delta^*}{U}\frac{\mathrm{d}U}{\mathrm{d}x_1}=\frac{0.123\times10^{-0.678\frac{\delta^*}{\theta}}}{\left(\frac{U\theta}{\nu}\right)^{0.268}} \tag{4.61}$$

Simultaneous solution of Eqs. (4.60) and (4.61) will yield $\delta^*(x_1)$ and $\theta(x_1)$. When these results are substituted into Eq. (4.54), one has $\tau_w(x_1)$. The skin-friction drag is then computed by integrating τ_w over both surfaces.

4.5.2 Transition

As has been indicated, the correct expression for τ_w depends on whether the boundary layer is laminar or turbulent. Generally, one would expect the boundary layer to be laminar over the forward portion of a body and turbulent over the aft portion. The change between laminar and turbulent motion is called transition. Equation (4.50) would give a good approximation expression for τ_w upstream of the transition point and Eq. (4.54) gives a good approximation downstream of this point. Because the boundary layer already has a finite thickness at the transition point, one chooses as a starting point for the turbulent calculation that point which will give the same δ as the laminar solution beginning at the leading edge. The laminar values of τ_w and δ^* are used up to the point of transition, and the turbulent values are used downstream. They are approximately the same at transition.

The beginning of transition has been found to occur at Reynolds numbers from 3×10^5 to 4×10^6 and depends on such factors as surface roughness, freestream turbulence, and $\mathrm{d}U/\mathrm{d}x_1$. The latter is the only one that actually can be determined before the wing is built. A laminar boundary layer is said to be unstable, that is, it tends to become turbulent, when a velocity disturbance in this boundary layer can grow.

Tollmein was able to show that a necessary and sufficient condition for neutral stability of disturbances in laminar boundary layers is the existence of a point of inflection in the boundary layer's velocity profile $u_1(x_2)$. Using a sixth-order polynomial to represent the velocity profile, Schlichting and Ulrich were able to plot a relationship between the value of $U\delta^*/\nu$ for which an inflection point exists and $(\delta^2/\nu)(\mathrm{d}U/\mathrm{d}x_1)$. With this plot one can take values of δ, δ^*, U, $\mathrm{d}U/\mathrm{d}x_1$, and ν and determine whether or not the boundary layer is unstable.

Most computer programs that perform complete front-to-back boundary-layer calculations over a body include a form of this plot or similar relationships as curve fits or table lookups from which they can determine whether to use the laminar form or the turbulent form of the equation for calculations. For our purpose we will not detail further the steps by which a determination of transition occurrence is made in specific codes but merely note that a criterion based on these considerations is generally included. The interested user can usually determine what is being done in a specific code by consulting the boundary-layer subroutine headers and the running comments in the source code.

4.6 Examples

In addition to an exposition of some elements of boundary-layer theory, consideration of some of the simple solutions to the exact equations for viscous flow can be instructive by demonstrating some of the other characteristics of viscous flows. We shall develop solutions for a few of these, as well as examine some classical results obtained with boundary-layer theory.

4.6.1 Steady Internal Axisymmetric Flow with Various Boundary Conditions

For this problem we will consider only incompressible flow in a tube long enough that we can assume $\partial v_z/\partial z = 0$. The momentum equations for this case reduce to

$$\frac{\mathrm{d}P}{\mathrm{d}z}=\mu\left(\frac{\mathrm{d}^2v_z}{\mathrm{d}r^2}+\frac{1}{r}\frac{\mathrm{d}v_z}{\mathrm{d}r}\right) \tag{4.62}$$

where in our cylindrical coordinate system z is the axial coordinate and r is the radial coordinate. We assume that there is no angular motion of the fluid about the centerline of our geometry. We are able to write this as an ordinary differential equation because we have assumed that $\mathrm{d}P/\mathrm{d}z$ may be considered to be a constant. We will consider the solution of this equation, termed the Hagen–Poiseuille equation, for the following cases: case I, flow in a tube of radius R, $\mathrm{d}P/\mathrm{d}z \neq 0$; case II, flow in the annular region between a tube of radius R_1 and a tube of radius R_2, $\mathrm{d}P/\mathrm{d}z \neq 0$; case III, same as case II except that $(R_2 - R_1)/R_1 \ll 1$; case IV, flow in the annular region between a tube of radius R_1 and a tube of radius R_2, $\mathrm{d}P/\mathrm{d}z = 0$, R_2 moves axially relative to R_1; and case V, same as case IV except that $\mathrm{d}P/\mathrm{d}z \neq 0$.

Case I. The boundary conditions are: $v_z = 0$ at $r = R$ and $\mathrm{d}v_z/\mathrm{d}r = 0$ at $r = 0$. Equation (4.62) can also be written

$$\frac{\mathrm{d}}{\mathrm{d}r}\left(r\frac{\mathrm{d}v_z}{\mathrm{d}r}\right)=\frac{r}{\mu}\frac{\mathrm{d}P}{\mathrm{d}z}$$

which can be integrated to

$$\frac{r\,\mathrm{d}v_z}{\mathrm{d}r}=\left(\frac{1}{2\mu}\frac{\mathrm{d}P}{\mathrm{d}z}\right)r^2+C$$

and integrated a second time to

$$v_z=\left(\frac{1}{2\mu}\frac{\mathrm{d}P}{\mathrm{d}z}\right)\frac{r^2}{2}+C\,\ell_n r+C_2 \tag{4.63}$$

Because $\mathrm{d}v_z/\mathrm{d}r = 0$ when $r = 0$, $C = 0$. Because $v_z = 0$ when $r = R$,

$$C_2=-\left(\frac{1}{2\mu}\frac{\mathrm{d}P}{\mathrm{d}z}\right)\frac{R^2}{2}$$

and

$$v_z = -\frac{1}{4\mu}\frac{dP}{dz}(R^2 - r^2) \tag{4.64}$$

Case II. The boundary conditions are now $v_z = 0$ at $r = R_1$ and $v_z = 0$ at $r = R_2$. When these are applied to Eq. (4.63) we have

$$0 = \left(\frac{1}{2\mu}\frac{dP}{dz}\right)\frac{R_1^2}{2} + C\,\ell n R_1 + C_2$$

$$0 = \left(\frac{1}{2\mu}\frac{dP}{dz}\right)\frac{R_2^2}{2} + C\,\ell n R_2 + C_2$$

a system of two equation we must solve for C and C_2. We can eliminate C_2 by subtracting the first equation from the second,

$$0 = \left(\frac{1}{4\mu}\frac{dP}{dz}\right)(R_2^2 - R_1^2) + C\,\ell n\frac{R_2}{R_1}$$

From this we can find C as

$$C = -\left(\frac{1}{4\mu}\frac{dP}{dz}\right)\left(\frac{R_2^2 - R_1^2}{\ell n\left(\frac{R_2}{R_1}\right)}\right)$$

and C_2 as

$$C_2 = \left(\frac{1}{4\mu}\frac{dP}{dz}\right)\left(\frac{R_2^2 - R_1^2}{\ell n\left(\frac{R_2}{R_1}\right)}\ell n R_1 - R_1^2\right)$$

Hence,

$$v_z = \frac{1}{4\mu}\frac{dP}{dz}\left[r^2 - R_1^2 - \left(\frac{R_2^2 - R_1^2}{\ell n\left(\frac{R_2}{R_1}\right)}\right)\ell n\frac{r}{R_1}\right] \tag{4.65}$$

Case III. For this case R_1 is approximately R_2 but both are large compared with their difference. As a result, the term on the right side of Eq. (4.62) $1/r \to 0$. The differential equation is then

$$\frac{d^2 v_z}{dr^2} = \frac{1}{\mu}\frac{dP}{dz}$$

The first integral is

$$\frac{dv_z}{dr} = \frac{1}{\mu}\frac{dP}{dz}r + C$$

and the second integral is

$$v_z = \frac{1}{\mu}\frac{dP}{dz}\frac{r^2}{2} + Cr + C_2$$

With the boundary conditions applied we have

$$0 = \frac{1}{\mu}\frac{dP}{dz}\frac{R_1^2}{2} + CR_1 + C_2$$

$$0 = \frac{1}{\mu}\frac{dP}{dz}\frac{R_2^2}{2} + CR_2 + C_2$$

As before, subtract the first from the second to eliminate C_2 with the result that

$$\frac{1}{2\mu}\frac{dP}{dz}(R_2^2 - R_1^2) + C(R_2 - R_1) = 0$$

and

$$C = -\frac{1}{2\mu}\frac{dP}{dz}\left[\frac{R_2^2 - R_1^2}{R_2 - R_1}\right]$$

Then C_2 is found by back substitution

$$C_2 = -\frac{1}{2\mu}\frac{dP}{dz}\left[R_2^2 - (R_2 + R_1)R_2\right]$$

The equation then reads

$$v_z = \frac{1}{2\mu}\frac{dP}{dz}[r^2 - (R_2 + R_1)r + R_1 R_2] \tag{4.66}$$

This is the equation of a parabola whose maximum value is located at

$$r = \frac{R_1 + R_2}{2}$$

Case IV. The boundary at R_1 has a velocity $-U$. The boundary at R_2 is fixed and $dP/dz = 0$. Then,

$$v_z = -U\frac{\ell n\left(\frac{R_2}{r}\right)}{\ell n\left(\frac{R_2}{R_1}\right)} \tag{4.67}$$

If R_1 is large and the distance h between R_1 and R_2 is small, then Eq. (4.67) can be written as

$$v_z = -U\left(\frac{h - r}{h}\right) \tag{4.67a}$$

which is essentially the classical Couette solution for plane flow if r is assumed to go from 0 to h.

Case V. The boundary at R_1 has a velocity $-U$. The boundary at R_2 is fixed and $dP/dz \neq 0$. For this case,

$$v_z = -\frac{1}{4\mu}\frac{dP}{dz}\left[R_2^2 - r^2 + \left(\frac{U + \left(\frac{1}{4\mu}\frac{dP}{dz}\right)(R_1^2 - R_2^2)}{\left(\frac{1}{4\mu}\frac{dP}{dz}\right)\ell n\frac{R_2}{R_1}}\right)\ell n\frac{R_2}{r}\right] \tag{4.68}$$

Depending on the signs and magnitudes of U and dP/dz, the velocity profiles may be quite unusual. In fact, it is possible to move the boundary at R_1 at such a velocity that there is no net fluid flow despite the presence of dP/dz.

To compute the volume of fluid flow in the channel we construct an element of area $r\,dr\,d\theta$, multiply this element of volume by its velocity, and integrate with respect to r and θ

$$Q = \int_0^{2\pi}\int_0^R v_z r\,dr\,d\theta$$

or, with the expression for the fluid velocity in case I,

$$Q = \int_0^{2\pi}\int_0^R \left[-\frac{1}{4\mu}\frac{dP}{dz}(R^2 - r^2)\right] r\,dr\,d\theta$$

The result of the first integration yields

$$Q = \int_0^{2\pi} \frac{-1}{4\mu}\frac{dP}{dz}\left[R^2\frac{r^2}{2} - \frac{r^4}{4}\right]_0^R d\theta$$

Finally, carrying out the indicated evaluation and integrating with respect to θ yields

$$Q = -\frac{\pi}{8\mu}\frac{dP}{dz}R^4 \tag{4.69}$$

If desired, the flow quantities in the other geometries can be computed in a similar manner.

4.6.2 Some Classical Boundary-Layer Solutions

In this section we will either briefly sketch methods for obtaining solutions or merely state the result for boundary layers on some simple bodies. The object is to give the reader an indication of the nature of these solutions.

The first problem we will consider is the steady flow over a circular cylinder normal to the stream. Following Blasius we will write the velocity as a power series (using the notation of Schlichting):

$$U(x) = u_1 x + u_3 x^3 + u_5 x^5 + \cdots \tag{4.70}$$

We will call y the spatial coordinate normal to the freestream direction and we will normalize it as follows:

$$\eta = y\sqrt{\frac{u_1}{\nu}} \tag{4.71}$$

This leads to the form

$$\psi = \sqrt{\frac{\nu}{u_1}}\,[u_1 f_1(\eta) + 4u_3 f_3(\eta) + 6u_5 f_5(\eta) + \cdots] \tag{4.72}$$

for the stream function and permits us to calculate $u = \partial\psi/\partial y$ and $v = -(\partial\psi/\partial x)$. Substituting these expressions into the equation of motion (4.24) and comparing coefficients of like powers permits us to write a series of ordinary differential equations, the first two of which are

$$f_1'^2 - f_1 f_1'' = 1 + f_1''' \tag{4.73a}$$

$$4f_1' f_3' - 3f_1'' f_3 - f_1 f_3'' = 1 + f_3''' \tag{4.73b}$$

The associated boundary conditions at $\eta = 0$ are

$$f_1 = F_1' = 0; \qquad f_3 = f_3' = 0 \tag{4.74a}$$

and at $\eta = \infty$ are

$$f' = 1; \qquad f_3' = \tfrac{1}{4} \tag{4.74b}$$

Now the potential flow solution for the velocity around a cylinder is

$$u(x) = U_\infty \sin\frac{x}{R}$$

where R refers to the radius of the cylinder. If we expand the sine function in a series and compare terms with Eq. (4.70) we obtain

$$u_1 = 2\frac{U_\infty}{R} \tag{4.75a}$$

$$u_3 = -\frac{1}{3}\frac{U_\infty}{R^3} \tag{4.75b}$$

$$\eta = \frac{y}{R}\sqrt{\frac{2U_\infty R}{\nu}} \tag{4.75c}$$

We may then proceed to solve Eq. (4.73). From the solutions we can obtain the velocity profiles for the boundary-layer flow over the cylinder, which are plotted in nondimensional form as $(y/R)\sqrt{U_\infty R/\nu}$ on the ordinate and u/U_∞ on the abscissa. Notice that the flow is accelerating from the stagnation point all of the way to the top of the cylinder. Because of the favorable pressure gradient, the boundary layer grows very slowly but still as $1/\sqrt{Re_N}$. However, once the flow begins to move over the lea side of the cylinder, the pressure gradient becomes increasingly unfavorable and the condition for separation is found at an angle from the stagnation point of 108 deg. (More terms than those used here must be retained in the series to obtain this value because of the existence of the increasingly adverse pressure gradient.)

How such knowledge can sometimes be put to good use in an unusual way may be illustrated by the following example. The author once wished to determine the discharge characteristics of a nozzle with an upstream wall that was turned using a tool with a rectangular shape from which a quarter-circle section had been

removed. The throat radius of the nozzle was a little less than one-third the wall radius. It was desired to find a semi-empirical expression for the displacement thickness of the boundary layer at the throat because this is related to the mass deficiency in the flow that passes through the throat. We assume that an expression of the sort

$$\left(\frac{r-\delta^*}{r}\right)^2 = \frac{r^2 - 2r\delta^* + (\delta^*)^2}{r^2} \tag{4.76}$$

represents the ratio of the actual flow area to the ideal. This expression is approximately

$$1 - 2\left(\frac{\delta^*}{r}\right)$$

and can be written approximately as

$$\frac{1}{1 + \dfrac{2\delta^*}{r}} \tag{4.77}$$

through use of the binomial theorem. Now, for such a flow we assume further that

$$\frac{\delta^*}{r} = \frac{C}{\sqrt{\frac{Ud}{\nu}}} \tag{4.78}$$

where C is a constant whose value can be estimated but whose actual value will be determined experimentally and d is the diameter of the nozzle throat, which can be related to the distance along the nozzle wall from the point where the nozzle wall is normal to the stream direction to the throat through a constant factor for any given nozzle of this general geometric shape. With Eq. (4.78) the discharge coefficient becomes

$$C_d = \frac{1}{1 + \dfrac{C}{\sqrt{Re_{N_d}}}} \tag{4.79}$$

The value of C was found to be about 3.9. Notice that as $Re_{N_d} \to \infty$, $C_d \to 1.0$, which is to be expected in a well-designed nozzle. Notice also that as $Re_{N_d} \to 0$

$$C_d = C_1\sqrt{Re_{N_d}} \tag{4.80}$$

which is again the correct behavior when the nozzle flow is completely viscous. As an aside we may note that for fully developed pipe flow the average velocity is

$$U_{\text{viscous}} = \frac{\pi \Delta P d^4}{128\mu L}$$

In inviscid flow the average velocity is

$$U_{\text{inviscid}} = \sqrt{2\Delta P/\rho}$$

By definition the discharge coefficient is a ratio of the two velocities

$$C_D = \left(\frac{\pi d^4}{128\mu L}\sqrt{\frac{\rho}{2}}\right)\sqrt{\Delta P}$$

which says that C_D is proportional to $\sqrt{\Delta P}$ when the geometry remains fixed. Because the velocity in viscous flow is proportional to ΔP and Eq. (4.80) gives

$$C_D = C_1\sqrt{\rho U \mathrm{d}/\mu}$$

we see that the discharge coefficients in Eq. (4.80) and that obtained from the ratio of the velocities have the same dependence on ΔP.

Experiments have shown that Eqs. (4.79) and (4.80) give the correct limiting forms for the flow of liquids or gases. However, the constant determined in one region may not be the most satisfactory one to use in the other flow regime. At still lower Reynolds numbers in gases the effects of rarefaction become significant, and then the discharge coefficient is also dependent on the pressure ratio across the nozzle.

Obviously, this type of relationship, e.g., Eq. (4.79) is better suited for use with nozzles where the boundary layer does not become turbulent on its journey from the upstream region on the nozzle wall to the throat as it may in a nozzle such as the contraction region of a large full-scale wind tunnel. Also note that difficulty in representing the transition from a flow characterized by Eq. (4.79) to one characterized by Eq. (4.80) is because, in this transition region, the entire nozzle throat is filled with viscous flow and many of the assumptions of boundary-layer theory are no longer valid. (It may interest the reader to know that once a supersonic nozzle throat is filled with viscous flow it is an experimental fact that the gas downstream of the throat can never go supersonic regardless of how low the exhaust pressure at the end of the nozzle is made. The author is unaware of the reason for this phenomenon but has observed it numerous times.)

As our next example we will consider the flow in the wake of a flat plate at zero incidence. We will assume that the station of interest is at least three plate lengths aft of the downstream end of the plate where the static pressure is constant from far below the plate to far above the plate. The wake is caused by a loss of momentum experienced by the flow because of its interaction with the plate. According to Newton's third law of motion the drag is equal to the force associated with the change in the momentum of the flow. If b is the span of the plate, u is the velocity at any distance y above or below the plate, and U is the freestream velocity, then the change in momentum due to the two wetted surfaces is

$$D = b\rho \int_{-\infty}^{\infty} u(U-u)\,\mathrm{d}y \tag{4.81}$$

Using an asymptotic expansion from Blasius's result at the end of the plate, Tollmein, as described by Schlichting,[24] found that the velocity distribution is given by

$$\frac{u}{U} = \left[\frac{0.664}{\sqrt{\frac{\pi x}{t}}}\right]\exp\left[-\left(\frac{1}{4}\frac{y^2 U}{x}\nu\right)\right] \tag{4.82}$$

Interestingly, this is a Gaussian distribution at every value of x/ℓ downstream of the plate. Unless there is large-scale separation, such a distribution is what is found experimentally. Surveying the loss of stagnation pressure in the wake has been a favorite method of determining the drag of bodies, such as two-dimensional airfoils, which could not easily be mounted on a drag balance.

Schlichting[24] provides a number of other exact solutions of the steady-state boundary-layer equations.

4.7 Closure

In this chapter we have sought to illustrate the approach by which the effects of the viscosity of the fluid flowing over a body's surface can be treated mathematically. To the continuity equation developed in Chapter 2 we have added the momentum equation—a statement of Newton's second law of motion. These two equations are sufficient to describe the motion of an incompressible viscous fluid. We have taken advantage of Prandtl's observation that for flows with moderate to high Reynolds numbers the effects of viscosity are confined to a relatively thin layer, called the boundary layer, next to the surface over which the fluid is flowing. Following order of magnitude arguments made by Prandtl we were able to reduce the complexity of the equations of motion and develop the boundary-layer equations. Through the use of a transformation we were able to convert this set of partial differential equations to a single ordinary differential equation. This we solved numerically for a flat plate using a simple fourth-order Runge–Kutta integrator. We listed the Fortran code for this process and presented a graph of the results. The solution of this equation can be used to show the velocity distribution in the laminar boundary layer and to determine the skin-friction drag on the surface over which the fluid flows. The latter represents that part of the body drag called skin-friction drag. We noted for streamlined bodies, the skin-friction drag represents about 80% of the total drag.

We also noted that for more general cases the equation contains terms representing functions of the longitudinal pressure distribuiton outside the boundary layer. This external pressure distribution is created by largely inviscid flowfields such as those discussed in Chapter 2. These functions of the external pressure distribution, when supplied to the integration routine for Eq. (4.50), determine the rate at which the boundary layer grows, whether it separates or not, and when it may become turbulent.

Our examination continued by looking at some simple solutions of the exact equations of motion for various axisymetric geometries and at solutions given in the literature for the boundary-layer flow over a cylinder normal to a stream and in the wake of a flat plate. We showed how the classical solution for the flow over a cylinder could be used as the basis of a semiempirical description of the discharge coefficient of one type of nozzle, the discharge coefficient being the ratio of the actual flow through a nozzle to the theoretical flow if there were no viscosity.

Our examination of viscous effects in this chapter is intended to provide a basis for understanding the manner by which these effects are treated in the computer programs described, in Chapters 5 and 7, which determine the aerodynamic characteristics of specified wings and bodies. Such an examination is necessary to permit the reader to gain an appreciation of the assumptions made in developing the methods and the consequences of such assumptions.

Problems

Although USCU units are used with these problems, SI units could be assumed without materially affecting the utility of the problems. The value for the coefficient of viscosity given in problem 4.1 would be in error, of course, but one might substitute the word fluid for water without indicating a particular fluid. A consistent units set could then be attached to the numbers given in the problems.

4.1. A long, annular flow channel containing water ($\mu = 674$ lb-s/ft) has an inner radius of 10 ft and an outer radius of 11 ft. Assume that $dp/dz = 10$ lb/ft^3 and that $U = -9$ ft/s. a) Plot as accurately as you can v_z against r from R_1 to R_2 and b) determine the net volumetric flow rate. You may wish to approximate the integral

$$\int_{R_1}^{R_2} v_z r \, dr$$

by the series

$$\sum_{R_1}^{R_2} v_z r \, \Delta r$$

where $\Delta r \leq 0.01$.

4.2. Repeat problem 4.1 with $R_1 = 1.0$ and $R_2 = 2.0$. Comment on the differences between the results for this problem and those for problem 4.1 both as to flow quantity and the shape of the velocity distribution.

4.3. Repeat problem 4.2 with $U = 0$

4.4. Repeat problem 4.1 with $dP/dz = 0$. How linear is dv_z/dr?

4.5. With $R_2 = 11$, $R_1 = 10$, $U = 0$, and $dP/dz = 10$, compute the flow through a tube of equal cross-sectional area. Compute the flow quantity through the annular area and compare with the flow quantity through the tube.

4.6. Repeat problem 4.1 for μ 10 times as large as that given for water. Is there any difference in the shape of the velocity distribution?

4.7. Repeat problem 4.1 for dP/dz 10 times as large as that given.

4.8. Can you find a value of U in problem 4.1 such that the net volumetric flow rate is zero? If so, what is the value?

4.9. Evaluate and plot Eq. (4.82) for the following conditions: $\ell = 1$, $x = 3\ell$, $U = 10$, and $\nu = 1.1$. At which value of y is $u_1 \geq 0.99U$?

4.10. What is the force required to move R_1 relative to R_2?

4.11. How would the force calculated in problem 4.10 change if R_2 were reduced to 10.1 ft? What is the shape of the velocity distribution in this case?

4.12. Consider the geometry described in problem 4.11. Let $dP/dz = 0$ and $U = 0$. Instead, R_1 rotates at constant velocity about its axis with a speed of π radians per second. a) Show that

$$u(r) = \frac{1}{R_2^2 - R_1^2}\left[\frac{R_1^2 R_2^2 \omega}{r} - R_1^2 \omega r\right]$$

represents the velocity distribution in the gap. Graph the results. b) Under what conditions is the velocity distribution approximately linear? c) How could such

a device be used to measure the viscosity of a fluid? d) Is the frictional resistance more when R_1 rotates about its axis or when R_1 moves axially? Assume that the boundary velocity is the same whether rotating axially or circumferentially.

4.13. It has been observed that as the flow velocity is reduced below a certain value, the drag coefficient on a circular cylinder placed normal to a stream increases. Because we consider a fixed cylinder in the same fluid, the Reynolds number of the cylinder is decreasing in this case. What does this fact imply about the vertical extent of the cylinder wake?

4.14. If you were to assume that the boundary layer separates from the $\phi = 90$ and 180 deg positions relative to the stagnation point on a circular cylinder and the flow proceeds straight downstream from those points, what should you estimate the drag coefficient of the cylinder to be? Assume the pressure in the wake is freestream.

4.15. If the measured drag coefficient is actually larger than that obtained by the method indicated in problem 4.14, what does this tell you about the extent of the region of separated flow?

4.16. At low Reynolds numbers the flow over bodies such as airfoils is laminar. Recall that the skin-friction coefficient varies as $1/\sqrt{Re_{N_x}}$ when the flow is laminar. At some value of Reynolds number, the flow becomes turbulent. The variation in skin-friction coefficient with Reynolds number has been observed to follow the law $Re_{N_x}^{\gamma}$ where γ has values varying from $-\frac{1}{7}$ to $-\frac{1}{4}$. Assuming that the turbulent skin friction is the same as the laminar value for a Reynolds number of 10^4, how would the skin friction coefficients compare at a Reynolds number of 10^7?

4.17. It has been observed experimentally that the skin-friction coefficient for turbulent flows over rough surfaces is greater than that for turbulent flow over smooth surfaces. In view of this, what would you expect to be the effect on drag of bug deposits, ill fitting pieces of wing skin, protruding rivets, or rain drops on the surface of a wing? How would these things affect the wake behind an airfoil for a given angle of attack?

4.18. The Prandtl number of a fluid indicates the rate at which heat is produced at a site by viscous dissipation relative to the rate at which it is conducted away from the site in the fluid. The Prandtl number for air is about 0.72. What is the implication of this value for the heating of a surface over which a boundary layer has developed?

4.19. Assume that a closed-circuit wind tunnel has a rectangular test section of 36×45 in. It is powered by a 50-hp motor driving a variable pitch propeller. Top speed of the test section air is 94 mph. When the tunnel has been run continuously for several hours at maximum speed, how much heat is being dissipated to the room by the wind-tunnel walls?

4.20. It is assumed that $dP/dz = C$ and $U = C$ for fluid flow in a long tube. What does this imply for the stagnation pressure from one end of the tube to the other?

4.21. Derive the equation of motion for the fluid surrounding a semi-infinite flat plate accelerated suddenly from rest. The fluid in which the plate resides is initially quiescent. a) Is this equation properly an ordinary differential equation or a partial differential equation? b) If it is a partial differential equation, what sort of transformation could be used to make it an ordinary differential equation? (Hint: an ordinary differential equation has only one independent variable. If the problem actually has two independent variables, it can be sometimes be transformed to an ordinary differential equation by devising a new independent variable that is some function of the two.) c) Why would we want the equation to an ordinary differential equation rather than a partial differential equation?

4.22. If we allowed the time the plate is in motion to approach infinity, could we see a boundary layer develop over the plate in the solution to the equation developed for problem 4.21 and why?

4.23. Given a flat plate over which water is flowing at 2 ft/s, what is the force per unit area on the plate at a point 10 ft behind the leading edge?

4.24. What is the effect on the integral of the surface pressures on an airfoil of a finite boundary-layer displacement thickness at the trailing edge?

4.25. By what factor is the boundary-layer displacement thickness decreased if twice the actual Reynolds number is used in the formula for δ^*? Explain.

4.26. On physical grounds, argue the relative sizes of the skin-friction drag and the form drag for a streamlined body aligned with the stream and operating at a speed such that the boundary layer is laminar.

4.27. A billboard 40 ft tall and 60 ft wide is placed so that the bottom of the billboard is 40 ft off the ground for the entire 60 ft length. It is supported by two posts. The structural designer is in a quandry about how big to make the posts. He does not know what bending moment at the ground he should design for. He does know that the maximum expected wind in the area is 80 mph. He wants an estimate from you as to what the bending moment would be in an 80-mph wind. a) Outline the steps you would need to take to arrive at such an estimate and put a number with it. Assume that you can use a sea level value of density. Assume also that the pressure in the wake region on the lea side of the billboard is atmospheric. b) Sketch the billboard wake.

4.28. Is the drag experienced by the billboard form drag or skin-friction drag?

4.29. Octofluorocyclobutane is an interesting gas. It has a molecular weight of 200 (vs 29 for air) and has a dynamic viscosity that is about 70% as large as that of air. It is nontoxic and, therefore, safe to use in wind tunnels. Boiling point at atmospheric pressure is near 0°C. If it has a velocity of 300 ft/s, by what factor can a model size be reduced when tested in it if the Reynolds number is to be the same as for testing in air at the same speed?

4.30. Repeat problem 4.29 with perfluoromethane (CF_4) gas.

4.31. a) Sketch a turbulent boundary layer and a laminar boundary layer. b) Which type of boundary layer applies the greater shear stress to the wall for a given Reynolds number? Suppose you have a material that sublimes under the action of shear stresses on the wall. Suppose, also, that the material is very reflective. c) Could you paint this material on a wing surface and by shining a light on it normal to the flow over the wing identify the location of transition? Assume that the wing is originally painted black and that a 35-mm movie camera records the condition of the wing surface as a function of time. d) Explain your reasoning.

4.32. Explain why it is desirable to have the point of minimum pressure as far back on an airfoil as possible while still allowing the boundary layer to remain attached all of the way to the trailing edge.

4.33. Consult a standard tabulation of airfoil wind-tunnel test results, such as NACA TR 824.[16] You will notice that the standard roughness drag values are much higher than for the smooth airfoil. Can you give a physical explanation for this? The roughness strip is affixed far forward on the airfoil.

4.34. Can you give an explanation in terms of the ability of the boundary layer to remain attached as to why airfoil thicknesses do not go beyond 24% of chord? If you wish, you can use the JOUKOW program to generate data on the most negative C_P for airfoils in a given family with only the thickness varying.

4.35. In general, boundary layers have a difficult time going around small radius turns without separating because the pressure gradients in the region are so high. Based on this idea, what would you expect to be the result of making the leading-edge radius of an airfoil very small, particularly at angle of attack?

4.36. If the separation point on a cylinder normal to a stream moves from 100 deg from the stagnation point to 120 deg from the stagnation point, what is the effect on the drag coefficient? Be as quantitative as you can.

5
Direct Computation of Airfoil Characteristics

5.1 Introduction

IN Chapter 3 we used the Joukowski transform to generate one class of airfoils. We noted, however, that this approach was rather impractical for engineering use because it is difficult to determine exactly what shape any particular circle may transform to a priori and because airfoils resulting from this transformation have their minimum pressure point too far forward, a situation that leads to higher drag and lower $C_{L_{max}}$ than are obtained with many other airfoil families. Without knowledge of the airfoil shape it is not possible to consider manufacturing difficulties, to undertake wing planform optimization, or to do any structural design involving the wing, items connected to the wing, or the wing–fuselage junction. In this chapter we consider a direct method for determining the aerodynamic characteristics of a given shape. Later we will consider what characteristics we should look for in given situations.

This direct method has been implemented as a computer program for ease of use. The program[25] was originally written at the Lockheed Georgia Company. It was modified internally at NASA Langley Research Center and then extensively modified at the Department of Mechanical and Aerospace Engineering of North Carolina State University (NCSU). The NCSU modifications are detailed in NASA Contractor's Report 2523.[26] The original Lockheed program was a multielement program; that is, it included the capability to treat airfoils plus flaps. Because the NCSU version was intended primarily for use with the general aviation class of airplane and for use on what was then a minicomputer, the multielement capability was removed. The NCSU modifications were directed toward improving the accuracy of the drag prediction, simplifying the code, reducing memory requirements, and reducing the running time.

Following is an outline of the programmed method. A number of vortices are distributed along the outline of the airfoil. The strengths of the individual vortices are chosen such that the flow velocity due to all vortices combined with that due to the freestream is parallel to the airfoil surface at control points between vortex locations. There is one control point for each vortex strength to be determined. Hence, we may write a system of N equations describing the contribution of all of the vortices and the freestream to the direction of the flow at each of the N control points on the airfoil where N is the number of vortices. Because the overall flow is not required to be parallel to the surface at any other points along the airfoil outline, the number of vortices and control points should be fairly numerous to adequately model the flow about the airfoil. After some experimentation it was determined that $N = 65$ (32 distinct upper surface points and 32 distinct lower surface points plus 1 common leading-edge point) yielded the best compromise between accuracy of representation and the time required to compute the aerodynamics characteristics of most conventional airfoils, that is, airfoils without a concavity on the lower surface, an important point as we shall see.

Because it is important in determining the conditions under which the program gives reliable results, we will now undertake a detailed exposition of the program algorithm.

5.2 Program Algorithm

Suppose we consider an arbitrary airfoil section, and at various points along its surface place mathematical vortices of undetermined strength. We will connect adjacent vortex centers by straight line segments so as to form a close approximation of the airfoil from the segments. The quality of the approximation depends on the number of vortices we choose and where we place them. We will designate the center of a particular vortex as being located at (x_{0_N}, y_{0_N}). Any other point in the two-dimensional flowfield has coordinates (x, y). The line segment between (x_{0_N}, y_{0_N}) and $(x_{0_{N+1}}, y_{0_{N+1}})$ is represented by

$$y = y_{0_N} + \left[\frac{y_{0_{N+1}} - y_{0_N}}{x_{0_{N+1}} - x_{0_N}}\right](x - x_{0_N}) \tag{5.1}$$

The midpoint of this line has coordinates given by

$$x_M = x_{0_N} + \tfrac{1}{2}(x_{0_{N+1}} - x_{0_N}) = \tfrac{1}{2}(x_{0_{N+1}} + x_{0_N}) \tag{5.2}$$

$$y_M = y_{0_N} + \tfrac{1}{2}(y_{0_{N+1}} - y_{0_N}) = \tfrac{1}{2}(y_{0_{N+1}} + y_{0_N}) \tag{5.3}$$

By reference to the expression for the velocity associated with a vortex developed in Chapter 2 the velocity components at (x, y) induced by a vortex of strength Γ_N at (x_{0_N}, y_{0_N}) can be seen to be

$$u = \frac{-(y - y_{0_N})\,\Gamma_N}{(y - y_{0_N})^2 + (x - x_{0_N})^2}\left(\frac{1}{2\pi}\right) \tag{5.4}$$

$$v = \frac{(x - x_{0_N})\,\Gamma_N}{(y - y_{0_N})^2 + (x - x_{0_N})^2}\left(\frac{1}{2\pi}\right) \tag{5.5}$$

Note that the denominator of Eqs. (5.4) and (5.5) represents the distance from (x_{0_N}, y_{0_N}) to (x, y) squared.

The net velocity at a point due to all K vortices representing the airfoil has as its components

$$u = -\frac{1}{2\pi}\sum_{N=1}^{K}\frac{(y - y_{0_N})\,\Gamma_N}{(y - y_{0_N})^2 + (x - x_{0_N})^2} \tag{5.6}$$

$$v = \frac{1}{2\pi}\sum_{N=1}^{K}\frac{(x - x_{0_N})\,\Gamma_N}{(y - y_{0_N})^2 + (x - x_{0_N})^2} \tag{5.7}$$

Now suppose we require that x and y be given by Eq. (5.2) and (5.3). Then,

$$u_M = -\frac{1}{\pi}\sum_{N=1}^{K}\frac{(y_{0_{N+1}} - y_{0_N})\,\Gamma_N}{(y_{0_{N+1}} - y_{0_N})^2 + (x_{0_{N+1}} - x_{0_N})^2} \tag{5.8}$$

$$v_M = \frac{1}{\pi}\sum_{N=1}^{K}\frac{(x_{0_{N+1}} - x_{0_N})\,\Gamma_N}{(y_{0_{N+1}} - y_{0_N})^2 + (x_{0_{N+1}} - x_{0_M})^2} \tag{5.9}$$

The direction of the surface of the airfoil at points (x_M, y_M) can be represented by

$$\left.\frac{dy}{dx}\right|_M - \tan\alpha \tag{5.10}$$

when the airfoil is at some angle of attack α to the oncoming stream. Now we will require that the combination of the freestream and the induced velocities due to all vortices be parallel to the surface of the airfoil at the same points. Thus,

$$\frac{v_M}{V + u_M} = \left.\frac{dy}{dx}\right|_M - \tan\alpha \tag{5.11}$$

where u_M and v_M are given by Eq. (5.8) and (5.9) and V is the freestream velocity.

Let us designate

$$a_{MN} = \frac{(y_{0_{N+1}} - y_{0_N})/\pi}{(y_{0_{N+1}} - y_{0_N})^2 + (x_{0_{N+1}} - x_{0_N})^2} \tag{5.12a}$$

$$b_{MN} = \frac{(x_{0_{N+1}} - x_{0_N})/\pi}{(y_{0_{N+1}} - y_{0_N})^2 + (x_{0_{N+1}} - x_{0_N})^2} \tag{5.12b}$$

With these definitions we can write Eq. (5.1) as

$$\frac{b_{M1}\Gamma_1 + b_{M2}\Gamma_2 + b_{M3}\Gamma_3 + \cdots + b_{MK}\Gamma_K}{V - a_{M1}\Gamma_1 - a_{M2}\Gamma_2 - a_{M3}\Gamma_3 - \cdots - a_{MK}\Gamma_K} = \left.\frac{dy}{dx}\right|_M - \tan\alpha \tag{5.13}$$

Suppose we now define the right-hand side of Eq. (5.13) as

$$B_M = \left.\frac{dy}{dx}\right|_M - \tan\alpha \tag{5.14}$$

then,

$$B_M = \frac{b_{M1}\Gamma_1 + b_{M2}\Gamma_2 + b_{M3}\Gamma_3 + \cdots + b_{MK}\Gamma_K}{V - a_{M1}\Gamma_1 - a_{M2}\Gamma_2 - a_{M3}\Gamma_3 - \cdots - a_{MK}\Gamma_K} \tag{5.15}$$

represents a system of K linear algebraic equations, which presumably we could solve for the unknown Γ. However, when $N = K$ in Eqs. (5.2) and (5.3), $(x_{0_{N+1}}, y_{0_{N+1}})$ is not defined. Thus, only $K - 1$ values of (x_M, y_M) are known.

We can identify a Kth set by closing the polygon and letting

$$x_{0_{K+1}} = x_{0_1} \tag{5.16a}$$

$$y_{0_{K+1}} = y_{0_1} \tag{5.16b}$$

Even though we have chosen to let $(x_{0_{K+1}}, y_{0_{K+1}})$ be (x_{0_1}, y_{0_1}) the midpoint of the line segment between (x_{0_K}, y_{0_K}) and (x_{0_1}, y_{0_1}) is not the same as any other (x_M, y_M). The system of equations is, therefore, not singular.

We will usually assume that the first vortex is located at the trailing edge. According to the Kutta condition, this must be a stagnation point. If the velocity at this point is zero, the vortex strength is zero. However, this statement determines the strength of one vortex and, thus, there is one more equation in Eq. (5.15) than necessary. However, if we place an additional vortex at $(x_{0_{K+1}}, y_{0_{K+1}})$ and require that

$$\Gamma_{K+1} = -\Gamma_1 \tag{5.17}$$

then the number of unknown vortex strengths matches the number of equations. By specifying the strengths in this fashion, we guarantee that a stagnation point exists at the trailing edge without having to specify Γ_1 a priori.

We ask now what happens when the angle of attack changes. The vortices, line segments, and midpoints are all defined with reference to a fixed coordinate system. Either we must redefine these values as α changes or we can assume that the airfoil remains fixed and the direction of the oncoming flow changes. The latter is easier to implement computationally. In that case, Eq. (5.11) is rewritten as

$$\frac{v_M + V\sin\alpha}{u_M + V\cos\alpha} = \left.\frac{\mathrm{d}y}{\mathrm{d}x}\right|_M = B_M \tag{5.18}$$

and Eq. (5.15) becomes

$$B_M = \frac{V\sin\alpha + b_{M1}\Gamma_1 + b_{M2}\Gamma_2 + b_{M3}\Gamma_3 + \cdots + b_{MK}\Gamma_K}{V\cos\alpha - a_{M1}\Gamma_1 - a_{M2}\Gamma_2 - a_{M3}\Gamma_3 - \cdots - a_{MK}\Gamma_K} \tag{5.19}$$

One additional aspect of the specification of vortex locations should be noted. For the line segment approximation to be reasonably close, the vortices need to be closer together in highly curved regions of the airfoil surface than in those regions where the surface is nearly flat. For airfoils without significant concavity, 65 vortices properly distributed over the surface do a reasonably good job of representing the flow. For airfoils with significant concavity, it has been found to be necessary to modify the program to accept additional vortices, perhaps as many as 100 or more. The program is easily modified to do this.

The program uses a curvature criterion to determine how to reposition the supplied vortex locations to obtain the best flow representation. Nevertheless, the user should carefully select vortex locations to avoid large movements of the supplied vortices. The application of the curvature criterion and the movement of the supplied vortices is a program detail that will not be discussed. Interested readers should consult the code directly for specifics.

As noted, the left-hand side of Eq. (5.19) is the slope of the airfoil surface at point M. The 65 values of B_M must be computed from a knowledge of the airfoil geometry. Then the system of 65 simultaneous equations represented by Eq. (5.19) can be solved for the 65 unknown values of Γ. Once these values

are known, the flow velocity can be computed at 65 values of M. From this it is possible to determine the pressure at 65 points on the airfoil surface. Assuming that the pressure is constant along a line segment representing a section of the airfoil surface permits us to determine a magnitude and direction for the force created by the pressure. Summing the components of these forces in the direction normal to the oncoming stream yields the lift created by the airfoil. The sum of the streamwise components yields the drag. The lift and drag together create the pitching moment.

5.2.1 *Treatment of Viscous Effects Within the Inviscid Formulation*

In Chapter 4 we developed a means for analyzing the flow in the boundary layer that surrounds the airfoil. In particular, we recall that the boundary-layer displacement thickness represents the distance displaced if the mass above the surface were inviscid. This concept suggests that by adding the boundary-layer displacement thickness to the airfoil ordinates one may be able to continue to treat the combination as an inviscid flow problem. Unfortunately, this must be done iteratively because the pressure distribution that governs boundary-layer growth changes as a result of the addition to the airfoil ordinates. Generally, five iterations are sufficient for the pressure distribution over the airfoil after the addition of the boundary-layer displacement thickness to be approximately the same as that used to determine the boundary-layer displacement thickness.

When the boundary displacement thickness is added to the airfoil, the trailing edge can no longer be a stagnation point because the effective thickness at this point is no longer zero. The stagnation point for purposes of the program must be placed somewhat downstream of the actual trailing edge. One possible device for determining this location is to determine the intersection of the lines made by extending

$$\begin{pmatrix} \delta^* \\ \dfrac{\mathrm{d}y}{\mathrm{d}x} \end{pmatrix}$$

from each surface. For example, if δ^* is $0.05C$ and $\mathrm{d}y/\mathrm{d}x = -0.25$ on the upper surface at $x = C$ and $\delta^* = 0.03C$ and $\mathrm{d}y/\mathrm{d}x = -0.05$ on the lower surface, then the intersection of the two extrapolations occurs at about $0.25C$ behind the trailing edge. Because the intersection is assumed to be a stagnation point, the pressure coefficient at this point must be $+1$. Because this is fairly close to the trailing edge, it implies that the pressures on the actual trailing edge may be somewhat higher than are usually found experimentally.

As we discuss subsequently, the program places the downstream stagnation point at $x = 2C$ and assumes an exponential decay in the dimensions of the wake body from the wake thickness at the trailing edge to zero thickness at the stagnation point to obtain a more realistic value. After the displacement thickness and the wake body are added to the airfoil, the inviscid computation determines the pressure distribution over this combination. Only the pressures over the airfoil plus displacement thicknesses are used to determine the lift, drag, and pitching moment, however. These are assumed to act unchanged through the boundary layer on to the airfoil surface. The pressures on the wake body are ignored.

Because the airfoil surface plus wake body is now somewhat longer than in the inviscid case we must accept fewer points on the physical airfoil at which

to evaluate the pressure or else increase the number of vortices representing the airfoil. Because the wake body has relatively little curvature, the vortex distribution algorithm will assign relatively few vortices to the wake body. Thus, the choice of whether to add a few additional vortices to the 65 originally specified or to redistribute the original 65 comes down to a decision as to which approach will be easier to implement computationally. For the airfoil, the choice was made to redistribute the 65 vortices.

Part of the result of the boundary-layer computations is the determination of the skin friction (which is a component of the vehicle drag) on the airfoil. For those cases where the wake is very small the skin friction may be 80% of the total drag. When the wake is larger, the form drag may become dominant. The form drag results from an excess pressure on the forward part of the airfoil acting in the streamwise direction relative to the pressure on the rearward portions of the airfoil that acts in the upstream direction. In separated flow, of course, the skin-friction drag disappears but the form drag is very high.

5.2.2 Algorithm Limitations

The model used in the program to calculate the boundary layer assumes the flow is always attached. Thus, when the angle of attack reaches a value where there is actually significant flow separation, the algorithm no longer models the flow accurately. On most airfoils this point seems to occur about $C_L = 0.8$. More recent airfoil analysis programs position one or two sources on the aft portion of the airfoil to model the separated wake. The strength of these sources are such that the flow separates from the airfoil at an angle roughly equal to that of the freestream. The separated wake may be closed at the downstream stagnation point by the addition of a sink. By this means the newer algorithms are able to compute $C_{L_{max}}$ with reasonable accuracy. Most such algorithms are proprietary, however, and cannot be distributed freely. Further, they differ from the algorithm discussed herein chiefly in what may be considered for our purposes to be details. For that reason no major pedagogical liability is incurred by restricting consideration at this level to the present algorithm.

5.2.3 Tuning Applied to the Program

Several semiempirical modifications were made to the basic program formulation to improve the agreement of the program output with experimental results. These can be thought of as a form of tuning or tweaking, which is commonly applied to theoretical models to take into account that they do not include a treatment of all known effects.

1) Instead of using point vortices as described in the development, the vorticity is assumed to be distributed at a constant strength over each of the line segments. The integral of the strength per unit length of the distributed vorticity over a line segment equals the strength of the point vortex for that segment. It has been found that the use of distributed vorticity leads to a less wavy line of $\psi = \text{const}$ than does the use of point vortices. In other words, it gives a better representation of the surface of an actual airfoil.

2) The Reynolds number was doubled for computations of the boundary layer. It is well known that the momentum integral method, which is used in the program, overpredicts the boundary-layer thickness. However, boundary-layer thickness

decreases with increasing Reynolds number. Thus, by doubling the actual Reynolds number for purposes of the computation, a displacement thickness somewhat closer to that found in practice was achieved.

3) The integration of the streamwise components of the pressures on the airfoil (those in the drag direction) before the boundary-layer displacement thickness is added did not equal zero as it must for an inviscid computation. This is probably because the circulation was assumed to be constant on a line segment. The drag results were improved considerably by subtracting this value as a tare from the final drag.

4) The ordinates of the wake body behind the symmetrical form of the airfoil are actually modeled by the relation

$$z = \pm\frac{1}{2}\left\{(z_{te} - z_\infty)\exp\left[-6.9\left(\frac{x}{C} - 1.0\right)\right] + z_\infty\right\}\left(2.0 - \frac{x}{C}\right) \tag{5.20}$$

where z_{te} is the trailing-edge thickness plus the finite wake thickness at the trailing edge, C is the airfoil chord, and $z_\infty = \frac{1}{2}C_D C$. The downstream stagnation point according to this model is at $x = 2C$.

5) A small correction was inserted to the calculated lift coefficient to account for wake effects. This is given by

$$C_{L_{wake}} = \left(1.0 - 0.214\sqrt{C_D}\right) C_{L_{\text{no wake}}} \tag{5.21}$$

The relation and the constant 0.214 come from the literature. However, even with this correction, the predicted lift coefficient for thick airfoils is somewhat optimistic at higher angles of attack. A better agreement with experiment can probably be had by replacing 0.214 with $3.57(t/C)$. No correction of this sort is available for the pressure distribution, however.

In addition to the semiempirical changes just noted, a change in the theoretical method for computing the magnitude of the distributed vorticity on the line segments representing the airfoil was made at the Langley Research Center prior to the program's acquisition by NCSU. These changes, based on the work of Oeller[27] and Chen[28] replace the requirement that the sum of the induced velocities and the freestream components be parallel to the airfoil surface with a requirement that the sum of the stream functions due to the freestream and to the distributed vortices trace the airfoil surface exactly, at least at the control points. This can be thought of as an integral version of the method previously described in this section. The advantage of such an approach is that integration tends to smooth out local variations. As a result, with the integral approach the representation of the airfoil surface is smoother between control points than it would be by determining the surface from the velocity components. To hasten the convergence to a solution when adding the boundary displacement thickness, Lockheed split the solution process into two parts: a camber solution and a thickness solution. The effect of adding the displacement thickness is to reduce the effective camber. The effect of the displacement thickness on the thickness solution is to move the rear stagnation point downstream as already indicated. The separate solutions are then added to obtain the overall solution.

The interested reader will find a more extended discussion of these changes, as well as those made to the orignal program for reasons of computational robustness and efficiency, in NASA CR-2523.[26] The latter changes need not concern us at

this time. We may note, however, that the implementation of simple concepts may not always be simple as this case illustrates. Although the alterations and additions needed to achieve a successful implementation seldom extend the range of applicability or validity of the underlying concepts, they do not obviate their study.

We may comment at this point that a process like the present calculation of aerodynamic characteristics is not one that could have been carried out in a routine manner before the availability of a computer with the computational capabilities of the mainframes of the early 1970s. Too many arithmetic processes are required. Conceptually the method is an extension of the thin airfoil theory, which had been in use since the 1920s, coupled with a boundary-layer calculation of like vintage. That concepts from several areas of research have been brought together to create a procedure of greater utility than that of its constituent parts separately is the significant achievement made possible by the availability of computer technology. Really new concepts evolve only sporadically. Synthesis of well-known concepts, however, can almost be produced to order through the use of this tool.

5.3 Program AIRFOIL

5.3.1 Features of the AIRFOIL Program

This program produces three output files, AIRFOIL.TXT, AIRFOIL.PS, and AERO.PS. The first provides tabulated results (in a 132 column format). The second draws the outline of the profile. The third plots the results of the computation as C_ℓ vs α, C_d vs C_ℓ, $C_{m_{c/4}}$ vs α, and C_P vs x/C with each plot presented on a separate page. As presently dimensioned, the program can compute 10 sets of such data during one run. Because a C_P vs x/C plot is produced for each α, there may be as many as 10 pages of C_P vs x/C plots.

AIRFOIL.PS draws a rather large profile to facilitate its inspection for input points that may be misplaced. The input points are connected by straight line segments. This enables the user to obtain an indication of the smoothness of the theoretical representation.

Program size is moderate. Both the source code and the executable (as made by Microsoft Powerstation) are slightly less than 200K. Running time on a 90-MHz Pentium varies from 15 to 18 s for a 10 alpha case depending on the amount of output requested.

The program permits the user to designate the Reynolds number at which the airfoil is expected to operate. This will affect primarily the computed drag because the program cannot compute $C_{L_{max}}$, the other characteristic that is primarily Reynolds number dependent.

The program can also be instructed to compute the characteristics at several different Mach numbers. Because the von Kármán–Tsien formula is employed for this purpose, requested Mach numbers should be less than 0.6 if reasonably accurate results are desired.

The program permits the user to designate the point of transition from laminar to turbulent boundary-layer flow on each surface or it can be instructed to compute the locations of the transition points. Fixing the transition point is not the same thing as applying standard roughness at that location. Applying material such as grains of sand to an otherwise smooth surface does in fact cause the boundary layer to become turbulent; however, even the small grain size used for this purpose is relatively large compared with the thickness of the boundary layer on the forward portions of the airfoil. As a result, the shearing stresses are much larger than


```
NACA 23012 AIRFOIL
   18   18    0    0    0
    0.0000    0.0125    0.0250    0.0500    0.0750    0.1000    0.1500    0.2000
    0.2500    0.3000    0.3500    0.4000    0.5000    0.6000    0.7000    0.8000
    0.9000    1.0000
    0.0000    0.0267    0.0361    0.0491    0.0580    0.0643    0.0719    0.0750
    0.0760    0.0755    0.0714    0.0614    0.0547    0.0436    0.0308    0.0168
    0.0092    0.0013
    0.0000    0.0125    0.0250    0.0500    0.0750    0.1000    0.1500    0.2000
    0.2500    0.3000    0.3500    0.4000    0.5000    0.6000    0.7000    0.8000
    0.9000    1.0000
    0.0000   -0.0123   -0.0171   -0.0226   -0.0261   -0.0292   -0.0350   -0.0397
   -0.0428   -0.0446   -0.0448   -0.0417   -0.0367   -0.0300   -0.0216   -0.0123
   -0.0070   -0.0013
   10
     .0000    1.0000    2.0000    3.0000    4.0000    5.0000    6.0000    7.0000
    8.0000    9.0000   10.0000
    1
     .300      .300
    1.0      1.000
  520.0        3.0        .7       1.0
      0        0.0       0.0       0.0
      0        0.0       0.0       0.0
END
```

Fig. 5.1 Output data from AIRFOIL program.

for natural transition. Consequently, the measured drag is greater than the drag predicted by the program for these conditions.

As a check on the drag computations, the program computes the profile drag by the Squire–Young formula. This result should agree closely with the drag coefficient calculated from the sum of the form drag and the skin-friction drag.

By specifying IPUNCH = 1 the program will create another output file AIRFOIL.PUN, which contains the two-dimensional characteristics at NA angles of attack in a form that can be used by F2D3D to convert section results to wing data.

5.3.2 Program Data Entry

For this version of the program the input data can be entered in response to a series of English language questions. The user responses to these questions are written in the correct format to the file AIRFOIL.DAT. This file can be edited separately and then processed without having to respond to the questions again. The number of input points on the airfoil may be greater less than 65 but should define the airfoil adequately, including the trailing-edge thickness. The current program limit is 50 points per surface.

Figure 5.1 shows a typical input file. Users desiring to edit this file should consult the source code (subroutine READIT) for identification of the various data fields. Subroutine READIT contains the questions that identify the data. The associated WRITE statements show the location and format of the information as it is written to AIRFOIL.DAT.

5.3.3 Typical Results

Results obtained from processing the typical input data are shown in Figs. 5.2 to 5.7.

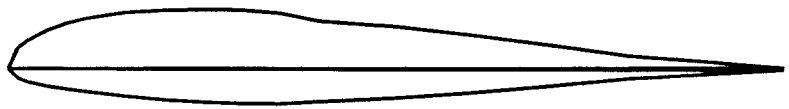

Fig. 5.2 NACA 23012 airfoil drawn from input data.

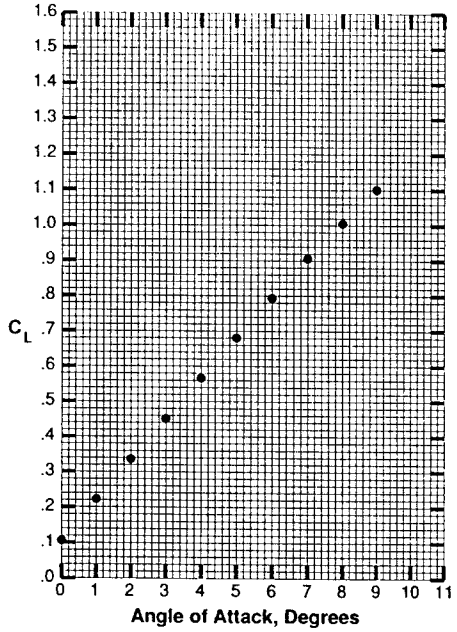

Fig. 5.3 Lift variation with angle of attack, NACA 23012 airfoil.

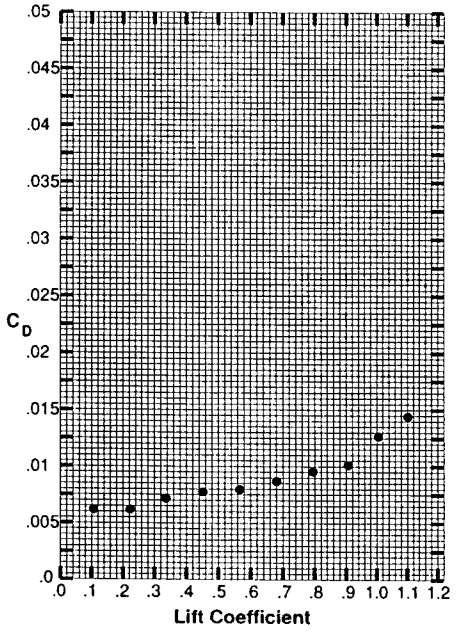

Fig. 5.4 Lift–drag characteristics, NACA 23012 airfoil.

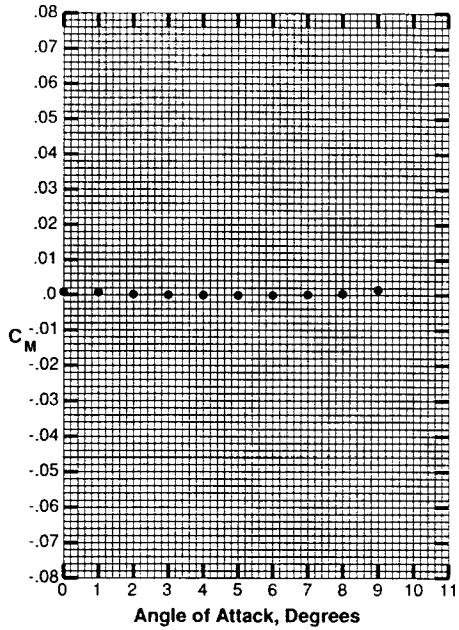

Fig. 5.5 Quarter-chord pitching moment characteristics.

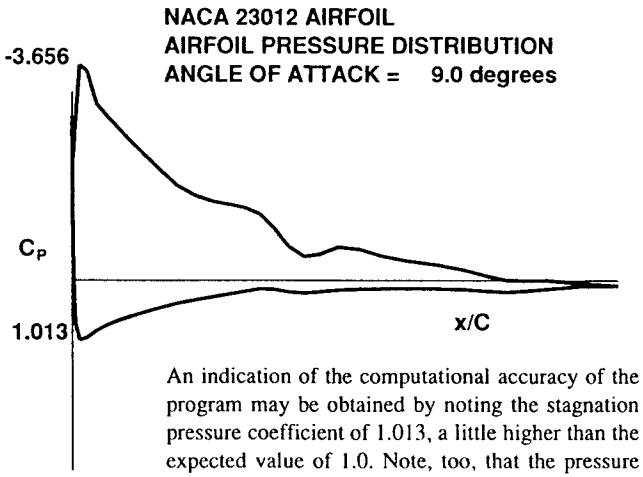

An indication of the computational accuracy of the program may be obtained by noting the stagnation pressure coefficient of 1.013, a little higher than the expected value of 1.0. Note, too, that the pressure distribution exhibits a dip in the same region as the defect in the upper surface contour.

Fig. 5.6 Pressure distribution, NACA 23012 airfoil.

```
1                    LOAD SUMMARY SHEET--ITERATION NUMBER 4

                     NACA 23012 AIRFOIL

MACH NUMBER       =  .30000        REFERENCE CHORD (BASIS FOR ALL COEFFICIENT NORMALIZATION) =  1.00000 FT.
REYNOLDS NO.      =  3.00000 MILLION  ANGLE OF ATTACK (VALUE OF IALPHA = 0)                   =  9.00000 DEG.
                                        (IALPHA=0--ANGLE DEFINED W.R.T. REFERENCE LINE)
LONGEST CHORDLINE =  1.00000 FEET      (IALPHA=1--ANGLE DEFINED W.R.T. LONGEST CHORDLINE)

ANGLE BETWEEN LONGEST CHORDLINE AND REFERENCE LINE =  .00000 DEG.  (POSITIVE FOR REFERENCE LINE BELOW THE LONGEST CHORDLINE)

                                                    LIFT COEFFICIENTS
NORMAL FORCE COEFFICIENTS                                (CL) PRESS.  =  1.10052
                    (CN) PRESS. =  1.08824               (CL) SHEAR   =   .00066
                    (CN) SHEAR  =   .00165               CL           =  1.10118
                    CN          =  1.08989

                                                    DRAG COEFFICIENTS
AXIAL FORCE COEFFICIENTS                                 (CD) PRESS.  =   .00812
                    (CA) PRESS. =  -.16413               (CD) SHEAR   =   .00636
                    (CA) SHEAR  =   .00618               CD           =   .01449
                    CA          =  -.15795

                                                    MOMENT COEFFICIENTS
MOMENT COEFFICIENTS                                      (CM) ABOUT NOSE        =  -.27096
(ABOUT NOSE)        (CM) PRESS  =  -.27112               (CM) QUARTER CHORD     =   .00151
                    (CM) SHEAR  =   .00016
                    CM          =  -.27096

DRAG COEFFICIENT COMPUTED BY SQUIRE-YOUNG FORMULA =  .01174
ZEROTH ITERATION PRESSURE DRAG =  -.00183          X/C(UPPER) =  .03570
TRANSITION POINTS:  X/C(LOWER) =  .39289

1NACA 23012 AIRFOIL          FSMACH =  .30000

 ALPHA       CL          CD          CM (NOSE)  CM (1/4-CHORD)
 .000000     .106393     .006192     -.025781    .000817
 1.000000    .223105     .006193     -.055059    .000736
 2.000000    .336017     .007168     -.083858    .000158
 3.000000    .451138     .007758     -.112719    .000012
 4.000000    .566448     .007994     -.141452    -.000046
 5.000000    .680761     .008728     -.169848    -.000115
 6.000000    .794064     .009591     -.197798    -.000119
 7.000000    .906054     .010167     -.225053    .000082
 8.000000    1.005502    .012724     -.249026    .000345
 9.000000    1.101179    .014487     -.270964    .001508
```

Fig. 5.7 Partial output listing of AIRFOIL program.

Notice that Fig. 5.2 does evidence some lack of smoothness. Because the smoothing algorithm creates a total of 65 points, the figure actually analyzed will be somewhat smoother than the one shown, which has only 36 points. (Notice, too, the finite trailing-edge thickness.)

The amount of output data written to AIRFOIL.TXT can vary from 3.5 Kbytes to 505 Kbytes depending on the value of IWRITE selected. Initially the user may wish to invoke the verbose option (IWRITE = 0) but for production runs IWRITE = 3 will probably be sufficient.

The value of the computed results ultimately depends on how well the results match experimental data for a variety of situations. The NASA contractor's report shows how well the computed results match wind-tunnel test data for 15 airfoils of varying camber and thickness. Eight of these, covering a range of thicknesses, are shown in Fig. 5.8. Lift and drag characteristics for these airfoils and one additional airfoil taken from the contractor's report are shown in Fig. 5.9.

5.3.4 Significance of Results

Some comments on the characteristics exhibited by these airfoils and the ability of the program to predict them would seem to be in order.

The airfoil designated S-14.1 is formed by two circular arcs. The entire lower surface is essentially concave as far as the oncoming flow is concerned up to a fairly large angle of attack. The effect of the program's inability to handle such geometries is shown clearly in the characteristics. They are actually very nonlinear, a fact not detected by the analysis. Only at $\alpha = 2$ deg is the lift coefficient approximately correct. At the same time, the predicted drag coefficient is less than half the actual value.

The variation of lift coefficient with angle of attack for the very thin NACA 63-006 airfoil is predicted accurately for angles of attack up to 8 deg. The predicted drag is reasonable over this angle range but does not evidence the familiar drag bucket, which occurs for lift coefficients between -0.1 and 0.1.

When the airfoil thickness is increased 50%, the prediction gets even better as evidenced by the characteristics of the 0009 airfoil. Both the lift and drag predictions are very good, the former to a C_L of 1.2.

The very thick NACA 2424 airfoil exhibits a nonconstant lift curve slope, which the predicted results fail to replicate, particularly for angles of attack greater than 6 deg. The drag characteristics underpredict the experimental values for C_L greater than 0.8. These results may be considered in light of the discussion regarding Eq. (5.21).

The lift characteristics of the moderate thickness NACA 63_2-615 airfoil are well predicted for angles of attack up to 8 deg and the drag characteristics agree closely with the experimental results for $C_L < 1.3$. Even the thicker NACA 63_4-421 airfoil gives similar results. However, when one attempts to maintain a laminar boundary layer even farther aft on the upper surface by specifying a NACA 64_4-421 airfoil, good agreement with experiment ceases when $\alpha > 8$ deg or $C_L > 1.0$ (for drag values).

As we have mentioned previously, when boundary-layer trips are affixed to the airfoil in the form of strips of sand paper, the changes in drag and $C_{L_{max}}$ are greater than predicted by fixing transition at the leading edge. For the NACA 4412

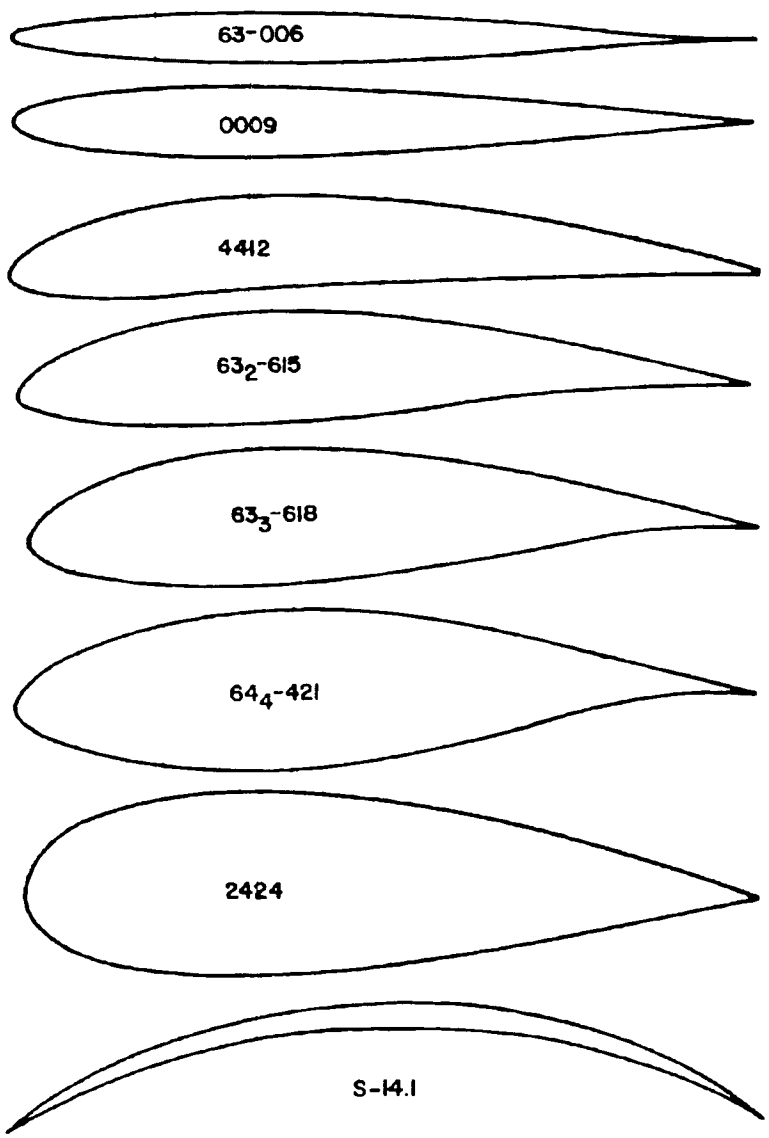

Fig. 5.8 Tested airfoils.

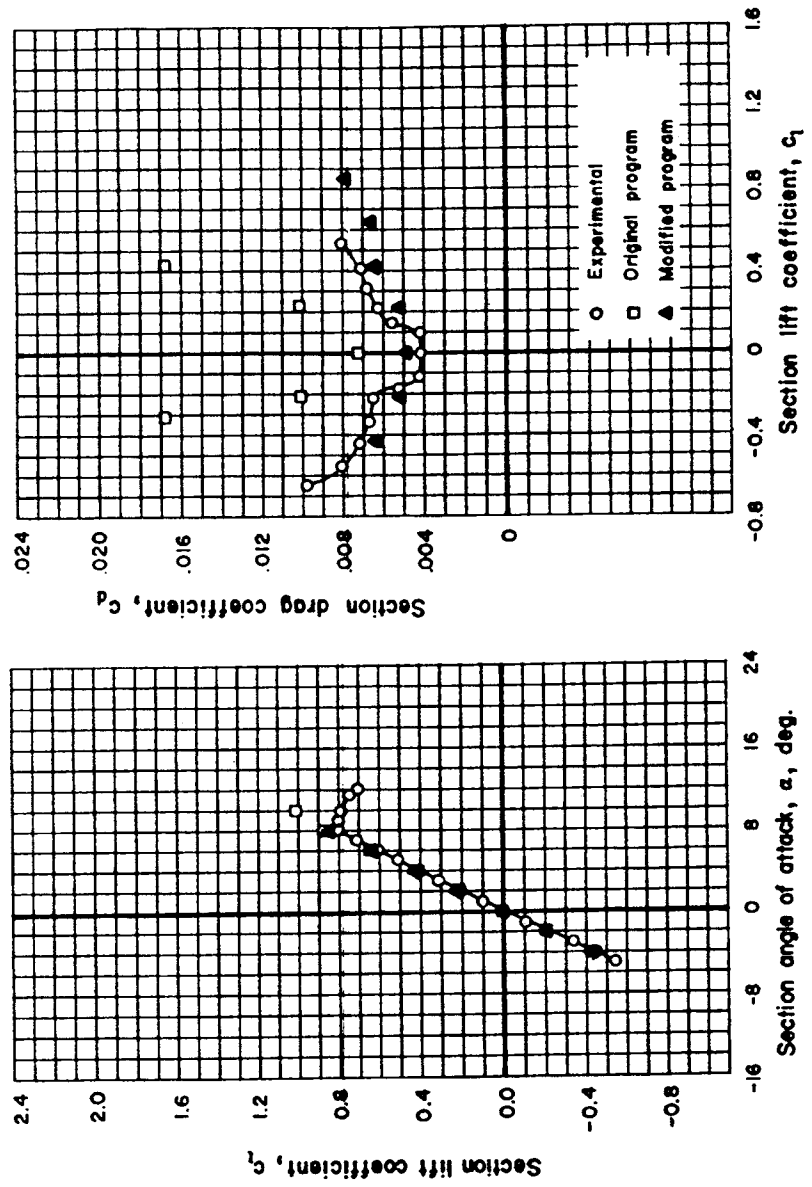

Fig. 5.9a Measured and predicted characteristics of NACA 63-006 airfoil.

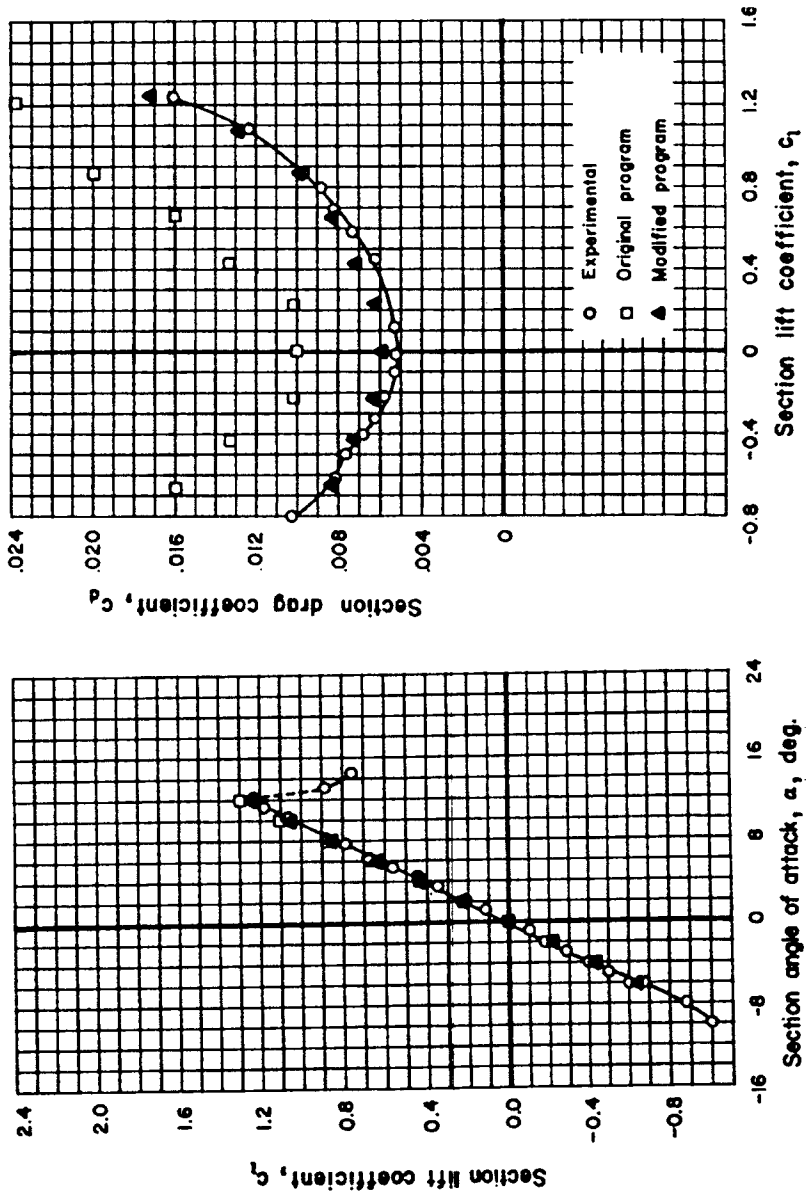

Fig. 5.9b Measured and predicted characteristics of NACA 0009 airfoil.

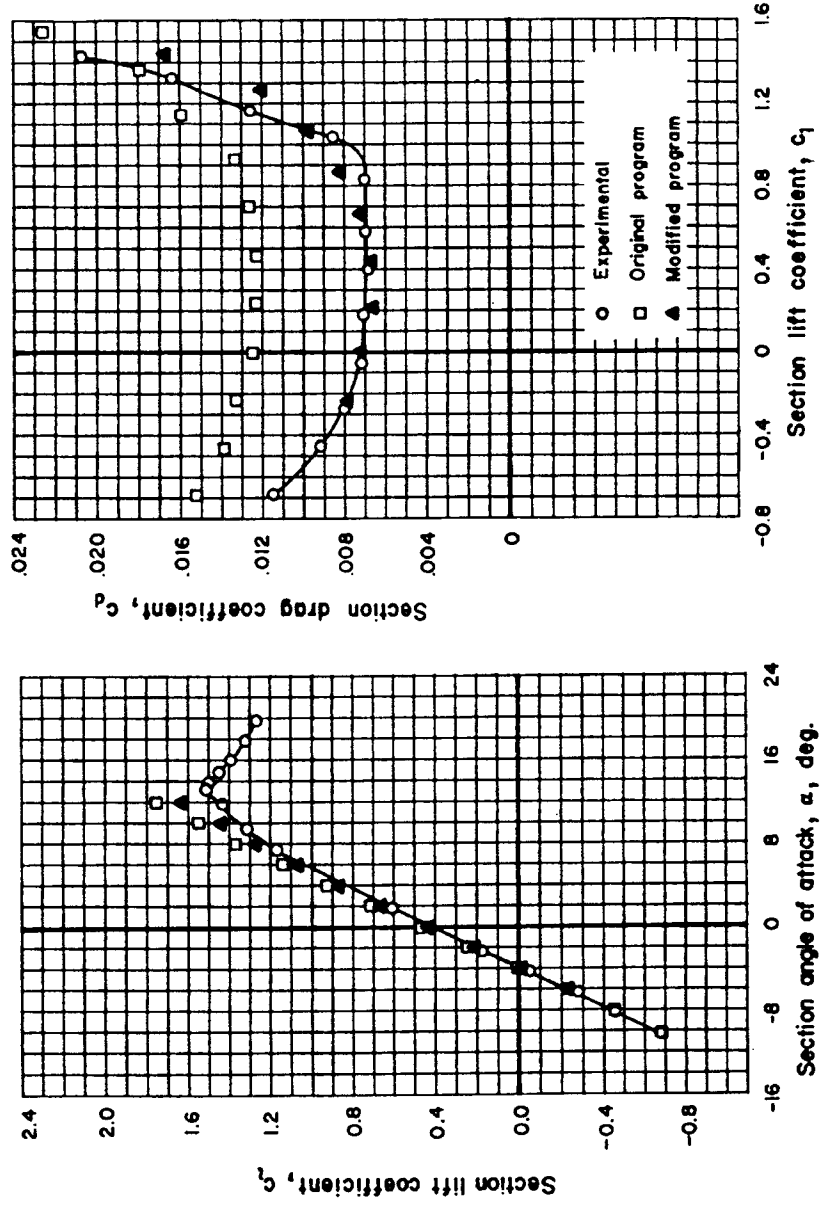

Fig. 5.9c Measured and predicted characteristics of NACA 4412 airfoil.

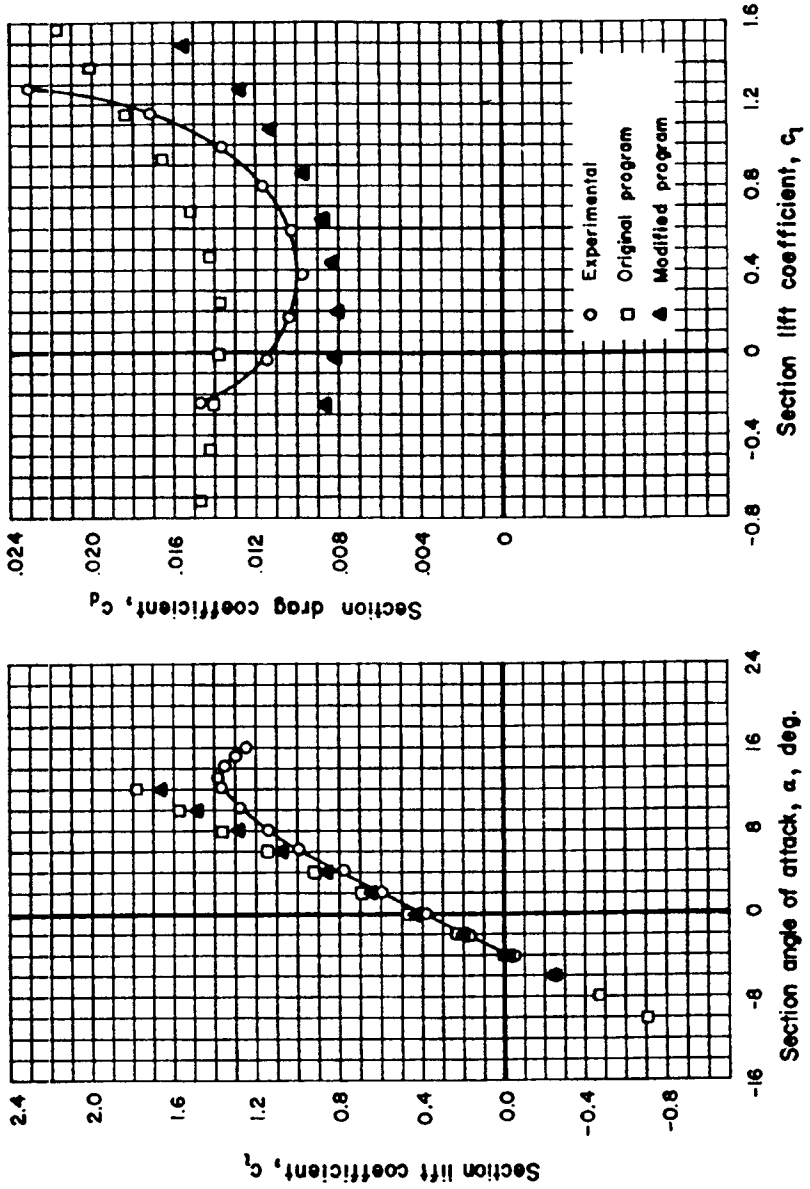

Fig. 5.9d Effect of roughness on characteristics of NACA 4412 airfoil.

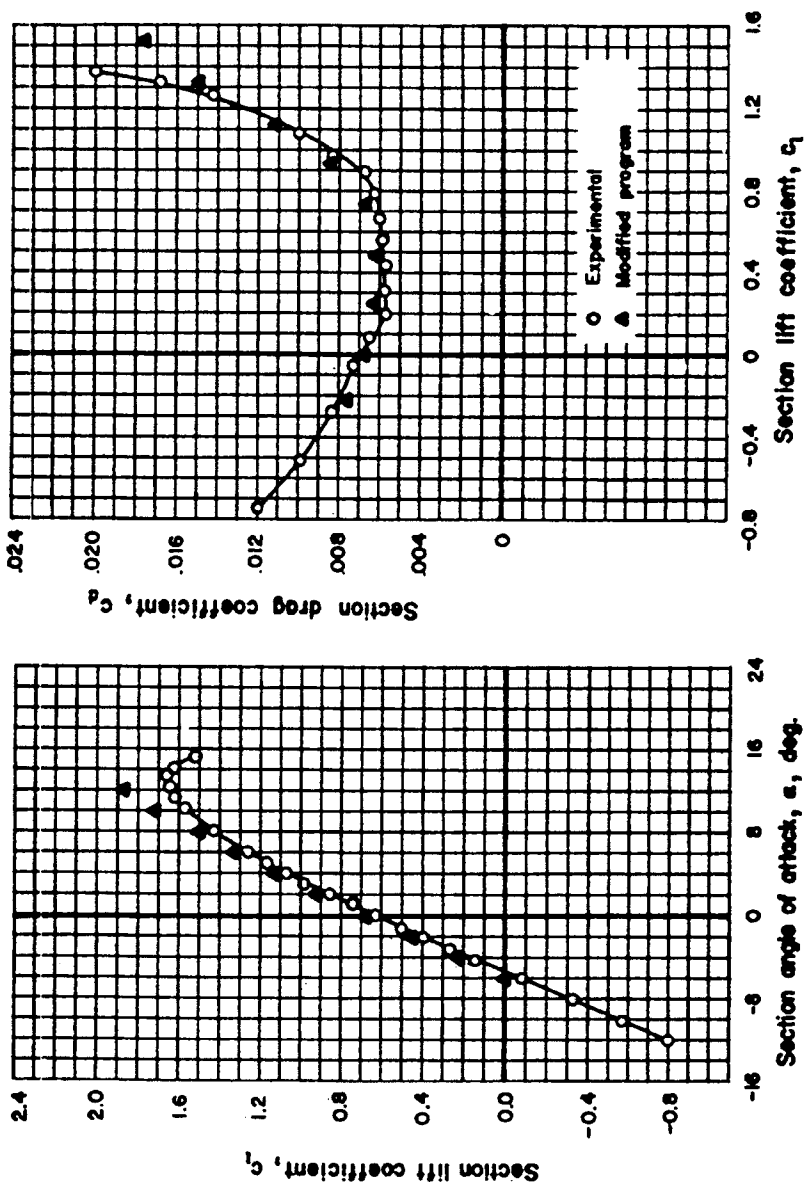

Fig. 5.9e Measured and predicted characteristics of NACA 65_2-615 airfoil.

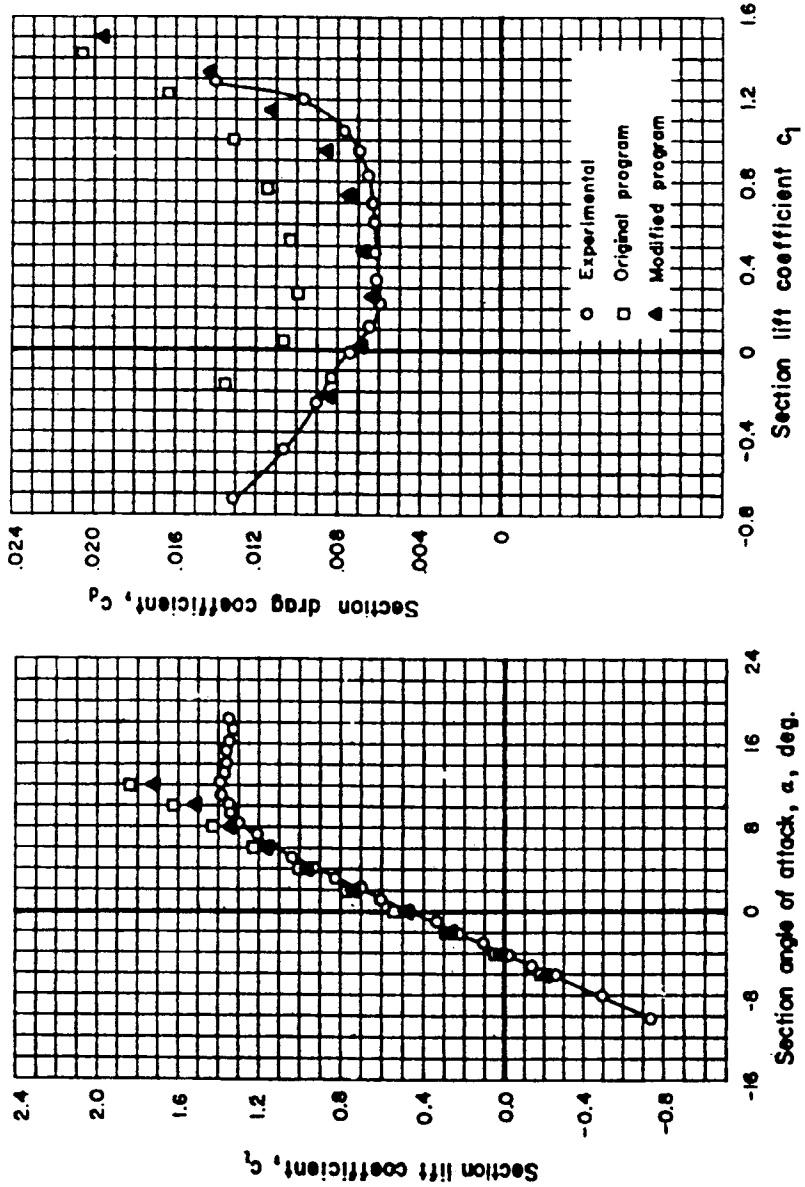

Fig. 5.9f Measured and predicted characteristics of NACA 63_3-618 airfoil.

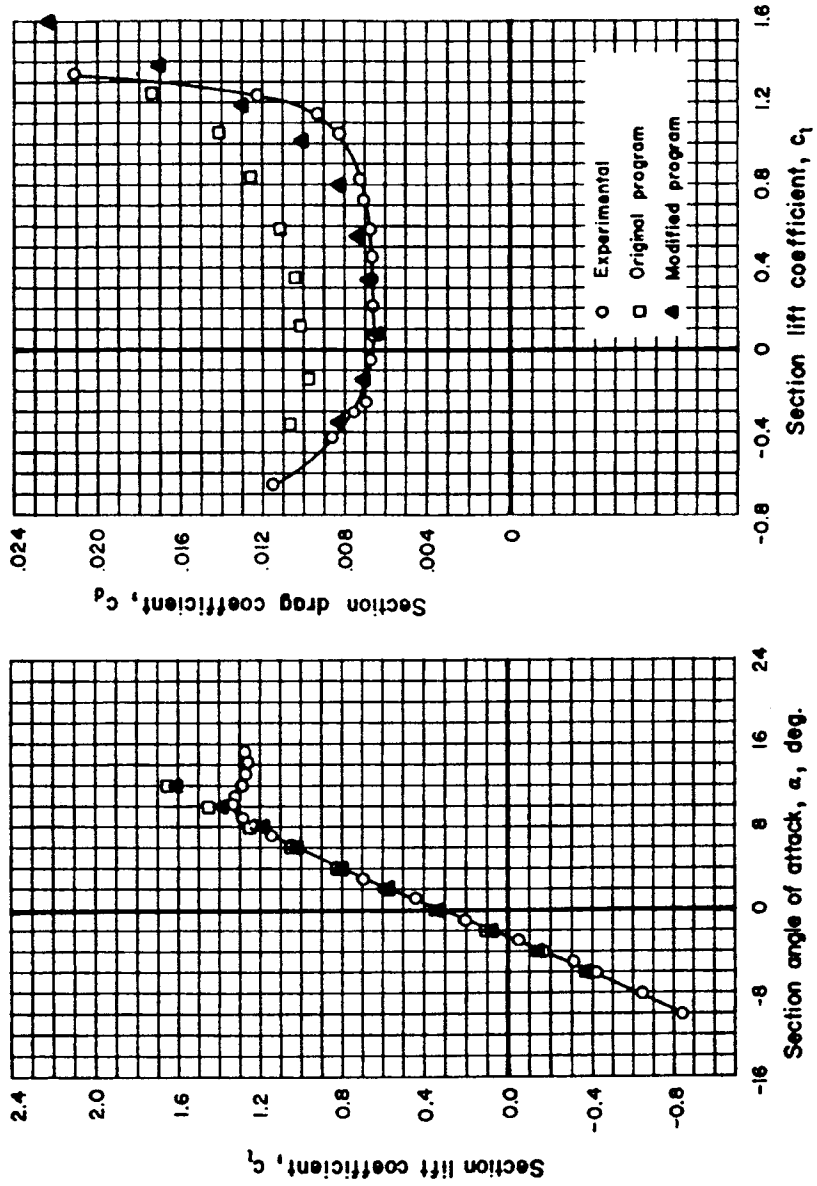

Fig. 5.9g Measured and predicted characteristics of NACA 63_4-421 airfoil.

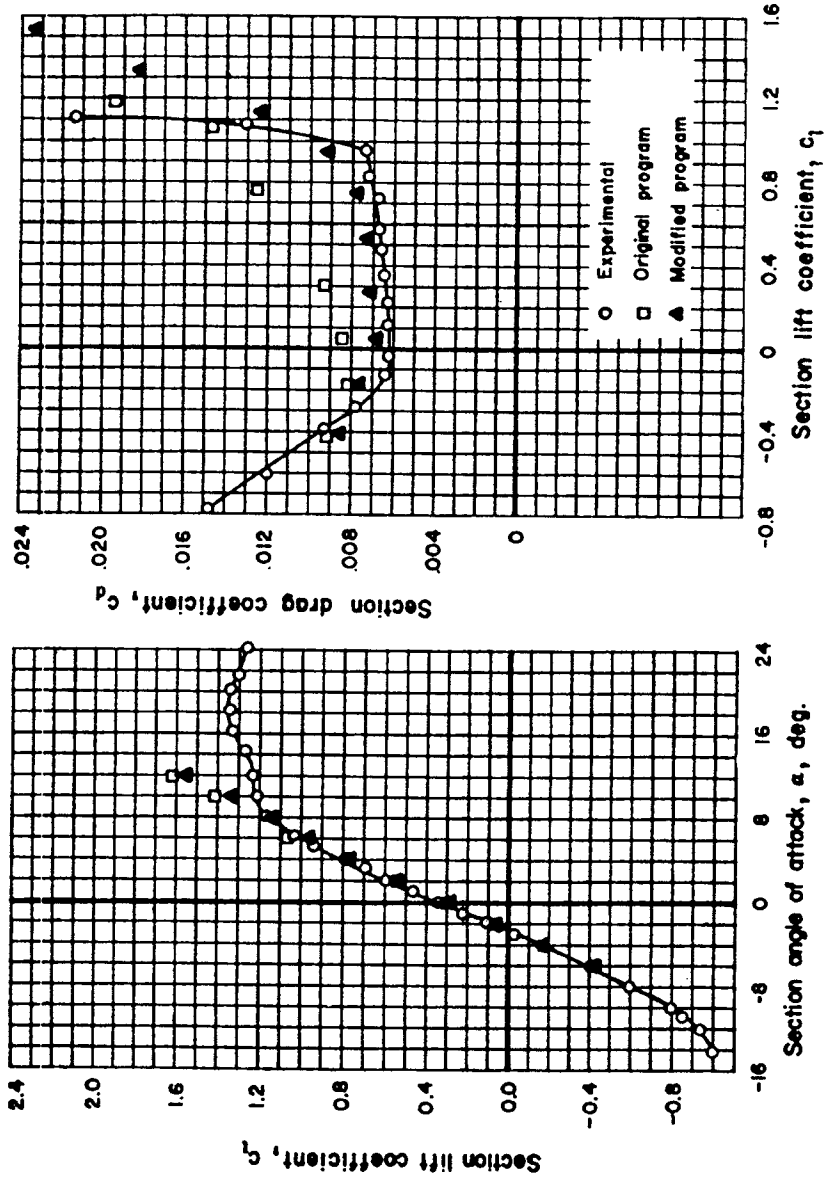

Fig. 5.9h Measured and predicted characteristics of NACA 64$_4$-421 airfoil.

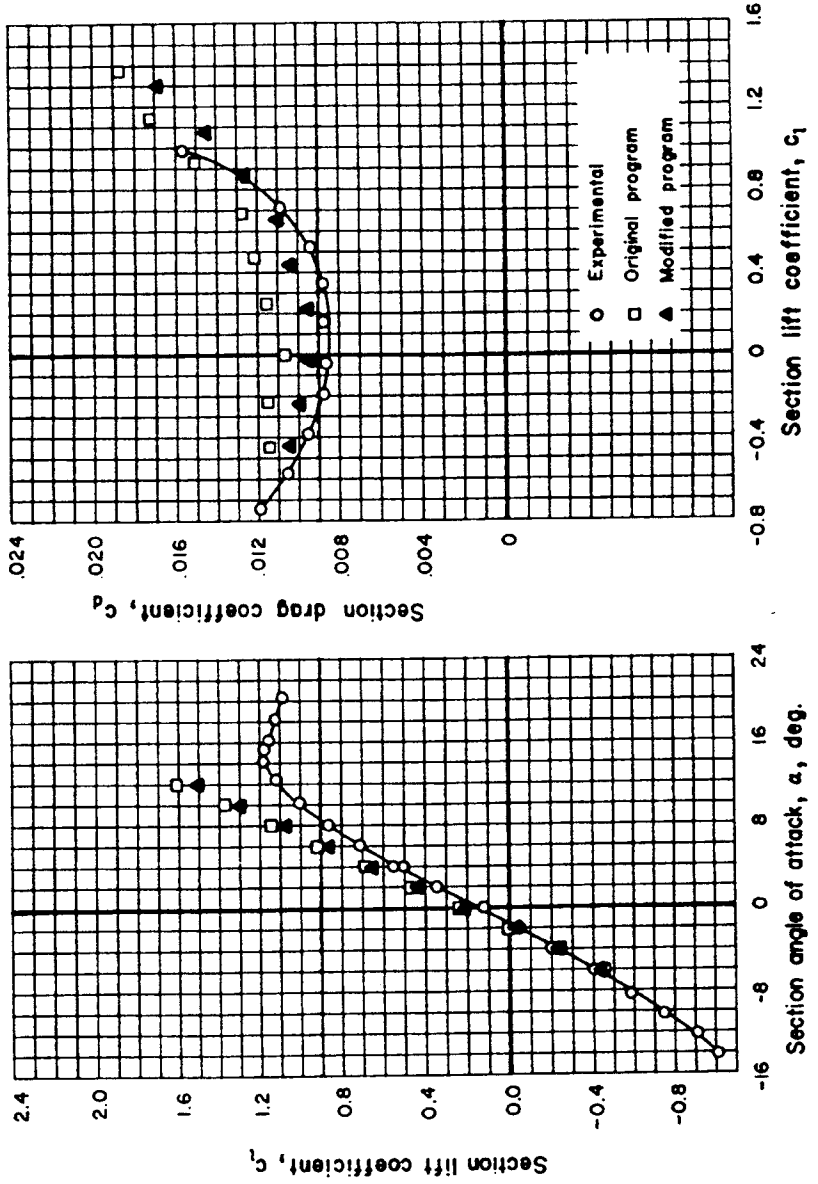

Fig. 5.9i Measured and predicted characteristics of NACA 2424 airfoil.

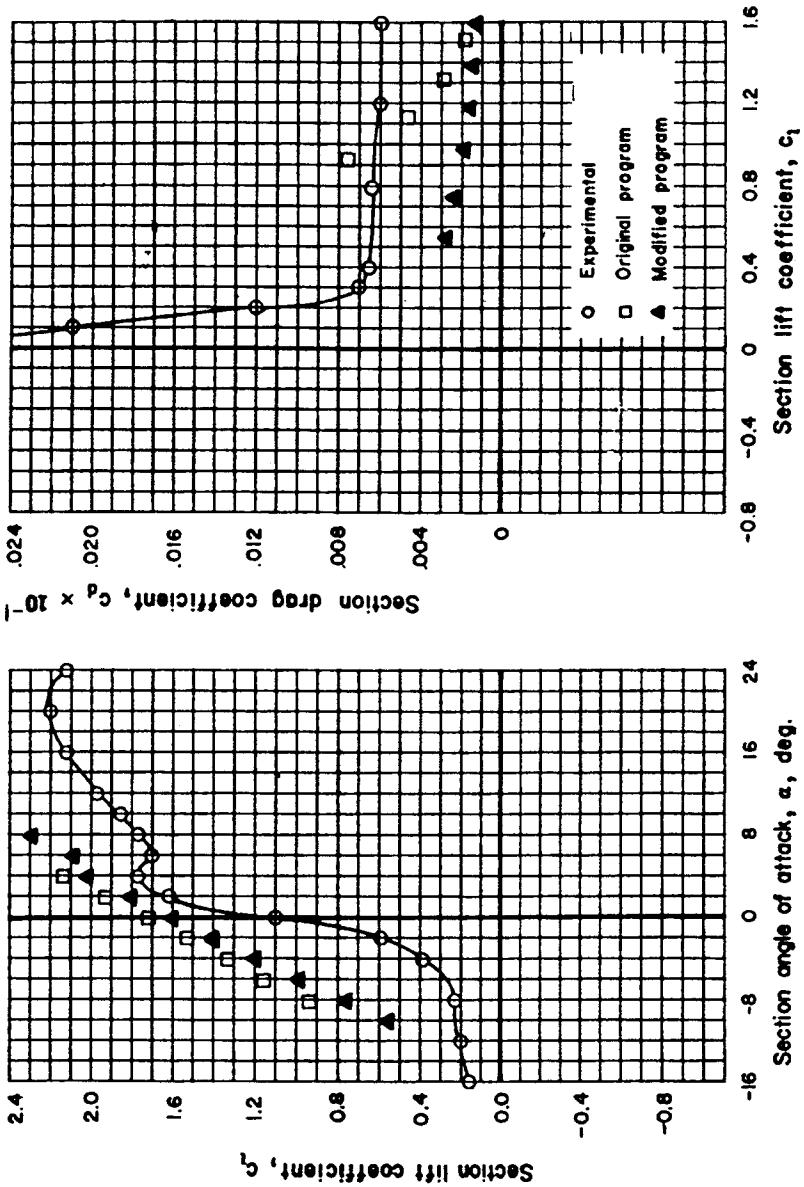

Fig. 5.9j Measured (Ref. 30) and predicted characteristics of S-14.1 airfoil.

airfoil the actual minimum drag coefficient is more than 25% greater than program prediction. The prediction becomes worse as C_L increases.

A review of these results indicates that for conventional airfoils, e.g., those without concave surfaces, the program yields good agreement with experiment for $C_L < 0.8$ and in some cases for higher values of C_L. Although we have chosen not to show them here, Ref. 26 gives comparisons between the predictions of our theory and experimental data from Ref. 29 for an unconventional airfoil. Drag results for dirty airfoils, e.g., those with bugs on them or with manufacturing irregularities, will probably be optimistic because the boundary-layer routine used in the program is simply not able to account for such disturbances. Thus, the program can be very useful for performing design analyses when the aircraft is in the cruise or climb configuration, but it is of limited utility for estimating the aerodynamic characteristics during approach when the lift coefficient is large. Depending on the individual design it may or may not be useful during takeoff. If the C_L exceeds 0.8 during takeoff or if extensive use of flaps is required, then more sophisticated routines or experimental results should be employed. Nevertheless, the relative simplicity of AIRFOIL and the quality of the results it produces should give the reader an indication of the theoretical bases of modern aerodynamic prediction programs and provide a guide to those areas where the present theory has been improved in more recent work.

The problems supplied later in this chapter provide the reader with some structured examples of how the program may be applied and some of the points to be noted in the results.

5.4 Airfoil Selection Criteria

With the ability to determine many of the aerodynamic characteristics of virtually any arbitrary airfoil now provided by a relatively simple computer program, the question naturally arises as to what characteristics are desirable. The answer to that question, not surprisingly, depends on the application to which the airfoil is put. We have alluded to some of the considerations used to make this choice. All of the applications we will consider are in the subsonic flight regime.

5.4.1 Long-Range Vehicle

To construct a long-range air-supported vehicle we need a wing with a high aspect ratio and a high lift-to-drag ratio. The latter condition is usually satisfied by ensuring that the wing surface is smooth and that the wing operates at angles of attack where the pressure gradient is favorable over a significant portion of the upper surface. A high aspect ratio minimizes induced drag, a type of drag of which we have not yet spoken. But for structural reasons a high aspect ratio is difficult to provide if the wing is not relatively thick. These considerations alone dictate an airfoil at least 12% thick. Then there is the question as to whether one wishes to use the wing to encase engines, landing gear, or other items. For example, the B-36 intercontinental bomber, which was the mainstay of the U.S. Air Force immediately following World War II, used the NACA 63(420)-422 airfoil. The root wing section on this aircraft was 8 ft thick and the span extended 320 ft. The six 3500-hp Pratt and Whitney R-4360 radial engines were enclosed in the wing and drove three-bladed pusher propellers. (In later models two turbojet engines

in an external pod were mounted outboard of the piston engines on each wing. The same pod was used on the first jet bomber, the B-47. The use of these pods enabled the gross takeoff weight of the B-36J to reach 450,000 lb.)

The wing on the B-36 was sufficiently thick that a mechanic could move along a passageway in the wing on a creeper to service the engines while in flight. This thick airfoil also provided an additional benefit: unmatched stall characteristics. Tests showed that $C_{L_{max}}$ could be maintained all of the way from 16-deg angle of attack to 24-deg angle of attack. One can well imagine the sight of this 230-ft-long aircraft landing. With its long, cylindrical fuselage it was said that the pilots were 100 ft in the air when the main wheels touched down.

A long-range aircraft must be relatively lightweight to carry a large amount of fuel. Making its wing stiff in torsion and in bending requires additional weight. The compromise selected by the designers of the B-36 was to limit the forward speed to 150 mph indicated. The means that the dynamic pressure is never more than 57.4 lb/ft^2 at any altitude. Although this might seem unduly slow considering the aircraft's mission, it should be remembered that the operational altitude of the aircraft was 50,180 ft. At that altitude 150 mph indicated is 383.6-mph true airspeed. At that altitude the speed of sound is 661 mph. For the thick airfoil used on the B-36 the critical Mach number is about 0.58 for a C_L of about 0.346. A true airspeed of 383.4 mph represents a flight Mach number of 0.58 at that altitude. Because the aircraft was Mach number limited to 150 mph indicated at its design altitude, the decision was made to design the structure to that limit as well. The supporting calculations for this rationale may be summarized as follows:

flight velocity = 150 mph at sea level = $1.467 \times 150 = 220$ ft/s
dynamic pressure = $\frac{1}{2}\rho v^2 = \frac{1}{2}(0.002378)(220)^2 = 57.4$ psf
density at 50,180 ft = 0.00036238 slugs/ft^3
true airspeed = $\sqrt{2(57.2)/0.00036238} = 383.6$ mph
temperature at 50,180 ft = 390°R
speed of sound at 50,180 ft = 661 mph
Mach number corresponding to true airspeed = 383.6/661 = 0.58
most negative C_P on airfoil at $\alpha = 0$ deg is -1.064
$C_L = 0.346$
M_{CR} see Fig. 5.10
weight at 50,180 ft and 383.6 mph = 178,681 lb
wing area = 9000 ft^2
maximum airfoil lift-to-drag ratio = 102.1, and
aspect ratio = 11.378.

Although the NACA 63(420)-422 airfoil has good stall characteristics it does not have a particularly high value of $C_{L_{max}}$ (about 1.3) at a Reynolds mumber of 3×10^6. Because of this one would ordinarily expect that a more complex flap arrangement would have to be used than for an airfoil with a higher $C_{L_{max}}$ to obtain the same landing speed. However, the root chord of the wing is over 36 ft long which means the Reynolds number for landing is on the order of 10^7. Because $C_{L_{max}}$ increases with increasing Reynolds number, the actual $C_{L_{max}}$ for landing will be somewhat greater than originally expected. Propeller driven aircraft, particularly those with pusher propellers in the plane of the wing, can energize a low-turbulence airstream over the wing by the application of power. This can make the effective Reynolds number over the wing during landing even higher.

5.4.2 High-Level Flight Speed

For highest level flight speed on a given amount of power one seeks to reduce the drag to the maximum extent possible. This means that the profile drag of the wing will be one of the drag factors one seeks to minimize. The induced drag at this condition is naturally very low because the aircraft will be operating at a $C_L \to 0$. Thin airfoils have inherently less profile drag than thick airfoils. Thus, for operation at the high-speed level flight condition one desires as thin an airfoil as is structually feasible. We may note that the X-3 research airplane used a 3% thick wing machined from a solid bar of aluminum alloy. Other requirements such as acceptable stall characteristics and the need for storage space within the wing may ameliorate the specification of such a thin wing.

By way of definition, the critical Mach number is the flight Mach number for which the velocity on the upper surface of the airfoil first reaches the speed of sound. The reason this is important is that flight velocities above this value but below sound speed cause regions of supersonic flow to develop on the wing, which must terminate in shock waves. The resultant pressure rise across the shock wave can cause the boundary layer to separate. The point on the upper surface where the flow first reaches the speed of sound is also the point where the pressure coefficient is a minimum. The location of this point and the minimum pressure coefficient may change with angle of attack or, to put it another way, with lift coefficient. As used, the pressure coefficient is defined in terms of incompressible theory. Prandtl and Glauert developed a simple correction to the pressure coefficient to account for the compressibility of air. They suggested that the compressible value could be obtained from the incompressible in the following manner:

$$C_{P_{comp}} = \frac{C_{P_{inc}}}{1 - M_\infty^2} \tag{5.22}$$

Beginning with the equation defining the stagnation pressure in a compressible stream in terms of the static pressure, Mach number, and ratio of specific heats γ, and assuming that the stagnation pressure is constant in the flow around the airfoil, one can derive the following equation relating the minimum incompressible pressure coefficient to the critical Mach number:

$$C_{P_{inc}} = \left(1 - M_{cr}^2\right)\left[\frac{\left(\dfrac{1 + 0.2M_{cr}^2}{1.2}\right)^{3.5} - 1}{\dfrac{\gamma}{2}M_{cr}^2}\right] \tag{5.23}$$

This equation is graphed in Fig. 5.10.

NACA TR-824[16] contains charts relating critical Mach number to lift coefficient for specific airfoils. The relationship is linear for most of the C_L range. In the case of the NACA 63(420)-422 airfoil, the chart gives the critical Mach number at $C_L = 0$ as 0.6 and 0.5 at a $C_L = 1$. Because the minimum pressure coefficient for a zero lift coefficient is about -0.84 and the minimum pressure coefficient for a lift coefficient of 1.0 is about -1.6 for this airfoil, it will be seen that the values in Fig. 5.10 agree with the NACA charts. The difference in the presentations is that the data in Fig. 5.10 are universal. However, to apply that graph to a specific airfoil,

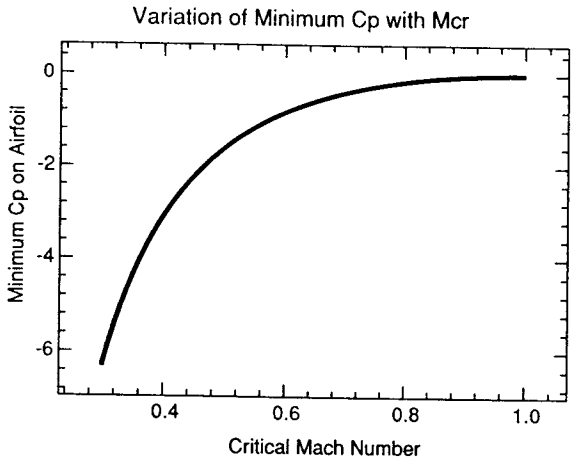

Fig. 5.10 Variation in critical Mach number with minimum pressure coefficient on airfoil.

the incompressible pressure distribution over that airfoil must be known at various lift coefficients. For greater understanding, the reader may wish to undertake the derivation of Eq. (5.23).

5.4.3 High $C_{L_{max}}$

When high $C_{L_{max}}$ becomes a dominant consideration driven, say, by a wish to obtain low landing speeds without the use of flaps or large wing areas, then special attention is paid to the exact Reynolds number at which $C_{L_{max}}$ is required and to the characteristics of airfoils at this Reynolds number. To obtain a favorable pressure gradient on the upper surface of the airfoil to as high an angle of attack as possible, it is necessary that the radius of curvature in this region be relatively large. Airfoils that achieve this condition often have rather bulbous noses with a nearly flat, but still convex, upper surface. Almost all of the shaping of the airfoil occurs on the lower surface. A $C_{L_{max}}$ of 2.1 at $Re = 9.2 \times 10^2$ is reachable in these designs.

5.4.4 Supercavitating Hydrofoils

Hydrofoils encounter a problem at high speeds that airfoils do not: cavitation. This refers to visible pitting, which occurs on shapes that move at high speed in water. The pitting is the result of the collapse of gas bubbles near the surface of the foil and the subsequent erosion due to the very high shear rates, which are created by the liquid rushing to fill the collapsed gas bubble. The gas bubbles are created when the velocity over the foil is sufficiently high that the local pressure drops below the local vapor pressure of the water. This erosion can be very severe in a relatively short period of time.

For years the onset of cavitation served to limit the speed that hydrofoils could be operated much like the speed of sound served to limit the speed of airfoils although for a different reason. The solution to the problem was the development of supercavitating hydrofoils. These foils are wedge shaped with blunt aft ends. Such foils have their minimum pressure points at the aft end of the foil. When

the gas bubble collapses, there is nothing but wake below it, and the foil itself suffers relatively little damage. However, there is a price to be paid for the ability to operate at speeds above those for which cavitation would occur on normal hydrofoils: higher drag than for hydrofoils with near zero trailing-edge angles.

The design of supercavitating hydrofoils is beyond the scope of the present text as is the design of supercritical airfoils, which are those that are shaped such that the shock wave due to the recovery from locally supersonic flow over the upper surface occurs very near the trailing edge and is relatively weak.

5.4.5 Sailplanes

A high cruise lift-to-drag ratio is desirable for many flight vehicles because it means that for a given weight the drag at cruise will be low. In a powered aircraft this translates to long range because the available fuel will burn at a lower rate and the flight can last longer at the same speed. In an unpowered vehicle a high lift-to-drag ratio translates into a shallower gliding angle and a lower sinking speed. Setting up a balance of the forces involved shows that

$$L\sin\gamma = D\cos\gamma$$

$$L\cos\gamma + D\sin\gamma = W$$

Hence, the glide path angle γ for steady-state glide is seen to be

$$\gamma = \tan^{-1}\left(\frac{D}{L}\right)$$

where the sinking speed V_s is

$$V_s = V\sin\gamma$$

For best sailplane performance, a very high lift-to-drag ratio is essential. This means we seek an airfoil section with very low profile drag but thick enough to support a very high aspect ratio. Because of the very high aspect ratio the wing chord and, therefore, the wing Reynolds number will be relatively small. We will not, therefore, be able to take advantage of airfoil sections that can achieve high values of C_L at high Reynolds numbers.

If we plot L/D vs C_L for airfoils we find that the peak value of L/D usually occurs in the range of $0.6 \leq C_L \leq 1.0$. The peak values are 100–133. A 15% thick airfoil probably has a minimum drag coefficient that is about 50% greater than a 6% thick airfoil. When all factors are considered, an airfoil 12–15% thick with a modest pitching moment coefficient (to keep the trim drag, i.e., the drag associated with the tail load necessary to balance the wing pitching moment, at moderate levels) will usually be selected. It will be built into a wing with a taper ratio of 0.5 to 0.7 and an aspect ratio of around 25. Taper ratio, a term we have not defined previously, is the ratio of the tip chord to the root chord. We show in the next chapter that an elliptical wing planform leads to minimum induced drag and that a trapezoidal planform with the proper taper ratio yields only slightly greater induced drag and is easier to build. The wing surface itself will be made as smooth as possible to ensure that the predicted value of C_D is actually achieved.

The airfoils chosen for sailplane are often of the NACA 65 and 66 series with design lift coefficients in the 0.4–0.6 range. Note, however, that because the

pitching moment coefficient cannot be permitted to become excessive the design lift coefficient may be restricted to the lower end of the range.

5.4.6 Maneuverable, Medium-Speed Vehicle

In this class of vehicle we may put such aircraft as World War II fighters and modern agricultural aircraft (crop dusters). Here the desire is for a wing that provides good high-lift characteristics without the use of auxillary high-lift devices. Good high-lift characteristics include high $C_{L_{max}}$ and benign stall characteristics. The NACA 4412 section was much used for such aircraft. Its characteristics are shown in Fig. 5.9c. Shown also are its characteristics with standard roughness (Fig. 5.9d) which in service might mean bug and dust deposits. It will be seen that this airfoil's lift characteristics are relatively unaffected, although the drag will increase significantly.

5.4.7 Piston Powered Transport Aircraft

Aircraft in this class may operate under conditions similar to those experienced by aircraft in the previous class. By operating at lower altitudes and smaller fields they may experience relatively greater amounts of bugs and dust than jets, which require longer runways and fly at higher altitudes. Money usually is not available for sophisticated high-lift devices and so inherently good $C_{L_{max}}$ from the airfoil itself is desired. Because very high cruise speeds are not achieved because the necessary power is not available in this class of aircraft, the selected airfoil need not have the absolute minimum profile drag. Again, the NACA 4412 section is a good selection but with higher aspect ratios (up to 11 or 12) than those in the previous class.

5.4.8 General Aviation Vehicle

New aircraft in this class are often kit built. The current trend is for wings to be constructed in molds from composite materials. This manufacturing process results in very smooth surfaces and makes it practical to think of using very low-drag sections. Use of such sections along with similarly smooth fuselages can yield sharply lower power requirements for a given speed. With sharply lower power requirements comes smaller, less expensive engines, greater range, and reduced operating costs while maintaining acceptable cruise speeds. Airfoils in the NACA 64 and 65 series with design C_L in the 0.2–0.4 range are usually considered first for this application. With aspect ratios in the 6–7 range, a 12% thick section is feasible with the fabrication techniques employed.

It is also possible to employ programs such as AIRFOIL to design custom airfoil sections for such aircraft. A marketing advantage may be seen by the designer from the use of a custom section. Perhaps a simpler structural layout or manufacturing simplicity may be realized with a custom design without compromising performance.

The flap arrangements in these aircraft are comparatively simple. A plain flap, split flap, or simple slotted flap may be used.

5.5 Other Approaches to Airfoil Design

AIRFOIL is what may be called an analysis program. It permits one to determine the aerodynamic characteristics of an existing airfoil. There is, however, an inverse procedure, one in which the pressure distribution is specified at a particular angle of attack. The program then generates an airfoil shape producing the specified pressure distribution if such a shape is possible. Such a procedure may be called a synthesis approach to airfoil design. We do not propose to discuss the details of such a procedure in this book but merely note that one popular program that operates in this manner was developed by Richard Eppler of Stuttgart University in Germany and Dan Sommers of NASA Langley Research Center. Analysis approaches usually are simpler to understand but often require iterative refinement to achieve optimal results. The synthesis approach trades somewhat greater mathematical complexity for a direct path to the optimal shape.

5.6 Concluding Remarks

In this chapter we looked in detail at a method for determining the lift, drag, and moment characteristics of a prespecified airfoil shape provided the airfoil has no concave surfaces. The method yields results that agree well with experimental data for smooth airfoils operating at lift coefficients up to 0.8 or so. The method does not include the ability to model large, separated wakes (for example, by additional sources whose strengths are set to produce separation from a predicted point at a particular angle) and, therefore, cannot predict $C_{L_{max}}$. The method can accommodate increases in Mach number up to about 0.55.

Although ostensibly an inviscid procedure, the method accounts for the effect of viscosity in the flow over the airfoil surface by adding a displacement thickness to the airfoil geometry and recomputing the inviscid flowfield outside the boundary layer. The iteration between airfoil pseudo-boundaries and the external pressure distribution is continued until the boundary-layer displacement thickness is that which one would calculate for the then existing pressure distribuion outside the boundary layer. The existence of displacement thicknesses on both upper and lower surfaces lead to the creation of an airfoil wake and associated form drag and necessitates the location of the downstream stagnation point at some place in the wake. The skin-friction drag is calculated as part of the boundary-layer routine. Integration of the surface pressures gives the lift coefficient and the moment coefficient. Integration of the streamwise components of the pressure around the airfoil gives the form drag.

Problems

5.1. Take a 65-point set of coordinates for a Joukowski airfoil and run the AIRFOIL program for this coordinate set. Compare the lift values with the results of JOUKOW.

5.2. For the same Joukowski airfoil take 65 other points and run AIRFOIL on them. Do you get the same results as for problem 5.1? What do you conclude as a result of this comparison?

5.3. The following data, written in AIRFOIL.DAT format, represent one of the NACA 6-series airfoils.

```
NACA 63(420)-422
26   26    2    0    0
   .0000     .1870     .3980     .8500    2.0410    4.4920    6.9770    9.4780
 14.5090   19.5630   24.6300   29.7050   34.7840   39.8610   44.9340   50.0000
 55.0570   60.1040   65.1400   70.1630   75.1720   80.1650   85.1420   90.1030
 95.0510  100.0000
   .0000    1.9595    2.4020    3.0880    4.3120    6.0500    7.3870    8.4960
 10.2310   11.4890   12.3770   12.8900   13.0340   12.8830   12.4930   11.9070
 11.1470   10.2770    9.1690    7.9880    6.7000    5.3290    3.9180    2.5130
  1.1810     .0000
   .0000     .8130    1.1020    1.6500    2.9590    5.5080    8.0230   10.5220
 15.4910   20.4370   25.3700   30.2950   35.2160   40.1390   45.0660   50.0000
 54.9430   59.8960   64.8600   69.8370   74.8280   79.8350   84.8580   89.8970
 94.9490  100.0000
   .0000   -1.7590   -2.1220   -2.6600   -3.5680   -4.7860   -5.6910   -6.4280
 -7.5390   -8.3050   -8.7970   -9.0020   -8.9140   -8.5990   -8.1130   -7.4950
 -6.7670   -5.9430   -5.0490   -4.1000   -3.1200   -2.1450   -1.2260    -.4450
   .0830     .000
```

The reference chord is 100.0 units. Run AIRFOIL for nine angles of attack, 0–8 deg in 1 deg increments. Base the Reynolds number on a real chord length of 36 ft and a flight Mach number of 0.223 when the absolute temperature is 520°R. Note that the graph of pitching moment coefficient about the quarter-chord may be off scale. The scale can be changed by changing the factor multiplying CM14 on line 2682 of AIRFOIL.FOR and recompiling. The numbers identifying the vertical scale in the figure then need to be changed to match. A factor of 10 is easiest to implement.

a) From the pressure distributions, deduce the largest angle of attack for which the pressure gradient is favorable over the forward portion of the upper surface.

b) What is the lift curve slope at $\alpha = 0$? Is it constant for the data available and if not, why not?

c) What is the minimum drag coefficient?

d) What is the drag coefficient for the angle of attack you deduce in problem 5.3a?

e) If the angle of attack is 5 deg and the dynamic pressure is 743 psf, what is the minimum pressure on the upper surface for these conditions? Assume the static pressure is 2116 psf and the absolute temperature is 520°R.

f) What is the highest Mach number over the upper surface for these conditions?

g) What application might be suitable for the use of this airfoil?

h) What is the lift coefficient for the minimum drag coefficient?

i) At what angle of attack is the maximum lift-to-drag ratio achieved?

j) In terms of application of this airfoil to airplanes, what is the implication of the values of $C_{m_{c/4}}$ found by the program?

k) Investigate the effect of changing Reynolds number and transition location on the aerodynamic characteristics of this airfoil. Consider Reynolds numbers from 1×10^6 to 10^8. Describe your results. Note particularly which characteristics are most affected.

l) See if you can find wind-tunnel test results for this airfoil and compare them to the results predicted by the program. Your best source of data will be NACA Report 824.[16] Comment also on the experimental stall characteristics of this airfoil.

m) At what flight Mach number does the Mach number on the upper surface first reach 1.0 when the angle of attack is 5 deg?

n) At what angle of attack is the design lift coefficient reached?

o) At what angle of attack should you expect to find a lift coefficient of zero?

p) Assume that you can model ice accumulation on the airfoil by forcing transition at the leading edge. What is the effect of ice accumulation on the aerodynamic characteristics? Referring now to experimental data, what generally is the effect of applying standard roughness to the airfoil?

5.4. Determine the thickness of the airfoil shown in Fig. P5.1 relative to the chord.

5.5. Is the airfoil in Fig. P5.1 cambered?

5.6. What technique is used in an effort to have AIRFOIL account for bugs smashed on the airfoil surface, manufacturing irregularities, or rain drops on the surface?

5.7. The airfoil in Fig. P5.1 is shown at $\alpha = 0$. Should you expect the lift coefficient at this angle of attack to be zero? Why?

5.8. Using the airfoil data given in problem 5.3, determine the variation in aerodynamic characteristics for negative angles of attack. (Note that the C_L vs α and C_L vs C_D plots may be blank because C_L may be negative for most α or α is negative. Note, too, that because of the downwardly curved trailing-edge data for α less than some value will probably be in error because this portion of the airfoil then will be operating as a concave surface in relation to the oncoming stream.) Is there an angle about which the lift coefficient is a mirror image? If so, what is the angle?

5.9. How would undesirable stall characteristics show up on the C_L vs α plot? Explain why a particular characteristic is undesirable.

5.10. Plot the airfoil data given in problem 5.3 to a large scale on graph paper. Then for about 30 points along the chord line determine the mean camber line by adding the ordinates of the upper surface to those of the lower surface including

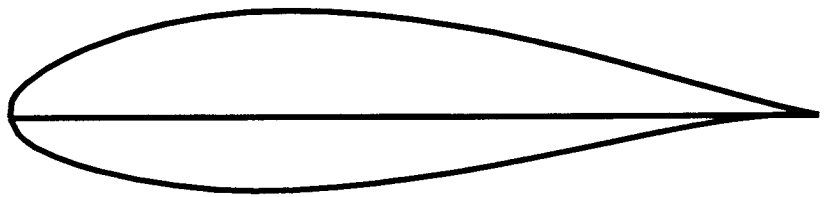

Fig. P5.1 Airfoil profile drawn using straight line segments between the 50 input points.

the signs on the lower surface ordinates. This sum should be the mean camber line. Now subtract the z value of the mean camber line from the upper surface ordinates and the lower surface ordinates. Submit the resulting data to AIRFOIL. In effect the new airfoil should be a symmetrical version of the original airfoil. Do the aerodynamic characteristics of the symmetrical airfoil match those of the cambered airfoil except for being shifted in α? Provide graphs to support your contention.

5.11. If the boundary layer on a 0024 airfoil at $\alpha = 0$ remains attached to the surface, how should you expect C_D to differ from that obtained on a 0006 airfoil at the same angle of attack? Discuss and, in particular, suggest how the magnitudes of the drag coefficients on the two airfoils may differ. If all else fails, run the AIRFOIL program to obtain the information.

5.12. The ordinates of a NACA 66-006 airfoil follow. Present a pressure coefficient plot for an angle of attack for which the drag coefficient lies in the drag bucket. This region should occur where the lift coefficient is near zero for this airfoil. Then, present a pressure coefficient plot for an angle of attack for which the drag coefficient is outside the drag bucket. Discuss the differences in the pressure coefficient plots.

```
NACA 66-006 AIRFOIL
26   26     2     1     0
  .0000      .5000      .7500     1.2500     2.5000     5.0000     7.5000    10.0000
 15.0000    20.0000    25.0000    30.0000    35.0000    40.0000    45.0000    50.0000
 55.0000    60.0000    65.0000    70.0000    75.0000    80.0000    85.0000    90.0000
 95.0000   100.0000
  .0000      .4610      .5540      .6930      .9180     1.2570     1.5240     1.7520
 2.1190     2.4010     2.6180     2.7820     2.8990     2.9710     3.0000     2.9850
 2.9250     2.8150     2.6110     2.3160     1.9430     1.5430     1.1070      .6650
  .2620      .0000
  .0000      .5000      .7500     1.2500     2.5000     5.0000     7.5000    10.0000
 15.0000    20.0000    25.0000    30.0000    35.0000    40.0000    45.0000    50.0000
 55.0000    60.0000    65.0000    70.0000    75.0000    80.0000    85.0000    90.0000
 95.0000   100.0000
  .0000     -.4610     -.5540     -.6930     -.9180    -1.2570    -1.5240    -1.7520
-2.1190    -2.4010    -2.6180    -2.7820    -2.8990    -2.9710    -3.0000    -2.9850
-2.9250    -2.8150    -2.6110    -2.3160    -1.9530    -1.5430    -1.1070     -.6650
 -.2620      .0000
```

5.13. Repeat problem 5.3(m) for the NACA 66-006 airfoil.

5.14. The drag force experienced by a wing in flight is given by $C_D \frac{1}{2}\rho S V^2$ where ρ is the atmospheric density, V is the flight velocity, and S is the wing area. Assuming that structural considerations can be ignored for the moment and that all other conditions and dimensions, such as wing area and wing chord, are the same except for the airfoil section, compare the drag associated with the NACA 65-006 airfoil relative to the NACA 63(420)-422 airfoil at sea level and a speed of 250 ft/s.

5.15. Considering the results of problems 5.13 and 5.14, what would be the motive in selecting the NACA 66-006 airfoil if high-speed flight is desired?

5.16. The deflection of a simple cantilever beam depends inversely on the depth cubed. What inference might one make as to the deflection under load of wings of the same span and chord if one wing uses a NACA 63(420)-422 airfoil and the other uses a NACA 66-006 airfoil? Which airfoil is better suited for use in wings of high aspect ratio?

5.17. Boundary layers separate in the face of steep adverse pressure gradients. (An adverse pressure gradient is one for which the pressure is increasing). When the boundary layer separates, there is a large region on the lea side of the airfoil over which the pressure is very low. Hence, the airfoil exhibits a significant drag. If the flow must negotiate a region with a small radius of curvature the velocities must change rapidly in a short distance and, hence, pressure gradients in such regions are likely to be steep. Considering this information, what are the likely stall characteristics of thin airfoils such as the NACA 65-006? By stall characteristics we mean the change in lift coefficient for a small change in angle of attack in the region near $C_{L_{max}}$. For many airfoils, the lift coefficient drops suddenly for a small increase in angle of attack. This is considered poor stall characteristics.

5.18. What are the expected stall characteristics of the NACA 63(420)-422 airfoil?

5.19. Consult a reference such as NACA TR 824[16] and determine the variation of C_L with α for α between 16 and 24 deg. Does this airfoil have good stall characteristics?

5.20. The NACA-6 series of airfoils were intended to provide varying amounts of laminary boundary-layer flow on the upper surface at design lift coefficient. The second number in the designation indicates the chord fraction over which there is a favorable pressure gradient and, therefore, the chord fraction over which the boundary layer should be laminar. Depending on the manufacturing technology used, the wing skin may be rather smooth or exhibit an occasional wrinkle. Which of the airfoil series, the 63, 64, 65, or 66, should you expect to be the most sensitive to manufacturing imperfections, rain, or bug splatter? For the clean condition, which of the series should you expect to have the lowest drag?

5.21. The center of gravity is the point about which the aircraft rotates in its x–z plane as a result of unbalanced forces or moments applied to the aircraft in this plane. When the wing lift is considered to be applied at the wing quarter chord, a pitching moment, represented by $C_{m_{c/4}}$, results because the center of pressure on the airfoil is actually located at some other place. When the center of pressure is farther aft than the quarter-chord, $C_{m_{c/4}}$ is negative, that is, the moment seeks to cause the aircraft nose to pitch down. In equilibrium flight, the forces and moments must be in balance. When the center of gravity is located near the leading edge

of the wing, there is a large negative moment around it due to the lift force times the distance from the quarter-chord to the center of gravity, in addition to the moment about the quarter-chord. These moments must be balanced by a moment produced by a download on the tail. When the forces involved are summed, it is seen that for such a case the wing lift must be equal to the aircraft weight plus the download on the tail. Associated with this additional lift is an additional drag. This is termed a trim drag because it arises from the need to balance or trim the aircraft. If one is going to design a flying wing, that is, an airplane without a tail to provide the trimming force, and needs to place the center of gravity slightly ahead of the quarter-chord for stability reasons, what sort of aerodynamic characteristics should one look for in an airfoil?

5.22. What changes would you make to the data set shown in problem 5.12 if the airfoil were to be used on a undersea vehicle traveling at 10 knots? How are these changes likely to affect the lift, drag, and pitching moment? Although the program does not compute the characteristics for angles of attack greater than 8–10 deg properly, generate some informed speculation on the effect that insertion into water has on the characteristics near $C_{L_{max}}$.

5.23. Both the Joukowski theory and thin airfoil theory find a lift curve slope of 2π per radian. Compare the results of programs calculations for the NACA 66-006 and NACA 63(420)-422 airfoils with this value. What are your conclusions?

5.24. Discuss how you might use Eqs. (5.18) and (5.19) to construct a picture of a specific airfoil in the manner of the stream function plots of Chapter 2. You are not being asked to do it. Just outline the steps involved. Is this something you might conceivably do by hand?

5.25. How does the boundary-layer displacement thickness on the aft portions of a specific airfoil vary with increasing flight velocity when the angle of attack remains constant? Be quantitative.

5.26. Locate the chordwise station on the NACA 63(420)-422 airfoil where the thickness is a maximum. For $\alpha = 0$, integrate the components of the pressure in the drag direction for all locations forward of the point of maximum thickness on the airfoil. Assume that the boundary layer separates from both surfaces at the point of maximum thickness and that the pressure on the airfoil surface aft of the point of maximum thickness is constant at the value of the C_P at the point of separation on the upper surface. For such an assumption, what is the drag coefficient?

5.27. Which airfoil, a NACA 66-006 or a NACA 63(420)-422 airfoil, has the highest maximum lift-to-drag ratio?

5.28. Modify the coordinates of the NACA 66-006 airfoil according to how you think some ice accumulation on the wing might cause the profile to appear. Then run AIRFOIL and compare the aerodynamic characteristics with those of the unmodified airfoil. Submit a listing of your modified coordinates. [Two approaches you may wish to consider are: a) a uniform coating over the entire airfoil surface and b) a buildup primarily in the nose region.]

5.29. If an airfoil section and wing planform are selected primarily to suit the power available at the cruise condition, what does the designer normally do to reduce the landing speed?

5.30. Based on the concept suggested in problem 5.26 estimate the wake thickness for the NACA 66-006 airfoil at $\alpha = 0$. Apply the concept to the NACA 63(420)-422 airfoil.

5.31. Rerun problem 5.30 for the same velocity but operating in water instead of air.

5.32. Before the development of programs such as AIRFOIL, NACA TR 824[16] was the principal source of information used by airframe designers to select airfoils for their subsonic vehicles. Discuss the change in subsonic airframe design practice permitted by the availablility of programs like AIRFOIL.

5.33. What traps can a user fall into by using AIRFOIL without understanding the theoretical basis of the program?

5.34. If the NACA 63(420)-422 airfoil were turned upside down and $\alpha = 5$ deg, at what Mach number would the velocity on the then upper surface first reach the speed of sound?

5.35. Construct a 22% Joukowski airfoil with roughly the same camber as the NACA 63(420)-422 airfoil. Compare the location of the minimum pressure on the upper surface for $\alpha = 4$ deg. Does your result support the contention that the minimum pressure point on the Joukowski profile is farther forward than on the NACA 63(420)-422?

5.36. As already noted, the NACA 6-series airfoils were intended primarily to produce low values of drag. Maximum lift coefficient on these airfoils is about 1.6 for a Reynolds number of 3×10^6. Some of the thicker airfoils have maximum lift coefficients of 1.3 or so at this Reynolds number. What sort of shapes might one use to obtain airfoils capable of higher maximum lift coefficients? For some hints, you may wish to consult NASA TN D-7071 (Ref. 30) or some of the work of Richard Whitcomb related to his supercritical airfoil shapes. A critical feature of such airfoils is that they are contoured to preserve a favorable pressure distribution at high angles of attack.

5.37. Discuss the correlation between lift coefficient at $\alpha = 0$ and the value of $C_{m_{c/4}}$.

5.38. Older 4-digit NACA airfoils such as the 4412 were used extensively on World War II military aircraft. Why would this airfoil be suitable for situations where manufacturing irregularities were difficult to prevent and where service factors might lead to frequent debris on the wing?

5.39. Using the coordinates for a 12% thick uncambered Joukowski airfoil, run AIRFOIL and determine the aerodynamic characteristics up to an angle of attack

of 12 deg. Then manually modify the coordinates on the upper surface alternately by 1% (so as to make the surface rough) and rerun AIRFOIL. Discuss your results.

5.40. Compare the minimum drag coefficient of the NACA 63(420)-422 airfoil with that of the NACA 66-006 airfoil. Assuming the aspect ratio and wing area were the same, how would the drag of the two airfoils compare?

5.41. Draw a supercavitating hydrofoil on paper. For simplicity let the chord be 10 cm long. Let the base have a thickness of 1 cm. If you wish you may put a small amount of camber into it. Let the nose radius be 1 mm. Now enter a set of ordinates describing this hydrofoil into AIRFOIL. Report your results and discuss. In your calculations consider a speed of 10 knots under water. Be sure to obtain data at several angles of attack.

5.42. Would you expect to use a cambered airfoil section as the dive planes on a submarine and why?

5.43. A Fowler flap is one which first extends rearward and then deflects the trailing edge downward. What does extension and/or deflection of a Fowler flap do the the airfoil's pitching moment.

5.44. What is the likely effect on C_L vs α of using some means to keep the boundary layer attached regardless of α? Devices used to accomplish this are multielement flaps and slats, suction of the boundary layer at a far rearward chordwise station, and blowing into the boundary layer along a line parallel to the airfoil surface.

5.45. Investigate the variation of the lift curve slope with airfoil thickness. You may use the data in Fig. 5.9 for this purpose.

5.46. The ordinates of a modified NACA 63_2-615 airfoil are given in the following data set against which you are to run AIRFOIL:

```
NACA 63-615 AIRFOIL (modified)
26   26     2     1     0
   .0000     .2050     .4180     .8660    2.0500    4.4920    6.9730    9.4730
 14.5040   19.5580   24.6250   29.7000   34.7780   39.8570   44.9320   50.0000
 55.0580   60.1050   65.1390   70.1590   75.1630   80.1530   85.1270   90.0890
 95.0420  100.0000
   .0000    2.1636    2.3882    2.9718    3.9170    5.3891    6.3294    7.1760
  8.3812    9.3560   10.000    10.4310   10.5870   10.5980   10.3840    9.9740
  9.3930    8.6650    7.8090    6.8470    5.8000    4.6930    3.5550    2.3980
  1.2450     .0000
   .0000     .7950    1.0820    1.6340    2.9500    5.5080    8.0270   10.5270
 15.4960   20.4420   25.3750   30.3000   35.2220   40.1430   45.0680   50.0000
 54.9420   59.8950   64.8610   69.8410   74.8370   79.8470   84.8730   89.9110
 94.9580  100.0000
   .0000   -1.8306   -1.9728   -2.2065   -2.6840   -3.1362   -3.5346   -3.8860
 -4.2020   -4.3500   -4.4300   -4.4990   -4.4070   -4.1720   -3.8140   -3.3560
 -2.8230   -2.2390   -1.6290   -1.0150    -.4300     .0830     .4830     .7040
   .6510     .0000
```


For the range of applicability of the program are any of the characteristics of this modified airfoil superior to those of the original airfoil for any of the uses discussed in Sec. 5.4?

5.47. Aircraft that are supposed to fly supersonically must still takeoff and land. One of the early supersonic airfoils developed from a consideration of inviscid compressible flow theory was in the shape of a diamond with two corners at $0.5C$ and the other two corners at 0.0 and $1.0C$. Although inviscid supersonic theory tells one the corners should be sharp, subsonic theory would prefer rounded corners. Construct a diamond airfoil with a maximum thickness of $0.09C$. Put a radius of $0.01C$ on all four corners. (Such an airfoil type was actually flown on the X-3 research airplane; however, the test wing was only 3% thick.) Analyze this airfoil with AIRFOIL. a) How reliable do you think the results are? b) Why? c) Assuming the results are reliable, would this be an airfoil one might consider using for a light aircraft wing? d) Why?

5.48. Submit the pressure distribution results for the airfoil in problem 5.47 in a report discussing the results.

5.49. Construct a 10% thick airfoil made with two circular arcs such that the airfoil has no concave surfaces. a) Analyze via AIRFOIL. b) Discuss the suitability of this airfoil for a light aircraft wing application based on your results. c) Under what conditions should you expect the results to require verification via a wind-tunnel test? d) Why?

5.50. Construct a 3% flat plate airfoil with nose and tail radii equal to 1.5% of chord. a) Analyze via AIRFOIL for Reynolds numbers 10^3, 10^4, 10^5, and 10^6 and several angles of attack. b) Discuss your results. Estimate the validity of the result as part of your discussion. In particular, consider the pressure gradient on the upper surface as the angle of attack increases.

5.51. For use in a wind powered electric generator one desires an airfoil with a high lift-to-drag ratio. Also, the blades should have a high length-to-chord ratio to minimize induced drag. Thus, very thin airfoils may not be satisfactory for this application. Determine the maximum lift-to-drag ratio and the angle of attack at which it occurs for the NACA 63_2-615 airfoil.

5.52. Draw an airfoil such as that shown in Fig. P5.2 on millimeter graph paper. Consider this a representation of the airfoil section used in an airplane made by folding a piece of paper. Develop a set or ordinates for this airfoil and analyze by AIRFOIL for several angles of attack and a Reynolds number less than 10,000. a) Discuss your results. b) Is AIRFOIL a suitable means to analyze such an airfoil? c) Explain.

Fig. P5.2 Representation of airfoil for paper airplane.

5.53. Consult a set of steam tables to determine the vapor pressure of water. At what speed in water would a NACA-0006 airfoil at zero angle of attack first find a mimimum pressure below the vapor pressure of water? Assume the hydrofoil is operating at a depth of 10 ft. The hydrofoil chord may be assumed to be 1 ft.

5.54. Develop the coordinates of an ellipse where the semimajor axis is 10 times the semiminor axis. Submit the configuration to AIRFOIL. a) Comment on the results. b) Discuss the problems the shape might have operating at an angle of attack of 180 deg. Angle of attack in this case is measured relative to the major axis.

5.55. Assume that you have been given the task of designing an airfoil that can produce the greatest possible value of $C_{L_{max}}$ without the use of slats, flaps, or other auxilliary devices at a given Reynolds number. Would AIRFOIL prove to be a useful tool in this endeavor and why?

5.56. Under what conditions (to what angle of attack) would AIRFOIL prove useful in analyzing the characteristics of a NACA 63(420)-422 airfoil at negative angles of attack and why?

5.57. The moment of inertia of a wing in bending is roughly proportional to the thickness squared. Assuming the chord remains constant, by how much could the span of a wing be increased for the same maximum bending stress by going from a NACA 0006 airfoil to a NACA 63(420)-422 airfoil? We will assume that the lift coefficient in the two cases is the same; hence, the lift force will increase directly with area, e.g., with span. We will also assume that the lift per unit span is constant. Bending stress is $\tau = Mc/I$ where c is half the maximum thickness of the wing. M is the product of the total lift times the distance from the center of lift to the fixed edge of the wing.

6
The Wing

6.1 Introduction

SELECTION of an airfoil profile or profiles is but the first task in the creation of a wing. There are structural considerations, considerations of the mission and the environment in which the wing will operate, consideration of the planform and the twist applied the wing so as to minimize induced drag, consideration of the effects of flexibility on the performance of aerodynamic surfaces attached to the wing and on wing flutter, and considerations of sweepback or sweepforward so as to minimize compressibility drag if the flight is to include speeds near Mach number 1. We will treat only those aspects related to the low-speed flight of a rigid wing. However, we may include the effects of stall on the performance of lateral control devices in assisting us to select suitable tip twist or section camber.

Early investigators soon realized that the characteristics of a complete wing were not the same as those of a two-dimensional airfoil. For example, the angle of attack at which a complete wing stalls is higher than the angle at which an airfoil section stalls. Also, the drag of a complete wing is higher than the drag of an airfoil section. Investigators noticed that aspect ratio, taper ratio, and twist all affect these differences. Twist refers to the angular difference between the angle of attack of the wing tip and the angle of attack of the wing root.

We could define sweepback as the angle between the wing leading edge and a line normal to the fuselage centerline. We could also use as our sweepback angle reference the wing quarter-chord or the wing half-chord lines. In cases where the airplane has tapered wings, it seems preferable to use the wing half-chord line as the sweepback reference, and we shall do so. Because we limit our consideration to wings with little or no sweepback, the choice of a half-chord sweepback reference helps make unambiguous the planform of the considered wings.

We will also restrict our consideration also to wings of moderate to high aspect ratio, which means aspect ratios of about 5 or greater. We do this because such wings better fit the assumptions of the lifting line theory, which will be the basis of our analysis. In this theory the actual wing is replaced by a vortex bundle, the ends of which trail into space behind the aircraft and come together at infinity. Looking at the bundle from the left wingtip, the vortices are clockwise. Looking at the trailing vortices from downstream, the left trailing vortex has clockwise circulation and the right trailing vortex has counterclockwise circulation. The horseshoe vortex system is shown schematically in Fig. 6.1.

We use the term vortex bundle to indicate that the wing is represented by a number of line vortices of different lengths, which may be laid on top of one another along the wing; the ends of each vortex leave the wing at different spanwise stations. The portion of each line vortex that lies in the plane of the wing is called a bound vortex. The bound vortex and the two trailing vortices together make up a horseshoe vortex. Because the components of the bound vortex vary in length the net vorticity can vary along the wing span. The shed portions of all of the vortices

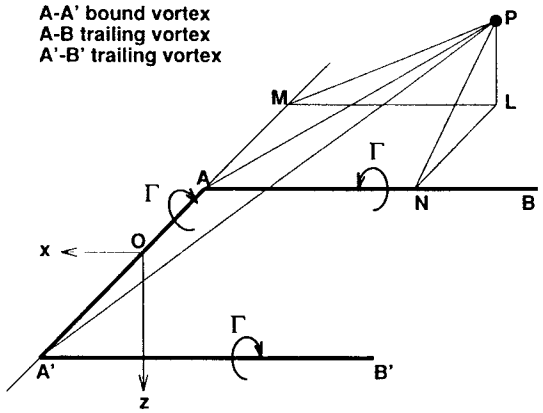

Fig. 6.1 Horseshoe vortex system.

roll up near the wing tips to form single vortex patterns, which can be made visible with smoke or, sometimes, with fine water droplets.

The lifting line theory is an inviscid theory. Therefore, it cannot include in its drag computation the form drag of the wing or its skin-friction drag. As a result, we shall be interested in how the F2D3D computer program does this. The F2D3D program also manages to include in its computation of the aerodynamic characteristics of complete wings the portion of the fuselage included in the wing planform area. This, too, is not usually a part of the lifting line theory; how the effect of a portion of the fuselage is included will also be of interest.

6.2 Induced Angle of Attack due to a Finite Wingspan and its Consequences

The first to provide what we now believe to be a correct description of the effect on lift of having a finite wingspan was the Englishman Frederick W. Lanchester,[31] who published his ideas somewhat belatedly in 1907. Because his exposition of the theory was easier to understand, Prandtl is usually given credit for developing the lifting line theory. However, in his 1927 Wilbur Wright Memorial Lecture to The Royal Aeronautical Society Prandtl[32] said:

> In England you refer to it as the Lanchester–Prandtl theory, and quite rightly so, because Lanchester obtained independently an important part of the results. He commenced working on the subject before I did, and this no doubt led people to believe that Lanchester's investigations, as set out in 1907 in his *Aerodynamics*, led me to the ideas upon which the aerofoil theory was based. But this was not the case. The necessary ideas upon which to build up that theory, so far as these ideas are comprised in Lanchester's book, had already occurred to me before I saw the book. In support of this statement I should like to point out that as a matter of fact we in Germany were better able to understand Lanchester's book when it appeared than you in England.... The truth of the matter, however, is that Lanchester's treatment is difficult to follow, since it makes very great demands on the reader's intuitive perceptions, and only because we had been working on similar lines were we able to grasp Lanchester's meaning at once. At the same time, however, I wish to be distinctly understood that in many particular respects Lanchester worked on different lines than we did, lines which were new to us, and that we were able to draw many useful ideas from his book.

Von Kármán[5], who knew both men well, summarized Prandtl's contribution to the development of the lifting theory in these words:

> Prandtl systematized and simplified the picture in the following ways: (1) the wing is replaced by a lifting line perpendicular to the flight direction; (2) the lifting line is assumed to consist of a bound vortex with circulation variable in order to account for the fact that the lift may change along the span; (3) in accordance with the change in circulation along the span, free vortices are born and extend downstream; (4) the flow produced by the vortex system is considered as a small perturbation of the fundamental stream relative to the wing, and therefore; (5) it is assumed that the free vortices approximately follow the original direction of the streamlines parallel and opposite to the flight direction, instead of winding up immediately into tip vortices as Lanchester assumed; (6) the flow in the immediate neighborhood of a wing section is determined by the two-dimensional solution given by Kutta and Joukowski.

6.2.1 *Calculation of Induced Angle of Attack*

We indicated that we would represent the wing by a group of horseshoe vortices which physically roll up aft of the tips to form a single trailing vortex. The circulation associated with these vortices will vary along the span, being symmetrical about the midspan point and falling to zero at the tips. Between y and dy on the span (see Fig. 6.1) the circulation decreases by an amount

$$-\frac{d\Gamma}{dy}dy \tag{6.1}$$

Ideally, a trailing vortex of this strength springs from each element of span dy. Therefore, there is a sheet of trailing vortices extending across the span, and the induced velocity normal to the freestream velocity must be obtained as the sum of the effects of all trailing vortices in this sheet.

To determine the form of the expression giving the sum of the effects of all trailing vortices consider the case of a wing represented by a single horseshoe vortex. The velocity induced by a vortex at a point depends on the distance from the point to the vortex filament. In Fig. 6.1 the distance from point P to the wing filament is PM. The total velocity, $\sqrt{u^2+v^2}$, is normal to the line, $\sqrt{x^2+y^2}$, connecting the filament to the point where the velocity is to be determined. Therefore, one could write

$$\sqrt{u^2+v^2} = \frac{\Gamma}{2\pi\sqrt{x^2+y^2}} \tag{6.2}$$

It seems reasonable to conclude that at any point the velocity induced by a semi-infinite vortex filament is half that induced by an infinite vortex. Let us ask, then,

what is the velocity induced at the point by a small segment of the vortex filament. We know that the velocity depends on the distance from the segment to the point. If we call $x^2 + y^2 = r^2$, then this distance from the vortex filament at A' is $r/\sin\theta_1$ where θ_1 is the angle $PA'M$ in Fig. 6.1.

Substitution of this expression for distance into an expression for the velocity induced at a point, say, in the XOZ plane, by a segment of semi-infinite vortex can be seen to yield

$$dV = \frac{\Gamma \sin\theta}{4\pi r} d\theta \tag{6.3}$$

Integration of this expression yields

$$V_1 = \frac{\Gamma}{4\pi r}\cos\theta_1 \tag{6.4}$$

Calculation of the contribution to the velocity from the part of the filament beyond 0 in the figure yields

$$V_2 = \frac{\Gamma}{4\pi r}\cos\theta_2 \tag{6.5}$$

so that the total induced velocity is

$$V = \frac{\Gamma}{4\pi r}(\cos\theta_1 + \cos\theta_2) \tag{6.6}$$

This is one form of the Biot–Savart law. Continuing in the notation of Fig. 6.1 the downwash velocity at point P (normal to PM) may be written

$$V = \frac{\Gamma}{4\pi PM}[\cos PA'A + \cos PAA'] \tag{6.7}$$

If we now assume that the point P is located along the span at, say, y_1, then the distance from y_1 to any other point is $y_1 - y$. Further, if Γ is variable along y, then

$$\Gamma = \int_{-b/2}^{b/2} \frac{d\Gamma}{dy} dy \tag{6.8}$$

Therefore, following Prandtl, one may write the induced velocity w at some point y_1 along the span as

$$w(y_1) = V\alpha_i(y_1) = \frac{1}{4\pi}\int_{-b/2}^{b/2} \frac{\frac{d\Gamma}{dy}dy}{y_1 - y}$$

Thus, the angle of attack of the induced flow is

$$\alpha_i(y_1) = \frac{1}{4\pi V}\int_{-b/2}^{b/2} \frac{\frac{d\Gamma}{dy}dy}{y_1 - y} \tag{6.9}$$

Unfortunately, the circulation Γ about an airfoil is not readily measured nor is it a quantity that is easily thought of in physical terms. More commonly, the characteristic of an airfoil is stated in terms of its lift coefficient, a quantity easily measured and important in aerodynamic and structural design. It can be shown on analytical grounds (see Chapter 3) that the lift per unit span of wing is $\rho V\Gamma$. The airfoil or section lift coefficient is, therefore,

$$C_\ell = \frac{\rho V\Gamma}{\frac{1}{2}\rho V^2 c} = \frac{2\Gamma}{Vc} \tag{6.10}$$

Hence,

$$\Gamma = \tfrac{1}{2}C_\ell V c \tag{6.11}$$

Because both C_ℓ and c can vary as functions of y we put

$$\frac{d\Gamma}{dy} = \frac{V}{2}\frac{d(C_\ell c)}{dy}$$

or in nondimensional form

$$\frac{d\Gamma}{dy} = \frac{Vb}{2}\frac{d(C_\ell c/b)}{dy} \tag{6.12}$$

from which we write

$$\bar{\alpha}_i(\bar{y}_1) = \frac{\bar{b}}{8\pi}\int_{-b/2}^{b/2} \frac{\frac{d\left(\frac{\bar{C}_\ell \bar{c}}{\bar{b}}\right)}{dy}}{y_1 - y}dy \tag{6.13}$$

The use of an overbar in the preceding equation indicates that the equation applies to variables in the transformed $\bar{u}$ plane, which is discussed in Sec. 6.3 of this chapter. At this point it will be sufficient to assert that the transformation does not affect geometric quantities in the chordwise direction so that $\bar{c} = c$. Wing twist is also not affected nor does the transformation affect quantities such as the local value of the circulation. Thus,

$$C_\ell(y)c = \bar{C}_\ell(\bar{y})\bar{c} \tag{6.14}$$

Let us now represent $C_\ell c/b$ by the series

$$\frac{c_\ell(y)c}{\bar{b}} = 4\sum_{n=1}^{\infty} A_n \sin\left[n\cos^{-1}\left(\frac{-2\bar{y}}{\bar{b}}\right)\right] \tag{6.15}$$

and call $\bar{\theta} = \cos^{-1}(-2\bar{y}/\bar{b})$. Then, we can write the expression for the induced angle of attack at any spanwise station in the $\bar{u}$ plane as

$$\bar{\alpha}_i(\bar{y}_i) = \frac{1}{4\pi}\int_0^{\pi} \frac{\sum_{n=1}^{\infty} nA_n \cos n\bar{\theta}}{\cos\bar{\theta}_i - \cos\bar{\theta}} d\bar{\theta} \tag{6.16}$$

However,

$$\int_0^{\pi} \frac{\cos n\theta}{\cos\phi - \cos\theta} d\theta = \pi \frac{\sin n\phi}{\sin\phi} \tag{6.17}$$

so that

$$\bar{\alpha}_i(\bar{y}_i) = \frac{\sum_{n=1}^{\infty} nA_n \sin n\bar{\theta}_i}{\sin\bar{\theta}_i} \tag{6.18}$$

Because y_i is an arbitrary spanwise location, we can discard the subscript.

We choose to evaluate the lift at m evenly spaced points along the span with a finite series of $r-1$ terms. We assume m and r are related by $\bar{\theta} = m\pi/r$ and $m = 1, 2, 3, \ldots$. The lift is assumed to be constant over each spanwise interval. Thus, to get a reasonably accurate representation it is necessary to consider a fairly large number of intervals. We write the lift in each interval as

$$\left(\frac{C_\ell(y)c}{\bar{b}}\right)_m = 4\sum_{n=1}^{r-1} A_n \sin n\frac{m\pi}{r} \tag{6.19}$$

for which

$$A_n = \frac{2}{r}\sum_{m=1}^{r-1}\left(\frac{C_\ell c}{\bar{b}}\right)_m \sin n\frac{m\pi}{r} \tag{6.20}$$

Substitution of this result into the expression for the induced angle of attack yields

$$\bar{\alpha}_i(\bar{y}) = \frac{1}{\sin\bar{\theta}}\left\{\sum_{n=1}^{\infty} n\left[\frac{2}{r}\sum_{m=1}^{r-1}\left(\frac{C_\ell c}{\bar{b}}\right)_m \sin n\frac{m\pi}{r}\right]\sin n\bar{\theta}\right\} \tag{6.21}$$

Now

$$\sin\alpha\sin\beta = \tfrac{1}{2}[\cos(\alpha-\beta) - \cos(\alpha+\beta)]$$

With the use of this identity we can write

$$\bar{\alpha}_i(\bar{y}) = \frac{1}{r\sin\bar{\theta}}\left\{\sum_{m=1}^{r-1}\left(\frac{C_\ell c}{\bar{b}}\right)_m \sum_{n=1}^{r-1} n\left[\cos n\left(\bar{\theta} - \frac{m\pi}{r}\right) - \cos n\left(\bar{\theta} + \frac{m\pi}{r}\right)\right]\right\} \tag{6.22}$$

For computational purposes we have chosen to terminate the series at $r-1$ terms.

We wish to evaluate the induced angle of attack at the same points at which we were required to find C_ℓ. To accomplish this we put $\bar{\theta} = k\pi/r$ and define

$$\beta_{mk} = \frac{1}{r\sin\dfrac{k\pi}{r}}\sum_{n=1}^{r-1} n\left[\cos n\frac{(k-m)\pi}{r} - \cos n\frac{(k+m)\pi}{r}\right] \tag{6.23}$$

Then,

$$\bar{\alpha}_i(\bar{y}) = \bar{\alpha}_{ik} = \sum_{m=1}^{r-1}\left(\frac{C_\ell c}{\bar{b}}\right)_m \beta_{mk} \tag{6.24}$$

Now if $k = m$

$$\beta_{mk} = \frac{1}{r\sin\dfrac{k\pi}{r}}\sum_{n=1}^{r-1} n\left[1 - \cos\frac{2kn\pi}{r}\right] \tag{6.25}$$

The sum of the series in Eq. (6.25) is not easily found. By evaluating series of varying length it can be shown to be $r^2/2$; hence,

$$\beta_{mk} = \frac{r}{2\sin\dfrac{k\pi}{r}} \tag{6.26}$$

When $k+m$ is even and $k \neq m$, then $\beta_{mk} = 0$. When $k+m$ is odd

$$\beta_{mk} = \frac{1}{r\sin\dfrac{k\pi}{r}}\left[\frac{1}{1-\cos\dfrac{(k+m)\pi}{r}} - \frac{1}{1-\cos\dfrac{(k-m)\pi}{r}}\right] \tag{6.27}$$

Note that the value of β_{mk} depends only on the number of spanwise stations used in the analysis and is independent of aspect ratio or taper ratio.

We will return to the evaluation of $\alpha_i(y)$ following our consideration of the effects of aspect ratio, planform shape, and the presence of a fuselage on the wing flowfield.

6.2.2 Effect of Aspect Ratio and Planform Shape

The effect of the induced flow is to reduce the effective angle of attack so that an additional physical angle of attack is required to produce the same lift. Mathematically, we can express this as

$$\alpha_e(y) = \alpha(y) - \alpha_i(y) \tag{6.28}$$

The term on the left side of Eq. (6.28) can also be expressed as

$$\alpha_e(y) = \frac{C_\ell(y)}{C_{L_\alpha}} = \frac{2\Gamma}{cVC_{L_\alpha}} \tag{6.29}$$

But

$$\Gamma = 2bV\sum_{n=1}^{\infty} A_n \sin n\theta \tag{6.30}$$

so that

$$\alpha_e(y) = \frac{4b}{cC_{L_\alpha}}\sum_{n=1}^{\infty} \sin n\theta \tag{6.31}$$

Now set $\mu = 4b/cC_{L_\alpha}$ and use Eq. (6.18) for $\alpha_i(y)$. Then Eq. (6.28) becomes

$$\frac{1}{\mu}\sum_{n=1}^{\infty} A_n \sin n\theta = \alpha(y) - \left[\frac{\sum_{n=1}^{\infty} A_n n \sin n\theta}{\sin\theta}\right] \tag{6.32}$$

or when fractions are cleared

$$\sum_{n=1}^{\infty} A_n \sin n\theta(\mu n + \sin\theta) = \mu\alpha \sin\theta \tag{6.33}$$

This is called the fundamental monoplane equation. By picking n locations (and, therefore, n values of θ) along the semispan at which the two-dimensional aerodynamics characteristics are known, it is possible to write n equations in A_n unknowns, which can then be solved. With these A_n known, one can evaluate the finite series for the sectional characteristics and then integrate over the semispan to obtain the overall three-dimensional characteristics. We discuss the procedure in somewhat more detail in our review of the F2D3D program.

Alternately, one may think of the effect of a finite wing span to be a rearward tilting of the lift vector. This rearward tilting reduces the lift and adds a component of force in the drag direction. This component is called the induced drag. Notice that this drag is not created by viscosity but is an unavoidable consequence of producing lift with a finite wing. Making use of the small angle approximation this induced drag is $L\alpha_i = L(w/V)_i$. But the induced velocity is

$$w = \frac{2L}{\rho\pi V b^2} \tag{6.34}$$

Hence,

$$D_i = \frac{2L^2}{\rho\pi V^2 b^2} = \frac{C_L^2 \rho V^2 S^2}{2\pi b^2} \tag{6.35}$$

In Eq. (6.35) S is the wing area. The induced drag coefficient is then simply

$$C_{D_i} = \frac{C_L^2 S}{\pi b^2} = \frac{C_L^2}{\pi A_R} \tag{6.36}$$

Here we have used the symbol $A_R = b^2/S$ to represent the aspect ratio.

From a force diagram it will be seen that C_{D_i} is $C_L\alpha_i$ so that the average induced angle of attack for the wing is, from Eq. (6.36),

$$\alpha_i = \frac{C_L}{\pi A_R} \tag{6.37}$$

We should note that the expressions we just obtained are not accurate for low aspect ratio wings, swept back wings, or swept forward wings. For those cases where they are properly applied, we see that the effect of a finite aspect ratio is to increase the geometric angle at which a given wing lift coefficient is obtained compared with the two-dimensional coefficient. We can write this effect in mathematical form as

$$(C_{L_\alpha})_1\left(\alpha + \frac{C_L}{\pi A_{R_1}}\right) = (C_{L_\alpha})_2\left(\alpha + \frac{C_L}{\pi A_{R_2}}\right) \tag{6.38}$$

If we take $A_{R_1} = \infty$ and $C_{L_{\alpha_1}} = 2\pi$, then Eq. (6.38) becomes

$$2\pi\alpha = C_{L_{\alpha_2}}\left(\alpha + \frac{C_L}{\pi A_{R_2}}\right)$$

from which we can construct a general expression for the effect of aspect ratio on thin airfoils,

$$C_{L_\alpha} = \frac{2\pi A_R}{A_R + 2} \tag{6.39}$$

For thicker airfoils we can replace 2π in Eq. (6.39) by the appropriate value.

A similarly useful relationship can be obtained for the change in the angle of attack required to achieve a given C_L. Let

$$\alpha_1 = \alpha_0 + \frac{C_L}{\pi A_{R_1}}$$

$$\alpha_2 = \alpha_0 + \frac{C_L}{\pi A_{R_2}}$$

with α_0 the angle of attack for infinite aspect ratio. Then it is easily seen that

$$\alpha_2 = \alpha_1 + \frac{C_L}{\pi}\left(\frac{1}{A_{R_1}} - \frac{1}{A_{R_2}}\right) \tag{6.40}$$

Now let us consider a distribution of circulation given by

$$\Gamma = \Gamma_0\sqrt{1 - \left(\frac{2y}{b}\right)^2} \tag{6.41}$$

and integrate this distribution over the span

$$L = \rho V \int_{-\frac{b}{2}}^{\frac{b}{2}} \Gamma_0 \sqrt{1 - \left(\frac{2y}{b}\right)^2}\, \mathrm{d}y \tag{6.42}$$

To facilitate the integration make the subsitutions

$$y = \frac{b}{2}\sin\theta$$

and

$$\mathrm{d}y = \frac{b}{2}\cos\theta$$

and change the limits of integration appropriately,

$$L = \rho V \Gamma_0 \int_{-\frac{\pi}{2}}^{\frac{\pi}{2}} \sqrt{1 - \sin^2\theta}\,\frac{b}{2}\cos\theta\,\mathrm{d}\theta \tag{6.43}$$

Then, as a result of the integration we can write

$$\Gamma_0 = \frac{4L}{\rho\pi V b} \tag{6.44}$$

If we had substituted

$$\Gamma = 2bV\sum_{n=1}^{\infty} A_n \sin n\theta \tag{6.45}$$

for Eq. (6.41) when integrating Eq. (6.42) we would have obtained

$$L = \rho V^2 b^2 \int_0^{\pi} A_n \sin n\theta \sin\theta\,\mathrm{d}y \tag{6.46}$$

However,

$$\int_0^{\pi} \sin n\theta \sin\theta\,\mathrm{d}\theta = 0$$

for $n \neq 1$. Thus,

$$L = \tfrac{1}{2}\rho V^2 \pi b^2 A_1 \tag{6.47}$$

By comparing Eqs. (6.44) and (6.47) we can evaluate A_1 for a wing with an elliptical planform,

$$A_1 = \frac{\Gamma_0}{2bV} \tag{6.48}$$

We can use the same approach to develop a general form for the induced drag,

$$D_i = \int_{-\frac{b}{2}}^{\frac{b}{2}} \rho V \Gamma \frac{w}{V}\mathrm{d}y \tag{6.49a}$$

or

$$D_i = \int_{-\frac{b}{2}}^{\frac{b}{2}} \rho V \left(2bV\sum_{n=1}^{\infty} A_n \sin n\theta\right)\left(\sum_{n=1}^{\infty} n A_n \frac{\sin n\theta}{\sin\theta}\right)\frac{b}{2}\sin\theta\,\mathrm{d}\theta$$

$$= \rho V^2 b^2 \int_0^{\pi} n A_n^2 \sin^2 n\theta\,\mathrm{d}\theta \tag{6.49b}$$

Because

$$\int_0^{\pi} \sin^2 n\theta\,\mathrm{d}\theta = \frac{\pi}{2}$$

Eq. (6.49b) can be written

$$D_i = \rho V^2 b^2 \frac{\pi}{2}\sum_{n=1}^{\infty} n A_n^2 \tag{6.50}$$

Now, because all A_n are squared in Eq. (6.50), the minimum D_i occurs when $n = 1$, which reduces Eq. (6.50) to

$$D_{i_{\min}} = \tfrac{1}{2}\rho\pi b^2 V^2 A_1^2 \tag{6.51}$$

Because

$$D_i = L\left(\frac{C_L}{\pi A_R}\right)$$

we can use Eqs. (6.47) and (6.51)

$$D_i = \frac{\rho}{2}V^2\pi b^2 A_1 \frac{C_L}{\pi A_R} = \frac{1}{2}\rho\pi b^2 V^2 A_1^2$$

to show that A_1 is

$$A_1 = \frac{C_L}{\pi A_R} \tag{6.52}$$

With Eq. (6.52), Eq. (6.51) becomes

$$D_{i_{\min}} = \rho V^2 b^2 \frac{\pi}{2}\left(\frac{C_L}{\pi A_R}\right)^2$$

or

$$D_{i_{\min}} = \frac{\rho}{2}SV^2\left(\frac{C_L^2}{\pi A_R}\right) \tag{6.53}$$

Equation (6.53) shows that the minimum induced drag is obtained through the use of an elliptical planform or a planform that, by means of appropriate taper and twist, achieves essentially the same thing aerodynamically. Readers interested in history may recall that the Supermarine Spitfire, the victorious fighter in the Battle of Britain in 1940, employed an elliptical planform. Later versions of the aircraft, however, employed more squared-off wing tips. A reason for this change

may be that the chord of an elliptical planform near the tip is very short and, thus, the Reynolds number is very small. At low Reynolds numbers the maximum lift coefficient is reduced and the drag coefficient is increased. As a consequence, the desired elliptical spanwise loading was probably not achieved. In addition, the difficulty of forming aerodynamically accurate sections in a small size on a production basis would seem to have contributed to the decision to use more squared-off tips.

6.3 Wing–Fuselage Interaction

The portion of the fuselage lying between the wings (see Fig. 6.2) is by definition included in the wing planform area. This is reasonable because this region contributes to the overall wing lift although in a manner that is not readily characterized. Multhopp[33] devised a transform similar to the Joukowsky transform, which squeezes an elliptical fuselage into a line along the major axis and distributes its upwash effects along a trace of the wing. As far as the flow is concerned, there is no fuselage in the $\bar{u}$ plane. A cross section of the wing–fuselage combination normal to the airflow is shown in Fig. 6.2a. Figure 6.2b displays the transformed wing–fuselage combination. The figure also identifies the nomenclature used in the following analysis.

We begin by writing the coordinates of the trace of the wing–fuselage combination as a complex variable

$$u = z + iy = a\cos\psi + ib\sin\psi \tag{6.54}$$

We use the angle ψ simply as an aid in some of the mathematical operations. After the transformation is applied, the coordinates of the wing–fuselage combination are written in terms of the complex variable

$$\bar{u} = \bar{z} + i\bar{y} \tag{6.55}$$

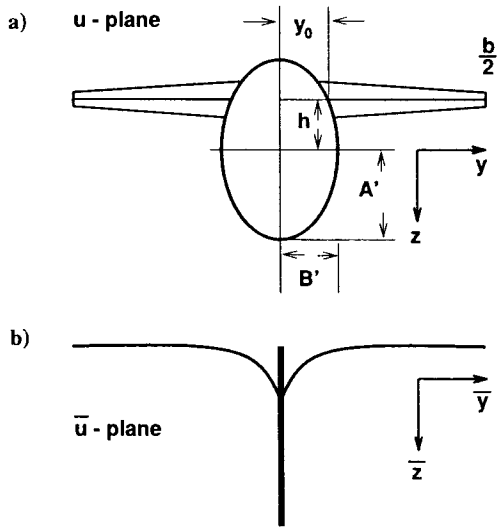

Fig. 6.2 a) Physical plane and b) transformed plane.

The trace of the wing–fuselage combination in the y–z plane is transformed from the physical u plane to the $\bar{u}$ plane according to the relation

$$\bar{u} = \frac{1}{A' - B'}\left[A'u - B'\sqrt{u^2 - A'^2 + B'^2}\right] \tag{6.56}$$

The following definitions also apply:

$$a = \tfrac{1}{2}\left[\sqrt{y^2 + (h - e')^2} + \sqrt{y^2 + (h + e')^2}\right] \tag{6.57a}$$

$$b = \sqrt{a^2 - e'^2} \tag{6.57b}$$

$$e' = \sqrt{A'^2 - B'^2} = \sqrt{a^2 - b^2} \tag{6.57c}$$

Substituting the trignometric form of u into the transformation relationship yields

$$\bar{u} = \frac{1}{A' - B'}\left[A'(a\cos\psi + ib\sin\psi) - B'(b\cos\psi + ia\sin\psi)\right] = \bar{z} + i\bar{y} \tag{6.58}$$

Comparing real and imaginary parts shows that

$$\bar{y} = \frac{1}{A' - B'}\left[A'y - B'a\sin\psi\right] \tag{6.59}$$

But because

$$y = b\sin\psi$$

$$\sin\psi = \frac{y}{\sqrt{a^2 - e'^2}} \tag{6.60}$$

Hence,

$$\bar{y} = \frac{y}{A' - B'}\left[A' - B'\frac{a}{\sqrt{a^2 - e'^2}}\right] \tag{6.61}$$

This relationship determines how points along the span in the physical plane or u plane transform into the $\bar{u}$ plane.

Now we seek to find how the flow in the neighborhood of the fuselage influences the flow direction and magnitude at each station along the wing's semispan. In effect, the real part of $d\bar{u}/du$ distributes the vertical components of the fuselage flow along the wing. If α_B is the fuselage angle of attack in the $\bar{u}$ plane, then the amount by which the flow angularity exceeds that due to geometric inclination at points along the span is given by

$$\Delta\alpha(y) = \left[\mathcal{R}\frac{d\bar{u}}{du} - 1\right]\alpha_B \tag{6.62}$$

where the symbol $\mathcal{R}$ indicates we are to consider only the real part of the derivative. Because of the nature of the transformation, α_B will have the same value in either

plane. Now the real part of $d\bar{u}/du$ is the vertical component of the flow. After some manipulation we find that

$$\mathcal{R}\frac{d\bar{u}}{du} = \frac{1}{A' - B'}\left[A' - B'\frac{\dfrac{a}{\sqrt{a^2 - e'^2}}}{1 + \dfrac{a'^2 y^2}{(a^2 - e'^2)^2}}\right] \tag{6.63}$$

If the wing is very thick at the junction with the fuselage, then the actual $\Delta\alpha$ obtained is less than predicted. It has been suggested that one should reduce $\Delta\alpha(y)$ by a factor T, taken as a constant across the wing span, which is the ratio of the body cross-sectional area above and below the wing to the total frontal area of the body. The area of an elliptical fuselage is, of course, $\pi A'B'$. The segment of the fuselage that represents a continuation of the wing has an area of approximately

$$T = 1 - \frac{2y_0 t_{\text{root}}}{\pi A'B'} \tag{6.64}$$

Using this relation we can write $\Delta\alpha(y)$ as

$$\Delta\alpha(y) = T\alpha_B\left[\mathcal{R}\frac{d\bar{u}}{du} - 1\right] \tag{6.65}$$

We could also have written this expression as

$$\Delta\alpha(y) = \alpha_B\left[\left(\mathcal{R}\frac{d\bar{u}}{du}\right)_T - 1\right] \tag{6.66}$$

if we had known how to write

$$\left(\mathcal{R}\frac{d\bar{u}}{du}\right)_T \tag{6.67}$$

explicitly. However, by comparing the two expressions for $\Delta\alpha(y)$ we choose to write as a first approximation

$$\left(\mathcal{R}\frac{d\bar{u}}{du}\right)_T = 1 + T\left[\mathcal{R}\frac{d\bar{u}}{du} - 1\right] \tag{6.68}$$

In addition to the flow angularity induced along the wing by the presence of a fuselage, there is also a flow downwash induced by the lift associated with the finite wing. This angle in the $\bar{u}$ plane is written as $\bar{\alpha}_i(\bar{y})$. Now we seek to transform this angle into the u plane so that we may more easily see its influence on the actual lift and drag of the local airfoil section. We note that the induced angle in the $\bar{u}$ plane multiplied by the real part of the change in $\bar{u}$ for a given change in u is just the induced angle in the u plane. Thus, for thick airfoils

$$\alpha_i(y) = \bar{\alpha}_i(\bar{y})\left[\mathcal{R}\frac{d\bar{u}}{du}\right]_T \tag{6.69}$$

This angle is negative in the usual sense. The geometric angle of attack can be given in terms of the angle of attack at the root and the twist relative to the root angle as a function of span: $\alpha_e(y) = \alpha_R + \epsilon(y)$. To the geometric angle we must add flow angularities due to body upwash, α_B, and due to wing lift, α_i. The result is that for thick wings, the effective section angle of attack in the physical plane is given by

$$\alpha_e(y) = \alpha_R + \epsilon(y) + [\alpha_B - \bar{\alpha}_i(\bar{y})]\left\{1 + \left(1 - \frac{2y_0 t_{\text{root}}}{\pi A'B'}\right)\right.$$
$$\left.\times\left[\frac{1}{A' - B'}\left(A' - B'\frac{\dfrac{a}{\sqrt{a^2 - e'^2}}}{1 + \dfrac{e'^2 y^2}{(a^2 - e'^2)^2}}\right) - 1\right]\right\} \tag{6.70}$$

with

$$a = \tfrac{1}{2}\left[\sqrt{y^2 + (h - A'^2 - B'^2)^2}\right] \tag{6.71a}$$

and

$$e = \sqrt{A'^2 - e'^2} \tag{6.71b}$$

Note that with the exception of $\bar{\alpha}_i(\bar{y})$ all of the quantities in Eq. (6.70) can be determined from the geometry of the design. The angle $\bar{\alpha}_i(\bar{y})$ is determined according to the analysis carried out in Sec. 6.2 and 6.4.

6.4 Characteristics of the Three-Dimensional Wing

Much of this section and portions of section 6.3 are based on the treatment given in Ref. 26. The present discussion provides the theoretical basis for program F2D3D, which is a modified version of the program presented in that document.

To this point we have developed an implicit relation giving the spanwise variation of induced angle of attack and a relationship distributing the upwash effects of the fuselage along the wing. We desire to develop a procedure similar to that arising from the use of Eq. (6.33) to determine explicitly the three-dimensional characteristics of the wing as a function of spanwise station that we can integrate to find the overall force and moment coefficients.

We begin by writing

$$\alpha_e = \alpha_k - \mathcal{R}\frac{d\bar{u}}{du}\sum_{n=1}^{r-1}\left(\frac{C_\ell c}{\bar{b}}\right)_m \beta_{mk} \tag{6.72}$$

As a first approximation, we will assume that the variation of lift coefficient with angle of attack C_{ℓ_α} at any spanwise location is constant. Then by writing

$$\alpha_e\left[C_{\ell_\alpha}\frac{c}{\bar{b}}\right]_k = \left(C_\ell\frac{c}{\bar{b}}\right)_k + \Delta_k \tag{6.73}$$

we can define Δ_k as the amount that must be added to the initial estimate for $(C_\ell c/\bar{b})$ to obtain a new value that includes in it the effects from other portions of the wing. A second iteration is formed as follows:

$$\left\{\alpha_k - \mathcal{R}\frac{d\bar{u}}{du}\sum_{n=1}^{r-1}\left[\left(\frac{C_\ell c}{\bar{b}}\right) + \Delta'\right]_m \beta_{mk}\right\}\left(C_{\ell_\alpha}\frac{c}{\bar{b}}\right)_k = \left(\frac{C_\ell c}{\bar{b}}\right)_k + \Delta'_k \tag{6.74}$$

Subtraction of Eq. (6.74) from Eq. (6.73) yields

$$\left(\frac{C_\ell c}{\bar{b}}\right)_k \left(\mathcal{R}\frac{d\bar{u}}{du}\right)_k \sum_{m=1}^{r-1}\Delta'_m\beta_{mk} = \Delta_k - \Delta'_k \tag{6.75}$$

If we define

$$\left(C_{\ell_\alpha}\frac{c}{\bar{b}}\right)_k \left(\mathcal{R}\frac{d\bar{u}}{du}\right)_k \frac{180r}{8\pi\sin(k\pi/m)} = G_{kk} \tag{6.76}$$

then Eq. (6.75) could be written as

$$\Delta'_k + G_{kk}\Delta'_k + \left[\sum_{m=1}^{r-1}\Delta'_k\beta_{mk}\right]_{k\neq m}\left(\frac{C_{\ell_\alpha}c}{\bar{b}}\right)_k\left(\mathcal{R}\frac{d\bar{u}}{du}\right)_k = \Delta_k \tag{6.77}$$

Dividing by G_{kk} yields

$$\left(1 + \frac{1}{G_{kk}}\right)\Delta'_k + \left[\sum_{m=1}^{r-1}\frac{\beta_{mk}}{\beta_{kk}}\Delta'_k\right]_{k\neq m} = \frac{\Delta_k}{G_{kk}} \tag{6.78}$$

Equation (6.78) represents $r/2$ simultaneous equations, which may be represented in matrix form as

$$[G_{ij}]\{\Delta'_i\} = \left(\frac{1}{G_{kk}}\right)\{\Delta_i\} \tag{6.79}$$

where G_{ij} is a matrix with all of the principal diagonal elements equal to $(1 + 1/G_{kk})$ and the other elements are β_{mk}/β_{kk}. The values to be added to one set of approximate values to obtain a better approximation, therefore, are given by

$$\{\Delta'_i\} = [G_{ij}]^{-1}\left(\frac{1}{G_{kk}}\right)\{\Delta_i\} \tag{6.80}$$

As a first approximation to the distribution of lift on the wing, we use the expression

$$\frac{C_\ell c}{\bar{b}} = C_\ell\left(\frac{A_R}{A_R + 1.8}\right)\left(\frac{c}{c_R}\right)\left(\frac{c_R}{b}\right)\left(\frac{b}{\bar{b}}\right)\left[1 + (1+\lambda)\sqrt{1 - \left(\frac{2\bar{y}}{\bar{b}}\right)^2}\right] \tag{6.81}$$

which, as can be seen, contains a simple aspect ratio correction and a single taper ratio λ correction to the typical elliptical lift distribution. In Eq. (6.81) c_R is the root chord. The value of C_ℓ on the right-hand side of Eq. (6.81) comes from the two-dimensional data corresponding to the local geometric angle of attack.

The flow in the tip regions and its effect on the overall wing characteristics are particularly difficult to determine quantitatively. The more inboard sections of a finite wing are influenced by the downwash generated by the horseshoe vortex system and the upwash due to the fuselage so that the primary effect on the more inboard sections is a change in effective angle of attack. In the tip region, on the other hand, there is a substantial spanwise flow that detracts from the flow moving chordwise; consequently, the tip region is able to generate less lift than one would normally expect for a given freestream flow velocity. This, of course, reduces the total lift of the wing somewhat. To accommodate this loss in lift within the idea of using two-dimensional data at an appropriate angle of attack, we modify α_e to read

$$\alpha'_e = \frac{(\alpha_e - \alpha_{ZL})\left[\sqrt{1 - \dfrac{4}{A_R^2}}\right]}{\sqrt{1 + \dfrac{4}{A_R^2}}} \tag{6.82}$$

We use α'_e to look up the three-dimensional value of the section lift coefficient from the two-dimensional data.

If $C_\ell c/\bar{b}$ computed in this fashion is not sufficiently close to the initial estimate of $C_\ell c/\bar{b}$, then a correction given by Eq. (6.80) is added. The process is repeated until a satisfactory agreement is obtained.

When a satisfactory lift distribution has finally been obtained, one can employ the same section data to find the profile drag and moment coefficient at each station along the wing. The local induced drag is simply a product of the lift and the induced angle of attack at that point. The overall force and moment coefficients are obtained by integrating the local values over the span. If one uses Simpson's rule for this integration, explicit relations for the lift, drag, and moment can be obtained.

$$C_L = \left(\frac{\bar{b}}{b}\right)^2 A_R \sum_{m=1}^{r-1}\left(\frac{C_\ell c}{\bar{b}}\right)_m \left\{\frac{\pi}{6r}[3 - (-1)^m]\sin\frac{m\pi}{r}\right\} \tag{6.83}$$

$$C_{D_i} = \frac{\pi}{180}\left(\frac{\bar{b}}{b}\right)^2 A_R \sum_{m=1}^{r-1}\left[\left(\frac{C_\ell c}{\bar{b}}\right)\alpha_i\right]_m \left\{\frac{\pi}{6r}[3 - (-1)^m]\sin\frac{m\pi}{r}\right\} \tag{6.84}$$

$$C_{D_0} = \left(\frac{\bar{b}}{b}\right)^2 A_R \sum_{m=1}^{r-1}\left(\frac{C_{d_0}c}{\bar{b}}\right)_m \left\{\frac{\pi}{6r}[3 - (-1)^m]\sin\frac{m\pi}{r}\right\} \tag{6.85}$$

$$C_m = \left(\frac{A_R\bar{b}}{b^2c'}\right)\sum_{m=1}^{r-1}(C_{m_i}c^2)\left\{\frac{\pi}{6r}[3 - (-1)^m]\sin\frac{m\pi}{r}\right\} \tag{6.86}$$

In Eq. (6.86)

$$C_m = C_{m_{\frac{c}{4}}} - (x/c)\left[C_\ell \cos(\alpha_B - \alpha_i + C_{d_0} \sin(\alpha_B - \alpha_i)\right]$$

$$- (z/c)\left[C_\ell \sin(\alpha_B - \alpha_i) - C_{d_0} \sin(\alpha_B - \alpha_i)\right] \qquad (6.87)$$

If c' is the mean aerodynamic chord, the preceding integrations are somewhat analogous to the process represented by

$$\frac{1}{bc'} \int_{-\frac{b}{2}}^{\frac{b}{2}} C_\ell c \, dy$$

Because the computation of $(C_\ell c/\bar{b})$ has really been carried out in the $\bar{u}$ plane as far as the wing span is concerned, we must multiply our result by $\bar{b}/b$ to transform it to the physical plane. A_R is just b/c', and the average (aerodynamic not geometric) value of c over the span is c'. The term in the braces in (6.83)–(6.86) is the multiplier employed by Simpson's rule. It is seen, therefore, that C_L is, in fact, an average over the span in the physical plane.

6.5 Curve Fitting Aerodynamic Characteristics: POLYFIT

The aerodynamics characteristics calculated by the AIRFOIL program are produced at discrete angles of attack. The present version of F2D3D requires that these data be in the form of the five coefficients of a fourth-order polynomial. POLYFIT (see Ref. 26) performs a least squares fit on the results produced by AIRFOIL to obtain the coefficients. Four sets of coefficients are produced: C_L vs α, C_D vs C_L, C_m vs C_L, and α vs C_L. Program output is divided between two files: POLYFIT.TXT and POLYFIT.DAT. The first provides printer plots of curves generated from the polynomials; the second is in a form that can be read directly by F2D3D.

Some renaming of the output files will be required, the amount depending on the airfoil sections chosen for the wing root and wing tip. F2D3D will require at least two input data files: one for the root and another for the tip. If the airfoil sections for the root and tip come from different families, then two sets of data must be input for the root and two for the tip. (A family consists of all of the sections with designations beginning with 230xx, for example; that is, members of one family differ from each other by their thicknesses.) The reason that two airfoil sections from one family must be used is so that the program can interpolate on thickness. For this reason some care must be exercised in selecting the second member of the family to use. For example, if the root section is to be 20% thick and the tip section is to be 12% thick, then the program will interpolate to find the correct thickness at each spanwise station. If the sections are from the same family, then only data for the 20% and 12% sections need be entered. However, if the root and tip are to use different families, then the data for the root family must include coefficients for a thinner member and the tip must include coefficients for a thicker family so that this interpolation can be carried out successfully. When only one family is used for both root and tip sections, the coefficients for the root section should reside in a file renamed POLYFIT.RT1, and those for the tip section should be in a file named POLYFIT.TP1. In the event that the root and tip sections are from different


```
23012 SERIES AIRFOIL / ALPHA=-4,-2,0,2,4,6,8,10,12 / RN=3.49 / MACH NO .2
        9
     -4.0000          -.31963          .78733E-02       -.50869E-02
     -2.0000          -.94990E-01      .75489E-02       -.66658E-02
      .00000           .12565          .64448E-02       -.85043E-02
     2.0000            .34962          .68430E-02       -.10548E-01
     4.0000            .57321          .70861E-02       -.12139E-01
     6.0000            .79169          .80974E-02       -.13172E-01
     8.0000           1.0056           .99529E-02       -.14259E-01
     10.000           1.1850           .14048E-01       -.12825E-01
     12.000           1.3580           .18434E-01       -.10255E-01
```

Fig. 6.3 Input data file for POLYFIT program.

families, there will be four files: POLYFIT.RT1, POLYFIT.RT2, POLYFIT.TP1, and POLYFIT.TP2.

Program 2DHELP generates input file AIRFOIL.PUN for POLYFIT. AIRFOIL.PUN must be manually edited or 2DHELP must be edited, recompiled, and executed when a different airfoil is to be analyzed.

6.5.1 Data Entry

For each airfoil the program requires the following input.

1) The 80 characters of the array TITLE is used as a header for identifying output. In this version of the program only one airfoil per run can be analyzed. The format is 20A4.

2) The number NUM is the variable that specifies the number of angles of attack that follow. The largest permissible value of NUM is 20. The format is I10.

3) The first element values of the arrays AL, CL, CD, and CM are the angle of attack and the two-dimensional coefficients of lift, drag, and pitching moment for that angle of attack. Similar lines with successive array elements follow until the number of point specified by NUM are read in. The format is G16.5.

In addition, two switches can be set in the program. When SWITCH is set to zero, printer plots are produced. When SWITCH is set to 1, no plots are produced. The other switch is PUNCH. It is set to zero to write output files for use in F2D3D. A typical input data set (AIRFOIL.PUN) is shown in Fig. 6.3

6.5.2 Typical Results

Results produced by the program for the example case in Fig. 6.3 are shown in Fig. 6.4. While the numbers shown in Fig. 6.3 are indeed those used to generate the results shown in Fig. 6.4, the horizontal location of the numbers in the figure has not been indicated. If in doubt, the READ statement in the program may be consulted to determine where in the formatted data field the program expects to find each column of numbers. Subsection 6.5.1 indicates that, for this case, each column occupies exactly 16 spaces with 5 digits to the right of the decimal point. Failure to observe this instruction will result in nonsense numbers if the program runs at all.

Note that the output file POLYFIT.TXT, although shown here as a series of figures, is actually produced as a single file using a print format of 132 characters per line. Printing it using 17 characters per inch on a dot matrix printer will render it in the correct form on 8.5 in. × 11 in. paper. If the file is printed with 6-point Courier bold type on a laser printer it will also have the desired appearance (8.5 × 11 paper).

TWO DIMENSIONAL AIRFOIL DATA INPUT

23012 SERIES AIRFOIL / ALPHA=-4,-2,0,2,4,6,8,10,12 / RN=3.49 / MACH NO .2
THE NUMBER OF DATA POINTS IS = 9

ALPHA	CL	CD	CM
-4.000000	-.319630	.007873	-.005087
-2.000000	-.094990	.007569	-.006666
.000000	.125650	.006445	-.008504
2.000000	.349620	.006843	-.010548
4.000000	.573210	.007086	-.012139
6.000000	.791690	.008097	-.013172
8.000000	1.005600	.009953	-.014259
10.000000	1.185000	.014048	-.012825
12.000000	1.358000	.018434	-.010255

TWO DIMENSIONAL CURVE FIT FUNCTION DATA
OF THE FORM Y=C(0)+C(1)*X+C(2)*X**2+...

23012 SERIES AIRFOIL / ALPHA=-4,-2,0,2,4,6,8,10,12 / RN=3.49 / MACH NO .2

	C(0)	C(1)	C(2)	C(3)	C(4)				
CL VERSUS ALPHA	.12631	.11213	.00014	-.00003	.00000	DOMAIN=	-4.0000	TO	12.0000
CD VERSUS CL	.00708	-.00202	.00195	.00058	.00269	DOMAIN=	-.3196	TO	1.3580
CM VERSUS CL	-.00751	-.00769	-.00095	-.00205	.00429	DOMAIN=	-.3196	TO	1.3580
ALPHA VERSUS CL	-1.13586	9.02353	-.05576	-.49731	.65991	DOMAIN=	-.3196	TO	1.3580

Fig. 6.4a Tabular results for curve fit.

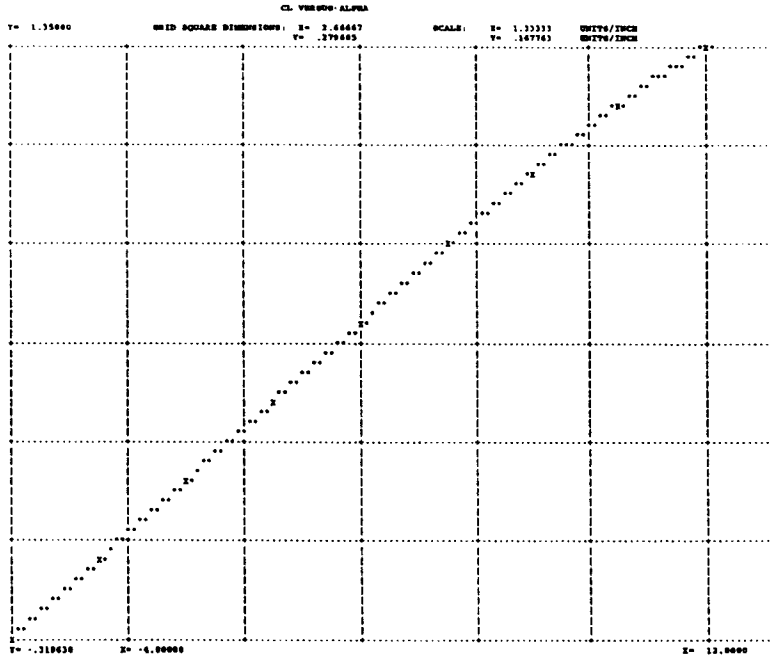

Fig. 6.4b C_L vs α curve produced by program.

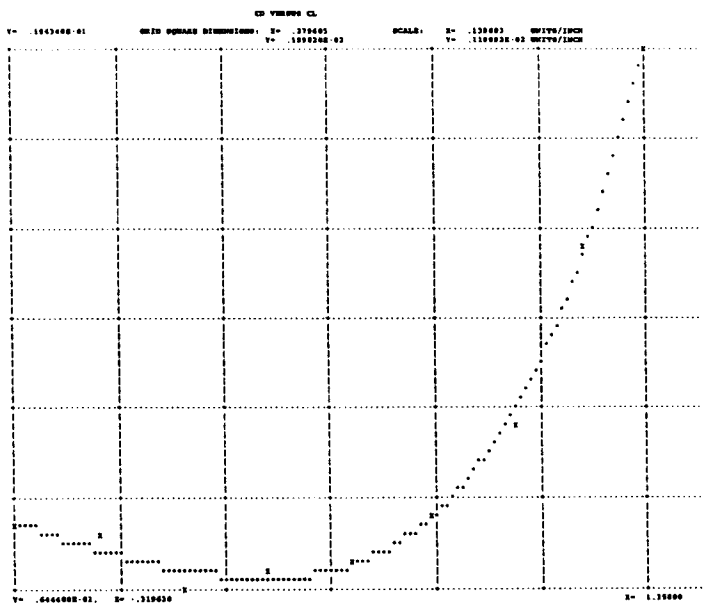

Fig. 6.4c C_D vs C_L curve produced by program.

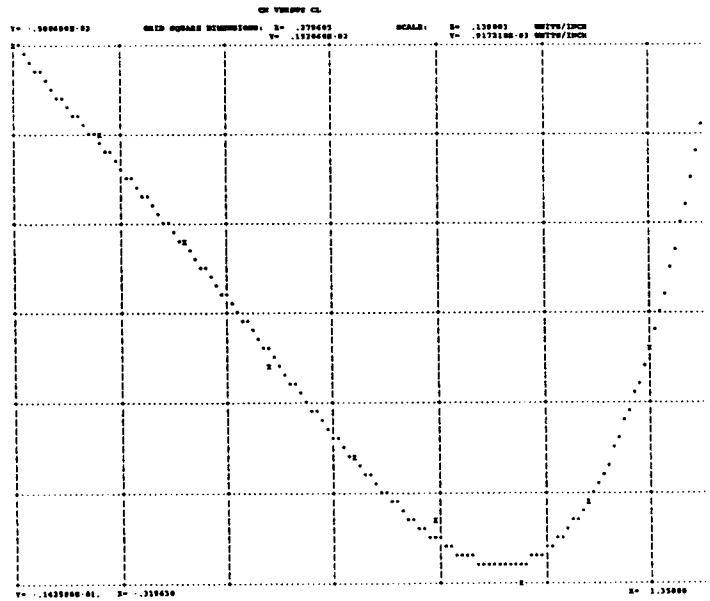

Fig. 6.4d C_m vs C_L curve produced by program.

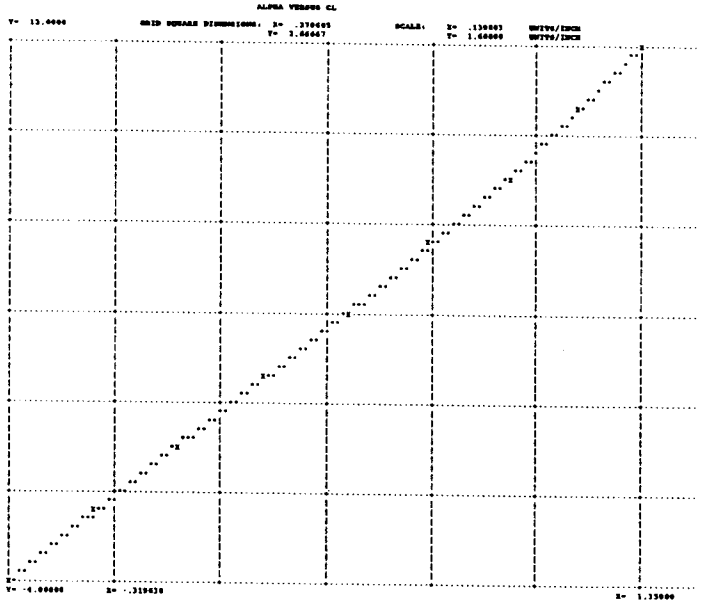

Fig. 6.4e Angle α vs C_L curve produced by program.

6.6 Converting Two-Dimensional Data to Three-Dimensional: Program F2D3D

Program F2D3D uses the lifting line theory discussed in Secs. 6.2 and 6.3 to determine the lift distribution of a complete wing in the manner of Sec. 6.4. (Note: F2D3D[26] is an extensive modification of the STALL program.[34]) It begins with the two-dimensional airfoil lift data for the root and tip airfoil sections as produced by program AIRFOIL and adds to these the effects of aspect ratio, taper ratio, and twist. The program can interpolate between the characteristics of sections of different thickness and even between the characteristics of sections from different families. The interpolations are linear along the semispan. Once the lift distribution is known, the program can then find the distribution of induced drag and induced angle of attack. The profile or form drag of the airfoil sections between the wing root and the wing tip are then interpolated from the root, and tip data supplied to the program. The pitching moment distribution is also determined by interpolation using input pitching moment characteristics as a function of section lift coefficient and the calculated section lift coefficient distribution. Each of these distributions is evaluated at 20 stations over the span. Overall wing characteristics are determined by integrating these distributions over the wing span using Simpson's rule. Interpolation in this manner is valid because there is little spanwise flow over a major portion of the span for straight wings of moderate to high aspect ratio.

On the following pages the data entry requirements for F2D3D are described. Translated into the files F2D3D.IN and POLYFIT1.DAT they are shown in Figs. 6.5a and 6.5b.

CL VERSUS ALPHA

DEGREE= 4

NUMBER OF DATA POINTS= 9
0VARIANCE= .794607E-04

THE FIT COEFFICIENTS ARE

C(0)= .126309
C(1)= .112130
C(2)= .141772E-03
C(3)= -.303841E-04
C(4)= -.377345E-05

0	X-VALUE	Y-VALUE	Y-FIT	X-VALUE	Y-VALUE	Y-FIT
	-4.000000	-.3196300	-.3187732	4.000000	.5732100	.5739952
	-2.000000	-.9499000E-01	-.9717796E-01	6.000000	.7916900	.7920923
	.0000000	.1256500	.1263086	8.000000	1.005600	.9998749
	2.000000	.3496200	.3508087	10.00000	1.185000	1.190669
	12.00000	1.358000	1.356352			

CD VERSUS CL

DEGREE= 4

NUMBER OF DATA POINTS= 9
0VARIANCE= .107878E-02

THE FIT COEFFICIENTS ARE

C(0)= .707615E-02
C(1)= -.201854E-02
C(2)= .195345E-02
C(3)= .575336E-03
C(4)= .269089E-02

0	X-VALUE	Y-VALUE	Y-FIT	X-VALUE	Y-VALUE	Y-FIT
	-.3196300	.7873300E-02	.7930206E-02	.5732100	.7086100E-02	.6959607E-02
	-.9499000E-01	.7548900E-02	.7285243E-02	.7916900	.8097400E-02	.8045048E-02
	.1256500	.6444800E-02	.6855173E-02	1.005600	.9952900E-02	.1035842E-01
	.3496200	.6843000E-02	.6673997E-02	1.185000	.1404800E-01	.1369064E-01
	1.358000	.1843400E-01	.1852986E-01			

CM VERSUS CL

DEGREE= 4

NUMBER OF DATA POINTS= 9
0VARIANCE= .276125E-03

THE FIT COEFFICIENTS ARE

C(0)= -.751337E-02
C(1)= -.769025E-02
C(2)= -.954965E-03
C(3)= -.204935E-02
C(4)= .428902E-02

0	X-VALUE	Y-VALUE	Y-FIT	X-VALUE	Y-VALUE	Y-FIT
	-.3196300	-.5086900E-02	-.5041208E-02	.5732100	-.1213900E-01	-.1215820E-01
	-.9499000E-01	-.6665800E-02	-.6789380E-02	.7916900	-.1317200E-01	-.1353219E-01
	.1256500	-.8504300E-02	-.8497716E-02	1.005600	-.1425900E-01	-.1391044E-01
	.3496200	-.1054800E-01	-.1034226E-01	1.185000	-.1282500E-01	-.1292013E-01
	1.358000	-.1025500E-01	-.1026347E-01			

ALPHA VERSUS CL

DEGREE= 4

NUMBER OF DATA POINTS= 9
0VARIANCE= .105227E-04

THE FIT COEFFICIENTS ARE

C(0)= -1.13586
C(1)= 9.02353
C(2)= -.557649E-01
C(3)= -.497311
C(4)= .659905

0	X-VALUE	Y-VALUE	Y-FIT	X-VALUE	Y-VALUE	Y-FIT
	-.3196300	-4.000000	-4.002625	.5732100	4.000000	3.995770
	-.9499000E-01	-2.000000	-1.993032	.7916900	6.000000	5.985492
	.1256500	.0000000	-.3759550E-02	1.005600	8.000000	8.050906
	.3496200	2.000000	2.000734	1.185000	10.00000	9.952416
	1.358000	12.00000	12.01410			

Fig. 6.4f Fit information.

```
    10.05       .12       .20       .40     -3.50     20.00      3.49      .001
      .00       .00       .00       .00       .00       .00    100.00
        1         0         0         0         1
23020 root series   23012 tip series
    -4.    -3.    -2.    -1.     0.     1.     2.     3.     4.     5.
     6.     7.     8.     9.    10.    11.    12.    99.
```

Fig. 6.5a Input file F2D3D.IN for a typical data set.

```
23012 SERIES AIRFOIL / ALPHA=-4,-2,0,2,4,6,8,10,12 / RN=3.49 / MACH NO .2
      .12000
      .12631          .11213          .14177E-03      -.33384E-04     -.37735E-05
    -4.0000          12.000
      .70761E-02     -.20185E-02      .19535E-02       .57534E-03      .26909E-02
    -.31963          1.3580
    -.75134E-02      -.76902E-02     -.95496E-03      -.20493E-02      .42890E-02
    -.31963          1.3580
    1.13580          9.0235          -.55860E-01      -.49714          .65984
    -.31963          1.3580
```

Fig. 6.5b Input file POLYFIT1.DAT for a typical data set.

6.6.1 Program Data Entry

For each configuration the program requires the following input data.

1) The aspect ratio ASPEC, the thickness ratio of the tip TAUT, the thickness ratio of the root TAUR, the taper ratio TAPER, the geometric twist TWIST in degrees (if geometric twist is specified the aerodynamic twist TWISA must be set to a value of 100.0), the number of spanwise stations R (R must be less than or equal to 20.0), Reynolds number in millions based on wing mean aerodynamic chord REYND, and a criterion for convergence of the lift distribution DISCR are required. The format for this line is 8F10.2.

2) Fuselage height to wing span ratio A; fuselage width to wing span ratio B; the height of the wing above the fuselage centerline H, again as a ratio to wing span; wing–body incidence angle ALPHR, in degrees; x coordinate of the moment reference X; z coordinate of the moment reference Z; and the aerodynamic twist TWISA, in degrees are required. The format for this line is 7F10.2.

3) The number of airfoil families (two tables per family) to be read in with this configuration IFAM, a control parameter for reading in the wing geometric parameters ISWIT(1), a control parameter for printing out the intermediate calculations as they are performed ISWIT(2), a control parameter for printing out matrices ISWIT(3), and an indicator that the tip airfoil is or is not of the same family as the root IRT are required. A yes action is implied when IRT = 1; otherwise, IRT = 0. The format for this line is 5I10.

4) The 80 characters of the array NAME are used as a header for identifying output. The format is 20A4.

5) The 80 characters of the array TITLE1 serve as identification for the first airfoil table. The format is 20A4.

6) The thickness ratio in the first table RT1 is required. The format is G16.5.

7) The five coefficients of the array for the lift polynomial CCLRT1 for the airfoil in the first table are required. The format is 5G16.5.

8) The domain is required for which the members of CCLRT1 are valid, XLO(1) and XHI(1).


```
*                                                                                *
*                          TWO DIMENSIONAL CURVE FIT FUNCTION DATA               *
*                            OF THE FORM Y=C(0)+C(1)*X+C(2)*X**2+...             *
*                                                                                *
*                                                                                *
*          23012 SERIES AIRFOIL / ALPHA=-4,-2,0,2,4,6,8,10,12 / RN=3.49 / MACH NO .2
*                                          THICKNESS RATIO=  .12                 *
*                      C(0)      C(1)      C(2)      C(3)      C(4)              *
* CL VERSUS ALPHA     .12631    .11213    .00014   -.00003    .00000   DOMAIN=  -4.0000  TO   12.0000 *
* CD VERSUS CL        .00708   -.00202    .00195    .00058    .00269   DOMAIN=   -.3196  TO    1.3580 *
* CM VERSUS CL       -.00751   -.00769   -.00095   -.00205    .00429   DOMAIN=   -.3196  TO    1.3580 *
* ALPHA VERSUS CL   1.13580   9.02350   -.05586   -.49714    .65984   DOMAIN=   -.3196  TO    1.3580 *
*                                                                                *
*          23021 SERIES AIRFOIL / ALPHA=-4,-2,0,2,4,6,8,10,12 / RN=3.49 / MACH NO .2
*                                          THICKNESS RATIO=  .21                 *
*                      C(0)      C(1)      C(2)      C(3)      C(4)              *
* CL VERSUS ALPHA     .13324    .11788   -.00013   -.00015    .00001   DOMAIN= -4.0000  TO   12.0000 *
* CD VERSUS CL        .00775   -.00047    .00338    .00154   -.00003   DOMAIN=  -.3295  TO    1.3580 *
* CM VERSUS CL       -.00176   -.01808   -.00626    .01679   -.00705   DOMAIN=  -.3295  TO    1.3580 *
* ALPHA VERSUS CL  -1.12080   8.48720   -.32278   1.16880   -.42162   DOMAIN=  -.3295  TO    1.4304 *
*                                                                                *
**********************************************************************************

                              SPECIAL FEATURES FOR THIS RUN

                              NO SWITCH SETTINGS  REGULAR RUN

                              23020 root series   23012 tip series


        SPANWISE STATIONS
( 1)   .98768840  ( 2)   .95105660  ( 3)   .89100670  ( 4)   .80901730  ( 5)   .70710720
( 6)   .58778590  ( 7)   .45399130  ( 8)   .30901800  ( 9)   .15643560  (10)   .12973930E-05
(11)  -.15643310  (12)  -.30901550  (13)  -.45398900  (14)  -.58778380  (15)  -.70710540
(16)  -.80901580  (17)  -.89100550  (18)  -.95105580  (19)  -.98768790  (

        THICKNESS / CHORD DISTRIBUTION
( 1)   .12241770  ( 2)   .12911920  ( 3)   .13873560  ( 4)   .14969090  ( 5)   .16069820
( 6)   .17094340  ( 7)   .18003350  ( 8)   .18786070  ( 9)   .19447550  (10)   .20000000
(11)   .19447560  (12)   .18786080  (13)   .18003370  (14)   .17094360  (15)   .16069840
(16)   .14969110  (17)   .13873580  (18)   .12911930  (19)   .12241780  (

        SECTION REYNOLDS NUMBERS
( 1)  1.9141270  ( 2)  2.0173960  ( 3)  2.1866850  ( 4)  2.4178240  ( 5)  2.7051210
( 6)  3.0415030  ( 7)  3.4186870  ( 8)  3.8273860  ( 9)  4.2575350  (10)  4.6985440
(11)  4.2575420  (12)  3.8273930  (13)  3.4186940  (14)  3.0415090  (15)  2.7051260
(16)  2.4178280  (17)  2.1866880  (18)  2.0173990  (19)  1.9141280  (

        CHORD DISTRIBUTION
( 1)   .40738700  ( 2)   .42936610  ( 3)   .46539600  ( 4)   .51458960  ( 5)   .57573560
( 6)   .64732840  ( 7)   .72760520  ( 8)   .81458920  ( 9)   .90613860  (10)   .99999920
(11)   .90614010  (12)   .81459070  (13)   .72760660  (14)   .64732970  (15)   .57573680
(16)   .51459060  (17)   .46539670  (18)   .42936660  (19)   .40738720  (

        TWIST DISTRIBUTION
( 1)  -3.3942270  ( 2)  -3.1010350  ( 3)  -2.6803180  ( 4)  -2.2010240  ( 5)  -1.7194530
( 6)  -1.2712250  ( 7)  -.87353400  ( 8)  -.53109620  ( 9)  -.24169580  (10)  -.18163520E-05
(11)  -.24169140  (12)  -.53109090  (13)  -.87352780  (14)  -1.2712180  (15)  -1.7194450
(16)  -2.2010160  (17)  -2.6803110  (18)  -3.1010290  (19)  -3.3942230  (
```

Fig. 6.6 File F2D3D.TXT: result of two-dimensional to three-dimensional conversion.

```
                    23020 root series   23012 tip series

BODY HEIGHT / SPAN . . . . . =      .00     BODY WIDTH / SPAN. . . . . =      .00
ASPECT RATIO . . . . . =    10.05     WING HEIGHT / SPAN . . . . . =      .00
WING BODY INCIDENCE, DEG . . =      .00     TIP THICKNESS CHORD. . . . . =      .12
ROOT THICKNESS CHORD . . . . =      .20     GEOMETRIC TWIST, DEG . . . . =    -3.50
NUMBER OF SPANWISE STATIONS. =    20.00     AERODYNAMIC TWIST, DEG . . . =    -5.45
TAPER RATIO. . . . . =      .40     REYNOLDS NUMBER. . . . . =     3.49
COORDINATES OF MOMENT REFERENCE POINT          X=      .00        Z=      .00
VALUE OF DISCRIMINANT. . . . =   .001000
```

THREE DIMENSIONAL LIFT, DRAG, AND MOMENT DATA

ALPHA	CL	CDP	CDI	CD	CM
-4.000000	-.350241	.008186	.004358	.012545	.000462
-3.000000	-.259806	.007969	.002563	.010532	-.000419
-2.000000	-.168407	.007776	.001287	.009063	-.001497
-1.000000	-.076028	.007623	.000542	.008166	-.002753
.000000	.016982	.007517	.000345	.007862	-.004127
1.000000	.110283	.007462	.000703	.008166	-.005562
2.000000	.203571	.007467	.001618	.009085	-.007007
3.000000	.296575	.007540	.003082	.010622	-.008415
4.000000	.389053	.007688	.005087	.012775	-.009752
5.000000	.480793	.007922	.007614	.015537	-.010988
6.000000	.571613	.008252	.010647	.018899	-.012105
7.000000	.661363	.008687	.014162	.022849	-.013091
8.000000	.749921	.009238	.018137	.027375	-.013942
9.000000	.837199	.009914	.022548	.032462	-.014662
10.000000	.923140	.010726	.027372	.038098	-.015258
11.000000	1.007723	.011684	.032586	.044270	-.015743
12.000000	1.090962	.012797	.038171	.050968	-.016135

Fig. 6.6 Contd.

9) The five coefficients of the drag polynomial CCDRT1 for the airfoil in the first table are required. The format is 5G16.5.

10) The domain is required for which the coefficients of CCDRT1 are valid, XLO(2) and XHI(2).

11) The five coefficients of the moment polynomial CCMRT1 for the airfoil in the first table are required. The format is 5G16.5.

12) The domain for which the coefficients of CCMRT1 are valid, XLO(3) and XHI(3), is required.

13) The five coefficients of the alpha polynomial CALRT1 for the airfoil in the first table are required.

14) The domain for which the coefficients of CALRT1 are valid, XLO(4) and XHI(4), is required.

15) A duplication of steps 4–14 is required for each additional airfoil.

16) The 20 elements of the array ALPHB are required representing the angles of attack for which the three-dimensional lift, drag, and pitching moment coefficients are to be calcuated. One element of this array must contain the value 99.0 to ensure a later return to the main portion of the program.

The program will continue execution until it encounters an ASPEC value of 99.0 followed by a blank line. For the present version of the program, input has

been divided among 3–5 files. F2D3D.IN contains the general program instructions. It may be produced by a user edited version of 3DHELP or it may be user edited. This method was chosen for general program data entry because a separate interactive program to write F2D3D.IN was regarded as too confusing given the quantity of data to be entered, particularly as regards to character strings identifying the various airfoils and other features of the wing design. The other input files are POLYFIT1.DAT and POLYFIT2.DAT and perhaps POLYFIT3.DAT and POLYFIT4.DAT. Figure 6.5 shows F2D3D.IN and POLYFIT1.DAT for a typical case. Note that the listings for 2DHELP.FOR and 3DHELP.FOR are provided on the accompanying disk as are personal computer executable versions.

6.6.2 *Typical Results*

Results produced by F2D3D appear in the file F2D3D.TXT. Operating on the input data shown in Fig. 6.5 the results given by F2D3D are shown in Fig. 6.6. No graphics are produced at the present time. However, the three-dimensional characteristics are produced in a compact tabular form at the end of the listing, which is easily converted to graphs by readily available plotting programs should the need for such a representation arise. At the beginning of the listing is a repeat of the input data so that it can be checked for accuracy in case the program fails to execute properly. In the middle are listed any special switch setting and the station by station values of the chord, the thickness, the Reynolds number, and the twist.

6.7 Other Methods of Analyzing Complete Wings

The moderate to high aspect ratio requirement makes the lifting line theory of little use to hydrodynamicists where, because of structural considerations, wings almost always have fairly low aspect ratios. Most modern corporate jets and commercial transports employ swept back wings to enable them to operate at higher Mach numbers (than unswept wings) before encountering the transonic drag rise. Some fighter designs carry the need for swept leading edges and thin wings to a logical conclusion by utilizing delta wing planforms. Such planforms have aspect ratios of three or less. Obviously, these planforms cannot be analyzed by the lifting line theory. There are also other classes of flight vehicle, such as sport aircraft, which find it desirable to employ moderate to low aspect ratio wings despite the increased induced drag that such use entails.

This situation lead researchers to develop what was called the lifting surface theory, a theory in which the wing's chord dimension was included. This theory was difficult to employ in practice because of its mathematical complexity. With the arrival of the digital computer it became possible to consider methods that although simple in concept required extensive computational effort. One such method applied to wing analysis is the vortex lattice method.[35] In this method the wing may be considered to be planar and is represented by many horseshoe vortices laid out in both the spanwise and chordwise directions, hence the name vortex lattice. The strengths of the individual vortices are determined from the requirement that the flow at a control point in each lattice element must be parallel to the wing surface. Several hundred vortices may be employed. An equation is written for the velocity induced at a control point by each vortex in the system. Additional equations are added to the system to define the net induced velocity

at all other control points on the wing until there is an equation for each of the unknown vortex strengths. Obviously, such a method would be attempted on a production basis only with the aid of a digital computer. One can see, however, how such a method is but a logical extension to the lifting line theory. The major wing analysis computer programs employed by the military and the major airframe constructors are generally refinements of the vortex lattice method.

In the next chapter we shall consider the representation of a body by a lattice structure where, instead of a vortex, there is a source and a control point in each of the lattice elements. Because the sources do not induce a circulation the body has no lift.

We will not discuss the lifting surface and vortex lattice methods in any additional detail because we believe them beyond the scope of an introductory text and because we have not provided one of the more complex computer programs that employ them with the book.

6.8 Concluding Remarks

In this chapter we have presented a method for converting two-dimensional airfoil section data for lift, drag, and pitching moment to three-dimensional wing characteristics including the effects of wing taper, wing twist, and fuselage upwash. Although based on the inviscid lifting line theory developed by Prandtl and others, the method permits one to determine the induced drag of medium to high aspect ratio wings, an inviscid phenomenon, as well as their profile drag, a result of viscosity. To obtain the latter result, the method serves merely to interpolate the readin section results and then integrates these values over the span. High-angle-of-attack lift characteristics can be handled in the same manner, that is, through interpolation and then integration over the span. By obtaining the induced angle of attack at up to 20 stations along the span, the program can give results of quite high accuracy. It is unable, however, to account properly for the unusual drag characteristics of some 6-series airfoils in their cruise configuration because the drag characteristics are fit with only a fourth-order polynomial.

Whereas the physical concepts behind F2D3D are readily appreciated, the mathematics by which these concepts are implemented in the program is more obtuse. When faced with such a situation, prior to using the program the reader would seem to have two choices: either spend the time necessary to become familiar with the mathematics or undertake to test the program results against known two- and three-dimensional data to gain confidence that the program is being used correctly and that it gives correct results. The latter course is recommended for the beginning student.

One may ask why, in light of this recommendation, the details of the program implementation are presented at all. The answer is that at some point in the user's career, when the program is applied to a case for which three-dimensional experimental results are unavailable and program output is perhaps suspicious, the user will want to check the procedure to determine what credance one should apply to the results for that case. Another reason for presenting the program implementation at this level is to give the student an indication of what is really involved in going on to make such conversions.

Also, at some point the user may have the opportunity to employ one of the various implementations of the vortex lattice method. For aircraft with unswept

moderate to high aspect ratio wings the method described in this chapter will be found to execute more rapidly, require fewer computational resources, and provide reliable estimates of wing profile drag (which other methods may be incapable of providing) as compared with most implementations of the vortex lattice method. On the other hand, if the problem involves low aspect ratio wings, whether on aircraft or on undersea vessels, the method of analysis described in this chapter may not be applied, and one must then have recourse to a vortex lattice or other lifting surface method.

Problems

6.1. Using the two-dimensional data in Fig. P6.1 determine the change in characteristics resulting from a) a change in aspect ratio from 10.05 to 5.8, b) a change in twist from −3.5 deg to 0.0 deg, c) a change in taper ratio from 0.4 to 1.0. Plot C_L vs α in each case. Comment on the differences.

6.2. Determine the spanwise lift distribution for the three cases in problem 6.1, then plot and discuss them. The program will display such results by setting ISWIT(2) = 1. Do not set ISWIT(1) = 1. Doing so will cause the program to crash because a portion of the code for which no data exists in F2D3D.IN is then invoked.

6.3. Compare the spanwise lift distributions for the three cases in problem 6.2 with an elliptical distribution. Which one is closest and which is least like an ellipse?

6.4. A certain wing has a 23012 root section, a 23020 tip section, a 0.4 taper ratio, a 10.05 aspect ratio, and −3.5-deg geometric twist. The Reynolds number based on the mean aerodynamic chord is 3.49×10^6. Compare the three-dimensional

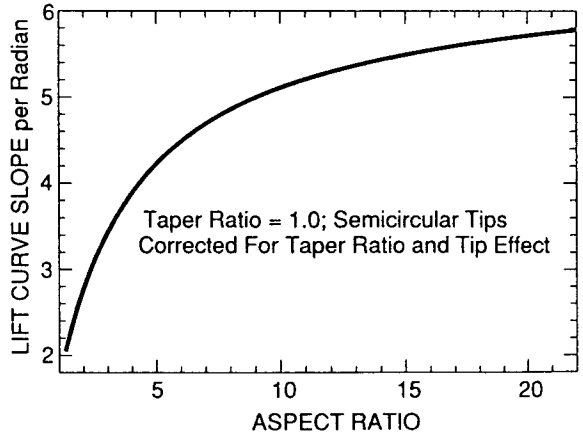

Fig. P6.1 Corrected C_{L_α} vs A_R curve for $\lambda = 1.0$.

aerodynamic characteristics of this wing with that shown in Fig. P6.1. Discuss them.

6.5. The AIRFOIL program cannot reliably predict the aerodynamic characteristics of an airfoil section when the lift coefficient exceeds about 0.8. When supplied with experimentally determined section data, however, the F2D3D program can function correctly up to and including the maximum lift coefficient of the section. Using the experimental data in Chapter 5, determine the angle of attack and spanwise location where stall first appears on the following wing: airfoil section NACA 4412, aspect ratio 6.0, taper ratio 0.5, twist -3.5 deg, and Reynolds number 3×10^6. [Stall is characterized by a failure of the lift to increase (and often to decrease) as the angle of attack is increased. A benign stall is one in which the decreases in lift are gentle as α increases. An undesirable stall is one in which the decrease in lift is large and sudden for small increases in α.] Note: it may be necessary to extrapolate the C_D vs C_L curve slightly to obtain a drag coefficient for $C_{L_{max}}$. To maintain lateral control near stall, it is desirable to ensure that the root area of the wing stalls before the tip area. That is one of the reasons for using washout, e.g., negative wing twist, at the tip region.

6.6. The first airplane to fly around the world unrefueled employed an aspect ratio of 22 and a taper ratio of about 0.4. Assuming a geometric twist of -3.5 deg, what percentage increase did the induced drag represent over the basic wing profile drag? Assume for purposes of this problem that the root and tip airfoil sections are the same as those in problem 6.1.

6.7. We wish to investigate how low the aspect ratio can be before F2D3D begins to yield results that are significantly in error. For purposes of this problem we will consider the standard of comparison to be the wing's lift curve slope. We will consider the characteristics of an untapered, untwisted wing with a NACA 0009 airfoil section. We will assume that the Reynolds number is 3×10^6. We will further assume that the wing tips are semicircles. For such a wing, the minimum aspect ratio is $4b^2/(\pi b^2) = 4/\pi$. (Experimental data exists for such wings. During the 1930s Charles Zimmermann of NACA conducted of series of wind-tunnel tests on such planforms the, results of which were published in a technical report or technical note. His interest in the circular planform led the Navy to support the construction of such an aircraft following World War II. Could the sight of this aircraft have led to stories of flying saucers?) Beginning with an aspect ratio of 6, run F2D3D at aspect ratio increments down to $4/\pi$. In Ref. 36 there is a formula for lift curve slope as a function of aspect ratio that for thin airfoils can be plotted as shown in Fig. P6.1. Compare the results given by F2D3D with the data shown on the graph. The curve on the graph is corrected for the fact that the wing is untapered and has a 9% thick airfoil section and semicircular tips.

6.8. What is the aspect ratio of a true delta wing?

6.9. If the airfoil used on a delta wing has a maximum lift coefficient of 1.5 at an angle of attack of 15 deg, what angle of attack should one expect the wing to reach for a lift coefficient of 1.5?

6.10. It can be shown that the maximum range of an aircraft is achieved when the aircraft flies at such a speed, weight, and altitude that the induced drag is equal to the profile drag. How does increasing the aspect ratio change the speed at which the aircraft reaches maximum range assuming that the weight, altitude, and wing area remain the same?

6.11. Discuss why a high aspect ratio is not desirable for all aircraft.

6.12. An undersea vessel has a hull diameter of 10 ft. Wings extending 10 ft from the hull on each side have a chord of 10 ft. What is the aspect ratio of the resulting wing?

6.13. How does the magnitude of the velocity induced by a vortex vary with distance from the vortex?

6.14. How does the bending moment on a wing vary with semispan?

6.15. If you assume that all of the airfoil's mass is concentrated at its maximum thickness from the mean chord line, how does the moment of inertia that resists bending vary with thickness ratio? Assume the mass is the same in each case; compare symmetrical sections 6, 12, 18, and 24% thick.

6.16. If you have studied charts of airfoil mimimum drag as a function of Reynolds number you would have discovered that the drag coefficient increases as the size of the wing and the flight velocity decrease. You should also be aware the maximum lift coefficient also decreases with decreasing Reynolds number. Given this information how would you expect the lift and profile drag of a paper airplane to compare with that of a typical general aviation craft? What should be your expectations of the induced drag?

6.17. Would you expect the aerodynamic characteristics of a GA class aircraft or a 747 to be more or less susceptible to a given amount of ice on the wing? Explain why.

6.18. Induced drag is a consequence of higher pressure air underneath the wing surface flowing spanwise and up over the tip to the lower pressure region over the upper surface. As a designer, if you place an external store such as a fuel tank projecting from the wing tip, what is the likely effect of that store on the induced drag? If the external tank is full, discuss what effect it has on the wing root bending moment.

7
Characteristics of Bodies at Small Angles of Attack

7.1 Introduction

IN this chapter we consider a method for modeling a body with a plane of symmetry from which we will be able to deduce the pressure distribution, the lift, and the drag when the body has little or no inclination to the oncoming flow. Therefore, the method is suitable for determining the aerodynamic characteristics of isolated bodies such as a fuselage or a nacelle; however, it is unable to determine the characteristics of such bodies in the presence of a wing. For those cases where wing–body interference effects are small and other restrictions on the method's accuracy are observed, it is superior to the use of common handbook values for accurate determinations of the drag of fuselages and nacelles.

It may be recalled that in Chapter 2 we showed that placing a separated source and sink in a uniform stream creates a two-dimensional body called the Rankine oval. In the present method, the body surface is represented by a sort of wire frame that divides the surface into a series of quadrilaterals. Each quadrilateral represents the edges of a flat surface. On each of these small surfaces is placed a source of unknown strength and a control point. We require that the exterior flow normal to the each quadrilateral surface is zero at the control point. This gives us the necessary information to write an equation giving the contribution of all sources to the flow over each quadrilateral. Solving this system of equations permits us to determine the value of the individual source strengths. Obviously, the greater the number of quadrilaterals used, the more accurately the surface can be represented. One can also expect the computation time and memory required to increase as n^2 where n is the number of quadrilateral panels in the analysis.

The idea of representing bodies in this manner seems to have originated with Hess and Smith[37] of the Douglas Aircraft Company who created a computer program in 1962 to perform the necessary calculations. Some of their Fortran code probably still exists within the present program, which is the result of many modifications and expansions of their original code. When the Hess–Smith program first appeared, computer memory was a very scarce commodity and so the authors were forced to spend most of their development effort on means to swap data and code in and out of main memory rapidly and efficiently and to devise means to solve the large system of equations in a piecemeal fashion. The situation had eased considerably by the mid 1970s when the first versions of BODY were written. Most of the elaborate I/O procedures were replaced; all code and data for the analysis of 225 panels on a half-body (some 5 Mbytes worth) could then be held in main memory, provided no other user was given a portion of the CPU memory. However, that memory requirement limited runs to nights and weekends on a large mainframe. Now, that amount of memory is available for program use on most home computers. Even when this quantity of memory is not available,

current personal computer operating systems will make the machine appear to have virtual memory. They do this by swapping portions of the code and data to disk in a manner tranparent to the user if there should be insufficient real memory. The use of virtual memory, however, entails a significant increase in program execution time because disk reads and writes are many times slower than writing to and reading from random access memory (RAM).

We must note that the original program was entirely inviscid. No drag values could be determined from it. The program was later modified and expanded at the Naval Ship Research and Development Center to include the ability to calculate on-body and off-body streamlines. At NCSU the boundary-layer routines from AIRFOIL were employed along the on-body streamlines. A wake body was created from the boundary-layer displacement thickness to simulate the body wake and permit a profile drag to be calculated. The skin-friction drag is calculated from the value of the skin-friction coefficient on each panel times the panel area. Several empirical tweeks and a more refined pressure integration routine were later employed to improve the agreement of the results with experimental data. One such tweek was to subtract the integral of the streamwise component of the pressures over the inviscid body from the final drag result. The force resulting from this integration should be zero. Depending on how many panels are used and the rapidity with which the pressure changes on the aft portions of the body the result may not be zero. Subtracting this tare usually improves the computed drag values.

The vehicle used for program evaluation was a prolate spheroid. NACA collected considerable wind-tunnel data early in the 1930s on fairly large models of the airship **Akron**. These data were very useful in helping to select the separation criteria for the boundary-layer flow from the physical body. These locations were then used as the points at which the wake body was attached to the physical body. No significant alterations have been made in the fundamental operation of the code since 1984, however.

The changes made for the present version of BODY deal with data I/O, the type of graphics routines used, and changes required by the evolving nature of the FORTRAN language and various operating systems. The NCSU version of the program was originally intended to drive a plotter; the plotter-specific routines have been replaced in the present version of the code by routines that write PostScript code. When the 1970s version of BODY was run the plots were created at the same time as the output text file was generated. With the present version, PostScript files are created at the same time that the text files are generated. One will then have to submit these PostScript files to a PostScript-equipped printer or to a software PostScript interpreter that can create a bitmap image for the screen or a laser, dot matrix, or inkjet printer to create the pictures. A four-view graphical description of a general ellipsoid produced by BODY is shown in Fig. 7.1. Notice the resemblence to a wire frame model.

One reason such pictures are still generated by the current version of the program is that they permit one to readily detect certain types of erroneous input data. Errors in the coordinates of panel corners stand out immediately when the wire frame image of the body is viewed; when they are buried in the mass of input data such errors are difficult to detect simply from a listing of the coordinates. It also enables one to see graphically the wake body that the program appends to the physical body.

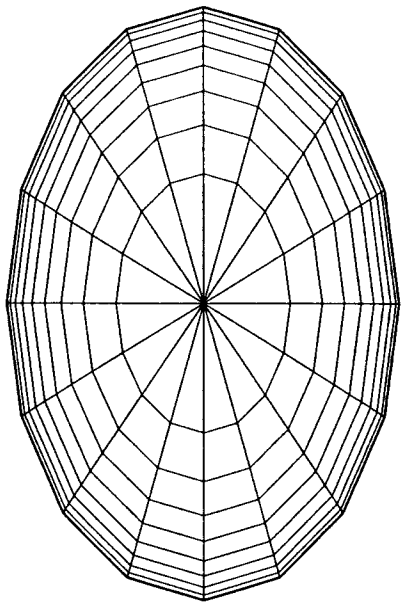

Fig. 7.1a Wire frame representation of general ellipsoid.

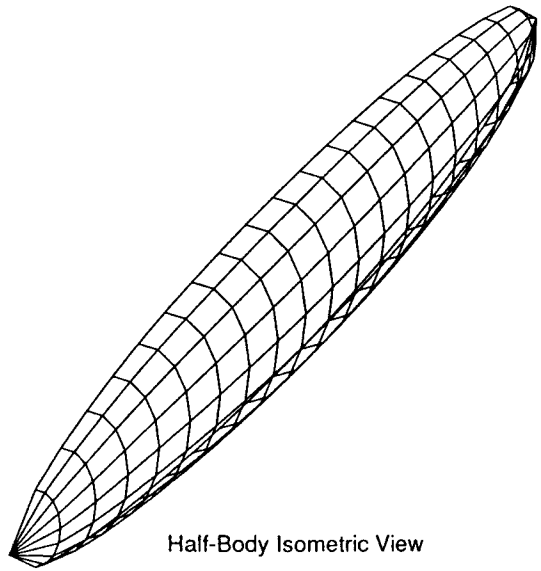

Fig. 7.1b Isometric view, general ellipsoid.

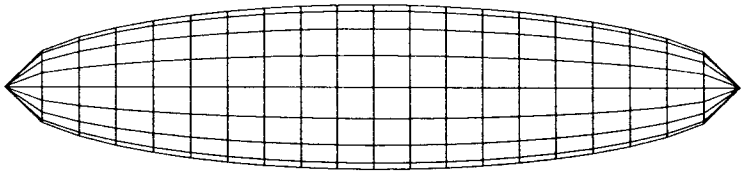

BODY Plan View

Fig. 7.1c Plan view, general ellipsoid.

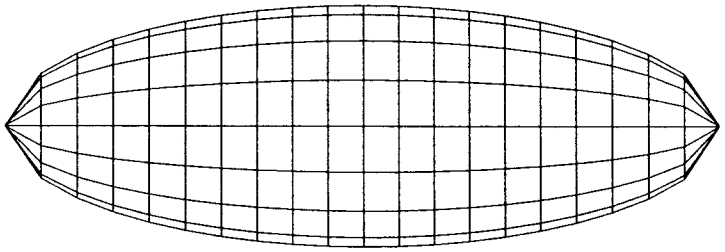

BODY Elevation View

Fig. 7.1d Elevation view, general ellipsoid wire frame representation with 320 panels.

7.2 Theory Behind Program BODY

7.2.1 Basic Hess–Smith Method

In the basic Hess–Smith[37] method the body surface is approximated by a set of plane quadrilaterals and the solution is constructed in terms of the source density on the surface of the body. Based on the assumption that the source density is constant on each quadrilateral, a system of algebraic equations is used to approximate the integral equation for the source density over the body. The source density in each quadrilateral is chosen so that the normal component of the velocity is zero at one point on each quadrilateral. The resulting matrix equation is solved by a simultaneous displacement iteration scheme with a two-eigenvalue extrapolation procedure to speed up convergence.

The fluid is assumed to have a uniform velocity $\mathbf{V}_\infty$, which is parallel with the x axis of the body. Because the fluid is assumed to be inviscid and irrotational a velocity potential exists, and we assume it satisfies the following equations:

$$\nabla^2\phi = 0 \tag{7.1}$$

in the fluid

$$\frac{\partial\phi}{\partial n} = 0 \tag{7.2}$$

on the surface of the body and

$$\phi = -x \cdot V_{\infty_x} - y \cdot V_{\infty_y} - z \cdot V_{\infty_z} \tag{7.3}$$

at infinity. Here, n is the direction normal to the surface. A solution to these equations is constructed in the form of a source density distribution $S(q)$ on the surface of the body

$$\phi(p) = \int_{\text{body}} \int_{\text{surface}} \left[\frac{S(q)}{r(p,q)}\right] \mathrm{d}A_q - x \cdot V_{\infty_x} - y \cdot V_{\infty_y} - z \cdot V_{\infty_z} \tag{7.4}$$

Here, $r(p,q)$ is the distance between the point p where we are interested in finding the potential and some other point q on the body. A_q denotes the area of the quadrilateral containing point q. Note that Eqs. (7.1) and (7.3) are satisfied by ϕ as defined by Eq. (7.4). The boundary condition on the body, Eq. (7.2) can be applied to obtain the equation for the source density at p:

$$0 = \frac{\partial\phi}{\partial n_p} = 2\pi S(p) - \int_{\text{body}} \int_{\text{surface}} \frac{\partial}{\partial n_p}\left(\frac{1}{r(p,q)}\right) \mathrm{d}A_q$$
$$-n_{px} \cdot V_{\infty_x} - n_{py} \cdot V_{\infty_y} - n_{pz} \cdot V_{\infty_z} \tag{7.5}$$

Because the surface of the body is approximated by a set of plane quadrilaterals that are generated from input points, in the limit Eq. (7.5) requires that the body surface be represented by an infinite number of panels with the flow normal to the surface zero at each panel. It is important to obtain satisfactory results with a finite number of panels and to properly size and position these panels on the body surface. Unfortunately, selection of panel size and panel placement is largely a matter of experience. Panels should be concentrated in regions where the source density is expected to vary rapidly. The method gives good results for convex surfaces. For rounded concave surfaces, however, a very large concentration of panels has been found to be required. Panel size also plays a role in determining the validity of the solution. Hess and Smith[37] found that if several small panels are in the vicinity of a large panel, the accuracy of the representation in that region is associated with the large panel. Thus, panel size should change gradually when going from a region of highly concentrated small panels to a region of sparce panel concentration. They recommend that the characteristics dimensions of adjacent panels should vary by no more than 50%.

The source density is assumed to be constant in each of the body panels and is computed by satisfying Eq. (7.5) at one point in each of the quadrilaterals. Thus, the Fredholm integral equation is approximated by the matrix equation

$$S_i = \sum_j C_{ij} S_j + V_i \tag{7.6}$$

where

$$C_{ij} = \frac{1}{2\pi} \int_{\text{quad}} \int_j \frac{\partial}{\partial n_i}\left(\frac{1}{r_{ij}}\right) \mathrm{d}A \tag{7.7}$$

$$C_{ii} = 0 \tag{7.8}$$

$$V_i = (1/2\pi)\left(n_x \cdot V_{\infty_x} + n_y \cdot V_{\infty_y} + n_z \cdot V_{\infty_z}\right) \tag{7.9}$$

Equation (7.6) is solved for S_i by the mentioned iteration procedure. The velocity components of each panel centroid are then computed from the following equations:

$$VX_i = \sum_j V1_{ij} S_j + V_{\infty_x} \tag{7.10}$$

$$VY_i = \sum_j V2_{ij} S_j + V_{\infty_y} \tag{7.11}$$

$$VZ_i = \sum_j V3_{ij} S_j + V_{\infty_z} \tag{7.12}$$

where

$$V1_{ij} = -\int_{\text{quad}} \int_j \frac{\partial}{\partial x}\left(\frac{1}{r_{ij}}\right) dA \tag{7.13}$$

$$V2_{ij} = -\int_{\text{quad}} \int_j \frac{\partial}{\partial y}\left(\frac{1}{r_{ij}}\right) dA \tag{7.14}$$

$$V3_{ij} = -\int_{\text{quad}} \int_j \frac{\partial}{\partial z}\left(\frac{1}{r_{ij}}\right) dA \tag{7.15}$$

The pressure coefficient is then computed from these velocity components.

An integral over a quadrilateral is evaluated by one of three methods depending on the distance of the ith point from the quadrilateral to the maximum dimension of the quadrilateral. If the ratio is greater than 4.0, the quadrilateral is approximated as a monopole (as if it were concentrated at one point); if the ratio is between 2.0 and 4.0, the quadrilateral is approximated by a quadrapole; if the ratio is less than 2.0, the integrals are evaluated exactly. The approximate methods are used because they require much less time than the exact method and yield effectively the same result for distant sources.

7.2.2 Streamline Determination

The on-body streamlines are computed once the velocities at the panel centroids are known. The method, developed by Dawson and Dean[38] of the Naval Ship Research and Development Center, may be outlined as follows.

1) The coordinates of a starting point within a particular quadrilateral are specified.

2) The two points are found at which the streamline, passing through the starting point, intersects the sides of the starting quadrilateral.

3) The intersection point, which is in the upstream flow direction, is retained.

4) A search is made of the adjacent quadrilaterals to determine which quadrilateral the streamline is entering in the upstream direction.

5) Using this quadrilateral as a starting quadrilateral, the point is found at which the streamline leaves the new quadrilateral in the upstream direction.

6) Steps 4 and 5 of the procedure are repeated until the streamline reaches the nose of the body.

7) The upstream portion of the streamline so traced is now defined by the coordinates of its intersection points on the sides of the quadrilaterals through which it passes.

8) It should be noted that as each point on the streamline is found the velocity at that point and the distance from that point to the previous streamline point are calculated.

9) After returning to the original starting quadrilateral the same procedure is used to trace the streamline in the downstream direction to the body tail.

10) The arc lengths from point to point are then all referenced to the nose of the body so that the distance of any point along a streamline is known.

To this point the entire procedure is still inviscid. With the streamline paths now known we can move on to a determination of the effects of viscosity. We will assume that the crossflow velocity along a streamline is small compared with the velocity in the streamline direction and that we are therefore justified in applying the two-dimensional boundary-layer method used in the AIRFOIL program to determine the boundary-layer displacement thickness and skin-friction coefficient at a point on each quadrilateral. From the boundary-layer displacement thickness and its rate of growth at the line of flow separation around the body, we can begin our determination of the shape of the wake body, a fictitious shape, which we append to the physical body to model the body wake. The use of this wake body enables us to apply the invicid theory we have been discussing to the combined body and thereby obtain the correct pressure distribution over the physical body. When this pressure distribution is integrated one obtains a form drag.

7.2.3 Addition of a Wake Body

For this version[26] of **BODY** we will make the assumption that the flow *always* separates from the body at the second from last N station. (In the version created by Fox[39] for his dissertation, the flow separates at the odd numbered N station just upstream of the point at which the flow separation criterion is satisfied along one of the streamlines.) This arbitrary selection of separation N station was made to keep the program as simple as possible and to reduce its execution time. This is also the reason there are no iterations on the initial wake body shape in the manner in which the airfoil shape was adjusted to account for the boundary-layer displacement thickness.

The assumptions used in **BODY** are not quite the large sources of error one may at first imagine them to be because the axial placement of N stations is restricted only by the requirment that the panels not vary too greatly in area. By selecting the second from last N station somewhere near where one might imagine separation to occur, the wake body size for purposes of the drag calculation is forced to be approximately correct. When we discuss the results of the computation we shall see how reliable the results can be when using an arbitrary number of equally spaced N stations.

From the point of its attachment to the physical body, the wake body extends downstream a distance that depends on the rate of growth of the displacement thickness on the after portion of the physical body. The formula developed to define the wake body shape is semiempirical, designed to yield approximately correct pressures on the body in the separated flow region. It must satisfy two criteria: 1) there must be a stagnation point at the downstream end of the wake

body and 2) the change in the wake body slope from the physical body aft should be monotonic; otherwise, the pressure distribution will exhibit confusing bumps. The procedure for generating the wake body can be described using the actual code instructions.

Begin by identifying the N station at which the wake body is to be attached. This station is identified in the program by the variable ISTART, defined as follows:

```
ISTART=(NMAXQD-3)*MMAXQD+1
```

Then, identify a second N station one station further downstream.

```
IST=ISTART+MMAXQD
```

The X values associated with these numbers are

```
XHOLD1=X(ISTART+1)
XHOLD2=X(IST+1)
```

Now let us determine the average value of the Z coordinate and load the XNEW, YNEW, and ZNEW arrays with the coordinates of the panel corners at the N station corresponding to ISTART,

```
      ZAV=0.0D0
      DO 405 I=1,MMAXQD
      XNEW(I)=X(ISTART+I-1)
      YNEW(I)=Y(ISTART+I-1)
      ZNEW(I)=Z(ISTART+I-1)
  405 ZAV=ZAV+ZNEW(I)
```

Then define two housekeeping variables and the average Z coordinate per panel,

```
      pi=DACOS(-1.0D0)
      THETA=-90.0D0*pi/180.0D0
      ZAV=ZAV/MMAXQD
```

Next find an average radius and convert it to a per panel value,

```
      RAV=0.0D0
      DO 410 I=1,MMAXQD
  410 RAV=RAV+DSQRT((YNEW(I))**2+(ZNEW(I)-ZAV)**2)
      RAV=RAV/MMAXQD
```

Define FAC in terms of XHOLD1, XHOLD2, and AVXCG, the average X coordinate of the panels whose upstream edge lies along N station ISTART,

```
FAC=(AVXCG-XHOLD1)/(XHOLD2-XHOLD1)
```

We now find the Y and Z coordinates of these same panels, the average radius at N station ISTART, the average radius at the panel centroids including twice the average boundary-layer displacement thickness AVDELS, which had been found

during the boundary-layer analysis, and the initial slope of the wake body and its per panel value

```
      AVSLOP=0.0D0
      DO 415 I=1,MMAXQD
      YCG=YNEW(I)-(YNEW(I)-Y(IST+I))*FAC
      ZCG=ZNEW(I)-(ZNEW(I)-Z(IST+I))*FAC
      R1=DSQRT((YNEW(I))**2+(ZNEW(I)-ZAV)**2)
      R2=DSQRT((YCG)**2+(ZCG-ZAV)**2)+2.0D0*AVDELS
      SLOPE=(R2-R1)/(XHOLD1-AVXCG)
  415 AVSLOP=AVSLOP+SLOPE
      AVSLOP=AVSLOP/MMAXQD
```

Then define the downstream extent of the wake body XINF, in terms of the average panel area AREAAV,

```
      AREAT=4.0*AREAAV*2.0*Dfloat(MMAXQD)
      XINF=XHOLD1-AREAT/(PI*RAV)
```

Next we use an exponential function to define the shape of the wake body and locate the N stations in it so that the panel areas are nearly the same as the upstream panel areas,

```
      DELTAZ=0.010D0
      KK=1
      XX1=XHOLD1
      ZZ2=0.0D0
      RR1=RAV
  425 ZZ2=ZZ2+DELTAZ
      XX2=ZZ2*(XINF-XHOLD1)+XHOLD1
      RR2=RAV*EXP(AVSLOP*ZZ2)*(1.0D0-ZZ2)
      DTHETA=PI/(MMAXQD-1)
      AREA2=(RR2+RR1)*DSIN(DTHETA/2.0)*DSQRT((RR2-RR1)**2
     1+(XX2-XX1)**2)
      IF (AREA2.LT.AREAAV) GO TO 425
      XK(KK)=XX2
      RK(KK)=RR2
      XX1=XX2
      RR1=RR2
      KK=KK+1
      IF (KK.GE.4) GO TO 430
      GO TO 425
  430 XK(4)=XINF
```

We now set up the loop to define the coordinates of the wake body at its various M and N stations,

```
      RK(4)=0.0D0
      X1=XK(1)
      X2=XK(2)
      X3=XK(3)
      X4=XK(4)
      R1=RK(1)
      R2=RK(2)
      R3=RK(3)
      R4=RK(4)
      NSTRT1=MMAXQD
      NSTRT2=2*MMAXQD
      NSTRT3=3*MMAXQD
      NSTRT4=4*MMAXQD
      YFAC=(-Y(1))/(XINF-XHOLD1)
      ZFAC=(ZAV-Z(1))/(XINF-XHOLD1)
      DO 435 I=1,MMAXQD
      COSTHT=DCOS(THETA)
      SINTHT=DSIN(THETA)
      XNEW(NSTRT1+I)=X1
      XNEW(NSTRT2+I)=X2
      XNEW(NSTRT3+I)=X3
      XNEW(NSTRT4+I)=X4
      YNEW(NSTRT1+I)=R1*qr1*COSTHT-(XNEW(NSTRT1+I)
     1-XHOLD1)*YFAC
      YNEW(NSTRT2+I)=R2*qr1*COSTHT-(XNEW(NSTRT2+I)
     1-XHOLD1)*YFAC
      YNEW(NSTRT3+I)=R3*qr1*COSTHT-(XNEW(NSTRT3+I)
     1-XHOLD1)*YFAC
      YNEW(NSTRT4+I)=R4*COSTHT-(XNEW(NSTRT4+I)
     1-XHOLD1)*YFAC
      ZNEW(NSTRT1+I)=R1/qr1*SINTHT+ZAV-(XNEW(NSTRT1+I)
     1-XHOLD1)*ZFAC
      ZNEW(NSTRT2+I)=R2/qr1*SINTHT+ZAV-(XNEW(NSTRT2+I)
     1-XHOLD1)*ZFAC
      ZNEW(NSTRT3+I)=R3/qr1*SINTHT+ZAV-(XNEW(NSTRT3+I)
     1-XHOLD1)*ZFAC
      ZNEW(NSTRT4+I)=R4*SINTHT+ZAV-(XNEW(NSTRT4+I)
     1-XHOLD1)*ZFAC
  435 THETA=THETA+DTHETA
```

For the example problem just given MMAXQD is 17, ISTART is 307, XHOLD1 is -8.0, and XHOLD2 is -9.0. In these equations $qr1$ is (ZMAX/YMAX) **0.49.

It magnifies the Z dimension and shrinks the Y dimension of the wake body so that it is elliptical and matches the shape of the physical body and also ensures that the wake body slope changes monotonically. The ability to treat elliptical bodies was first added for the version of the program to accompany this book. It requires no user intervention.

Wake bodies generated by the program are quasiconic sections with a length about three times that of the base diameter. This ratio was selected after studies showed that making the wake body too short resulted in excessive pressures on the aft surfaces of the physical body. Making it too long resulted in pressures on the aft surfaces of the body that were too low. (In Fox's[39] version, the wake body length can vary over a significantly greater range than in the present version.)

As indicated previously, the body plus wake body is treated as a physical body for purposes of an inviscid flow computation. Then the pressures, which are calculated to exist on this pseudobody, are applied to the region of the physical body that lies beneath the wake body. Because the pressures in this region are now lower than those calculated for the physical body alone, the physical body experiences a pressure drag. (In the program, the pressure drag is obtained by summing the product of the pressure coefficient on a panel centroid, the panel area, and the direction cosine in the streawise direction for that panel over all panels on the body surface. Increasing the number of panels used can improve the accuracy of this approximation, but the greatest improvement can be obtained, as Fox[39] found, by recognizing that the pressures on the triangular panels at the downstream end of the wake body change rapidly. The pressure at the geometric centroid of the panel does not represent the average pressure over the panel. Therefore, Fox employed a bicubic spline to represent the data in this region of the body. In the interests of simplicity and rapid execution, this feature was not incorporated into the present version of the program.) When the pressure drag is combined with the skin-friction drag calculated during the boundary-layer analysis, one thereby obtains the total drag on the physical body.

7.3 General Program Description

The present version of the **BODY** source code consists of 3000 lines of Fortran instructions including the comments. It consumes 219,264 bytes of storage space. The executable file made with MicroSoft PowerStation Fortran is 186,880 bytes long with no unusual optimization or the use of 486 specific commands. The input data file is BODY.DAT. The output files are BODY.TXT, BODYWK.PS, and BOLD.PS. Temporary data files, which are left on the hard disk after the program has executed, are BODY7.DAT, BODY8.DAT, BODY9.DAT, and BODY10.DAT. BODY11.DAT usually contains the coordinates of the panel corners after the wake body has been added in the format used by BODY.DAT. Therefore, BODY11.DAT can be used as an input file if desired.

The input file generation program **BODYGEN** is 250 lines and 10,496 bytes long. The executable file has a length of 110,080 bytes.

The average running time of **BODY** is about 10 min on a 90-MHz Pentium. This is for a case with 320 panels on the half-body. Generally, the running time is proportional to the number of panels squared. This time estimate is for a situation where less than 23 iterations are required to achieve a satisfactory source strength

distribution, that is, one that meets the error criterion set in the program. Because the program limits the number of iterations to 150, it is easily seen that the program may run 50 min or longer. The maximum number of body panels permitted on the half-body including those on the wake body by the current array dimensions is 650.

All of the comments from the 1975 version of the program have been retained, and a few new ones have been added. In addition, some notes were added to the source code file header. This version of the program contains two subroutines, which write PostScript vector files. These files show the body in orthographic three view plus a pseudoisometric view, both with and without wake body, as well as the symmetry plane pressure distribution with and without wake body. These files can be rendered on any device having a hardware or software PostScript interpreter.

The intermediate data files can be quite large. For the 320 panel case, BODY9.DAT may be more than 7.7 Mbytes and BODY10.DAT more than 2.6 Mbytes. About 13 Mbytes of free disk space should be available to run **BODY** with a problem having 320 panels. The intermediate data files remain on the hard disk after the program has completed execution. Normally, these intermediate data files can be discarded after program execution. If problems arise during execution these file often can be used after the fact to locate the source of the trouble. The intermediate data files are simply a relic of the days when computer memory was very scarse and small hard disks were common. The intermediate results were then written off to tape. Of course, this slowed the program considerably but it was the only practical solution for the large memory requirements. For this version, hard disk space, rather than RAM, replaced the tapes. This strategy permits somewhat larger problems to be run on machines with modest complements of RAM. The read/write speeds of modern hard drives are now fast enough that this does not appear to be a major factor limiting program execution time.

In Fox's[39] version these intermediate files are assigned to arrays in RAM. If the amount of memory required for a program is not available, most modern operating systems spool intermediate data to a hard drive. Thus, in practice, there may be little actual difference in hard drive usage for large problems.

Figure 7.2a is a depiction of how the wake body is related to the original physical body. It will be seen that the first two sets of panels on the wake body do not exactly cover the last two sets of physical body panels, whereas the last two sets of the wake body panels become increasingly long in order to obtain panel areas that are about the same as the average panel area on the physical body. Figure 7.2a shows quite clealy why the application of the pressures developed over the wake body to the physical body beneath result in a pressure drag on the physical body.

Figures 7.2b and 7.2c show the location of the axis reference and the order of the panel numbering on the physical body. Note, particularly, that panel numbering must begin at the ventral centerline and proceed to the dorsal centerline at each N station. Note, too, that the axis reference is usually taken to be the maximum area cross section.

Figure 7.2d shows how the wire frame grid can be used to describe more complex bodies such as complete aircraft. Of course, only one, non-lifting body at a time can be analyzed by **BODY**. The program also has no means by which it can account for the interaction between two major components, particularly the interaction of viscous flows.

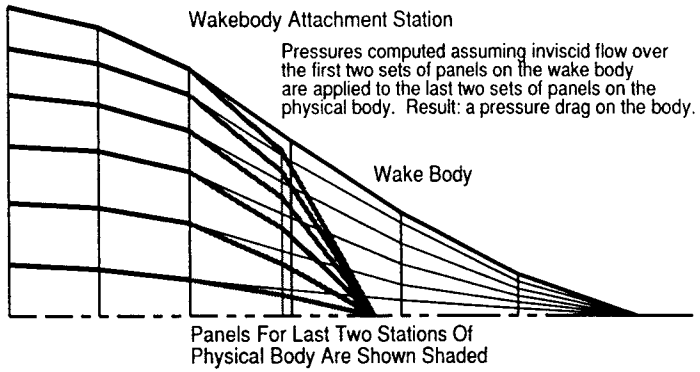

Fig. 7.2a How the wake body is related to the physical body.

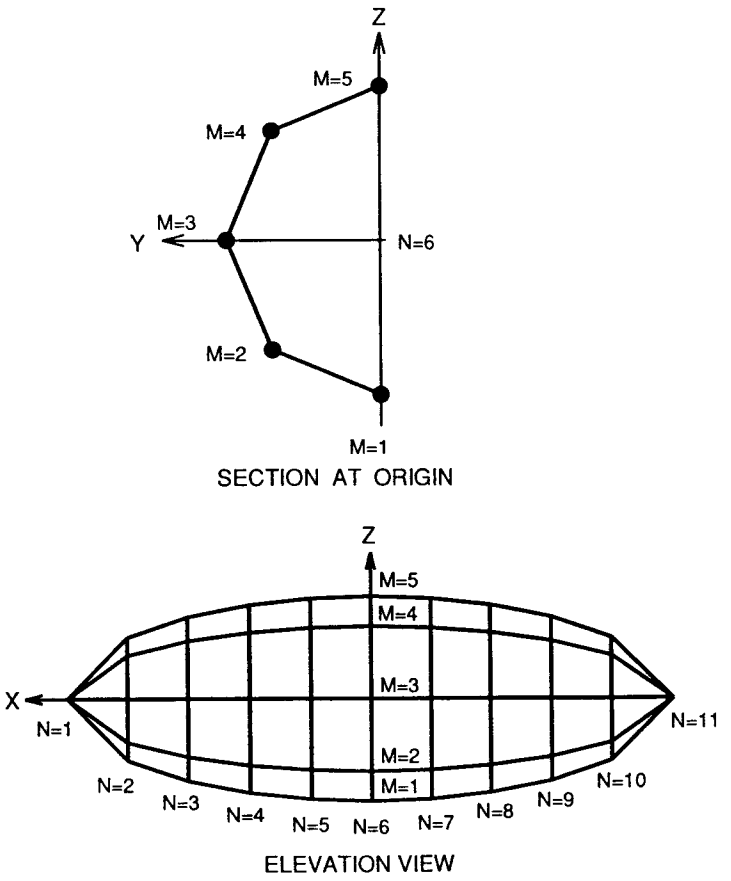

Fig. 7.2b Reference quantities and nomenclature.

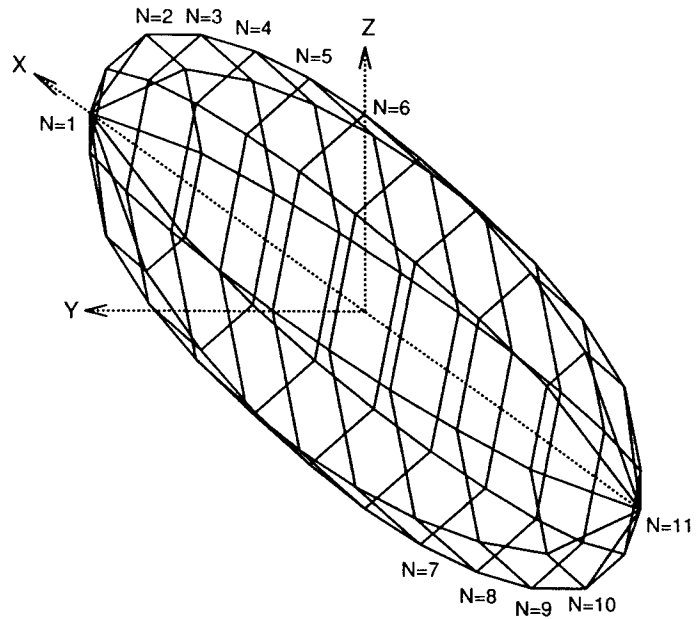

Fig. 7.2c Reference quantities and nomenclature, hidden lines not removed.

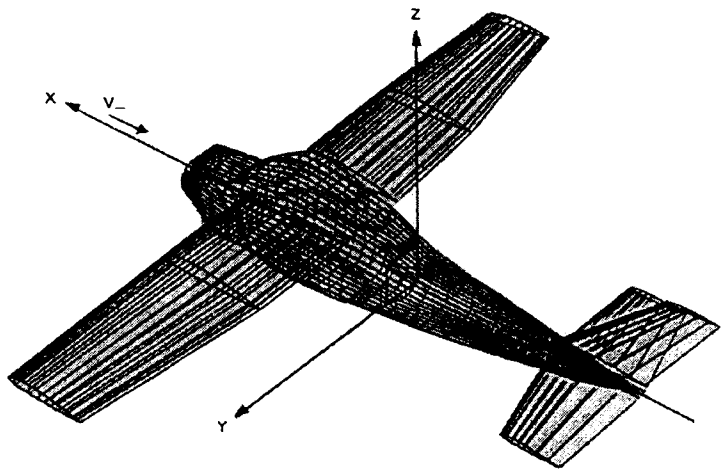

Fig. 7.2d Wire frame model of complete aircraft.

7.4 Program Data Entry

The lines in the input data file each replace a card in the version of the program described in NASA CR-2523.[26] The first line carries the problem identification in a 16A4 format. To enter this data in response to an on screen request, it may be necessary to separate each four characters by a carriage return. The second line provides values for the following five program flow control variables.

1) VINF is the reference freestream flow velocity in units per second where the units are those used to input the body coordinates.

2) V0 is the kinematic viscosity of the fluid. If the velocity is in feet per second, then V0 has units of square foot per second; it is the dynamic viscosity of the fluid divided by its density.

3) ROE is the density of the fluid in which the body moves in slugs per cubic foot, taken as 0.002378 for standard sea-level conditions in air; for fresh water the density is about 1.94 slugs/ft^3; for sea water, the density is about 2.0 slugs/ft^3.

4) REFA is the reference area on which the aerodynamic coefficients will be based, usually taken as the maximum cross-sectional area; for an ellipitcal body this is πAB where A is the semimajor axis dimension and B is the semiminor axis dimension.

5) IWRITE is a parameter to indicate how much of the program output is to be printed. IWRITE = 0 yields maximum information. IWRITE = 1 deletes the information about each input point. IWRITE = 2 deletes streamline and boundary-layer information as well.

The format for this line is 4F10.5,I5.

The third line holds the parameter NQE, an integer in I4 format, which must be right justified.

Lines 4, 5, 6, ... contain six values that describe a point on the body surface: X1, the X coordinate of the input point; Y1, the Y coordinate of the input point; Z1, the Z coordinate of the input point; N1, the N body (axial) station index; M1, the M body (circumferential) station index; and NS, section identification number.

A separate line must appear at this position in the input file for each point used to describe the body surface. It is absolutely essential that the input point coordinates be entered in the following order: For the first N station, which is usually the front of the body, the M points are numbered consecutively from the ventral centerline to the dorsal centerline as viewed from the front of the body. Then, the points for the next N station are entered in like manner and so on. Failure to follow this numbering scheme will cause the program to give erroneous results.

A small program **BODYGEN** is provided on the accompanying disk to assist the user in entering input data points for a general ellipsoid. This can be quite a chore if done manually because the present example has 357 points on the half-body. **BODYGEN** can create wireframe bodies for which the three axes dimensions are either equal or unequal. For the general ellipsoid shown in Figs. 7.1 and 7.2 $A = 10$, $B = A/4.5$, and $C = A/3.0$. A prolate spheroid (ellipsoid with B and C equal) is shown subsequently in Sec. 7.5.

To obtain the data **BODYGEN** writes on the first two lines of the file **BODY.DAT**, the user is asked to respond to questions displayed on the screen. A typical input file is shown in Fig. 7.3.

```
general ellipsoid
100.000000    .000100  0.002378 23.250000     2
 320
 10.000000000    .000000000    .000000000   1   1   1   0
 10.000000000    .000000000    .000000000   1   2   1   0
 10.000000000    .000000000    .000000000   1   3   1   0
 10.000000000    .000000000    .000000000   1   4   1   0
 10.000000000    .000000000    .000000000   1   5   1   0
 10.000000000    .000000000    .000000000   1   6   1   0
 10.000000000    .000000000    .000000000   1   7   1   0
 10.000000000    .000000000    .000000000   1   8   1   0
 10.000000000    .000000000    .000000000   1   9   1   0
 10.000000000    .000000000    .000000000   1  10   1   0
 10.000000000    .000000000    .000000000   1  11   1   0
 10.000000000    .000000000    .000000000   1  12   1   0
 10.000000000    .000000000    .000000000   1  13   1   0
 10.000000000    .000000000    .000000000   1  14   1   0
 10.000000000    .000000000    .000000000   1  15   1   0
 10.000000000    .000000000    .000000000   1  16   1   0
 10.000000000    .000000000    .000000000   1  17   1   0
  9.000000000    .000000000  -1.452966315   2   1   1   0
  9.000000000    .188973111  -1.425047974   2   2   1   0
  9.000000000    .370684091  -1.342365839   2   3   1   0
  9.000000000    .538149889  -1.208097338   2   4   1   0
  9.000000000    .684934889  -1.027402334   2   5   1   0
  9.000000000    .805398225   -.807224834   2   6   1   0
  9.000000000    .894910560   -.556026136   2   7   1   0
  9.000000000    .950031983   -.283459666   2   8   1   0
  9.000000000    .968644210    .000000000   2   9   1   0
  9.000000000    .950031983    .283459666   2  10   1   0
  9.000000000    .894910560    .556026136   2  11   1   0
  9.000000000    .805398225    .807224834   2  12   1   0
  9.000000000    .684934889   1.027402334   2  13   1   0
  9.000000000    .538149889   1.208097338   2  14   1   0
  9.000000000    .370684091   1.342365839   2  15   1   0
  9.000000000    .188973111   1.425047974   2  16   1   0
  9.000000000    .000000000   1.452966315   2  17   1   0
  8.000000000    .000000000  -2.000000000   3   1   1   0
  8.000000000    .260120429  -1.961570561   3   2   1   0
  8.000000000    .510244576  -1.847759065   3   3   1   0
  8.000000000    .740760311  -1.662939225   3   4   1   0
  8.000000000    .942809042  -1.414213562   3   5   1   0
  8.000000000   1.108626150  -1.111140466   3   6   1   0
  8.000000000   1.231839377   -.765366865   3   7   1   0
  8.000000000   1.307713707   -.390180644   3   8   1   0
  8.000000000   1.333333333    .000000000   3   9   1   0
  8.000000000   1.307713707    .390180644   3  10   1   0
  8.000000000   1.231839377    .765366865   3  11   1   0
  8.000000000   1.108626150   1.111140466   3  12   1   0
  8.000000000    .942809042   1.414213562   3  13   1   0
```

Fig. 7.3 Sample input file.


```
  8.000000000    .740760311   1.662939225   3  14   1   0
  8.000000000    .510244576   1.847759065   3  15   1   0
  8.000000000    .260120429   1.961570561   3  16   1   0
  8.000000000    .000000000   2.000000000   3  17   1   0
  7.000000000    .000000000  -2.380476143   4   1   1   0
  7.000000000    .309605238  -2.334735961   4   2   1   0
  7.000000000    .607312521  -2.199273186   4   3   1   0
  7.000000000    .881681124  -1.979293576   4   4   1   0
  7.000000000   1.122167215  -1.683250823   4   5   1   0
  7.000000000   1.319529050  -1.322521685   4   6   1   0
  7.000000000   1.466182124   -.910968781   4   7   1   0
  7.000000000   1.556490641   -.464407857   4   8   1   0
  7.000000000   1.586984095    .000000022   4   9   1   0
  7.000000000   1.556490641    .464407857   4  10   1   0
  7.000000000   1.466182124    .910968781   4  11   1   0
  7.000000000   1.319529050   1.322521685   4  12   1   0
  7.000000000   1.122167215   1.683250823   4  13   1   0
  7.000000000    .881681124   1.979293576   4  14   1   0
  7.000000000    .607312521   2.199273186   4  15   1   0
  7.000000000    .309605238   2.334735961   4  16   1   0
  7.000000000    .000000000   2.380476143   4  17   1   0
  6.000000000    .000000000  -2.666666667   5   1   1   0
  6.000000000    .346827239  -2.615427414   5   2   1   0
  6.000000000    .680326102  -2.463678753   5   3   1   0
  6.000000000    .987680414  -2.217252299   5   4   1   0
  6.000000000   1.257078722  -1.885618083   5   5   1   0
  6.000000000   1.478168200  -1.481520621   5   6   1   0
  6.000000000   1.642452502  -1.020489153   5   7   1   0
  6.000000000   1.743618276   -.520240859   5   8   1   0
  6.000000000   1.777777778    .000000000   5   9   1   0
  6.000000000   1.743618276    .520240859   5  10   1   0
  6.000000000   1.642452502   1.020489153   5  11   1   0
  6.000000000   1.478168200   1.481520621   5  12   1   0
  6.000000000   1.257078722   1.885618083   5  13   1   0
  6.000000000    .987680414   2.217252299   5  14   1   0
  6.000000000    .680326102   2.463678753   5  15   1   0
  6.000000000    .346827239   2.615427414   5  16   1   0
  6.000000000    .000000000   2.666666667   5  17   1   0
  5.000000000    .000000000  -2.886751346   6   1   1   0
  5.000000000    .375451500  -2.831283228   6   2   1   0
  5.000000000    .736474609  -2.667010484   6   3   1   0
  5.000000000   1.069195412  -2.400246022   6   4   1   0
  5.000000000   1.360827635  -2.041241452   6   5   1   0
  5.000000000   1.600164015  -1.603793118   6   6   1   0
  5.000000000   1.778006989  -1.104711913   6   7   1   0
  5.000000000   1.887522152   -.563177250   6   8   1   0
  5.000000000   1.924500897    .000000000   6   9   1   0
  5.000000000   1.887522152    .563177250   6  10   1   0
  5.000000000   1.778006989   1.104711913   6  11   1   0
  5.000000000   1.600164015   1.603793118   6  12   1   0
```

Fig. 7.3 Contd.

5.000000000	1.360827635	2.041241452	6	13	1	0
5.000000000	1.069195412	2.400246022	6	14	1	0
5.000000000	.736474609	2.667010484	6	15	1	0
5.000000000	.375451500	2.831283228	6	16	1	0
5.000000000	.000000000	2.886751346	6	17	1	0
4.000000000	.000000000	-3.055050463	7	1	1	0
4.000000000	.397340519	-2.996348525	7	2	1	0
4.000000000	.779411465	-2.822498594	7	3	1	0
4.000000000	1.131530065	-2.540181624	7	4	1	0
4.000000000	1.440164600	-2.160246899	7	5	1	0
4.000000000	1.693454416	-1.697295098	7	6	1	0
4.000000000	1.881665729	-1.169117197	7	7	1	0
4.000000000	1.997565684	-.596010779	7	8	1	0
4.000000000	2.036700309	.000000000	7	9	1	0
4.000000000	1.997565684	.596010779	7	10	1	0
4.000000000	1.881665729	1.169117197	7	11	1	0
4.000000000	1.693454416	1.697295098	7	12	1	0
4.000000000	1.440164600	2.160246899	7	13	1	0
4.000000000	1.131530065	2.540181624	7	14	1	0
4.000000000	.779411465	2.822498594	7	15	1	0
4.000000000	.397340519	2.996348525	7	16	1	0
4.000000000	.000000000	3.055050463	7	17	1	0
3.000000000	.000000000	-3.179797338	8	1	1	0
3.000000000	.413565124	-3.118698424	8	2	1	0
3.000000000	.811237173	-2.937749678	8	3	1	0
3.000000000	1.177733832	-2.643904860	8	4	1	0
3.000000000	1.498970840	-2.248456261	8	5	1	0
3.000000000	1.762603240	-1.766600748	8	6	1	0
3.000000000	1.958499785	-1.216855760	8	7	1	0
3.000000000	2.079132283	-.620347687	8	8	1	0
3.000000000	2.119864892	.000000000	8	9	1	0
3.000000000	2.079132283	.620347687	8	10	1	0
3.000000000	1.958499785	1.216855760	8	11	1	0
3.000000000	1.762603240	1.766600748	8	12	1	0
3.000000000	1.498970840	2.248456261	8	13	1	0
3.000000000	1.177733832	2.643904860	8	14	1	0
3.000000000	.811237173	2.937749678	8	15	1	0
3.000000000	.413565124	3.118698424	8	16	1	0
3.000000000	.000000000	3.179797338	8	17	1	0
2.000000000	.000000000	-3.265986324	9	1	1	0
2.000000000	.424774882	-3.203231312	9	2	1	0
2.000000000	.833225904	-3.017377918	9	3	1	0
2.000000000	1.209656522	-2.715568382	9	4	1	0
2.000000000	1.539600718	-2.309401077	9	5	1	0
2.000000000	1.810378922	-1.814484783	9	6	1	0
2.000000000	2.011585279	-1.249838856	9	7	1	0
2.000000000	2.135487542	-.637162324	9	8	1	0
2.000000000	2.177324216	.000000023	9	9	1	0
2.000000000	2.135487542	.637162324	9	10	1	0
2.000000000	2.011585279	1.249838856	9	11	1	0

Fig. 7.3 Contd.

2.000000000	1.810378922	1.814484783	9	12	1	0
2.000000000	1.539600718	2.309401077	9	13	1	0
2.000000000	1.209656522	2.715568382	9	14	1	0
2.000000000	.833225904	3.017377918	9	15	1	0
2.000000000	.424774882	3.203231312	9	16	1	0
2.000000000	.000000000	3.265986324	9	17	1	0
1.000000000	.000000000	-3.316624790	10	1	1	0
1.000000000	.431360932	-3.252896775	10	2	1	0
1.000000000	.846144906	-3.064161761	10	3	1	0
1.000000000	1.228412005	-2.757672729	10	4	1	0
1.000000000	1.563471920	-2.345207880	10	5	1	0
1.000000000	1.838448486	-1.842618008	10	6	1	0
1.000000000	2.042774507	-1.269217359	10	7	1	0
1.000000000	2.168597850	-.647041398	10	8	1	0
1.000000000	2.211083194	.000000000	10	9	1	0
1.000000000	2.168597850	.647041398	10	10	1	0
1.000000000	2.042774507	1.269217359	10	11	1	0
1.000000000	1.838448486	1.842618008	10	12	1	0
1.000000000	1.563471920	2.345207880	10	13	1	0
1.000000000	1.228412005	2.757672729	10	14	1	0
1.000000000	.846144906	3.064161761	10	15	1	0
1.000000000	.431360932	3.252896775	10	16	1	0
1.000000000	.000000000	3.316624790	10	17	1	0
.000000000	.000000000	-3.333333333	11	1	1	0
.000000000	.433534049	-3.269284268	11	2	1	0
.000000000	.850407627	-3.079598442	11	3	1	0
.000000000	1.234600518	-2.771565374	11	4	1	0
.000000000	1.571348403	-2.357022604	11	5	1	0
.000000000	1.847710250	-1.851900777	11	6	1	0
.000000000	2.053065628	-1.275611441	11	7	1	0
.000000000	2.179522845	-.650301073	11	8	1	0
.000000000	2.222222222	.000000000	11	9	1	0
.000000000	2.179522845	.650301073	11	10	1	0
.000000000	2.053065628	1.275611441	11	11	1	0
.000000000	1.847710250	1.851900777	11	12	1	0
.000000000	1.571348403	2.357022604	11	13	1	0
.000000000	1.234600518	2.771565374	11	14	1	0
.000000000	.850407627	3.079598442	11	15	1	0
.000000000	.433534049	3.269284268	11	16	1	0
.000000000	.000000000	3.333333333	11	17	1	0
-1.000000000	.000000000	-3.316624790	12	1	1	0
-1.000000000	.431360932	-3.252896775	12	2	1	0
-1.000000000	.846144906	-3.064161761	12	3	1	0
-1.000000000	1.228412005	-2.757672729	12	4	1	0
-1.000000000	1.563471920	-2.345207880	12	5	1	0
-1.000000000	1.838448486	-1.842618008	12	6	1	0
-1.000000000	2.042774507	-1.269217359	12	7	1	0
-1.000000000	2.168597850	-.647041398	12	8	1	0
-1.000000000	2.211083194	.000000000	12	9	1	0
-1.000000000	2.168597850	.647041398	12	10	1	0

Fig. 7.3 Contd.

-1.000000000	2.042774507	1.269217359	12	11	1	0
-1.000000000	1.838448486	1.842618008	12	12	1	0
-1.000000000	1.563471920	2.345207880	12	13	1	0
-1.000000000	1.228412005	2.757672729	12	14	1	0
-2.000000000	.424774882	-3.203231312	13	2	1	0
-2.000000000	.833225904	-3.017377918	13	3	1	0
-2.000000000	1.209656522	-2.715568382	13	4	1	0
-2.000000000	1.539600718	-2.309401077	13	5	1	0
-2.000000000	1.810378922	-1.814484783	13	6	1	0
-2.000000000	2.011585279	-1.249838856	13	7	1	0
-2.000000000	2.135487542	-.637162324	13	8	1	0
-2.000000000	2.177324216	.000000023	13	9	1	0
-2.000000000	2.135487542	.637162324	13	10	1	0
-2.000000000	2.011585279	1.249838856	13	11	1	0
-2.000000000	1.810378922	1.814484783	13	12	1	0
-2.000000000	1.539600718	2.309401077	13	13	1	0
-2.000000000	1.209656522	2.715568382	13	14	1	0
-2.000000000	.833225904	3.017377918	13	15	1	0
-2.000000000	.424774882	3.203231312	13	16	1	0
-2.000000000	.000000000	3.265986324	13	17	1	0
-3.000000000	.000000000	-3.179797338	14	1	1	0
-3.000000000	.413565124	-3.118698424	14	2	1	0
-3.000000000	.811237173	-2.937749678	14	3	1	0
-3.000000000	1.177733832	-2.643904860	14	4	1	0
-3.000000000	1.498970840	-2.248456261	14	5	1	0
-3.000000000	1.762603240	-1.766600748	14	6	1	0
-3.000000000	1.958499785	-1.216855760	14	7	1	0
-3.000000000	2.079132283	-.620347687	14	8	1	0
-3.000000000	2.119864892	.000000000	14	9	1	0
-3.000000000	2.079132283	.620347687	14	10	1	0
-3.000000000	1.958499785	1.216855760	14	11	1	0
-3.000000000	1.762603240	1.766600748	14	12	1	0
-3.000000000	1.498970840	2.248456261	14	13	1	0
-3.000000000	1.177733832	2.643904860	14	14	1	0
-3.000000000	.811237173	2.937749678	14	15	1	0
-3.000000000	.413565124	3.118698424	14	16	1	0
-3.000000000	.000000000	3.179797338	14	17	1	0
-4.000000000	.000000000	-3.055050463	15	1	1	0
-4.000000000	.397340519	-2.996348525	15	2	1	0
-4.000000000	.779411465	-2.822498594	15	3	1	0
-4.000000000	1.131530065	-2.540181624	15	4	1	0
-4.000000000	1.440164600	-2.160246899	15	5	1	0
-4.000000000	1.693454416	-1.697295098	15	6	1	0
-4.000000000	1.881665729	-1.169117197	15	7	1	0
-4.000000000	1.997565684	-.596010779	15	8	1	0
-4.000000000	2.036700309	.000000000	15	9	1	0
-4.000000000	1.997565684	.596010779	15	10	1	0
-4.000000000	1.881665729	1.169117197	15	11	1	0
-4.000000000	1.693454416	1.697295098	15	12	1	0
-4.000000000	1.440164600	2.160246899	15	13	1	0

Fig. 7.3 Contd.

-4.000000000	1.131530065	2.540181624	15	14	1	0
-4.000000000	.779411465	2.822498594	15	15	1	0
-4.000000000	.397340519	2.996348525	15	16	1	0
-4.000000000	.000000000	3.055050463	15	17	1	0
-5.000000000	.000000000	-2.886751346	16	1	1	0
-5.000000000	.375451500	-2.831283228	16	2	1	0
-5.000000000	.736474609	-2.667010484	16	3	1	0
-5.000000000	1.069195412	-2.400246022	16	4	1	0
-5.000000000	1.360827635	-2.041241452	16	5	1	0
-5.000000000	1.600164015	-1.603793118	16	6	1	0
-5.000000000	1.778006989	-1.104711913	16	7	1	0
-5.000000000	1.887522152	-.563177250	16	8	1	0
-5.000000000	1.924500897	.000000000	16	9	1	0
-5.000000000	1.887522152	.563177250	16	10	1	0
-5.000000000	1.778006989	1.104711913	16	11	1	0
-5.000000000	1.600164015	1.603793118	16	12	1	0
-5.000000000	1.360827635	2.041241452	16	13	1	0
-5.000000000	1.069195412	2.400246022	16	14	1	0
-5.000000000	.736474609	2.667010484	16	15	1	0
-5.000000000	.375451500	2.831283228	16	16	1	0
-5.000000000	.000000000	2.886751346	16	17	1	0
-6.000000000	.000000000	-2.666666667	17	1	1	0
-6.000000000	.346827239	-2.615427414	17	2	1	0
-6.000000000	.680326102	-2.463678753	17	3	1	0
-6.000000000	.987680414	-2.217252299	17	4	1	0
-6.000000000	1.257078722	-1.885618083	17	5	1	0
-6.000000000	1.478168200	-1.481520621	17	6	1	0
-6.000000000	1.642452502	-1.020489153	17	7	1	0
-6.000000000	1.743618276	-.520240859	17	8	1	0
-6.000000000	1.777777778	.000000000	17	9	1	0
-6.000000000	1.743618276	.520240859	17	10	1	0
-6.000000000	1.642452502	1.020489153	17	11	1	0
-6.000000000	1.478168200	1.481520621	17	12	1	0
-6.000000000	1.257078722	1.885618083	17	13	1	0
-6.000000000	.987680414	2.217252299	17	14	1	0
-6.000000000	.680326102	2.463678753	17	15	1	0
-6.000000000	.346827239	2.615427414	17	16	1	0
-6.000000000	.000000000	2.666666667	17	17	1	0
-7.000000000	.000000000	-2.380476143	18	1	1	0
-7.000000000	.309605238	-2.334735961	18	2	1	0
-7.000000000	.607312521	-2.199273186	18	3	1	0
-7.000000000	.881681124	-1.979293576	18	4	1	0
-7.000000000	1.122167215	-1.683250823	18	5	1	0
-7.000000000	1.319529050	-1.322521685	18	6	1	0
-7.000000000	1.466182124	-.910968781	18	7	1	0
-7.000000000	1.556490641	-.464407857	18	8	1	0
-7.000000000	1.586984095	.000000022	18	9	1	0
-7.000000000	1.556490641	.464407857	18	10	1	0
-7.000000000	1.466182124	.910968781	18	11	1	0
-7.000000000	1.319529050	1.322521685	18	12	1	0

Fig. 7.3 Contd.

-7.000000000	1.122167215	1.683250823	18	13	1	0
-7.000000000	.881681124	1.979293576	18	14	1	0
-7.000000000	.607312521	2.199273186	18	15	1	0
-7.000000000	.309605238	2.334735961	18	16	1	0
-7.000000000	.000000000	2.380476143	18	17	1	0
-8.000000000	.000000000	-2.000000000	19	1	1	0
-8.000000000	.260120429	-1.961570561	19	2	1	0
-8.000000000	.510244576	-1.847759065	19	3	1	0
-8.000000000	.740760311	-1.662939225	19	4	1	0
-8.000000000	.942809042	-1.414213562	19	5	1	0
-8.000000000	1.108626150	-1.111140466	19	6	1	0
-8.000000000	1.231839377	-.765366865	19	7	1	0
-8.000000000	1.307713707	-.390180644	19	8	1	0
-8.000000000	1.333333333	.000000000	19	9	1	0
-8.000000000	1.307713707	.390180644	19	10	1	0
-8.000000000	1.231839377	.765366865	19	11	1	0
-8.000000000	1.108626150	1.111140466	19	12	1	0
-8.000000000	.942809042	1.414213562	19	13	1	0
-8.000000000	.740760311	1.662939225	19	14	1	0
-8.000000000	.510244576	1.847759065	19	15	1	0
-8.000000000	.260120429	1.961570561	19	16	1	0
-8.000000000	.000000000	2.000000000	19	17	1	0
-9.000000000	.000000000	-1.452966315	20	1	1	0
-9.000000000	.188973111	-1.425047974	20	2	1	0
-9.000000000	.370684091	-1.342365839	20	3	1	0
-9.000000000	.538149889	-1.208097338	20	4	1	0
-9.000000000	.684934889	-1.027402334	20	5	1	0
-9.000000000	.805398225	-.807224834	20	6	1	0
-9.000000000	.894910560	-.556026136	20	7	1	0
-9.000000000	.950031983	-.283459666	20	8	1	0
-9.000000000	.968644210	.000000000	20	9	1	0
-9.000000000	.950031983	.283459666	20	10	1	0
-9.000000000	.894910560	.556026136	20	11	1	0
-9.000000000	.805398225	.807224834	20	12	1	0
-9.000000000	.684934889	1.027402334	20	13	1	0
-9.000000000	.538149889	1.208097338	20	14	1	0
-9.000000000	.370684091	1.342365839	20	15	1	0
-9.000000000	.188973111	1.425047974	20	16	1	0
-9.000000000	.000000000	1.452966315	20	17	1	0
-10.000000000	.000000000	.000000000	21	1	1	0
-10.000000000	.000000000	.000000000	21	2	1	0
-10.000000000	.000000000	.000000000	21	3	1	0
-10.000000000	.000000000	.000000000	21	4	1	0
-10.000000000	.000000000	.000000000	21	5	1	0
-10.000000000	.000000000	.000000000	21	6	1	0
-10.000000000	.000000000	.000000000	21	7	1	0
-10.000000000	.000000000	.000000000	21	8	1	0
-10.000000000	.000000000	.000000000	21	9	1	0
-10.000000000	.000000000	.000000000	21	10	1	0
-10.000000000	.000000000	.000000000	21	11	1	0

Fig. 7.3 Contd.

-10.000000000	.000000000	.000000000	21	12	1	0
-10.000000000	.000000000	.000000000	21	13	1	0
-10.000000000	.000000000	.000000000	21	14	1	0
-10.000000000	.000000000	.000000000	21	15	1	0
-10.000000000	.000000000	.000000000	21	16	1	0
-10.000000000	.000000000	.000000000	21	17	1	0

Fig. 7.3 Contd.

7.5 Typical Results

Results produced by the program for this sample case are shown in Figs. 7.4, 7.5, and 7.6. Figure 7.4 shows the appearance of the half-body when the wake body has been appended. Notice that the body slope changes reasonably smoothly from the physical body, over the wake body, to the point where the wake body terminates and that the length of the body plus wake body is about 5/4 that of the physical body alone.

Figure 7.5 compares the pressure distribution over the physical body to that over the physical plus wake body as calculated in the plane of symmetry. Notice that the pressures over the physical body approach the stagnation value as the end of the body is approached. As a result, the drag coefficient of the body is zero. However, when the wake body is added, the pressures on the aft portions of the physical body never exceed about 0.2 times the stagnation value. Consequently, there is a positive pressure drag coefficient for this case. Both Figs. 7.4 and 7.5 are produced by the program.

Shown in Fig. 7.6 is a partial listing of the program output produced by the program. Even for IWRITE = 2 there is a significant quantity of output most of which was deleted when creating Fig. 7.6. There are, however, a number of very interesting results displayed in the figure. Notice that both the pressure drag and the lift are zero for the inviscid case. The effect of fluid viscosity is shown by the frictional drag coefficient result. Also an effect of fluid viscosity is the pressure or form drag coefficient, which is given here as 0.07065. The pressure drag coefficient was computed as 0.02078, and the lift coefficient with wake body is calculated as −0.00005, a value that indicates that the symmetry of the attached wake body with the original physical body is good. The fact that the pressure drag coefficient is less than 1/3 of the frictional drag coefficient shows that the body, even with the wake body attached, is quite streamlined. Finally, a total drag coefficient of 0.09143 is 4–12% greater than the values reported in the literature for similarly shaped bodies (prolate spheroids). This is because the pressure at the center of the last set of panels is much lower than it is toward the rear of the panels. Fox[39] circumvented the problem by integrating the pressure distribution (represented by a bicubic spline) over these panels rather than assuming the pressure to be constant at the center value.

The listing also shows the coordinates of the panel corners and the velocity components over each of the panels, as well as the normal velocity at the panel control point. This value is unusually significant because it provides a direct indication of the accuracy to which the computation as been performed. The reader may recall that the condition imposed on the induced flows was that the sum of all of the induced velocities plus the component of the freestream flow should be zero at the control point on each panel. It will be seen that the normal

BODY Plan View
Wake Body Attached

Fig. 7.4a Body with added wake body, plan view.

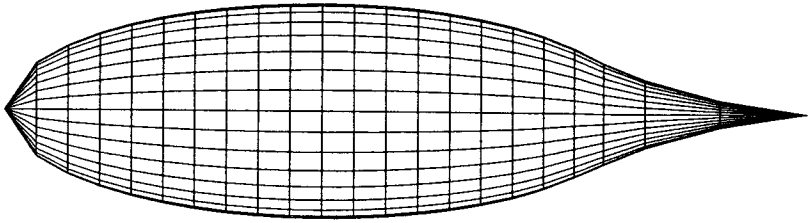

BODY Elevation View
Wake Body Attached

Fig. 7.4b Body with added wake body, elevation view.

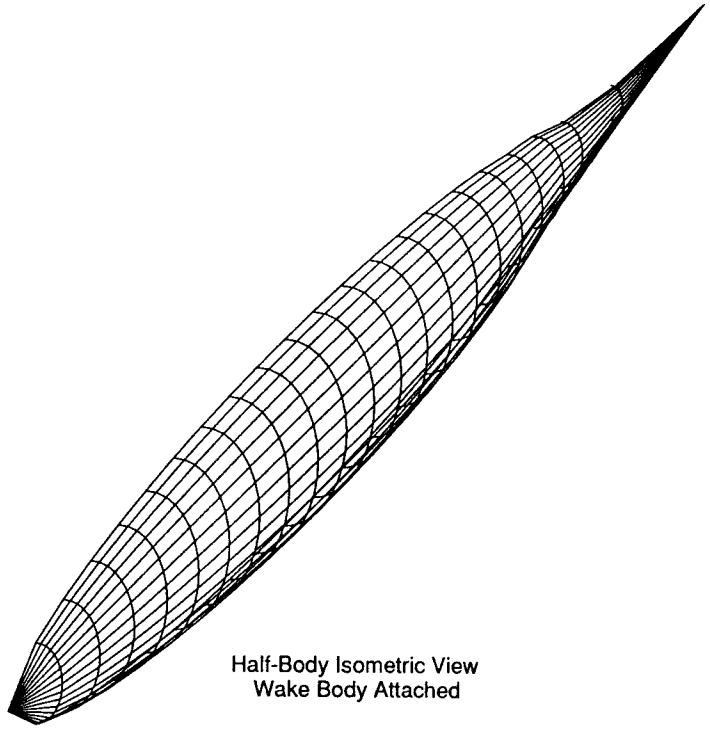

Half-Body Isometric View
Wake Body Attached

Fig. 7.4c Body with added wake body, isometric view.

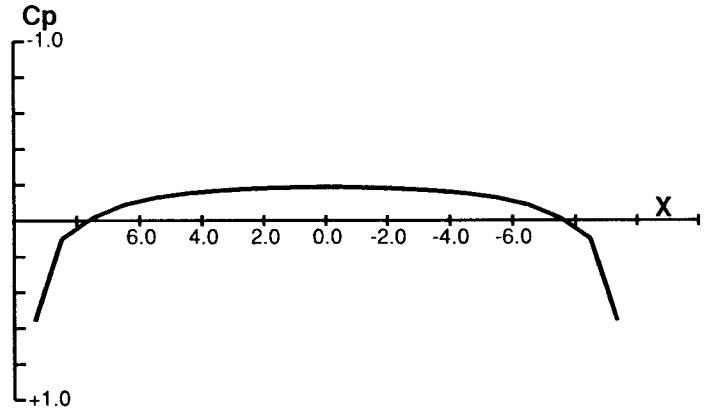

Fig. 7.5a Pressure distribution over general ellipsoid as calculated by program body; flow left to right.

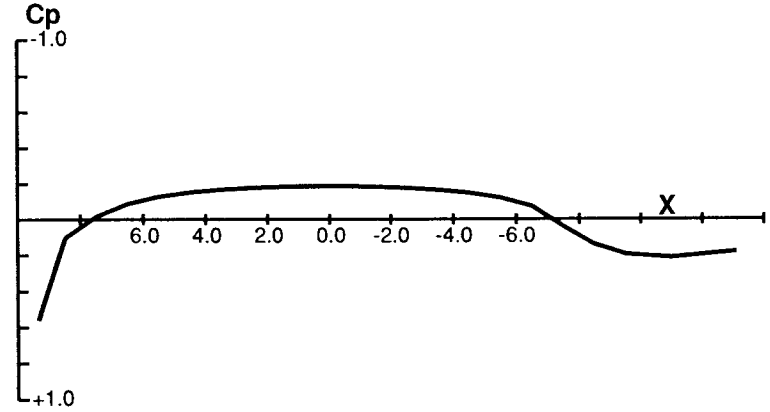

Fig. 7.5b Pressure distribution over general ellipsoid with added wake body as calculated by BODY.

velocities vary from less than 1.0D-4 to less than 1.0D-6 ft/s. In other words, the error in satisfying the condition of no flow normal to a panel surface at any control point is less than 1 part in 1×10^6 (recall the freestream value of the velocity is 10^2) and less than 1 part in 10^8 at some points. (See Figs. 7.7 and 7.8.)

Figure 7.9 shows a comparison between the pressure distribution obtained using **BODY** and that obtained using an analytical solution for a 3 to 1 prolate spheroid. Considering all of the assumptions that had to be made to put together this version of **BODY** the agreement is remarkably good.

The drag coefficient of the prolate spheroid was found to be about 20% smaller than that of the general ellipsoid. (Compare Figs. 7.6 and 7.8.) Most of this

```
general ellipsoid
NO. OF QUADS.  = 320
NO. OF SECTIONS=  1
MAX. NO. OF ITERATIONS X FLOW 150
VINF = 100.000000   VO =  .000100   ROE =  .002378   REFA = 23.271057   IWRITE =  2
1 PLANES OF SYMMETRY
CONVERGENCE CRITERIA ,  .00010
general ellipsoid                                              PAGE =    1
 X FLOW
PT.       X       Y       Z        VX      VY       VZ      ABS.V     CP     SOURCE   V NORMAL
  1    9.33333  .06299  -.95934   -.43310  .07812  -.49615   .66320  .56016   .07135   .55E-06
  2    8.47360  .11321 -1.72420   -.83689  .06509  -.44036   .94791  .10146   .04173   .27E-06
                                .
                                .
                                .
                      PRESSURE LIFT AND DRAG COEFFICIENTS
                       ****************************
                          PRESSURE CL =      .00000
                          PRESSURE CD =      .00000
                        REFERENCE AREA =   23.27106
                       REYNOLDS NUMBER =   .2000E+08
                       ****************************
POTENTIAL FLOW PROGRAM SECTION 5
SUMMARY OF BOUNDARY LAYER INFORMATION FOR QUADRILATERALS
 NQUAD     X       Y       Z       DSTAR   SKIN
     1  9.33333  .06299  -.95934    .00036  .00041
     2  8.47360  .11321 -1.72420    .00108  .00122
                                .
                                .
                                .
                       FRICTION DRAG COEFFICIENT
                       ****************************
                          FRICTION CD =      .07065
                        REFERENCE AREA =   23.27106
                       REYNOLDS NUMBER =   .2000E+08
                          BODY LENGTH =   20.00000
                       ****************************
                                BEGIN WAKE BODY GEOMETRY
AVERAGE SLOPE = -.93816  AVERAGE PANEL AREA = .28351  AVERAGE X-CENTROID = -8.47360
END OF BODY AT X = -15.21116
 X VELOCITY=-1.0     Y VELOCITY= 0.0     Z VELOCITY= 0.0
 POTENTIAL FLOW PROGRAM SECTION 4
general ellipsoid                                              PAGE =    1
 X FLOW
PT.       X       Y       Z        VX      VY       VZ      ABS.V     CP     SOURCE   V NORMAL
  1    9.33333  .06299  -.95934   -.43309  .07812  -.49615   .66320  .56017   .07135   .66E-05
  2    8.47360  .11321 -1.72420   -.83688  .06509  -.44036   .94791  .10147   .04172   .52E-05
                                .
                                .
                                .
general ellipsoid                                              PAGE =    8
 X FLOW
PT.       X       Y       Z        VX      VY       VZ      ABS.V     CP     SOURCE   V NORMAL
351   -11.22330  .05295   .77431   -.84611 -.03307  -.23724   .87936  .22672  -.01912   .99E-05
352   -13.43240  .01890   .27633   -.89684 -.02649  -.15600   .91070  .17063  -.01213   .16E-04
```

Fig. 7.6 BODY program output listing greatly condensed as to quantity of data and vertical spacing on the page.


```
PRESSURE LIFT AND DRAG COEFFICIENTS
 ****************************
    PRESSURE CL =     -.00005
    PRESSURE CD =      .02078
  EFERENCE AREA =    23.27106
REYNOLDS NUMBER =    .2000E+08
 ****************************
   TOTAL BODY COEFFICIENTS
 ****************************
  TOTAL BODY CL =     -.00005
  TOTAL BODY CD =      .09143
  REFERENCE AREA =    23.27106
REYNOLDS NUMBER =    .2000D+08
   BODY LENGTH =     20.00000
 ****************************
```

Fig. 7.6 Contd.

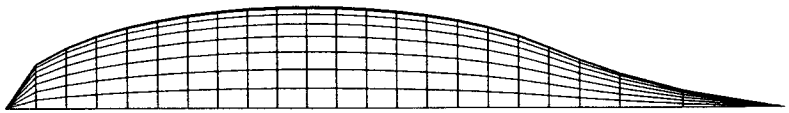

BODY Plan View
Wake Body Attached

Fig. 7.7a Plan view of 3 to 1 prolate spheroid.

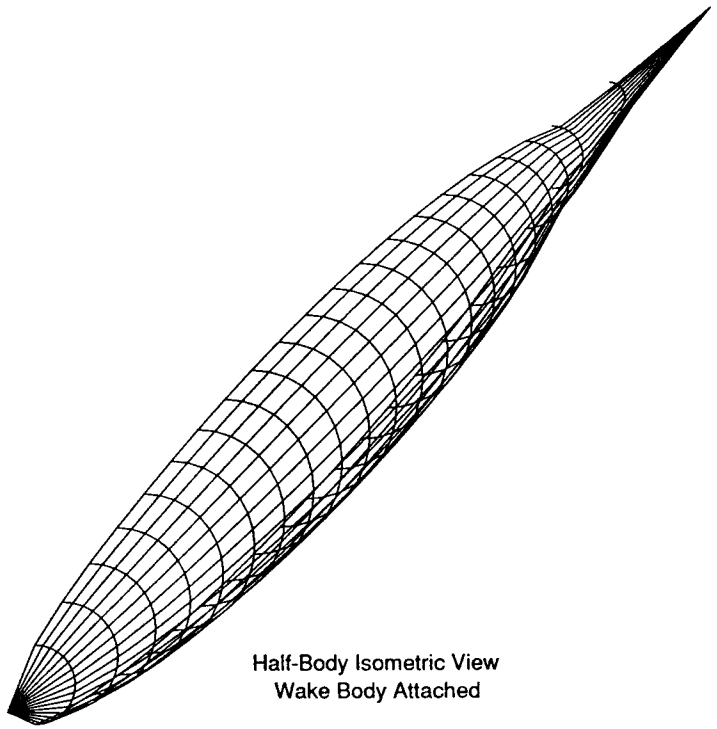

Half-Body Isometric View
Wake Body Attached

Fig. 7.7b Isometric view of 3 to 1 prolate spheroid.

```
prolate spheroid
NO. OF QUADS.  = 320
MAX. NO. OF ITERATIONS X FLOW 150
VINF = 100.000000      VO =.000100      ROE =.002378
  REFA =34.790000      IWRITE = 2
CONVERGENCE CRITERIA = 0.00010

 X VELOCITY=-1.0     Y VELOCITY= 0.0     Z VELOCITY= 0.0

                PRESSURE LIFT AND DRAG COEFFICIENTS
                  ****************************
                      PRESSURE CL =       .00000
                      PRESSURE CD =       .00000
                   REFERENCE AREA =     34.79000
                  REYNOLDS NUMBER =    .2000E+08
                  ****************************

                    FRICTION DRAG COEFFICIENT
                  ****************************
                      FRICTION CD =       .05823
                   REFERENCE AREA =     34.79000
                  REYNOLDS NUMBER =    .2000E+08
                      BODY LENGTH =     20.00000
                  ****************************

                PRESSURE LIFT AND DRAG COEFFICIENTS
                  ****************************
                      PRESSURE CL =      -.00004
                      PRESSURE CD =       .01928
                   REFERENCE AREA =     34.79000
                  REYNOLDS NUMBER =    .2000E+08
                  ****************************

                     TOTAL BODY COEFFICIENTS
                  ****************************
                    TOTAL BODY CL =      -.00004
                    TOTAL BODY CD =       .07751
                   REFERENCE AREA =     34.79000
                  REYNOLDS NUMBER =    .2000D+08
                      BODY LENGTH =     20.00000
                  ****************************
```

Fig. 7.8 General results for 3 to 1 prolate spheroid; normal velocities are less than 1.0D-06 for all panels.

difference is due to the smaller frictional drag coefficient exhibited by the prolate spheroid. That the surface area of the general ellipsoid is proportionally greater than the surface area of the prolate spheroid for the same cross-sectional area probably accounts for this. Notice that the reference area of the prolate spheroid is about 50% greater than for the general ellipsoid.

That the prolate spheroid has smaller velocities normal to its surface panels and has a lower lift coefficient are indications that source strengths, which vary only in the axial direction, are easier for the program to accommodate than the source strengths that vary circumferentially as well as axially.

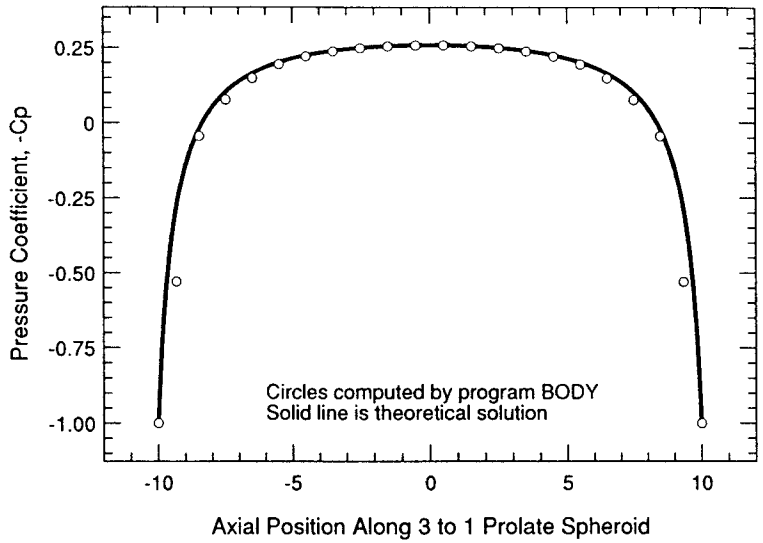

Fig. 7.9 Comparison of the results produced by BODY program with those obtained from an analytical determination of the pressure distribution on a prolate spheroid.

Data reported in Ref. 26 indicates that the results given by **BODY** for more complex bodies such as general aviation fuselages are similar to but slightly lower than drag coefficients determined by the well-known C_{D_π} or drag buildup method.

7.6 Concluding Remarks

In this chapter we have attempted to show how a relatively simple yet rigorous concept can be used to determine the drag coefficients of isolated nonlifting bodies. We began by representing the body by an ensemble of linked, flat quadrilaterals, a sort of wire frame model of the body. On each of these panels we placed a fluid dynamic source of unknown strength. We determined the source strengths by requiring that the flow velocity induced by all sources plus the freestream normal to the panel surface be zero at one point on each panel. The solution of this problem gave us the inviscid pressure distribution over the body. When the forces due to these pressures are summed in the lift and drag directions one should, if the computations were carried out with sufficient accuracy and precision, obtain zero lift coefficient and zero drag coefficient.

The program also determines the flow streamlines on the body surface. Combined with the pressure distribution it is possible to determine the skin friction along streamlines, as well as the boundary-layer displacement thickness. The skin-friction results in a drag on the body regardless of whether there is a pressure drag. It is well known that for very streamlined bodies the skin-friction drag may represent 80% of the total drag. For less streamlined bodies, however, viscosity causes a wake to form behind the body. The pressure in the wake is less than one would predict from inviscid theory and, as a result, a pressure drag exists on the body.

To model this effect within the framework of the general inviscid theory, we applied the concept of a wake body, a ficticious extension of the physical body about which we perform an inviscid flow analysis. Then, when the pressures developed over the wake body are applied to the physical body, a drag of approximately the correct magnitude is developed. For the **BODY** program we have chosen to attach the wake body 2 N stations upstream of the end of the physical body. We select as the initial slope of the wake body the slope of the physical body plus twice the boundary-layer displacement thickness. Finally, we locate the terminus of the wake body downstream in the physical wake at a point such that the wake body slope can vary monotonically from its inital value in an exponential manner. We note that to retain the concept of inviscid flow over the body plus wake body, a stagnation point must exist at the vertex of the wake body.

Using this model to acccount for viscous flow over a body with a plane of symmetry causes the computation time to be somewhat greater than twice as long as for inviscid flow alone because 1) the streamlines must be determined, 2) the skin friction and boundary-layer displacement thickness must be determined along a streamline passing through the centroid of each panel used to represent the surface, 3) a wake body must be created and attached to the physical body, and 4) the pressure distribution over this combined body must be determined. Although such a computation is more difficult than an inviscid computation alone, it is far less resource intensive than a solution of Navier–Stokes equations with the physical body as the boundary condition. We will have a bit more to say on this point in the chapter on computational fluid dynamics.

The results obtained with this method for determining the drag of slender, isolated bodies have proven to be fairly accurate; unfortunately, there is little data available in the literature that could be used to compare the results for more complex body shapes. Also, generating the grid describing more complex bodies is a tedious task. Nevertheless, the success of this method indicates the progress made in calculating the aerodynamic characteristics of complete configurations in a fairly rigorous manner from first principles. As computers become more powerful, it can be expected that the procedures will be refined to eliminate some of the assumptions made in this version. Automatic gridding schemes will be of enormous assistance in analyzing complex shapes. The ability to treat bodies with concavities, a feat that the present method cannot accomplish in a practical manner, can also be expected. (An inward normal on a panel is an indication that the local surface is concave. The program reports these inward normals when it finds them.)

Readers interested in more detail regarding the inviscid theory treated herein are urged to consult the references.

Problems

To spare the user the arduous task of identifying and recording the coordinates of more than 100 points on a general body, the following problems are intended to be solved using the **BODYGEN** program to create input files for analysis by **BODY**.

7.1. Let $N = 21$ and $M = 17$ (for a half-body). Then generate a prolate spheroid with the semimajor axis equal to 10.0 and the semiminor axis equal to 5.0. Use sea level air as the medium through which the body is moving. Determine the pressure and frictional and total drag of the body when its velocity is 100 ft/s. Compare these with the results for the 3 to 1 prolate spheriod and comment on the differences. Are the trends in the directions to be expected?

7.2. Repeat problem 7.1 for a 6 to 1 prolate spheroid. Choose the semimajor axis to be 10.0 ft.

7.3. Repeat problem 7.1 for a 2 to 1 prolate spheroid. Choose the semimajor axis to be 10.0 ft.

7.4. A 3 to 1 prolate spheroid is traveling at 100 ft/s in sea level air. It has a semimajor axis of 10.0 ft. Choose $N = 21$ and $M = 7$ (for the half-body). Generate the drag values using **BODY**. Compare the results with those for the case where $M = 17$. Comment on the differences.

7.5. Repeat problem 7.4 for the case where $N = 29$ and $M = 17$.

7.6. For the 3 to 1 prolate spheroid traveling in air let the semimajor axis be 10.0 ft. Choose $N = 21$ and $M = 17$. Let the velocity be 1 ft/s. Run BODY and compare the results with the case where the velocity is 100 ft/s. Comment on any differences observed.

7.7. Repeat problem 7.6 for a speed of 0.1 ft/s.

7.8. Choose a 3 to 1 prolate spheroid running in sea water at 100.0 ft/s. Let $N = 21$ and $M = 17$. Let the semimajor axis be 10.0 ft. Determine the drag coefficient and compare with the case where the medium is air.

7.9. Repeat problem 7.8 for a velocity of 10.0 ft/s.

7.10. Repeat problem 7.8 for a velocity of 1.0 ft/s.

7.11. Repeat problem 7.8 for a speed of 0.1 ft/s.

7.12. From all of the data you have collected on the 3 to 1 prolate spheroid, plot C_D vs Reynolds number. Discuss your results.

7.13. Repeat problem 7.8 with the semimajor axis 1.0 ft. Compare the results with those obtained for problem 7.8 and those obtained for problem 7.9.

7.14–7.25. Repeat the problems involving a 3 to 1 prolate spheroid for a body with semimajor axis equal to 10.0 ft, semiminor axis in the plane of symmetry of 3.33333 ft, and semiminor axis normal to the plane of symmetry equal to 2.22222 ft.

7.26–7.35. Repeat the problems with the two semiminor axes reversed.

7.36–7.46. Repeat the problems for a body with the ratio of the two semiminor axes equal to 1.25. The semimajor axis in the plane of symmetry is 3.0 ft. The semimajor axis is 9.0 ft.

7.47. A prolate spheroid has a semimajor axis of 10.0 ft and a semiminor axis of 1.0 ft. Develop the drag coefficients for this body when the speed is 100.0 ft/s in sea water. Determine the ratio of the frictional drag coefficient to the pressure drag coefficient for this configuration and discuss.

7.48. The program creates a file in input data format giving the coordinates of the panel corners when a wake body has been attached. Submit to the program a body that results from the analysis of the 2 to 1 prolate spheroid. Describe in detail the results and in particular how the aft end of the body has been changed.

7.49. A body is formed by rotating the figure described by positive values of y from the equation

$$x^2 + 4y^2 = 81$$

for $x > -5.4$ and by the equation

$$y = 3.6 + (3.6/9.6)(x + 5.4)$$

for $x < -5.4$ about the x axis. Let $dx = -0.9$ for $x \geq -5.4$. For $x < -5.4$ the values of x are -6.5, -7.8, -9.3, -11.0, -12.9 and -15.0. The body formed is a 2 to 1 prolate spheroid with a conical afterbody such that the slope of the cone is equal to the slope of the body at the point of attachment. The semimajor axis is 9.0, and the semiminor axis is 4.5. Choose the number of M stations to be 15. The number of N stations is 23. How does the drag of this body compare with the drag of the basic 2 to 1 prolate spheroid? Compare pressure drag and skin-friction drag separately.

7.50. Based on your experience with general ellipsoids (bodies for which the three principal axes are unequal) what should you expect relative to the program's ability to determine the drag coefficient of bodies like light aircraft fuselages? Discuss. Does the same reasoning apply to fuselages of commercial transport aircraft or submarine hulls?

7.51. If you were asked to determine the drag of a 1 to 2 ellipsoid by the use of the program **BODY** what should be your reply and why?

7.52. If you were asked to determine the pressure distribution for inviscid flow about a 1 to 2 ellipsoid using **BODY** could you legitimately do so and why?

8
Characteristics of Wing Wakes

8.1 Introduction

THE horizontal tailplane on conventional aircraft flies in the wake of the main wing. Because the wing is lifting, the flow behind the wing exhibits a downwash, which varies along the wing semispan. (Simple momentum considerations tell us that because the flow has created an upward force on the wing, there is an equal and opposite force on the flow that imparts a downward velocity component to it.) Inboard of the tips, the downwash can be thought of as a downward component in the flow relative to the direction of flight. In the tip regions, however, there is a significant outward component in the flow below the wing and a similar inward component in the flow above the wing in addition to a downward component. These spanwise flow components eventually cause the flow leaving the tip regions to roll up into vortices. The strength of these vortices depends on the lift being generated by the wing. Large transport aircraft, for example, are heavy and, thus, generate considerable lift (equal to their weight) and, hence, very strong vortical flows immediately aft of the aircraft.

The generation of lift can be treated as a purely inviscid matter. However, the finite drag of the main wing causes a momentum defect to exist in the flow at the center of the downwash field. Locating the horizontal tailplane in or near the center of this downwash field can reduce its effectiveness by 15% or more. In particular, locating the horizontal tailplane in a region where it is impacted by the flow at the center of the downwash field only during high-angle-of-attack situations causes this loss in effectiveness to be felt just at the occasion where the maximum contribution of the tailplane to aircraft control is desired.

To minimize the size of the horizontal tailplane and thus minimize overall aircraft drag, it is necessary that the tailplane operate in a flow region where there is little momnentum loss at high-lift situations. If designers are to find such locations they must be able to develop fairly complete knowledge of the direction and magnitude of the flow at stations 2–10 chord lengths aft of the wing. It is the purpose of the programs in this chapter to provide such information.

WASH is an inviscid program that calculates the local direction of the flow from the trailing edge of the wing to as far downstream as one is able to track the streamlines successfully. The methodology is very similar to that used to find the flow over airfoils and bodies. **WAKE** is a program that determines the momentum loss in the flow sheet immediatly downstream of the wing. Together they can be used to create a three-dimensional picture of the directions and magnitudes of the flow in the field downstream of the wing.

8.2 Program WASH

A review of previous literature in the area and a detailed discussion of the theory leading to the creation of **WASH** are provided in Ref. 40. Here we relate the theory necessary to the understanding of program operation.

We begin with a consideration of the horseshoe vortex system such as that shown schematically in Fig. 6.1, Chapter 6, page 132. Note that we are representing the wing surface by what is called a lifting line approximation, which is satisfactory for wings with little or no sweep and moderate to high aspect ratios. Along the lifting line we place a bundle of horseshoe vortices. Each of these vortices has a different circulation strength and spanwise extent. As a group they define the spanwise lift distribution. (In more exact representations of the wing we use a chordwise as well as a spanwise distribution of horseshoe vortices.) If the dark line in Fig. 6.1, A–A', is thought of as representing all the horseshoe vortices, then Γ varies in a symmetrical manner with respect to point 0. Lines A'–B' and A–B represent all the trailing vortices which eventually roll up into two large tip vortices. According to the Biot–Savart law all these vortices induce velocity components into the flowfield whose strengths are inversely proportional to their distances from the point of consideration.

One form of the Biot–Savart law is given by

$$dW = \frac{\Gamma}{4\pi}\frac{\sin\theta\, d\ell}{r^2} \tag{8.1}$$

where:

dW = total velocity induced at a particular point by a filament $d\ell$
Γ = strength of the vortex filament
r = distance to increment of filament at the point the velocity is induced
θ = angle between the length r and the filament

The contibution of the bound vortex is calculated by integrating Eq. (8.1) from the negative wing tip to the positive wing tip. Expressing $\sin\theta$ and r in terms of x, y, and z, and noting that $d\ell$ becomes dy, the induced velocity at a point (x, y, z) can be expressed by

$$W_b = \int_{-1}^{1} \frac{\Gamma(y_0)(b/2)\sqrt{(x-x_2)^2+(z-z_b)^2}\, dy_0}{4\pi\left[(x-x_b)^2+(y-y_b)^2+(z-z_b)^2\right]^{\frac{3}{2}}} \tag{8.2}$$

where all coordinates are nondimensionalized by the semispan. Equation (8.2) may be solved numerically or, if the functional for $\Gamma(y_0)$ is known, it may be integrated in closed form. To use the closed-form technique, two successive specified values of $\Gamma(y)$ for the bound vortex were fitted using a cubic spline. The coefficients in the spline relationship were obtained by matching the first and second derivatives at the endpoints. We recall that the cubic spline is of the form

$$\Gamma(y) = A_{1j}y^3 + A_{2j}y^2 + A_{3j}y + A_{4j} \tag{8.3}$$

where $y_j \le y \le y_{j+1}$, $j = 1, 2, 3, \ldots, 19$.

Note that for each of the 19 intervals the coefficients of the spline function over the interval y_j–y_{j+1} are constant. However, a different set of constant coefficients may apply to the interval y_{j+1}–y_{j+2}. Using Eq. (8.3) in Eq. (8.2) permits us to integrate Eq. (8.2) to yield the total velocity induced by the bound vortex at point $p(x, y, z)$. The total velocity can be divided into a freestream component u and a downwash component w,

$$u_b = \frac{W_b\,(x - x_b)}{\sqrt{(x-x_b)^2+(z-z_b)^2}} \tag{8.4a}$$

$$w_b = \frac{W_b\,(z - z_b)}{\sqrt{(x-x_b)^2+(z-z_b)^2}} \tag{8.4b}$$

The subscript b refers to the bound vortex. Here, w and W are defined as positive in the negative z direction, and u is positive in the positive x direction. Because the bound vortex is always parallel to the y axis there is no sidewash component in W_b. The streamwise component is usually very small compared with the freestream velocity.

The velocity induced by a trailing vortex is calculated by summing the effects of each straight line segment of the vortex. The total velocity induced at a point by a straight line segment is also calulated by Eq. (8.1); however, the evaluation is much simpler than the bound contribution because Γ is constant along all segments of the trailing vortex. Suppose we call the distance along a straight line segment ℓ. Expressing $d\ell$ and r in terms of θ, that is, $r\,d\theta = d\ell$, we can write the equation for the velocity induced by a trailing vortex segment as

$$w_t = \frac{\Gamma}{4\pi}\int_{\theta_A}^{\theta_B} \frac{\sin\theta}{h} d\theta \tag{8.5}$$

where:

w_t = total velocity induced at point $p(x, y, z)$ by a vortex of length AB, see Fig. 6.1
θ_A = angle PAB between the length r or PA and the filament at point A
θ_B = angle PBA between the length r or PB and the filament at point B
h = perpendicular distance from p to the filament, PN in Fig. 6.1

Carrying out the integration indicated in Eq. (8.5) we have

$$w_t = (\Gamma/4\pi h)(\cos\theta_A - \cos\theta_B) \tag{8.6}$$

This inital induced velocity must also be divided into its component parts: freestream, sidewash, and downwash velocities. As shown in Fig. 8.1 the total induced velocity p_0 due to a line vortex from p_1 to p_2 of strength Γ may be written as

$$w_t = \frac{\Gamma\,(\cos\theta_1 + \cos\theta_2)}{4\pi\,(b/2)\,d_{01}\sin\theta_1} \tag{8.7}$$

The three lengths shown in the figure are defined as follows:

$$d_{21} = \sqrt{(x_2-x_1)^2+(y_2-y_1)^2+(z_2-z_1)^2} \tag{8.8a}$$

$$d_{01} = \sqrt{(x_0-x_1)^2+(y_0-y_1)^2+(z_0-z_1)^2} \tag{8.8b}$$

$$d_{02} = \sqrt{(x_0-x_2)^2+(y_0+y_2)^2+(z_0-z_2)^2} \tag{8.8c}$$

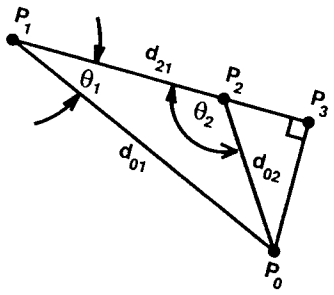

Fig. 8.1 Schematic showing velocity induced at P_0 due to a vortex from P_1 to P_2.

The angles θ_1 and θ_2 are defined in terms of these lengths by the relationships

$$\theta_1 = \cos^{-1}\left[\frac{(d_{21}^2 + d_{01}^2 - d_{02}^2)}{(2d_{21}d_{01})}\right] \tag{8.9a}$$

$$\theta_2 = \cos^{-1}\left[\frac{(d_{21}^2 + d_{02}^2 - d_{01}^2)}{(2d_{21}d_{02})}\right] \tag{8.9b}$$

In terms of these quantities and the locations of points 1 and 2, the location of point 3 is given by

$$x_3 = x_1 + d_{01} \cdot (\cos\theta_1) \cdot [(x_2 - x_1)/d_{21}] \tag{8.10a}$$

$$y_3 = y_1 + d_{01} \cdot (\cos\theta_1) \cdot [(y_2 - y_1)/d_{21}] \tag{8.10b}$$

$$z_3 = z_1 + d_{01} \cdot (\cos\theta_1) \cdot [(z_2 - z_1)/d_{21}] \tag{8.10c}$$

We will define three additional quantities as

$$A = (y_2 - y_1)(z_3 - z_1) - (y_3 - y_1)(z_2 - z_1) \tag{8.11a}$$

$$B = (x_2 - x_1)(z_3 - z_1) - (x_3 - x_1)(z_2 - z_1) \tag{8.11b}$$

$$C = (x_2 - x_1)(y_3 - y_1) - (y_2 - y_1)(x_3 - x_1) \tag{8.11c}$$

so that we can write the components of the velocity induced by the trailing vortices as

$$u_t = W_t(A/\sqrt{R}) \tag{8.12a}$$

$$v_t = W_t(B/\sqrt{R}) \tag{8.12b}$$

$$w_t = W_t(C/\sqrt{R}) \tag{8.12c}$$

where

$$R = A^2 + B^2 + C^2 \tag{8.12d}$$

We note that the induced velocity components at a point are determined from contributions due to the bound vortex given by Eqs. (8.4) and to the trailing vortices given by Eqs. (8.7) and (8.12). The velocity induced by the entire vortex system

is computed by summing the contributions of the bound vortex and each segment of the 18 trailing vortices.

The curvature in the trailing vortex system is modeled by representing each vortex by a number of straight line segments, which are free to follow the local direction of flow. Their position is found by marching stepwise in the x direction, determining the flow direction at a particular value of x from the v and w components due to all vortices at that point, and aligning the segment with the flow by use of the equations

$$\Delta y = v\Delta x \tag{8.13a}$$

$$\Delta z = w\Delta x \tag{8.13b}$$

(A marching procedure is required because the position of each segment and, therefore, the velocity components it induces is unknown a priori)

8.2.1 Features of WASH Program

The current version of WASH produces, in addition to listings of the locations of shed vortices, PostScript views of the downwash field, as shown in Fig. 8.2. In these views the locations of the centers of the 9 vortices shed from each half of the wing are shown at 15 stations downstream of the wing trailing edge. As many as 5 additional downstream stations can be added. One view is a quasiplan view, and the other shows their appearance as seen by an observer in the region of the horizontal tailplane. Figure 8.2 was computed for an angle of attack of 11 deg and a lift coefficient of about 1.0. Notice that for this lift coefficient the vortices do not appear to roll up completely, at least over the field of observation. (A rollup would be indicated by having, say, the center of the most outboard vortex move to the inside of the next most outboard vortex at some X station; however, the figure does appear to show the beginning of this situation.) Figure 8.2b indicates that there is a relatively large upward displacement of the vortex centers as one moves outward along the wing semispan. The figure maintains the correct Y–Z scale relationships. Different scaling was used for the three axes in Fig. 8.2a to highlight the characteristics of the vortex sheet.

In addition to providing data from which to construct these views, the program offers options to compute the downwash field in the X–Z plane behind the wing or the upwash field in the X–Z plane ahead of the wing. Typical results are shown in Fig. 8.5b. The significance of the results in this figure is discussed in Sec. 4.0. Figure 8.5a shows the sidewash components in the Y–Z plane at six inboard Y-locations for a specified value of X. The data appear in **WASH.TXT**. The PostScript file created from these data is called **SWASH.PS**. If the user wishes to plot these data in some other fashion they are available for this purpose in **WASH.OUT**, a permanent file.

Two additional executables, **WASHDAT1** and **WASHDAT**, have been provided with the present version of **WASH** to assist the user in creating input files for **WASH**. These are described in more detail in the next section.

Programs sizes are as follows.

NAME	NUMBER OF LINES	BYTES IN SOURCE	BYTES IN EXECUTABLE
WASHDAT1	39	1,792	89,088
WASHDAT	125	5,504	90,624
WASH	1900	83,456	133,120

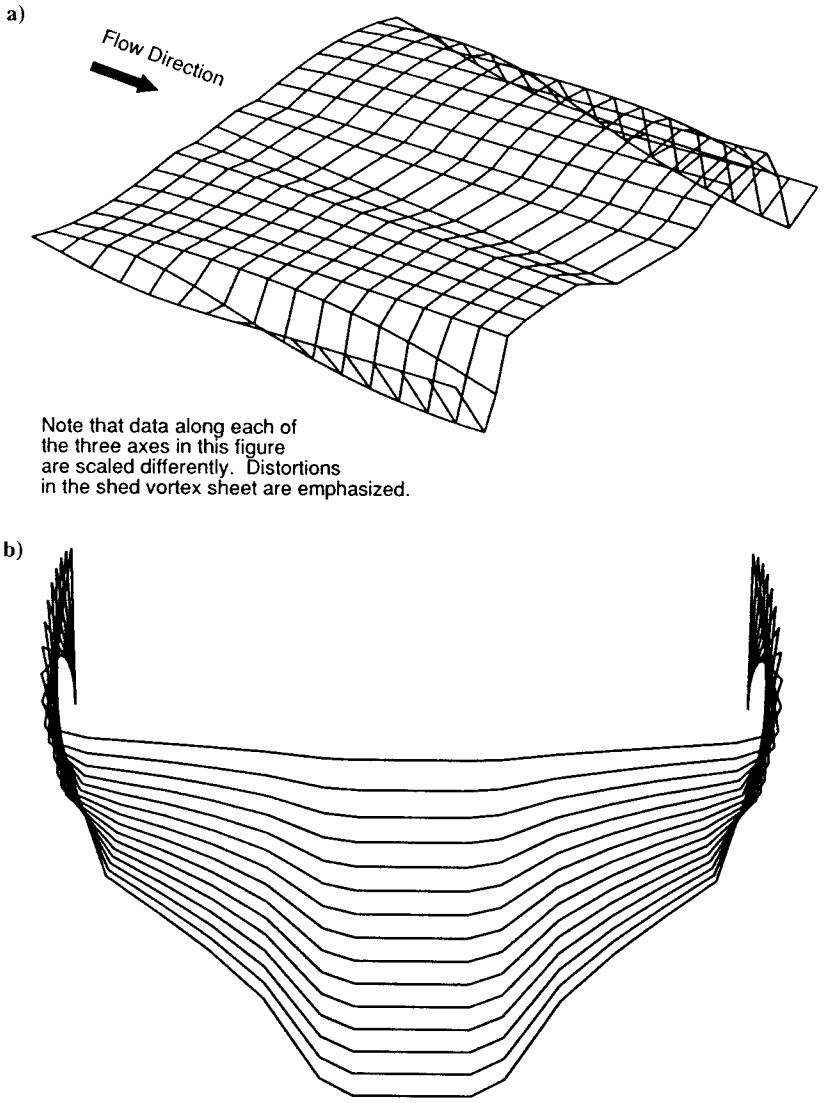

Fig. 8.2 Two views of downwash field: a) shed vortex sheet and b) view from region of horizontal tailplane.


```
wing
      15         1
11.00000  20.00000     .49000    4.00000     .25000
  .98769     .95106     .89101     .80902     .70711     .58779     .45399     .30902
  .15644     .12974
  .45462     .75759     .92777    1.02802    1.09002    1.12809    1.14835    1.15099
  .13458    1.08261
       1     .75000
       0     .75000
```

Fig. 8.3 Typical input date file for WASH program.

8.3 Program Data Entry

A typical input data file is shown in Fig. 8.3. On the first line is the name one wishes to assign to the job. The next line shows the number of the downstream station at which the downwash is to be computed and the type of computation desired. The number 1, which follows, tells the program to generate file WASH.OUT. The next two lines show the stations on the semispan for which section lift coefficient values are available. These are given in the following two lines. Next are two numbers, the first of which indicates the type of computation desired. The number 1 indicates that the views shown in Fig. 8.2 are desired. For 2, the downwash in the $X-Z$ plane behind the wing is produced. For 3, the upwash in the $X-Z$ plane is produced. The second number indicates the downstream separation between planes of computation in semispans. In the last line the first number has been changed to zero to signal the program to halt following one set of computations. A provision to enable the program to read a second set of input data at this point was eliminated from this version. This input file is produced by program **WASHDAT**. **WASHDAT** in turn uses a file, WASHDAT.DAT, made by **WASHDAT1** from an edited version of F2D3D.TXT called CODE.DAT. All files can also be created with an editor.

8.4 Typical Results

Results produced by the program for the input data file given in Fig. 8.3 are shown in Fig. 8.4.

Some of the values in the figure are self-explanatory. The circulation values, of course, are determined from the section lift coefficients. These are then spline fitted to give a smooth variation over the wing semispan. The next item in the listing is the locations of the centers of the shed vortices at each of the downstream planes for which computation was desired. This is the information that is plotted in Fig. 8.2. Finally, the last three sets of numbers in the listing are the total flow deviation, the sidewash, and the downwash in $X-Z$ planes at six spanwise locations 0.75 semispans aft of the wing trailing edge (roughly the region in which the horizontal tailplane would be located). These data give the actual directions of the flow components at the specified locations. Note that Y and Z values have been normalized by dividing by $b/2$.

The strength of the tip vortex and, hence, the amount of rollup that will be seen in the figures is dependent on the aspect ratio, the taper ratio, and the lift. A taper ratio of about 0.5 makes the lift distribution nearly elliptical and, therefore, spreads the vorticity over the span. Increasing aspect ratio has the same effect. In the example, the aspect ratio is about 10. For this example, therefore, a high degree of rollup is not expected, even at maximum lift coefficient where the tip vortex is strongest. Notice, too, that the rollup takes time (or distance) to develop.

```
000D+02  DEGREES
000D+02  FEET
000D+00
000D+01  FEET
000D+00  SEMISPANS
244D+00  SEMISPANS
213D-01  SEMISPANS

ALUES
        CLS(I)
)0      .454620D+00   TIP VALUE (Y-POSITIVE)
)0      .757590D+00       |
)0      .927770D+00       |
)0      .102802D+01       |
)0      .109002D+01       |
)0      .112809D+01       |
)0      .114835D+01       |
)0      .115099D+01       |
)0      .113458D+01       |
)0      .108261D+01   ROOT VALUE
 VALUES
        CLS(I)          C(I)          GAM(I)
)0      .454620D+00     .198511D+01     .451236D+00   TIP VALUE (Y-NEGATIVE)
)0      .757590D+00     .205984D+01     .780256D+00       |
)0      .927770D+00     .218234D+01     .101235D+01       |
)0      .102802D+01     .234960D+01     .120772D+01       |
)0      .109002D+01     .255750D+01     .139386D+01       |
)0      .112809D+01     .280091D+01     .157984D+01       |
)0      .114835D+01     .307386D+01     .176493D+01       |
)0      .115099D+01     .336960D+01     .193919D+01       |
)0      .113458D+01     .368086D+01     .208812D+01       |
)0      .108261D+01     .373533D+01     .202195D+01       |
)0      .108261D+01     .373533D+01     .202195D+01       |
)0      .113458D+01     .368086D+01     .208812D+01       |
)0      .115099D+01     .336960D+01     .193919D+01       |
)0      .114835D+01     .307386D+01     .176493D+01       |
)0      .112809D+01     .280091D+01     .157984D+01       |
)0      .109002D+01     .255750D+01     .139386D+01       |
)0      .102802D+01     .234960D+01     .120772D+01       |
)0      .927770D+00     .218234D+01     .101235D+01       |
)0      .757590D+00     .205984D+01     .780256D+00       |
)0      .454620D+00     .198511D+01     .451236D+00   TIP VALUE (Y-POSITIVE)
 OF THE 9 SHED VORTICES ON THE NEGATIVE Y-AXIS
IMAGE IS ASSUMED FOR POSITIVE AXIS)
        GAMS(I)
)0     -.329020D+00   TIP VALUE (Y-NEGATIVE)
)0     -.232098D+00       |
)0     -.195363D+00       |
)0     -.186143D+00       |
)0     -.185978D+00       |
)0     -.185095D+00       |
)0     -.174254D+00       |
)0     -.148929D+00       |
)0      .66?534D-01   ROOT VALUE

ORTEX STRENGTHS VERSUS Y

 GAMMA
 .29496022
 .78702135
 .98914547
1.11428501
```

Fig. 8.4 Typical WASH output slightly condensed.


```
 -.800          1.22664068
 -.750          1.32158156
 -.700          1.40539683
 -.650          1.48447691
 -.600          1.56124217
 -.550          1.63692988
 -.500          1.70818065
 -.450          1.76930779
 -.400          1.81983732
 -.350          1.87578828
 -.300          1.95633746
 -.250          2.05722452
 -.200          2.11893155
 -.150          2.07414920
 -.100          1.95363527
 -.050          1.87864287
  .000          1.85364540
  .050          1.87864287
  .100          1.95363527
  .150          2.07414920
  .200          2.11893155
  .250          2.05722452
  .300          1.95633746
  .350          1.87578828
  .400          1.81983732
  .450          1.76930779
  .500          1.70818065
  .550          1.63692988
  .600          1.56124217
  .650          1.48447691
  .700          1.40539683
  .750          1.32158156
  .800          1.22664068
  .850          1.11428501
  .900           .98914547
  .950           .78702135
 1.000           .29496022

 COORDINATES FOR DOWNSTREAM SHED VORTICES ALONG THE POSITIVE Y-AXIS (FROM WING ROOT TO WING TIP)
 S DENOTES PATH DISTANCE DOWNSTREAM FROM TRAILING EDGE FOR EACH VORTEX AT THE GIVEN STEP

TRAILING EDGE
   X   .000000   .000000   .000000   .000000   .000000   .000000   .000000   .000000   .000000
   Y   .143090   .232730   .381505   .520890   .647450   .758065   .850015   .921035   .969375
   Z   .000000   .000000   .000000   .000000   .000000   .000000   .000000   .000000   .000000
   S   .000000   .000000   .000000   .000000   .000000   .000000   .000000   .000000   .000000

 STEP 1
   X   .250000   .250000   .250000   .250000   .250000   .250000   .250000   .250000   .250000
   Y   .143984   .232817   .382258   .521974   .648964   .760332   .853875   .928128   .973796
   Z  -.022468  -.021898  -.018595  -.016289  -.014382  -.012848  -.011403  -.007702   .008567
   S   .251009   .250957   .250692   .250532   .250418   .250340   .250290   .250219   .250186

 STEP 2
   X   .500000   .500000   .500000   .500000   .500000   .500000   .500000   .500000   .500000
   Y   .144488   .232959   .382612   .522401   .649522   .761234   .855846   .933954   .969278
   Z  -.039406  -.038205  -.031814  -.027657  -.024397  -.021989  -.020015  -.014573   .019780
   S   .501583   .501489   .501041   .500791   .500619   .500509   .500446   .500381   .500478
                                                  .  .
                                                  .  .
                                                  .  .
 STEP 15
   X  3.750000  3.750000  3.750000  3.750000  3.750000  3.750000  3.750000  3.750000  3.750000
   Y   .156020   .245240   .392773   .534388   .668241   .804516   .953388   .898712   .886099
   Z  -.210121  -.200511  -.156468  -.129880  -.108960  -.088926   .003273   .094423   .007110
   S  3.756101  3.755582  3.753462  3.752437  3.751799  3.751586  3.753374  3.755558  3.752393
```

Fig. 8.4 Contd.

TOTAL FLOW ANGULAR DEVIATION INFORMATION FOR POSITIVE Y-AXIS AT THE X STATION OF 7500 SEMI-SPANS

Y = .1450		Y = .2332		Y = .3830		Y = .5228		Y = .6501		Y = .7623	
Z	ANGLE	Z	ANGLE	Z	ANGLE	Z	ANGLE	Z	ANGLE	Z	ANGLE
.1955	1.79	.1974	1.85	.2068	1.96	.2127	2.11	.2172	2.26	.2204	2.34
.1455	1.94	.1474	1.97	.1568	2.08	.1627	2.25	.1672	2.43	.1704	2.50
.0955	2.05	.0974	2.05	.1068	2.17	.1127	2.38	.1172	2.62	.1204	2.69
.0455	2.05	.0474	2.06	.0568	2.21	.0627	2.48	.0672	2.84	.0704	2.91
-.0045	1.86	-.0026	1.96	.0068	2.18	.0127	2.53	.0172	3.08	.0204	3.19
-.0545	1.64	-.0526	1.83	-.0432	2.11	-.0373	2.51	-.0328	3.20	-.0296	3.34
-.1045	1.81	-.1026	1.88	-.0932	2.10	-.0873	2.45	-.0828	3.01	-.0796	3.12
-.1545	1.92	-.1526	1.95	-.1432	2.10	-.1373	2.36	-.1328	2.72	-.1296	2.81
-.2045	1.85	-.2026	1.91	-.1932	2.04	-.1873	2.25	-.1828	2.47	-.1796	2.56
-.2545	1.72	-.2526	1.81	-.2432	1.94	-.2373	2.11	-.2328	2.27	-.2296	2.35
-.3045	1.57	-.3026	1.69	-.2932	1.82	-.2873	1.97	-.2828	2.09	-.2796	2.17

SIDEWASH INFORMATION FOR POSITIVE Y-AXIS AT THE X STATION OF .7500 SEMI-SPANS

Y = .1450		Y = .2332		Y = .3830		Y = .5228		Y = .6501		Y = .7623	
Z	ANGLE	Z	ANGLE	Z	ANGLE	Z	ANGLE	Z	ANGLE	Z	ANGLE
.1955	-1.46	.1974	-1.23	.2068	-.99	.2127	-.71	.2172	-.35	.2204	-.48
.1455	-1.54	.1474	-1.28	.1568	-1.02	.1627	-.72	.1672	-.33	.1704	-.51
.0955	-1.55	.0974	-1.25	.1068	-.99	.1127	-.70	.1172	-.28	.1204	-.53
.0455	-1.39	.0474	-1.10	.0568	-.86	.0627	-.60	.0672	-.17	.0704	-.52
-.0045	-.85	-.0026	-.68	.0068	-.52	.0127	-.36	.0172	-.02	.0204	-.38
-.0545	.21	-.0526	.09	-.0432	.06	-.0373	.05	-.0328	.08	-.0296	.05
-.1045	1.19	-.1026	.84	-.0932	.63	-.0873	.45	-.0828	.15	-.0796	.45
-.1545	1.57	-.1526	1.22	-.1432	.94	-.1373	.68	-.1328	.25	-.1296	.57
-.2045	1.59	-.2026	1.32	-.1932	1.05	-.1873	.76	-.1828	.33	-.1796	.56
-.2545	1.50	-.2526	1.30	-.2432	1.05	-.2373	.76	-.2328	.36	-.2296	.52
-.3045	1.37	-.3026	1.23	-.2932	1.01	-.2873	.73	-.2828	.36	-.2796	.48

DOWNWASH INFORMATION FOR POSITIVE Y-AXIS AT THE X STATION OF .7500 SEMI-SPANS

Y = .1450		Y = .2332		Y = .3830		Y = .5228		Y = .6501		Y = .7623	
Z	ANGLE	Z	ANGLE	Z	ANGLE	Z	ANGLE	Z	ANGLE	Z	ANGLE
.1955	1.03	.1974	1.38	.2068	1.70	.2127	1.99	.2172	2.23	.2204	2.29
.1455	1.17	.1474	1.50	.1568	1.81	.1627	2.13	.1672	2.41	.1704	2.45
.0955	1.33	.0974	1.62	.1068	1.93	.1127	2.27	.1172	2.60	.1204	2.64
.0455	1.51	.0474	1.74	.0568	2.04	.0627	2.41	.0672	2.83	.0704	2.87
-.0045	1.65	-.0026	1.84	.0068	2.12	.0127	2.50	.0172	3.08	.0204	3.16
-.0545	1.63	-.0526	1.83	-.0432	2.11	-.0373	2.51	-.0328	3.19	-.0296	3.34
-.1045	1.36	-.1026	1.68	-.0932	2.00	-.0873	2.41	-.0828	3.01	-.0796	3.09
-.1545	1.10	-.1526	1.52	-.1432	1.87	-.1373	2.26	-.1328	2.71	-.1296	2.75
-.2045	.94	-.2026	1.38	-.1932	1.75	-.1873	2.12	-.1828	2.45	-.1796	2.50
-.2545	.84	-.2526	1.26	-.2432	1.63	-.2373	1.97	-.2328	2.24	-.2296	2.29
-.3045	.77	-.3026	1.16	-.2932	1.51	-.2873	1.83	-.2828	2.06	-.2796	2.11

Fig. 8.4 Contd.

In most conventional aircraft, the horizontal tailplane is set 3–4 chord lengths aft of the aircraft c.g. (which is approximately at the wing quarter-chord). In the example problem, the wing semispan is 5 times the wing chord. With a stepsize of 0.25 semispans one would expect to find the horizontal tailplane at about the third step of the net in Fig. 8.2 behind the wing. Although tip vortex rollup is unlikely to impact the horizontal tailplane of the aircraft that generates it, the diameter of the vortex grows as the vortex moves downstream. When this is coupled with the fact that the strength of the vortex is dependent on the actual lift being generated, one can easily see the hazard created when a small aircraft enters the vortex field of a much larger aircraft.

Although the wing tip vortex is unlikely to impact the aircraft's own horizontal tailplane, the downwash field associated with it can have a very significant impact on the control of the aircraft. The reader may recall that the lift of the horizontal

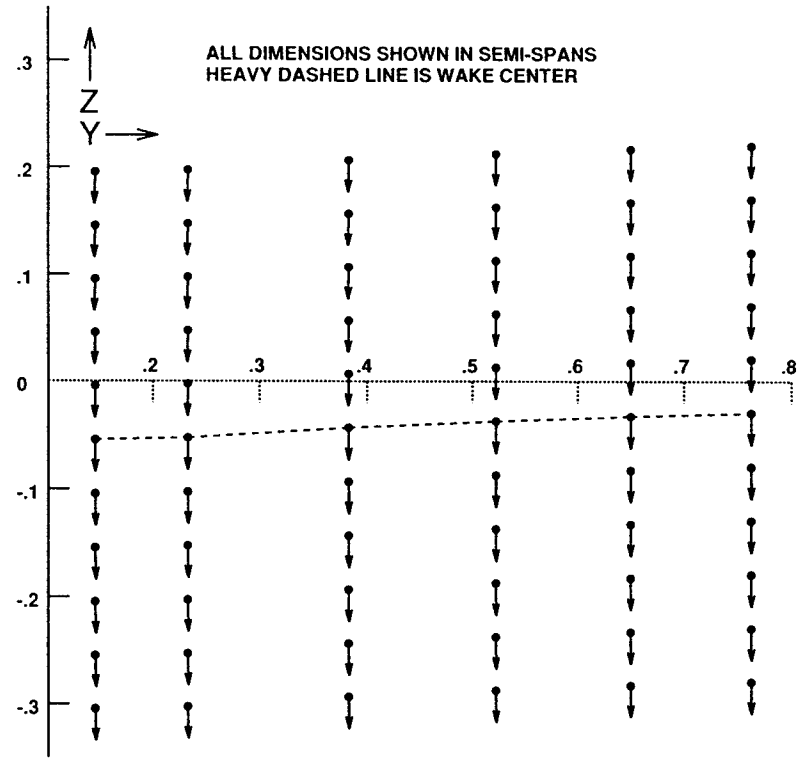

Fig. 8.5a Flowfield in Y–Z plane. The magnitude of the sidewash is dependent on the value of C_L, here about 1.0. To make it more apparent, add a scale factor of 20 to line 1157 in the program.

tailplane generates a pitching moment about the aircraft c.g., one that is needed to balance the wing's pitching moment. Because the tailplane lift is dependent on its angle of attack relative to the oncoming stream, the effect of the downwash is to reduce the tailplane's angle of attack and, hence, its lift. At high values of wing lift coefficient, the downwash angle at some values of Z near the aircraft's plane of symmetry may exceed 10 deg. If this had not been accounted for during the aircraft's design by changing the tailplane's incidence angle and locating the tailplane vertically in a position where the downwash is weaker, the most forward c.g. location at which the aircraft could be trimmed (balanced in steady flight) would be severly restricted.

The sidewash shown in Fig. 8.5a indicates the degree of spanwise flow taking place at various locations in the flowfield at $X = 0.75$ semispans. Note that the data plotted in the figure do not include Y values near the tip. Although this view does not depict the tip vortex field, it does show the sidewash in the flowfield through which the horizontal tail will fly. Note also that the lengths of all arrows are the same so that only the deviation from vertical of the arrow has meaning:

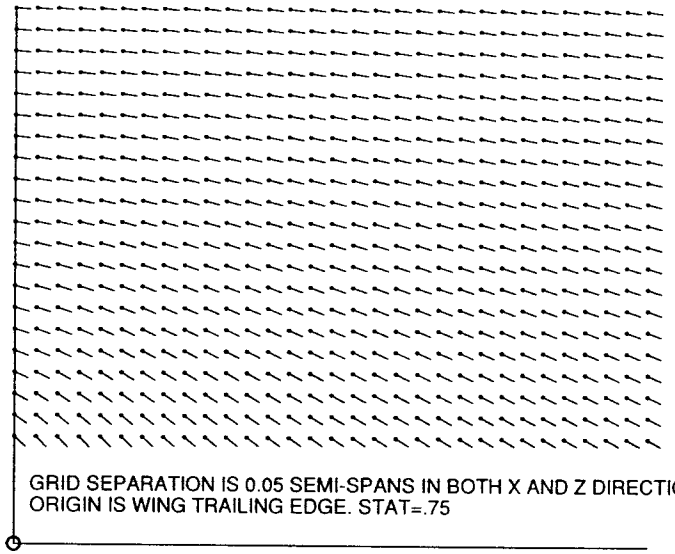

Fig. 8.5b Downwash in X–Z plane at $Y = 0$; vertical flow displacement is emphasized by a factor of 15.

vertical arrow equals zero sidewash. The deviation is shown here unamplified. The flow direction shown is that which exists at the origin of an arrow. The data from which this figure was made are available only when NXORY = 1.

In addition to a downwash effect, there is a momentum defect in the flow downstream of the wing resulting from the wing's profile drag. If the horizontal tailplane should encounter the momentum defect at its most severe, it can lose 10% or more of its effectiveness. Notice that the vertical location of the most severe momentum defect changes with changes in lift coefficient. For the spanwise stations of interest, this vertical location lies within the vortex sheet shown in Fig. 8.2. Hence, the computations used to determine the path of the shed vortex sheet also provide the starting point for the **WAKE** calculations.

There are several ways in which the downwash data could be presented graphically. The usual method is to draw contours of constant downwash angle. This is somewhat tedious because it is necessary to interpolate the available data to find the actual Z location for a specific contour at each X station. One could also show the direction by a short line tangent to the flow in the same manner as one depicts streamlines. This is essentially what is done experimentally with a tuft grid. If necessary, the angle of the line can be amplified (as was done in Fig. 8.5b) to render the flow angle changes more visible. The resulting figure is qualitative in nature rather than quantitative. Quantitative data can be obtained from the file. In any case, this technique is easily incorporated into the program or made into an auxillary program such as **DWASH.FOR**, which obtains its input from a portion of **WASH.TXT**. Note that the parameter STAT has a value of 0.75 for both figures but means the X distance to the Y–Z plane in the first case and Z value of the center of the X–Z plane in the second.

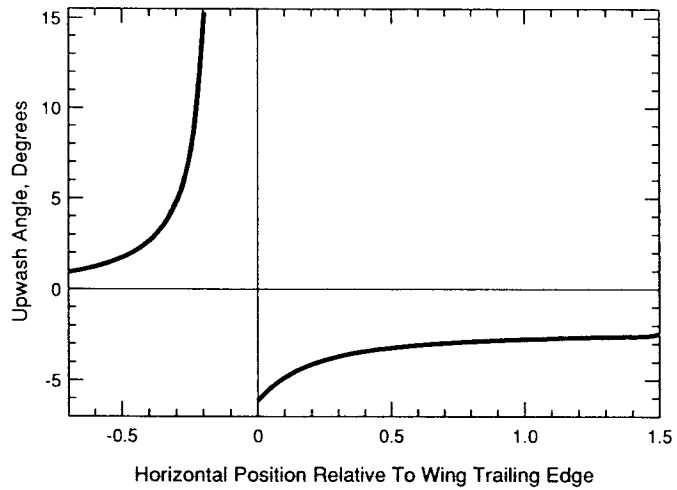

Fig. 8.5c Upwash and downwash magnitudes in the X–Y plane, which lies along the wing chord line. Generated with options NXORY = 2 and NXORY = 3.

Other data of interest also appear in the file **WASH.TXT**. The distribution of circulation along the span, for instance, is listed and thus may be easily plotted, if desired.

Figure 8.5b shows the flow direction in the plane of symmetry for the portion of the X–Z plane where one might expect the horizontal tail to located on a low-wing aircraft. Notice that the downwash diminishes as one moves up from the trailing edge and also as one moves downstream. This figure is generated for a value of STAT = 0.75. When STAT = 0.0, Z goes from -0.5 to $+0.5$. To use **DWASH** with STAT = 0.0, it will be necessary to change the value of ZZ0 on line 101 of **DWASH.FOR** and change the bias value on line 74 to 550 to shift the reference upward on the page. The vertical location of the text may have to be moved as well.

Figure 8.5c shows the magnitude of the downwash and the upwash ahead of the wing in the X–Y plane. (This is taken from a run with STAT = 0.0 and NXORY = 2. The data for $X < 0.0$ are obtained from a run with NXORY = 3.) Notice that the flow angle magnitudes are considerably greater than those in Fig. 8.5b. Perusal of the listing shows that, in general, the greatest downwash is at or below the $Z = 0$ line. The maximum downwash angle decreases as X increases. In the area of the tail it is about one-half that at the trailing edge. The flow would appear to be headed toward a 0-deg asymptote.

8.5 Program WAKE

We have been able to treat the problem of determining the Y–Z coordinates at specified values of X of the constituent parts of the vortex sheet that is shed from the wing by an integral technique, that it, a technique that did not require us to solve any differential equations. Such a technique can tell us the net result of fluid dynamic activity inside a volume but cannot give us any details of that activity. Thus, having determined the path of the shed vortex sheet and the associated inviscid downwash field, we now seek to find the magnitude and extent of the

velocity defect at various downstream locations in the viscous wing wake. For such a problem we are interested in fluid dynamic details; hence, we will have to solve some sort of differential equation.

The general problem is obviously three dimensional and so we will resort to experimental observations in an effort to find some reasonable assumptions to simplify the problem. To begin we recognize that we are interested in a region of flow whose extent in the Y direction is probably no more than 1/3 semispan from the fuselage and whose extent in the X direction is on the order of 3/4 semispan. In this region we observe that 1) vortex rollup is still minimal, 2) streamline curvature in either the Y or Z directions is very gradual, and 3) the wake centerline lies along the shed vortex sheet of inviscid theory. As a result of these observations we will assume that 1) we can treat the flow along the wake centerline as two dimensional 2) the position of the wake centerline is known a priori, and 3) because of the low curvature the pressure is constant across the wake and the describing differential equations are the two-dimensional boundary-layer equations. Therefore, we look for a method of solving these equations that yields the variation in streamwise velocity across the wake.

One technique for solving partial differential equations, which these are, is to first find a new independent variable that is a combination of the two previous independent variables. If we are successful, the transformed equations become ordinary differential equations and can be solved by one of the many analytical or numerical procedures available for this purpose. Even if we are not completely successful we may be able to transform the equations into a form that is easier to solve. We will assume that a suitable combination of independent variables is

$$\eta = \frac{y}{\sqrt{100 c_d t x}} \tag{8.14a}$$

$$\xi = x/c \tag{8.14b}$$

where:

c = wing chord at some value of wing semispan
t = wing thickness at this value of wing semispan
c_d = section profile drag coefficient
y = physical coordinate normal to the streamline
x = physical coordinate along the stream

In addition, we will assume that the flow can be described by the stream function

$$\psi(x, y) = U_\infty \sqrt{100 c_d t x}\, f(\xi, \eta) \tag{8.15}$$

where $f(\xi, \eta)$ is a function of the new independent variables whose explicit form is given by the solution of the equations.

We recall that the two-dimensional boundary-layer equations are written as follows.

$$u\frac{\partial u}{\partial x} + v\frac{\partial u}{\partial y} = \frac{1}{\rho}\frac{\partial \tau}{\partial y} \qquad \text{Equation for } x \text{ momentum} \tag{8.16a}$$

$$\frac{\partial u}{\partial x} + \frac{\partial v}{\partial y} = 0 \qquad \text{Continuity equation} \tag{8.16b}$$

We will consider the wake to be turbulent and, therefore, we should write

$$\tau = \rho \epsilon \frac{\partial u}{\partial y} \tag{8.17}$$

where ϵ is called the eddy viscosity coefficient. We will defer for the moment discussion on how ϵ is evaluated.

Substitution of the expression for τ into Eq. (8.16a) yields

$$u\frac{\partial u}{\partial x} + v\frac{\partial u}{\partial y} = \epsilon \frac{\partial^2 u}{\partial y^2} \tag{8.18a}$$

$$\frac{\partial u}{\partial x} + \frac{\partial v}{\partial y} = 0 \tag{8.18b}$$

If we substitute the expression for the stream function into the continuity equation, we have seen in Chapter 2 that the equation vanishes. To transform the remaining equation we first write the values of the following derivatives:

$$\frac{\partial \eta}{\partial y} = \frac{1}{\sqrt{100 c_d t x}} \tag{8.19a}$$

$$\frac{\partial \xi}{\partial x} = \frac{1}{c} \tag{8.19b}$$

$$\frac{\partial \psi}{\partial y} = u$$

$$u = \frac{\partial \psi}{\partial \eta}\frac{\partial \eta}{\partial y} = U_\infty \sqrt{100 c_d t x}\,\frac{\partial f}{\partial \eta}\frac{1}{\sqrt{100 c_d t x}} = U_\infty f' \tag{8.19c}$$

$$-\frac{\partial \psi}{\partial x} = v$$

$$= -U_\infty \left(\frac{f}{2x}\frac{100 c_d t x}{\sqrt{100 c_d t x}} + \sqrt{100 c_d t x}\,\frac{\partial f}{\partial \xi}\frac{\partial \xi}{\partial x} + \sqrt{100 c_d t x}\,\frac{\partial f}{\partial \eta}\frac{\partial \eta}{\partial x} \right)$$

$$= -U_\infty \sqrt{100 c_d t x} \left(\frac{f}{2x} + \frac{1}{c}\frac{\partial f}{\partial \xi} + f'\frac{\partial \eta}{\partial x} \right) \tag{8.19d}$$

$$\frac{\partial u}{\partial y} = \frac{U_\infty}{\sqrt{100 c_d t x}} f'' \tag{8.19e}$$

$$\frac{\partial^2 u}{\partial y^2} = \frac{U_\infty}{100 c_d t x} f''' \tag{8.19f}$$

$$\frac{\partial u}{\partial x} = U_\infty \frac{\partial f'}{\partial \xi}\frac{\partial \xi}{\partial x} + U_\infty \frac{\partial f'}{\partial \eta}\frac{\partial \eta}{\partial x} = \frac{U_\infty}{c}\frac{\partial f'}{\partial \xi} + U_\infty f''\frac{\partial \eta}{\partial x} \tag{8.19g}$$

When these expression are substituted into Eq. (8.18a) we have

$$(U_\infty f')\left(\frac{U_\infty}{c}\frac{\partial f'}{\partial \xi}+U_\infty f''\frac{\partial \eta}{\partial x}\right)$$
$$-U_\infty\sqrt{100c_d t x}\left(\frac{f}{2x}+\frac{1}{c}\frac{\partial f}{\partial \xi}+f'\frac{\partial \eta}{\partial x}\right)\left(\frac{U_\infty}{\sqrt{100c_d t x}}f''\right)=\frac{U_\infty \epsilon}{100c_d t x}f''' \tag{8.20}$$

Clearing the second term, dividing by U_∞^2, and multiplying by x gives

$$\xi f'\frac{\partial f'}{\partial \xi}-\frac{ff''}{2}-\xi f''\frac{\partial f}{\partial \xi}=\frac{\epsilon f'''}{100U_\infty c_d t}$$

or

$$\frac{\epsilon f'''}{100U_\infty c_d t}+\frac{ff''}{2}+\xi\left(f''\frac{\partial f}{\partial \xi}-f'\frac{\partial f'}{\partial \xi}\right)=0 \tag{8.21}$$

This is the equation that must be solved at every ξ to find $u=u(\eta)$. It is a third-order partial differential equation in a single dependent variable f and requires three boundary conditions,

$$u(x, y\to\infty)=U_\infty; \qquad f'(\xi,\infty)=1 \tag{8.22a}$$
$$u(x, y\to-\infty)=U_\infty; \qquad f'(\xi,-\infty)=1 \tag{8.22b}$$
$$v(x, y=0)=0; \qquad f(\xi,0)+2\xi\left.\frac{\partial f}{\partial \xi}\right|_{\xi=0}=0 \tag{8.22c}$$

The left-hand expressions give the boundary conditions in physical coordinates, and the right-hand expressions given them in transformed coordinates.

We will now make the substitution

$$T=f' \tag{8.23a}$$

so that our equation reads

$$\frac{\epsilon}{100U_\infty 100c_d t}T''+\frac{fT'}{2}+\xi\left(T'\frac{\partial f}{\partial \xi}-T\frac{\partial T}{\partial \xi}\right)=0 \tag{8.23b}$$

Now let

$$c_1=\frac{100U_\infty c_d t}{\epsilon} \tag{8.23c}$$

so that

$$T''+\frac{fc_1}{2}T'+c_1\xi\left(T'\frac{\partial f}{\partial \xi}-f'\frac{\partial T}{\partial \xi}\right)=0 \tag{8.24}$$

Then take

$$\alpha_1=c_1\left(\frac{f}{2}+\xi\frac{\partial f}{\partial \xi}\right) \tag{8.25a}$$
$$\alpha_2=-c_1\xi f' \tag{8.25b}$$

from which

$$T''+\alpha_1 T'+\alpha_2\frac{\partial f}{\partial \xi}=0 \tag{8.26}$$

We shall solve Eq. (8.26) by assuming a solution for α_1 and α_2. Then T can be found by integrating Eq. (8.26) numerically, and α_1 and α_2 can be updated. With the updated values a new solution for T can be found. The process is continued in this fashion until convergence is achieved. A finite difference scheme is employed in **WAKE** to convert Eq. (8.26) into a set of algebraic equations. Following Cebeci and Smith[41] we write

$$\left.\frac{\partial^2 T}{\partial \eta^2}\right|_{n,m+1}=\frac{T_{n+1,m+1}-2T_{n,m+1}+T_{n-1,m+1}}{(\Delta\eta)^2} \tag{8.27a}$$

$$\left.\frac{\partial T}{\partial \eta}\right|_{n,m+1}=\frac{T_{n+1,m+1}-T_{n-1,m+1}}{2\Delta\eta} \tag{8.27b}$$

$$\left.\frac{\partial T}{\partial \xi}\right|_{n,m+1}=\left[\frac{h_2}{h_1(h_1+h_2)}\right]T_{n,m-1}$$
$$-\left[\frac{h_1+h_2}{h_1h_2}\right]T_{n,m}+\left[\frac{h_1+2h_2}{h_2(h_1+h_2)}\right]T_{n,m+1} \tag{8.27c}$$

$$h_1=\xi_m-\xi_{m-1} \tag{8.27d}$$
$$h_2=\xi_{m+1}-\xi_m \tag{8.27e}$$

The subscripts refer to points on the grid as shown in Fig. 8.6.

These grid points are the only points at which the solution is actually obtained. Note that in contrast to the solutions of a differential equation, which, in this context, is found for any position in the ξ, η space, the solutions obtained by a finite difference technique are valid only at discrete points. The solution is not known anywhere else in the field. However, if the grid is reasonably fine this is not an obstacle of practical importance. The advantage achieved by making this approximation is that the system of algebraic equations is readily solved on a computer by modern matrix techniques, as we shall now demonstrate.

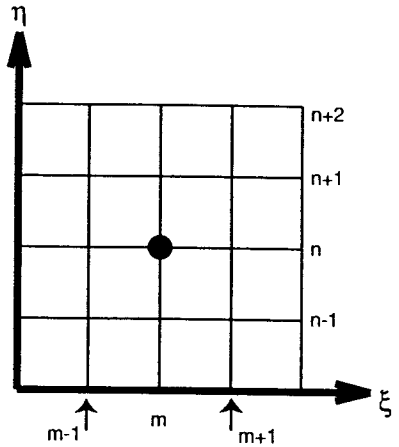

Fig. 8.6 Grid on which finite difference solution is evaluated.

When the approximations for the derivatives are subtituted into Eq. (8.26) we obtain

$$\left[\frac{1}{(\Delta\eta)^2}+\frac{\alpha_1}{2\Delta\eta}\right]T_{n+1,m+1}+\left[\frac{-2}{(\Delta\eta)^2}+\alpha_2\left(\frac{h_1+2h_2}{h_2(h_1+h_2)}\right)\right]T_{n,m+1}$$
$$+\left[\frac{1}{(\Delta\eta)^2}-\frac{\alpha_1}{2\Delta\eta}\right]T_{n-1,m+1}+\alpha_2\left[\left(\frac{h_2}{h_1(h_1+h_2)}\right)T_{n,m-1}\right.$$
$$\left.-\left(\frac{h_1+h_2}{h_1h_2}\right)T_{n,m}\right]=0 \tag{8.28}$$

or

$$A_nT_{n+1,m+1}+B_nT_{n,m+1}+C_nT_{n-1,m+1}=D_n \tag{8.29}$$

If we let

$$A_n=\frac{1}{(\Delta\eta)^2}+\frac{\alpha_1}{2\Delta\eta} \tag{8.30a}$$

$$B_n=\frac{-2}{(\Delta\eta)^2}+\alpha_2\frac{h_1+2h_2}{h_2(h_1+h_2)} \tag{8.30b}$$

$$C_n=\frac{1}{(\Delta\eta)^2}-\frac{\alpha_1}{2\Delta\eta} \tag{8.30c}$$

$$D_n=\alpha_2\left(\frac{-h_2}{h_1(h_1+h_2)}\right)T_{n,m-1}+\left(\frac{H_1+h_2}{H_1h_2}\right)T_{n,m} \tag{8.30d}$$

The total number, n_{max}, of η stations must be odd. The bottom of the wake ($\eta \to -\infty$) is defined by $n = 1$, while the top ($\eta \to \infty$) is defined by $n = n_{max}$. The wake center is definded by $n_{mid}[(n_{max}-1)/2]+1$. Therefore, the boundary conditions can be specified using the index n.

At $n = 1$,

$$T_{n,m+1}=1 \tag{8.31a}$$

At $n = n_{mid}$

$$f(\xi,0)+2\xi\left.\frac{\partial f}{\partial\xi}\right|_{(\xi,0)} \tag{8.31b}$$

At $n = n_{max}$

$$T_{n,m+1}=1 \tag{8.31c}$$

When written in matrix form, Eq. (8.29) is

$$\begin{bmatrix}1&0&0&0&&&&\\C_2&B_2&A_2&0&&&&\\0&C_3&B_3&A_3&&&&\\&&&&\ddots&&&\\&&&&&C_{n-2}&B_{n-2}&A_{n-2}&0\\&&&&&0&C_{n-1}&B_{n-1}&A_{n-1}\\&&&&&0&0&0&1\end{bmatrix}\begin{bmatrix}T_1\\T_2\\T_3\\\cdot\\\cdot\\\cdot\\T_{n-2}\\T_{n-1}\\T_n\end{bmatrix}=\begin{bmatrix}1\\D_2\\D_3\\\cdot\\\cdot\\\cdot\\D_{n-2}\\D_{n-1}\\1\end{bmatrix} \tag{8.32}$$

Because the matrix is tridiagonal the solution procedure can be greatly simplified. If the left matrix in Eq. (8.32) is designated as **A**, then

$$\mathbf{AT}=\boldsymbol{D} \tag{8.33}$$

where we employ the notation of a boldface upright character to represent a rectangular matrix. Equation (8.33) shows the two column matrices in Eq. (8.32) in boldface, also a commonly used representation. Readers unfamiliar with this notation may notice that one can write the system of equations this represents by inspection:

$T_1 = 1$

$T_1C_2 + T_2B_2 + T_3A_2 + \cdots = D_2$

etc.

Now let

$$\mathbf{A}=\mathbf{LX} \tag{8.34}$$

where

$$\mathbf{L} = \begin{bmatrix} \omega_1 & 0 & 0 & & & \\ \beta_2 & \omega_2 & 0 & & & \\ 0 & \beta_3 & \omega_3 & & & \\ & & \cdot & & & \\ & & & \cdot & & \\ & & & & \cdot & \\ & & & & \beta_{n-1} & \omega_{n-1} & 0 \\ & & & & 0 & \beta_n & \omega_n \end{bmatrix} \tag{8.35a}$$

$$\mathbf{X} = \begin{bmatrix} 1 & -E_1 & 0 & & & \\ 0 & 1 & -E_2 & & & \\ & & \cdot & & & \\ & & & \cdot & & \\ & & & & \cdot & \\ & & & & 0 & 1 & -E_{n-1} \\ & & & & 0 & 0 & 1 \end{bmatrix} \tag{8.35b}$$

and

$$\mathbf{LX} = \begin{bmatrix} \omega_1 & -\omega_1 E_1 & 0 & 0 & 0 \\ \beta_2 & (-E_1\beta_2 + \omega_2) & -E_2\omega_2 & 0 & 0 \\ 0 & \beta_3 & (-E_2\beta_2 + \omega_3) & -E_3\omega_3 & 0 \\ 0 & 0 & \beta_4 & (-E_3\beta_4 + \omega_4) & 0 \\ & & & & \cdot \\ & & & & \cdot \\ & & & & \cdot \end{bmatrix} \tag{8.35c}$$

Equations (8.35a), (8.35b), and (8.35c) use a bold equals sign. There is no particular significance to this. It was done simply to improve the visual appearance of the equation. The centered dots, of course, are meant to indicate that many rows of the matrix have simply not been written down because the form of the terms in these rows is similar to those in the rows above or below with appropriate changes in subscript values. The use of such matrix notation is usually a convenient and compact way to write what would otherwise be a dense page full of innumerable terms in a very large system of equations.

A finite difference scheme such as this for determining the the flowfield velocities is really feasible only through the use of a computer and is written to make use of the strengths of a computer. Assuming that one could find an analytical solution to the partial differential equation with these boundary conditions, it would be of an entirely different character, perhaps making use of a new class of functions or some special mathematical insight. This is another example showing that solution techniques are developed to take advantage of the tools at hand. As the tools change and become more powerful, the methods that employ them should also change.

Thus,

$$\begin{array}{lll} \beta_2 = C_2 & \omega_1 = 1 & -\omega_1 E_1 = 0 \\ \beta_3 = C_3 & -E_1\beta_2 + \omega_2 = B_2 & -\omega_2 E_2 = A_2 \\ \beta_4 = C_4 & -E_2\beta_3 + \omega_3 = B_3 & -\omega_3 E_3 = A_3 \\ \cdot & \cdot & \cdot \\ \cdot & \cdot & \cdot \\ \cdot & \cdot & \cdot \\ \beta_n = C_n & -E_{n-1}\beta_n + \omega_n = B_n & \omega_n E_n = A_n \end{array} \tag{8.36}$$

Applying these equations a step by step procedure is used to evaluate the β, ω, and E given the A_n, B_n, and C_n. From Eqs. (8.33) and (8.34)

$$\mathbf{LXT} = \mathbf{D} \tag{8.37}$$

and if

$$\mathbf{XT} = \mathbf{e} \tag{8.38}$$

then

$$\mathbf{Le} = \mathbf{D} \tag{8.39}$$

or

$$\begin{bmatrix} \omega_1 & 0 & 0 & 0 & & & & \\ \beta_2 & \omega_2 & 0 & 0 & & & & \\ 0 & \beta_3 & \omega_3 & 0 & & & & \\ 0 & 0 & \beta_4 & \omega_4 & & & & \\ & & & & \cdot & & & \\ & & & & & \cdot & & \\ & & & & & & \cdot & \\ & & & & & & \beta_{n-1} & \omega_{n-1} & 0 \\ & & & & & & 0 & \beta_n & \omega_n \end{bmatrix} \begin{bmatrix} e_1 \\ e_2 \\ e_3 \\ e_4 \\ \cdot \\ \cdot \\ \cdot \\ e_{n-1} \\ e_n \end{bmatrix} = \begin{bmatrix} D_1 \\ D_2 \\ D_3 \\ D_4 \\ \cdot \\ \cdot \\ \cdot \\ D_{n-1} \\ D_n \end{bmatrix} \tag{8.40}$$

If $e_1 = 1$ and $E_1 = 0$, then all of the e and E are evaluated using the relations

$$e_n = \frac{D_n - C_n e_{n-1}}{B_n + C_n E_{n-1}} \tag{8.41a}$$

and

$$E_n = \frac{-A_n}{B_n + C_n E_{n-1}} \tag{8.41b}$$

With these relations, Eq. (8.38) may be written as

$$\begin{bmatrix} 1 & -E_1 & 0 & 0 & & & & \\ 0 & 1 & -E_2 & 0 & & & & \\ 0 & 0 & 1 & -E_3 & & & & \\ & & & \ddots & & & & \\ & & & & \ddots & & & \\ & & & & & \ddots & & \\ & & & & & 0 & 1 & -E_{n-1} \\ & & & & & 0 & 0 & 1 \end{bmatrix} \begin{bmatrix} T_1 \\ T_2 \\ T_3 \\ \cdot \\ \cdot \\ \cdot \\ T_{n-1} \\ T_n \end{bmatrix} = \begin{bmatrix} e_1 \\ e_2 \\ e_3 \\ \cdot \\ \cdot \\ \cdot \\ e_{n-1} \\ e_n \end{bmatrix} \tag{8.42}$$

Starting with T_n, the n values of T are obtained by using the recursive relation

$$T_n = e_n + E_n T_{n+1} \tag{8.43}$$

These T_n values represent the solution at the ξ station $m + 1$. With these values known, one can then march forward to find all T_n at ξ station $m + 2$ and so forth. This type of recursive procedure is possible because the first matrix in Eq. (8.32) is tridiagnonal.

8.5.1 Procedure Summary

1) The solution is assumed to be known at station ξ_m for all n.

2) An approximate solution, T_{old}, is assumed at station ξ_{m+1} to evaluate the A_n, B_n, C_n, D_n, e_n, and E_n. (This approximate solution at station $m + 1$ is usually taken to be the solution for station m.)

3) Using the computed values of e_n and E_n, the solution T_{new} is calculated using Eq. (8.43).

4) T_{old} and T_{new} are compared to see whether they are the same at every n station to within a certain accuracy; if not, the T_{old} is set equal to T_{new} and steps 2 and 3 are repeated.

5) This iteration procedure is continued until T_{old} and T_{new} are sufficiently close, signaling a converged solution at the ξ station $m + 1$. Usually, no more than 2 or 3 iterations are required.

6) Steps 1–5 are repeated for each downstream station.

As noted in step 1, the finite difference technique requires that a solution be known at some ξ station to compute solutions downstream. Although an actual velocity profile is not known in general, a profile shape can be found at the trailing edge of an airfoil on both the upper and lower surfaces whenever the flow over an airfoil is calculated. One method of finding the viscous solution over an airfoil is given, as we have seen, in Chapter 5. There the flow is computed by solving the boundary-layer equations by a momentum integral technique. Using the output from the **AIRFOIL** program the velocity profiles on both surfaces may be determined from their respective boundary-layer thicknesses, form factors, and the equations

$$\frac{u_u}{U_\infty} = \left(\frac{y}{\delta_u}\right)^{\frac{H_u - 1}{2}} \tag{8.44a}$$

$$\frac{u_\ell}{U_\infty} = \left(\frac{y}{\delta_\ell}\right)^{\frac{H_\ell - 1}{2}} \tag{8.44b}$$

Although Eq. (8.44) do yield an initial velocity profile, there is still a problem due to the singular nature of the boundary-layer equations at the airfoil trailing edge. From Eqs. (8.14) it is evident that η is unbounded at $x = 0$ and, therefore, at $\xi = 0$. Therefore, some procedure or technique must be used to provide an initial profile downstream of the trailing edge. Examination of some experimental data suggested that the velocity profile a short distance downstream from the trailing edge is much the same as it is at the trailing edge. Consequently, the assumption was made that the velocity profile at 0.01 chord lengths downstream of the trailing edge is the same as at the trailing edge.

8.5.2 Eddy Viscosity

The eddy viscosity model used in **WAKE** is

$$\epsilon = \tilde{c} b_{\text{wake}} (u_{\max} - u_{\min}) \tag{8.45}$$

This model was derived by Prandtl for a fully developed wake flow. In general, the velocity term in parentheses represents the difference between the maximum and minimum velocity in the profile. Traditionally, b_{wake} represents the wake thickness or height at a velocity station halfway between the maximum and minimum velocity values. Also, $\tilde{c}$ is a constant whose value is to be determined. These parameters can be estimated given the velocity profile in a fully developed wake; but if the the initial profile is the trailing-edge profile, then another set of parameters must be defined, which will correlate with experimental measurements, because $u_{\max} - u_{\min}$ is always $u_{\max}$ at the trailing edge and b_{wake} is always smaller at the trailing edge than for a fully developed flow.

A value for the constant $\tilde{c}$ in the eddy viscosity model must also be chosen. Earlier, in Eq. (8.23a), the eddy viscosity appeared in the expression

$$c_1 = \frac{100 c_d t U_\infty}{\epsilon}$$

where

$$\epsilon = b_{\text{wake}} \tilde{c} (u_{\max} - u_{\min})$$

We could have also defined ϵ as

$$\epsilon = \frac{b_{\text{wake}} \tilde{c} (u_{\max} - u_{\min})}{U_\infty} \tag{8.46}$$

As a results of some experimental correlations, it was decided to redefine b_{wake} in Eq. (8.46) as the distance between the points in the wake where the velocities are 75% of the freestream value and to give $\tilde{c}$ a constant value of 0.03. These choices gave good agreement with experiment for small values of c_d. Such values are generally found only for $C_\ell < 0.8$, that is, for unseparated boundary-layer flows on the aft portions of the airfoil.

It may be remarked at this point that the whole idea of an eddy viscosity is an attempt to fit what is obviously not a laminar flow process within the confines of the mathematical description for laminar flow (traditional Navier–Stokes formulation for fluid motion). Turbulent flow involves additional motions by large groups of molecules, some of which may appear to be random, which are over and beyond the mass mean, or average, motion of the flow. It has proven to be difficult, if not impossible, to devise a solvable mathematical representation for these motions that matches our physical understanding of the nature of turbulence. Since Prandtl's time, therefore, it has been customary to use the eddy viscosity concept in place of or in addition to the dynamic viscosity associated with laminar flows when using the general Navier–Stokes model to represent such flows. Because the mathematical representation of turbulence within this model is semiempirical, one can devise many forms by which to express it. Each, it seems, has a limited range of applicability. None of the proposed models has been shown to work well over a large range of Reynolds numbers and pressure gradients. If truth be told, there has really been no significant advance in describing such flows for engineering purposes since Prandtl.

8.5.3 Caveats

To create a program without undue complexity, it was necessary to make a number of simplying assumptions. The limitations these assumptions place on the input data and on the results should be clearly understood by the program user. The first of these assumptions is that there is no pressure variation across the wake. Second, we will also assume that the section lift coefficient will always be less than about 0.8, which generally implies that there is no boundary-layer separation over the rear portion of the airfoil and that the section drag coefficient is near its minimum value. Third, we assume that the node spacing in Fig. 8.6 is sufficiently fine that the approximation of the partial differential equation by a set of finite difference equations will yield comparable results when the resulting system of algebraic equations is solved. Fourth, we assume that the initial velocity profile we obtain from the airfoil program is adequate to serve as our initial estimate.

8.6 Features of Program WAKE

The **WAKE** program solves the finite difference approximations to the boundary-layer equations as described in the preceding section. Running time is generally under 1 min on a Pentium 90 but may be longer if the number of iterations required for convergance becomes large or the number of X stations for which results are desired exceeds about 5.

The primary output is a listing of the velocity deficit at various positions above and below the wake centerline. Up to 20 such results can be computed at user selected X stations. A secondary form of output, added especially for the present version, is a PostScript file of the velocity profile at a particular X station. As many as 20 such files may be produced during a run. The data from which the PostScript figures are made are taken from the arrays used to print the results. The data in the arrays are then scaled to show the velocity defect a little more clearly. However, the Y dimension and the velocity magnitude scales are not shown on the PostScript graphs to permit them to be combined more readily into a single figure.


```
joukowski airfoil
     1601        20       156         4   1.00000   0.00001   0.00125   0.00005
  0.01000   0.03000   0.11800   0.01039   0.01378   0.05000
113 128 136 157
  0.02429   0.02429   1.41390   1.41390
```

Fig. 8.7 Typical data entry file for WAKE program.

8.7 Program Data Entry

Data are entered into **WAKE** via the file WAKE.DAT, a typical copy of which is shown in Fig. 8.7.

The first line contains title of the job in a 20A4 format.

On the second line are the number of mesh points (see Fig. 8.6) in the η direction, NPTS; the number of η steps between prints of the result in the η direction, NETAPT; the number of steps in the x or ξ direction, NXSTEP; the number of profiles for which results are requested, NXPRT; a proportionality constant for uneven stepsize in the η direction, AK; the accuracy for solution convergence, EPS; the stepsize in the η direction, DETA; and the stepsize in the X direction, DX, in chord lengths. The format is 4I10,4F10.5.

The first item on the third line is the X station at which the initial velocity profile is assumed, X(1). A value of 0.01 is generally used. The second item is the value of a constant used to evaluate the eddy viscosity model, CEDDY. A value of 0.03 correlates best with experimental data. The third item is the airfoil thickness at the station of interest, T, in chord lengths. The fourth item is the profile drag coefficient at the spanwise station of interest, CD. The last item is the minimum drag coefficient at the spanwise station of interest, CDMIN. CD and CDMIN are the same unless there is a significant amount of boundary-layer separation from the airfoil. These five items are entered in an F10.5 format. Most of the data can be obtained from **AIRFOIL**.

The fourth line gives the X stations at which printing of a velocity profile is desired. In this case these are the inital solutions, one for step 113, one for step 128, one for step 136, and one for step 157. These are in an I4 format.

The fifth line gives the boundary-layer thickness on the upper surface of the airfoil at its trailing edge, DELTAU; the boundary-layer thickness on the lower surface of the airfoil at the trailing edge, DELTAL; the form factor on the upper surface, HU; and the form factor on the lower surface, HL. The reader will recall that H is the boundary-layer displacement thickness divided by the momentum thickness. These are in an F10.5 format. The data may be obtained from **AIRFOIL**. No actual data from **WASH** are required; it is assumed that the analysis is carried out with repect to the centerline of the shed vortex sheet whose position is determined by **WASH**.

8.8 Typical Results

The first part of the output file produced by **WASH** is shown in Fig. 8.8.

The graphical output produced by **WAKE** for five X stations is shown in Fig. 8.9. **WAKE** actually produces each profile as a separate figure. They have been show here in the same figure to better illustrate the lateral growth of the wake and the decrease in the velocity deficit as the flow moves downstream. At the first X station, located at the trailing edge of the wing, as one should expect, the wake

```
joukowski airfoil
     NPTS   = 1601
     NMID   =  801
     NETAPT =   20
     NXSTEP =  156
     NXPRT  =    4
     NXPRNT =  113 128 136 157
     AK     =   .10000000D+01
     EPS    =   .10000000D-04
     DETA   =   .12500000D-02
     DX     =   .50000000D-04
     X(1)   =   .10000000D-01
     CEDDY  =   .30000000D-01
     B12    =   .60494085D-02
     T      =   .11800000D+00
     UMUDEL = -.32627526D+00
     CD     =   .10390000D-01
     DXSTEP =   .50000000D-01
     C1     =   .50936572D+03

     DELTAU =   .24290000D-01
     DELTAL =   .24290000D-01
     HU     =   .14139000D+01
     HL     =   .14139000D+01

       CONVERGENCE ATTAINED AFTER   1 ITERATIONS

       RESULTS FOR X/C STATION   1     X =    .10000000D-01
joukowski airfoil
```

ETA	U/UDEL	F	Y/C	(U/UDEL)**2
.10000000D+01	.10000000D+01	.88093587D+00	.35014568D-01	.10000000D+01
.97500000D+00	.10000000D+01	.85593587D+00	.34139204D-01	.10000000D+01
.95000000D+00	.10000000D+01	.83093587D+00	.33263840D-01	.10000000D+01
.92500000D+00	.10000000D+01	.80593587D+00	.32388476D-01	.10000000D+01
.90000000D+00	.10000000D+01	.78093587D+00	.31513112D-01	.10000000D+01
.87500000D+00	.10000000D+01	.75593587D+00	.30637747D-01	.10000000D+01
.85000000D+00	.10000000D+01	.73093587D+00	.29762383D-01	.10000000D+01
.82500000D+00	.10000000D+01	.70593587D+00	.28887019D-01	.10000000D+01
.80000000D+00	.10000000D+01	.68093587D+00	.28011655D-01	.10000000D+01
.77500000D+00	.10000000D+01	.65593587D+00	.27136291D-01	.10000000D+01
.75000000D+00	.10000000D+01	.63093587D+00	.26260926D-01	.10000000D+01
.72500000D+00	.10000000D+01	.60593587D+00	.25385562D-01	.10000000D+01
.70000000D+00	.10000000D+01	.58093587D+00	.24510198D-01	.10000000D+01
.67500000D+00	.99435732D+00	.55598848D+00	.23634834D-01	.98874648D+00
.65000000D+00	.98662128D+00	.53122577D+00	.22759469D-01	.97342156D+00
.62500000D+00	.97864556D+00	.50665942D+00	.21884105D-01	.95774713D+00
.60000000D+00	.97041268D+00	.48229563D+00	.21008741D-01	.94170076D+00
.57500000D+00	.96190309D+00	.45814109D+00	.20133377D-01	.92525756D+00
.55000000D+00	.95309484D+00	.43420297D+00	.19258013D-01	.90838978D+00
.52500000D+00	.94396312D+00	.41048905D+00	.18382648D-01	.89106638D+00
.50000000D+00	.93447977D+00	.38700775D+00	.17507284D-01	.87325244D+00
.47500000D+00	.92461259D+00	.36376826D+00	.16631920D-01	.85490844D+00
.45000000D+00	.91432457D+00	.34078063D+00	.15756556D-01	.83598942D+00
.42500000D+00	.90357280D+00	.31805590D+00	.14881192D-01	.81644381D+00
.40000000D+00	.89230716D+00	.29560627D+00	.14005827D-01	.79621206D+00
.37500000D+00	.88046852D+00	.27344532D+00	.13130463D-01	.77522481D+00
.35000000D+00	.86798644D+00	.25158821D+00	.12255099D-01	.75340047D+00
.32500000D+00	.85477600D+00	.23005207D+00	.11379735D-01	.73064202D+00
.30000000D+00	.84073341D+00	.20885635D+00	.10504371D-01	.70683266D+00
.27500000D+00	.82572981D+00	.18802341D+00	.96290063D-02	.68182971D+00
.25000000D+00	.80960232D+00	.16757922D+00	.87536421D-02	.65545592D+00
.22500000D+00	.79214053D+00	.14755441D+00	.78782779D-02	.62748661D+00

Fig. 8.8 First portion of WAKE program output as given in the WAKE.TXT file: notice that η goes from -1.0 to +1.0, whereas Y/C goes to ± 0.035.

.20000000D+00	.77306537D+00	.12798563D+00	.70029137D-02	.59763006D+00
.17500000D+00	.75199471D+00	.10891774D+00	.61275495D-02	.56549604D+00
.15000000D+00	.72838358D+00	.90407019D-01	.52521853D-02	.53054264D+00
.12500000D+00	.70141264D+00	.72526467D-01	.43768210D-02	.49197969D+00
.10000000D+00	.66975823D+00	.55375200D-01	.35014568D-02	.44857609D+00
.75000000D-01	.63104741D+00	.39096803D-01	.26260926D-02	.39822083D+00
.50000000D-01	.58025635D+00	.23921663D-01	.17507284D-02	.33669743D+00
.25000000D-01	.50271489D+00	.10296684D-01	.87536421D-03	.25272226D+00
.00000000D+00	.00000000D+00	.00000000D+00	.00000000D+00	.00000000D+00
-.25000000D-01	.50271489D+00	-.10296684D-01	-.87536421D-03	.25272226D+00
-.50000000D-01	.58025635D+00	-.23921663D-01	-.17507284D-02	.33669743D+00
-.75000000D-01	.63104741D+00	-.39096803D-01	-.26260926D-02	.39822083D+00
-.10000000D+00	.66975823D+00	-.55375200D-01	-.35014568D-02	.44857609D+00
-.12500000D+00	.70141264D+00	-.72526467D-01	-.43768210D-02	.49197969D+00
-.15000000D+00	.72838358D+00	-.90407019D-01	-.52521853D-02	.53054264D+00
-.17500000D+00	.75199471D+00	-.10891774D+00	-.61275495D-02	.56549604D+00
-.20000000D+00	.77306537D+00	-.12798563D+00	-.70029137D-02	.59763006D+00
-.22500000D+00	.79214053D+00	-.14755441D+00	-.78782779D-02	.62748661D+00
-.25000000D+00	.80960232D+00	-.16757922D+00	-.87536421D-02	.65545592D+00
-.27500000D+00	.82572981D+00	-.18802341D+00	-.96290063D-02	.68182971D+00
-.30000000D+00	.84073341D+00	-.20885635D+00	-.10504371D-01	.70683266D+00
-.32500000D+00	.85477600D+00	-.23005207D+00	-.11379735D-01	.73064202D+00
-.35000000D+00	.86798644D+00	-.25158821D+00	-.12255099D-01	.75340047D+00
-.37500000D+00	.88046852D+00	-.27344532D+00	-.13130463D-01	.77522481D+00
-.40000000D+00	.89230716D+00	-.29560627D+00	-.14005827D-01	.79621206D+00
-.42500000D+00	.90357280D+00	-.31805590D+00	-.14881192D-01	.81644381D+00
-.45000000D+00	.91432457D+00	-.34078063D+00	-.15756556D-01	.83598942D+00
-.47500000D+00	.92461259D+00	-.36376826D+00	-.16631920D-01	.85490844D+00
-.50000000D+00	.93447977D+00	-.38700775D+00	-.17507284D-01	.87325244D+00
-.52500000D+00	.94396312D+00	-.41048905D+00	-.18382648D-01	.89106638D+00
-.55000000D+00	.95309484D+00	-.43420297D+00	-.19258013D-01	.90838978D+00
-.57500000D+00	.96190309D+00	-.45814109D+00	-.20133377D-01	.92525756D+00
-.60000000D+00	.97041268D+00	-.48229563D+00	-.21008741D-01	.94170076D+00
-.62500000D+00	.97864556D+00	-.50665942D+00	-.21884105D-01	.95774713D+00
-.65000000D+00	.98662128D+00	-.53122577D+00	-.22759469D-01	.97342156D+00
-.67500000D+00	.99435732D+00	-.55598848D+00	-.23634834D-01	.98874648D+00
-.70000000D+00	.10000000D+01	-.58093587D+00	-.24510198D-01	.10000000D+01
-.72500000D+00	.10000000D+01	-.60593587D+00	-.25385562D-01	.10000000D+01
-.75000000D+00	.10000000D+01	-.63093587D+00	-.26260926D-01	.10000000D+01
-.77500000D+00	.10000000D+01	-.65593587D+00	-.27136291D-01	.10000000D+01
-.80000000D+00	.10000000D+01	-.68093587D+00	-.28011655D-01	.10000000D+01
-.82500000D+00	.10000000D+01	-.70593587D+00	-.28887019D-01	.10000000D+01
-.85000000D+00	.10000000D+01	-.73093587D+00	-.29762383D-01	.10000000D+01
-.87500000D+00	.10000000D+01	-.75593587D+00	-.30637747D-01	.10000000D+01
-.90000000D+00	.10000000D+01	-.78093587D+00	-.31513112D-01	.10000000D+01
-.92500000D+00	.10000000D+01	-.80593587D+00	-.32388476D-01	.10000000D+01
-.95000000D+00	.10000000D+01	-.83093587D+00	-.33263840D-01	.10000000D+01
-.97500000D+00	.10000000D+01	-.85593587D+00	-.34139204D-01	.10000000D+01
-.10000000D+01	.10000000D+01	-.88093587D+00	-.35014568D-01	.10000000D+01

Fig. 8.8 Contd.

center velocity is 0.0. The small values, which would have extended the figure far to the left (those which correspond to 0.0), have been removed from the figure in the interests of obtaining a more compact representation. The significant aspects of the figure are just how small the vertical extent of the actual wake region is in the neighborhood of the horizontal tail location and what the magnitude of the momentum deficit is. It will be seen in the figure that the total momentum deficit region is about 1/3 chord lengths wide at 2 chord lengths aft of the wing trailing edge. The maximum value of the velocity deficit is 9%.

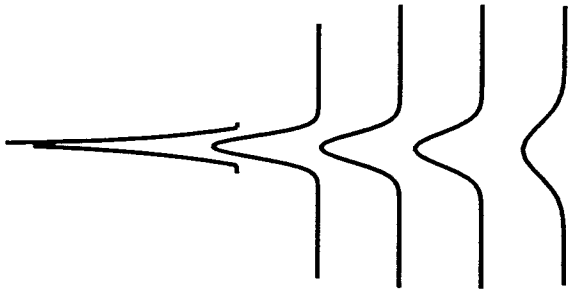

Fig. 8.9 Velocity profiles in wing wake at $X = 0.01$, $X = 0.245$, $X = 0.5$, $X = 0.734$, and $X = 2.03$ measured from trailing edge in chords. Note: X positions of profiles are not shown to scale; vertical extent of profiles is approximately ± 0.2 chords; maximum velocity deficit at $X = 2.45$ is 9%.

This region of velocity deficit moves up and down in the Z direction as the angle of attack changes. The case selected here for analysis has a fairly large value of profile drag and so corresponds to a fairly high angle of attack. The direction and position of the shed vortex sheet is also related to the angle of attack. Together there is enough effect to warrant running these analyses if the use of a low mounted horizontal tailplane is contemplated. A horizontal tailplane mounted on top of the vertail tail almost never encounters a momentum defect due to the wing wake unless the wing, too, is mounted high.

8.9 Concluding Remarks

In this chapter we have sought to present rigorous methods by which the direction and magnitude of the flow approaching the horizontal tailplane of an airplane can be determined. We found that the flow direction could be determined by an inviscid method similar to that used to determine the induced drag of a wing, provided we ignored the interaction of the downwash field with flow around the fuselage. Particularly for the case where the wings emanate from the middle of the fuselage, this effect is expected to be small. We also ignored the effect of the small upwash field created by the horizontal tailplane on the downwash field of the main wing. Upwash fields are smaller than downwash fields for a given wing (see Fig. 8.5b) and their strength is proportional to the area of the wing creating them. Given that the horizontal tailplane is usually on the order of 20% of the area of the main wing, this assumption seems reasonable.

We determined the magnitude of the flow in the downwash field by the use of the **WAKE** program. Here we assumed that the analysis could be applied along the centerline of the wake as shed from the wing trailing edge, that the curvature of the wake was sufficiently small that the pressure across the wake could be considered to be constant, that in the region of interest the spanwise flow component was sufficiently small that we could employ a two-dimensional analysis, and that as a result of these assumptions the governing equations are the turbulent boundary-layer equations, which we solved by a finite difference scheme. Such a scheme transforms the partial differential equation into a set of algebraic equations, which are readily solved on a computer by the techniques

of linear algebra. From the solution we were able to determine the magnitude of the velocity deficit as a function of distance above and below the centerline of the wake. The aircraft designer's task is then to keep the horizontal tailplane out of the wake region over as much of the aircraft's angle-of-attack range as possible.

The **WAKE** and **WASH** programs provide the tools to enable the designer to identify the regions to avoid and to compute the penalty involved when avoidance is not possible.

Problems

8.1. It is desired to obtain a graphical indication of the downwash field behind a wing near stall. Run **F2D3D** for a case where the lift coefficient is about 1.5. Transfer the necessary data and create an input file for **WASH**. Modify **WASH** so that the downwash data are also written to the file **WASHT.DAT** in the format required for **DWASH**. Create a PostScript plot of the downwash field. From this plot and the output file determine how much of an incidence angle should be applied to a horizontal tailplane that is to be located 0.25 semispans above and 0.8 semispans behind the wing trailing edge to compensate for the downwash. Note that the PostScript file is easily enlarged by changing the scaling directive on the second line. To alter the amplification of the flow angle, change the value on line 1157 of **DWASH.FOR**, recompile, and then execute.

8.2. If the horizontal tailplane is to located 0.8 semispans aft of the wing trailing edge and 1.0 semispan above it, how would your answer change?

8.3. If the vertical position of the horizontal tailplane is in line with the wing at a point 0.8 semispans behind it, what compensation is required?

8.4. You have probably noticed that at each of the three previous locations the required compensation angle was different. At each of these locations the compensation required also changes with lift coefficient (or speed). Unless the airplane has an all movable tail with automatic compensation adjustment, a single incidence angle must be chosen that does not give the proper compensation at any other lift coefficient. What is an effective strategy to minimize this problem? (The strategy, however, may not be available in all cases.)

8.5. Figure 8.5c shows the downwash angle slowing approaching zero as X increases. Argue the validity or nonvalidity of this result on physical grounds.

The following seven problems test semiempirical equations related to wakes found in the literature.

8.6. Use the results of a **WAKE** run and attempt to match the velocity profile at some downstream point in the wake by the following equation:

$$\frac{u(y/d_{\text{wake}})}{U_\infty} = \cos^2\left(\frac{\pi}{2}\frac{y}{d_{\text{wake}}}\right)$$

Note your results will depend somewhat upon your selection of the definition of d_{wake}, the width of the half-wake. a) Report and graph your results. Be sure you identify your selection of the definition of d_{wake}. b) Try the problem with the left side of the equation equal to

$$\left(\frac{u(y/d_{\text{wake}})}{U_\infty}\right)^2$$

8.7. a) Repeat problem 8.6 for the following equation:

$$\frac{u(y/d_{\text{wake}})}{U_\infty} = \left[1 - \left(\frac{y}{d_{\text{wake}}}\right)^{1.75}\right]^2$$

b) Also try this equation with the left-hand side equal to

$$\left(\frac{u(y/d_{\text{wake}})}{U_\infty}\right)^2$$

Which equation or variation thereof gives the best fit?

8.8. If ζ is the width of the half-wake divided by the wing chord and ξ is the distance behind the wing chord divided by the wing chord generate a plot of ζ vs ξ. On the same graph plot the equation

$$\zeta = 0.68\sqrt{c_{d_0}}\sqrt{\xi + 0.15}$$

How do they compare?

8.9. If η is $(u/U_\infty)^2$, how well does the equation

$$\eta = \frac{2.42\sqrt{c_{d_0}}}{\xi + 0.3}$$

fit the data?

8.10. At a downstream location, say, $X = 0.5c$, evaluate the equation

$$d_0 = \rho \int_{-d_{\text{wake}}}^{d_{\text{wake}}} u\,(U_\infty - u)\,\mathrm{d}y$$

Then divide your result by $\rho U_\infty^2/2$ and compare with the value of c_{d_0} you used in problem 8.8 or problem 8.9. Show all steps and report your results.

8.11. Use the following nomenclature:

d = cylinder diameter
C_D = cylinder drag coefficient
u = velocity in the wake at a point y above or below the wake centerline
x = distance downstream of the cylinder
ϵ_0 = constant of eddy viscosity
η = nondimensionalized y coordinate, $y\sqrt{U_\infty/\epsilon_0 x}$
U_∞ = freestream velocity

and generate a plot of the equation

$$\frac{u}{U_\infty} = \frac{1}{4\sqrt{\pi}}\left(\frac{U_\infty C_D d}{\epsilon_0}\right)^{0.5}\left(\frac{x}{C_D d}\right)^{-0.5} e^{-\eta^2/4}$$

Consult a fluid mechanics text to find a suitable C_D value of a cylinder with a turbulent wake. Make d and U_∞ consistent with the Reynolds number for which you have selected the drag coefficient. Let

$$\epsilon_0 = 0.47\left(2b_{\frac{1}{2}}u_{\max}\right)$$

where:

$b_{\frac{1}{2}}$ = half the wake width between $u_{\max}$ and $u_{\min}$ at some x station
$u_{\max}$ = the maximum value of u in the wake at that x station

Does it appear to possess the correct variation with x and y?

8.12. Repeat problem 8.11 for the following equation:

$$\frac{u}{U_\infty} = \frac{\sqrt{10}}{18(0.18)}\left(\frac{x}{C_D d}\right)^{-0.5}\left\{1 - \left(\frac{y}{b}\right)^{1.5}\right\}^2$$

Which equation gives the better result?

8.13. Run **WAKE** for a Reynolds number of 10^7 and again for a Reynolds number of 10^4. Note any differences in results. This will require that you get two sets of data from **AIRFOIL**.

8.14. Attempt to determine at what value of X the vortex rollup becomes too great for program **WASH** to accommodate. Determine if this distance is sufficient to permit the program to be used to determine potential upsets encountered by aircraft following behind larger aircraft and explain.

8.15. Explain why a finite difference technique was used to solve the boundary-layer equation in program **WAKE** rather than a momentum integral technique such as was used in program **AIRFOIL**.

9
Computational Fluid Dynamics

9.1 Introduction

WE saw in Chapter 8 that when the problem of analyzing the velocity distribution in the wake of an airfoil was formulated in such a way as to take advantage of those computational processes that computers perform very efficiently, we employed a finite difference scheme from which we obtained solutions to the governing equation only at discrete points in the flowfield, or, we might say, on the nodes of a net. In this chapter we briefly consider the task of extending this concept of devising analysis techniques tailored to the strengths of the computer to treat more complex fluid dynamics problems. The purpose is to indicate the direction, mathematically speaking, in which these newer design and analysis techniques for determining the forces developed by moving wings and bodies are evolving. Because these methods all involve the solution of partial differential equations, first we will consider how such equations are classified because this determines how the boundary conditions (and initial conditions, if required) must be specified.

9.2 Classification of Partial Differential Equations

Partial differential equations, we recall, are those differential equations where there is more than one independent variable. Equations (4.9) are one form of the momentum equations that are part of the complete Navier–Stokes equations. In their most general form they are written for unsteady flow of compressible, heat conducting gases and require, in addition to the continuity and three momentum equations, an energy equation and an equation of state. The momentum equation in Chapter 4 [Eq. (4.9)] is written for steady flow of an incompressible medium and, therefore, has put ρ outside the partial derivative symbols. It can be shown that if the velocity changes are small enough for this approximation to be valid, then the energy equation and the equation of state are not needed.

Written as shown in Eq. (4.9), the partial differential equation is first order. If we write the velocity components in terms of a stream function, however, the resulting equation is second order. This is the form commonly used for many analyses. We may recall from our study of analytical geometry that the equation for an ellipse can be written as

$$\frac{x^2}{A^2} + \frac{y^2}{B^2} = 1 \tag{9.1}$$

whereas the equation for the trace of a hyperboloid can be written as

$$\frac{x^2}{A^2} - \frac{y^2}{B^2} = 1 \tag{9.2}$$

The equation for a parabola contains one first-order term and one second-order term,

$$y = Ax^2 \tag{9.3}$$

By analogy with these geometric figures, two-dimensional second-order partial differential equations are classified as elliptical, such as

$$\frac{\partial^2 \psi}{\partial x^2} + \frac{\partial^2 \psi}{\partial y^2} = 0 \tag{9.4}$$

hyperbolic, such as

$$\frac{\partial^2 \psi}{\partial x^2} - \frac{\partial^2 \psi}{\partial y^2} = 0 \tag{9.5}$$

or parabolic, such as

$$\frac{\partial T}{\partial t} - \frac{\partial^2 T}{\partial x^2} = 0 \tag{9.6}$$

Each of these equation types have different requirements for specifying their boundary conditions. The boundary conditions for elliptical partial differential equations (PDEs), for example, are specified on the outer surface of the flow regime, often at infinity. A change in a boundary condition is immediately reflected as a change in the dependent variable throughout the entire flow regime. As a result, we say that the velocity of signal propagation in such a flow is infinite.

When one of the independent variables in Eq. (9.5) is time, the equation is called the wave equation. It requires two boundary conditions and two initial conditions to obtain a solution. Hyperbolic PDEs such as Eq. (9.5) have regions of influence. The flow outside of these regions is unaffected by a change in the flowfield inside the region. The velocity of signal propagation in such flowfields is finite.

Steady supersonic flows can also be described by a hyperbolic PDE, often written as

$$(1 - M_\infty^2)\phi_{xx} + \phi_{yy} = 0 \tag{9.7}$$

This equation is hyperbolic as long as $M_\infty > 1$ and elliptic if $M_\infty < 1$. In supersonic flow the boundary between the region of influence and that which does not perceive the flow is formed in two ways: first by a shock wave, the so-called strong solution or, second, by two straight lines (called characteristics), which emanate from the point of interest and extend in the streamwise direction, one with a slope of $1/\sqrt{M_\infty^2 - 1}$ and the other with a slope of $-1/\sqrt{M_\infty^2 - 1}$, the weak solution. In three dimensions the zone of influence is conical. The speed of signal propagation along the characteristics is the speed of sound. Strong disturbances travel at a higher speed (up to 2.5 times the speed of sound), which is why attempts to measure the speed of sound by timing the interval between the appearance of a muzzle flash and the report of a cannon give values higher than the speed of sound.

When $M_\infty^2 \to 0$, Eq. (9.7) becomes elliptic.

Parabolic PDEs exert an influence over a semi-infinite region. The unsteady, one-dimensional heat conduction equation is an example of a parabolic PDE. The velocity of signal propagation in a parabolic PDE is generally finite, which means that it takes a finite amount of time for the heat injected at one end of an insulated rod to travel to its other end. The amount of heat present at any point along the rod is indicated by the local temperature. This will change with time and with the type of boundary conditions (either a fixed temperature or a definite heat transfer rate).

The Laplace equation is an example of an elliptical PDE. In such a PDE, the velocity of signal propagation is infinite.

When approximate methods are devised to solve these equations, the requirements for proper specification of the boundary conditions, the regions of influence, and the speed of disturbance propagation must all be taken into account.

Reference 42 is a very detailed exposition of many of the finite difference methods, their strengths, weaknesses, computational problems, etc., for solving fluid dynamic and heat transfer problems, which have been developed over the years. Readers seriously interested in pursing advanced computational methods for solving such problems will find this source an unexcelled primer.

9.2.1 Euler Formulation

When the viscous terms are removed from the Navier–Stokes equations one has what are called the Euler equations after Leonhard Euler, who published his studies of these equations beginning in 1755. These equations are suitable for the analysis of flow phenomena wherein viscosity is not a significant mechanism. From the standpoint of computational fluid dynamics, one is concerned with finding algorithms that permit rapid and accurate solution of the set of equations that approximate the PDEs and with algorithms that set up suitable computational nets, the nodes of which are the points at which the solutions for the velocity components are determined. The nets must have a sufficiently fine mesh to define the geometry adequately yet not so fine that the problem becomes computationally impossible. The Euler equations are either elliptic or hyperbolic depending on the magnitude of the Mach number.

Around $M_\infty = 1$ there exists what is called the transonic flow regime. For small disturbances the describing equation can be written

$$\left[\frac{1 - M_\infty^2}{M_\infty^2} - (\gamma + 1)\frac{u'}{U}\right] M_\infty^2 \phi'_{xx} + \phi'_{yy} = 0 \tag{9.8}$$

where we use the prime as a way of expressing the small difference between a dependent variable and a constant value at any time, such as in the expression

$$u = U + u'$$

This nonlinear equation is either elliptic or hyperbolic depending on the magnitude of the Mach number. The reader will recognize that at flight near $M_\infty = 1$ some regions of the flowfield around a body or wing will be subsonic while others will be supersonic, which adds greatly to the difficulty.

9.2.2 Navier–Stokes Formulation

In the Navier–Stokes formulation, one has the additional complication of the effects viscosity to consider. Not only are the individual equations more complex, there are more of them and they are of a higher order than the Euler equations, which means additional boundary conditions are required. The unsteady, compressible Navier–Stokes equations are a set of mixed hyperbolic–parabolic equations, whereas the unsteady, incompressible Navier–Stokes equations are a mixed set of elliptic–parabolic equations. As a consequence, different numerical techniques must be used to solve the Navier–Stokes equations in compressible and incompressible flow regimes.

9.3 Major Problems in Computational Fluid Dynamics

The straightforward concept of representing the derivatives in the equations of fluid motion by finite differences to transform these equations into a system of algebraic equations is one that modern digital computers are optimized to solve. Problems arise when one attempts to implement the concept. Principal among these are the stability of the solution (i.e., does the solution go rapidly to infinity or does it tend toward a physically meaningful result?), the time required to compute a solution, and the selection and construction of a computational grid, which is at the same time sufficient to yield the desired flow detail yet not overly consuming of computer resources. We will consider each of these problems briefly.

9.3.1 Solution Stability

Reference 42 explains,

> The stability problem in numerical analysis is similar to the problem of stability encountered in a modern control system. The transfer function plays the role of difference operator.... The stability of such a system depends upon the operations performed by the black box (transfer function) on the input data.... A controls system engineer would require that the transfer function have no poles in the right-half plane. Without this requirement, input signals would be falsely amplified and the output would be useless; in fact it would grow without bound. Similarly, the way in which the difference operator alters the input information to produce the solution at the next time level is the central concern of stability analysis.

Needless to say, different algorithms operate differently. Part of the problem is how they respond to roundoff and discretization. Roundoff error is that error resulting from a change or no change in the least significant digit retained in a number to account for the values of even less significant digits. If we designate the solution obtained by a machine using an infinite number of digits as D and the solution obtained by a machine with a finite number of digits as N, then the roundoff error is $N - D$. The difference between D and the analytical solution A we call the discretization error. Fortunately, there are procedures that indicate the stability of the various methods in a manner similar to the Routh–Hurwitz criteron in control theory. Examination of its stability should be an integral part of the process of selecting an algorithm.

9.3.2 Time Required to Effect a Solution

Depending on the type of problem, certain algorithms are more efficient in arriving at a solution than are others. There is no one method that is superior for all types of problem. If the problem is relatively simple this may not be of great concern; however, if the problem is complex, the choice of an efficient algorithm may be the difference between solving the problem or not solving it. Because the times required for certain algorithms to solve certain kinds of problems are known and are reported in the literature, selection of an algorithm to solve a given problem should include an investigation of the projected computational time requirements. An absolutely stable algorithm that takes too long to reach a solution is of no use.

9.3.3 Selection of Computational Grid

On the selection of a computational grid, Ref. 42 comments:

> The solution of a system of partial differential equations can be greatly simplified by a well-constructed grid. It is also true that a grid that is not well suited to the problem can lead to an unsatisfactory result. In some problems, improper choice of grid point locations can lead to apparent instability or lack of convergence. One of the central problems in computing numerical solutions to partial differential equations is that of grid generation.

Many procedures can be followed in developing grids. One popular method described in Ref. 42 is as follows:

> ...transform the physical domain into a computational domain. Numerous advantageous accrue when this procedure is followed. For example, the body surface can be selected as a boundary in the computational plane permitting easy application of the surface boundary condition.... Several requirements must be placed on such mappings. A partial list can be stated as follows:
>
> 1. The mapping must be one on one.
> 2. The grid lines should be smooth to promote continuous transformation derivatives.
> 3. Grid points should be closely spaced in the physical domain where large numerical errors are expected.
> 4. Excessive grid skewness should be avoided...since it...sometimes exagerates truncation errors.

Several methods for grid generation follow explicit rules and thus can be automated. The various processes involved, however, are details beyond the view we wish to bring to the present discussion. For example, Ref. 42 devotes an entire 30-page chapter to the subject. Grid generation remains one of the most difficult aspects of the task of applying computational fluid dynamics (CFD) to the analysis of the characteristics of real configurations.

9.4 Practical Application

An indication[43] of the accuracy and cost achievable with current CFD codes is that the predicted maximum reverse thrust produced by a 10 passenger twin engine business jet in ground effect was within 5% of the value obtained from actual

test data. The three-dimensional calculation employed approximately 0.5×10^6 grid points and required 5 h of CPU time on an SGI Indigo 2, a very powerful workstation that can run the problem in about 1/5 the time that would be required by a 133-MHz Pentium. The company that ran the problem developed the code, as well as three other CFD codes of various capabilities over a 20–25 year period, primarily with government sponsorship. It now derives a significant portion of its income by acting as a service bureau, that is, by applying its codes to customer problems for a fee.

9.5 Other Methods

In addition to the finite difference methods such as that discussed in Chapter 8, some problems are amenable to solution by integral techniques. An example of this approach is the determination of the temperature distribution in an infinite rod as a function of time given some initial temperature distribution. (Although we are using temperature as the dependent variable in this problem, any scalar fluid property with a distribution described by the same equation could have been used in the place of temperature.) We assume for this example that all surfaces of the rod are insulated so that no heat enters or leaves the rod. To simplify the problem we will take

$$\frac{\partial T}{\partial x} = 0 \qquad \text{at} \qquad x = 0 \tag{9.9a}$$

This implies that the temperature distribution is symmetrical with respect to the origin of the coordinate system. We will say the initial temperature distribution is given by

$$T(x, 0) = f(x) \tag{9.9b}$$

The equation describing the temperature distribution in the rod as a function of time and distance is

$$\frac{\partial T}{\partial t} = \frac{\partial^2 T}{\partial x^2} \tag{9.9c}$$

for $t \geq 0$ and $0 < x < \infty$. Applying the Laplace transform to this equation yields

$$\frac{\partial \Phi}{\partial t} - S^2 \Phi = 0 \tag{9.10}$$

where

$$\Phi(S, t) = \int_0^\infty e^{-Sx} T(x, t)\, dx \tag{9.11}$$

and

$$\int_0^\infty \frac{\partial^2 T}{\partial x^2} e^{-Sx} dx = S^2 \Phi(S, t) - ST(0+) - \frac{\partial T}{\partial x}(0+) \tag{9.12}$$

The last two terms on the right are boundary conditions, which we will assume to be zero.

The solution of the transformed PDE (9.10) is

$$\Phi = Ae^{S^2 t} \tag{9.13}$$

where

$$A = \int_{-\infty}^{\infty} f(\lambda) e^{-S\lambda} d\lambda \tag{9.14}$$

In this expression, $f(\lambda)$ represents the distribution of temperature along x at $t = 0$. We use a dummy variable to enable us to perform unambiguous integrations over the entire length of the rod when this is required to determine the variation in temperature with time at a particular value of x. With this definition for A, we can write the solution to the PDE as

$$\Phi(S, t) = e^{S^2 t} \int_0^\infty f(\lambda) e^{-S\lambda} d\lambda \tag{9.15}$$

Inversion of Eq. (9.15) to the time domain yields

$$\begin{aligned} T(x, t) &= \frac{1}{2\pi j} \int_{-\infty}^{\infty} e^{S^2 t} \left[\int_0^\infty f(\lambda) e^{-S\lambda} d\lambda \right] e^{Sx} dS \\ &= \frac{1}{2\pi j} \int_{-\infty}^{\infty} f(\lambda) d\lambda \int_0^\infty e^{S^2 t - S\lambda + Sx} dS \end{aligned} \tag{9.16}$$

But

$$S^2 t - S(x - \lambda) = \left\{ S\sqrt{t} - \frac{(x - \lambda)}{2\sqrt{t}} \right\}^2 - \frac{(x - \lambda)}{4t} \tag{9.17}$$

Now, call

$$S\sqrt{t} - \frac{x - \lambda}{2\sqrt{t}} = u \tag{9.18a}$$

and

$$du = \sqrt{t}\, dS \tag{9.18b}$$

Then,

$$T(x, t) = \frac{1}{2\pi j} \int_{-\infty}^{\infty} f(\lambda) e^{\frac{(x-\lambda)^2}{4t}} d\lambda \int_0^\infty e^{-u^2} \frac{du}{\sqrt{t}} \tag{9.19}$$

But

$$\int_0^\infty e^{-u^2} du = \sqrt{\pi} \tag{9.20}$$

so that

$$T(x,t) = \frac{1}{2\sqrt{\pi t}} \int_{-\infty}^{\infty} f(\lambda) \exp[(x-\lambda)^2/4t] \mathrm{d}\lambda \tag{9.21}$$

is the desired solution. Notice that if we specify a position along the rod and a time of interest, then carrying out the indicated integration in Eq. (9.21) permits us to determine the temperature.

9.5.1 Similar Solutions

A variation on the foregoing solution may be achieved by first finding a new independent variable, which is a combination of the two existing variables. If such a variable can be found, say,

$$\eta = \frac{x}{2\sqrt{t}} \tag{9.22a}$$

and we let

$$f(\eta) = \frac{T}{T_0} \tag{9.22b}$$

then the equation becomes

$$\frac{\partial\left(\frac{T}{T_0}\right)}{\partial t} = \frac{\partial^2\left(\frac{T}{T_0}\right)}{\partial x^2}$$

or

$$\frac{\partial f}{\partial \eta}\left(\frac{-\eta}{2t}\right) = \frac{\partial^2 f}{\partial \eta^2}\left(\frac{1}{4t}\right) \tag{9.23}$$

an ordinary differential equation,

$$\frac{\mathrm{d}^2 f}{\mathrm{d}\eta^2} + 2\eta \frac{\mathrm{d}f}{\mathrm{d}\eta} = 0 \tag{9.24}$$

Whereas the original boundary conditions could have been written

$$T(0,x) = 0 \tag{9.25a}$$

$$T(t,\infty) = 0 \tag{9.25b}$$

$$T(t,0) = T_0 \tag{9.25c}$$

they become

$$f(0) = 1 \tag{9.26a}$$

$$f(\infty) = 0 \tag{9.26b}$$

in the transformed case. The ordinary differential equation (ODE) may then be solved to yield

$$T = T_0\left(1 - \frac{2}{\sqrt{\pi}} \int_0^{\eta} e^{-\eta^2} \mathrm{d}\eta\right) \tag{9.27a}$$

or

$$T = T_0[1 - \mathrm{erf}(\eta)] \tag{9.27b}$$

Tables of the error function, $\mathrm{erf}(\eta)$, are found in many collections of standard tabulated functions.

Solutions obtained with this device are called similar solutions because the solution is the same for all cases with the same value of $x/\sqrt{t}$.

9.5.2 Finite Element Technique

Still another technique for solving a problem properly described by PDEs is to model the distributed phenomena by a large collection of mathematical representations of equivalent phenomena, the finite element method. In this process one may replace a single PDE by a system of ODEs. Although conceptually an infinite number of finite elements would be required to achieve an accurate representation of a PDE, a reasonable number, say, 10–30 finite elements, may be sufficient to achieve the desired level of accuracy.

The actual means by which the describing PDEs are best solved involves consideration of 1) the least accurate solution acceptable and 2) the least costly of several possibile algorithms available to solve the problem at hand. The latter depends heavily on the available computational tools. For example, if a problem can be structured so that it can be solved piecemeal by a group of networked workstations working on the problem in parallel, it may be less expensive to use this algorithm than to employ an algorithm that solves the problem serially on a supercomputer in the same time.

Engineers who have the task of designing flight vehicles today have been hearing from CFD scientists for the past 30 years that within the next few years it will be possible to determine fluid flows around complex configurations with an accuracy and reliability sufficient to obviate the need for wind tunnel or flight testing. While great strides have indeed been made in this direction in terms of computer capacity and speed, as well as algorithmically, the complexity of configuration for which this vision has been realized is still embarrassingly simple. Nevertheless, it is because the potential for cost savings and accuracy improvements is so great that work continues at a relatively high level on developing improved algorithms at the same time that computer designers seek to develop better computational topologies and faster components. The vehicle designer should remain cognizant of such developments and appropriate for use those which appear to offer cost effective solutions to current problems.

9.6 Concluding Remarks

In this chapter, we have attempted to indicate something of the configuration that the task of computing the aerodynamics and hydrodynamic characterics of wings

and bodies appears to be taking as we approach the new century. We have already moved from a time of basing new designs on correlations of empirical data to a period where design methods are based on integral forms of the fundamental fluid dynamic relationships. As computational horsepower increases, we can expect the preferred design methods to rely increasingly on accurate approximate solutions of the governing PDEs, methods probably developed from one of the techniques mentioned in this chapter. Nevertheless, the need for experimental verification of predicted results will remain, even though its scope and thoroughness may be reduced by the increased confidence one may then place in the theoretical computations. Engineering judgement, however, still has its place in balancing the use of the two technologies.

Problems

9.1. Assume the initial temperature distribution in an infinite, insulated rod is constant. a) Using Eq. (9.21) determine the variation in temperature at $x = 1.0$. Perform the integration numerically. b) From physical considerations, what answer should you expect? Did you obtain the expected answer?

9.2. How does representing derivatives by finite differences make the equations of fluid motion easier to solve?

9.3. Comment on the type of PDEs one may use to describe the motion of a body through air at 400 ft/s vs the type of PDEs one should use to described the motion of the same body through C_4F_8 at the same speed.

9.4. Look up Chapman.[44] From a perusal of the *AIAA Journal* for the last two years prepare a rather detailed commentary, with citations, on the extent to which Chapman's vision has been realized at the present time.

9.5. What would be the utility of CFD methods, such as those mentioned in this chapter, in the design of small, personal use aircraft? In your answer consider the application of the methods to determining the lift and drag characteristics of the vehicle, the aerodynamic or hydrodynamic stability derivatives for control and navigation system design, and the pressures on the vehicle surface, which can translate into some of the structural characteristics that the craft requires.

9.6. In what class of flight vehicles would the methods mentioned in the chapter be expected to find their inital application? Explain why.

References

[1]Woods, F. S., *Advanced Calculus*, Ginn and Co., 1934.

[2]Navier, C. L. M. H., "Mémoire sur les lois du mouvement des fluides," *Mémoires de l'Académie des Sciences*, Vol. 6, 1832, pp. 389–416.

[3]Stokes, G., "On the Theories of the Internal Friction of Fluids in Motion," *Transactions of the Cambridge Philosophical Society*, Vol. 8, 1845, pp. 287–305.

[4]Gerhart, P. M., and Gross, R. J., *Fundamentals of Fluid Mechanics*, Addison–Wesley, Reading, MA, 1985.

[5]von Kármán, T., *Aerodynamics: Selected Topics in the Light of Their Historical Development*, Cornell Univ. Press, Ithaca, New York, 1954.

[6]von Helmholtz, H., "Über Integrale der hydrodynamischen Gleichungen, welche den Wirbelbewegungen ensprechen," *Zeitschrift für die reine und angewandte Mathematik*, Vol. 55, 1858, pp. 25–55.

[7]von Helmholtz, H., "Über discontinuirliche Flüssingheitsbewegungen," *Monatberichte der Königlichen Akademie der Wissenchaften zu Berlin*, 1868, pp. 215–228.

[8]Kirchhoff, G., "Zur Theorie freier Flüssigkeitsstrahlen," *Zeitschrift für die reine und angewandte Mathematik*, 70, 1869, pp. 289–298.

[9]Kutta, M. W., "Auftriebkräfte in strömenden Flüssikeiten," *Illustrierte aeronautische Mitteilungen*, Vol. 6, 1902, pp. 133–135.

[10]Kutta, M. W., "Über eine mit den Grundlagen des Flugproblems in Bezeichung stehende zweidimensionale Strömung," *Sitzungsberichte der Bayerischen Academie der Wissenschaften*, 1910, pp. 1–58.

[11]Joukowski, N., "Über die Konturen der Tragflächen der Drachenflieger," *Zeitschrift für Flugtechnik und Motorluftschiffahart*, I, 1910, pp. 281–284.

[12]von Kármán, T., and Trefftz, E., "Potentialströmung um gegebene Tragflächenquerschnitte," *Zeitscrift für Flugtechnik und Motorluftschiffahart*, Vol. 9, 1918.

[13]Müller, W., "Zur Konstruktion von Tragflächenprofilen," *ZAMM*, 1924.

[14]Munk, M. M., "General Theory of Wing Sections," NACA Rept. 142, 1922.

[15]Theodorsen, T., "Theory of Wing Sections of Arbitrary Shape," NACA Rept. 411, 1932.

[16]Abbott, I. H., von Doenhoff, A. E., and Stivers, L. S., "Summary of Airfoil Data," NACA Rept. 824, 1945.

[17]Abbott, I. H., and von Doenhoff, A. E., *Theory of Wing Sections*, McGraw–Hill, New York; reprint Dover, 1959.

[18]Houghton, E. L., and Brock, A. E., *Aerodynamics for Engineering Students*, St. Martins Press, New York, 1970.

[19]Prandtl, L., "Über Flüssigkeitsbewegung bei sehr kleiner Reibung," *Verhandlungen des dritten internationalen Mathematiker-Kongress*, Heidelberg, 1904, pp. 484–491.

[20]Blasius, H., "Grenzschichten in Flüssigkeiten mit kleiner Reibung," *Zeitschrift für Mathematisch Physik*, Vol. 56, 1908, pp. 1–37.

[21]Howarth, L., "On the Solution of the Laminar Boundary Equations," *Proceedings of the Royal Society of London A*, Vol. 164, 1938, pp. 547–579.

[22]von Kármán, T., "Über laminare und turbulente Reibung," *ZAMM*, Vol. 1, 1921, pp. 233–253.

[23]Polhausen, K., "Zur näherungsweisen Integration der Differentialgleichung der Grenzschicht," *ZAMM*, Vol. 1, 1921, pp. 252–268.

[24]Schlichting, H., *Boundary Layer Theory*, 7th ed., McGraw–Hill, New York, 1979.

[25]Stevens, W. A., Goradia, S. H., and Braden, J. A., "Mathematical Model for Two-Dimensional, Multi-Component Airfoils in Viscous Flow," NASA CR-1843, July 1971.

[26]Smetana, F. O., Summey, D. C., Smith, N. S., and Carden, R. K., "Light Aircraft Lift, Drag, and Moment Prediction—A Review and Analysis," NASA CR-2523, May 1975.

[27]Oeller, H. J., "Die Inkompressible Potentialstromung in Ebener Gitterstufe," *Jahrbuch 1962 Wissenschaftlichen Gesellschaft für Luft und Raumfahrt*, e.v. pp. 349–353.

[28]Chen, A. W.-S., "The Determination of the Geometries of Multiple Element Airfoils Optimized for Maximum Lift Coefficient," Ph.D. Thesis, Univ. of Illinois, Urbana-Champaign, IL, 1971.

[29]Bingham, G. J., and Chen, A. W.-S., "Low Speed Aerodynamic Characteristics of an Airfoil Optimized for Maximum Lift Coefficient," NASA TN D-7071, Dec. 1971.

[30]Milgram, J. H., "Section Data for Thin, Highly Cambered Airfoils in Incompressible Flow," NASA CR-1767, July 1971.

[31]Lanchester, F. W., *Aerodynamics*, Constable and Co., London, 1907.

[32]Prandtl, L., "The Generation of Vortices in Fluids of Small Viscosity," *Journal of the Royal Aeronautical Society*, Vol. 31, 1927, pp. 720–741.

[33]Multhopp, H., "Aerodynamics of the Fuselage," NACA TM-1036, Dec. 1942 (translation of earlier work in German).

[34]McVeigh, M. A., and Kisielowski, E., "A Design Summary of Stall Characteristics of Straight Wing Aircraft," NASA CR-1646, June 1971.

[35]Margason, R. J., and Lamar, J. E., "Vortex-Lattice Fortran Program for Estimating Subsonic Aerodynamic Characteristics of Complex Planforms," NASA TND-6142, Feb. 1971.

[36]Pope, A., *Basic Wing and Airfoil Theory*, McGraw–Hill, New York, 1951.

[37]Hess, J. L., and Smith, A. M. O., "Calculation of Non-Lifting Potential Flow About Arbitrary Three-Dimensional Bodies," Douglas Aircraft Co. Rept. E. S. 40622, March 15, 1962.

[38]Dawson, C. W., and Dean, J. S., "The XYZ Potential Flow Program," Naval Ship Research and Development Center, Rept. 3892, Bethesda, MD, June 1972.

[39]Fox, S. R., "An Automated Technique for Encasing Specific Payloads in Low-Drag Fairings," Ph.D. Dissertation, Dept. of Mechanical and Aerospace Engineering, North Carolina State Univ., NC, 1984.

[40]Summey, D. C., and Smetana, F. O., "Prediction of Light Aircraft Horizontal Tail Onset Flows—A Review and Analysis," NASA CR-2774, April 1977.

[41]Cebeci, T., and Smith, A. M. O., "A Finite Difference Solution to the Incompressible Turbulent Boundary Layer Equation by an Eddy Viscosity Concept," McDonnell-Douglas Aircraft Co., Inc., Long Beach, CA, Rept. DAC-67130, Oct. 1968.

[42]Anderson, D. A., Tannehill, J. C., and Pletcher, R. H., *Computational Fluid Mechanics and Heat Transfer*, Hemisphere, New York, 1984.

[43]Anon, "Advertisement by Analytical Methods, Inc., Redmond, WA," *Aerospace America*, Sept. 1996.

[44]Chapman, D. R., *AIAA Journal*, Vol. 17, 1979, pp. 1293–1313.

Index